Tow Scale Dry Fibre Architectures for High-Performance Ductile Composites

A thesis submitted to The University of Manchester for the degree of

Doctor of Philosophy

In the Faculty of Science and Engineering

2019

Mohammad Hamidul Islam

Robotics and Textile Composites Group

Department of Materials

School of Natural Sciences

The University of Manchester

Table of Contents

Words count: 45,925

List of Figures

List of Tables

List of Abbreviations

UD	Unidirectional
LS	Low strain
HS	High strain
GF	Glass fibre
E-G	E-glass
S-E	S-glass
T700	Carbon T700-60E
M55	Carbon M55J
MW	Micro-wrapped
SHMW	Single helix micro-wrapped
DHMW	Double helix micro-wrapped
ASTM	American Society for Testing and Materials
SBS	Side by side
2D	Two dimensional
3D	Three dimensional
TRM	Resin transfer moulding
VARTM	Vacuum assisted resin transfer moulding
RTCR	Room temperature curing resin
HTCR	High temperature curing resin
PP	Polypropylene
UDW	Unidirectional woven
CNT	Carbon nanotube
SEM	Scanning electron microscope
NCF	Non-crimp fabric
ROM	Role of mixture

FVF	Fibre volume fraction
MVF	Matrix volume fraction
SD	Standard deviation
MPa	Mega pascal
GPa	Giga pascal

Abstract

High-performance fibre reinforced composites have excellent mechanical properties such as high specific strength and stiffness, excellent corrosion resistance and high fatigue life. Therefore, they have been in use for advanced lightweight application such as aero-structures, spacecraft, automobile, wind turbine blade and sports equipment. However, one key limitation of conventional composites is their brittleness and catastrophic failure under the tension, without sufficient warning or residual load-carrying ability. The lack of warning before failure leads to safety concerns which can limit their applications due to the unpredictable failure behaviour. Hence, it is necessary to fabricate a new generation of high-performance composite that overcomes the key limitations of composites and fail gradually with plastic deformations while still carrying the load. To attain such an ambitious outcome, development of new inherent ductile reinforced material with novel architectures is required.

This research work aims to design and develop novel processes for dry fibre architecture for reinforced (preform) materials to improve the ductility or pseudo-ductility of high-performance composites. Two different processes have been investigated to prepare hybrid preform for ductile composites. The first process, commingled hybrid tow was prepared from carbon and glass fibre spread tow using air-assisted spreading and commingling technology where carbon and glass fibres were partially hybridised at the tow level. A comparative study of the tensile properties of the thin ply layer by layer hybrid and commingled hybrid composites with epoxy resin were carried out. It was found that both hybrid composites failed more gradual and exhibited improved tensile failure strain compared to carbon fibre spread tow composite.

The second process, the hybridisation of two different dry fibres with dissimilar failure strain was done through the micro-wrapping process where low strain to failure fibres helically wrapped with high strain to failure fibres and produced core-shell type hybrid tow. Micro-wrapped hybrid tows were produced using two different types of wrapping arrangement, single helix and the double helix. In order to compare micro-wrapped hybridisation process to another kind of hybridisation, a side-by-side parallel placement hybridisation process was considered. Four different types of hybrid configurations (T700/E-G, T700/S-G, M55/S-G and M55/T700) tows have been prepared and studied their structural and tensile properties. A detailed study on the effect of micro-wrap hybrid architecture on the ductile or pseudo-ductile properties of the composite has been carried out and compared with side by side hybrid architecture. The investigations were carried out in three stages-mesoscale composites (single hybrid tow composite rod), UD composite laminates and UD woven composites laminates. Additionally, the influence of two epoxy resin systems (room temperature and high-temperature curing resin) on the composite mechanical properties was also studied. Tensile test results revealed that micro-wrapped hybrid composites (rods and laminates) demonstrated excellent pseudo-ductile behaviour with little stress drop after low strain fibre failure for all four hybrid configurations. On the other hand, a significant stress drop was observed in side by side hybrid composites after LS fibre failure. The matrix properties played a significant role in the composites ultimate failure strain. About 27% higher failure strain was attained with room temperature curing resin compared to high temperature curing resin composites. Double helix micro-wrapped hybrid tow composite also demonstrated similar results of single helix micro-wrapped hybrid composites. Therefore, the novel micro-wrapped hybrid architecture could be a suitable approach to produce low-cost textile preform for high performance ductile or pseudo-ductile composites.

Declaration

No portion of the work referred to in the thesis has been submitted in support of an application for another degree or qualification of this or any other university or other institutes of learning.

Copyright Statement

Acknowledgement

I would like to express my sincere gratitude to my supervisor Prof. Prasad Potluri for his excellent guidance, spiritual direction, motivation, helpful discussion and financial support throughout the research. I would also like to express my gratitude to my other supervisor Prof. Michael R Wisnom from the University of Bristol for his patient guidance, valuable suggestions and helpful discussions during this research. They have always been sharing their extensive knowledge and valuable expertise in composite materials for my work. I am honoured to work with both of them.

I would like to thanks Dr. Vivek Koncherry, Dr. Sree Shankhachur Roy, Dr. Mayank Gautam and Dr. Alan Nesbitt for their kind help and advice during the study and critical review of my PhD thesis manuscript. They were always ready to help with my difficulties during this study.

I would like to express my gratitude to UK Engineering and Physical Sciences Research Council (EPSRC) for providing partial financial support for my research via Programme Grant EP/I02946X/1 on High-Performance Ductile Composite Technology (HiperDuCT) in collaboration with the University of Bristol.

I also want to extend my gratitude towards: Mr. Thomas Kerr, Mr. Christopher Cowan, and Mr. Roy Conway for all their help.

I also would like to thank all the team members of the Robotics and Textile composites group for their help and support during this work.

I am grateful to my wife Laila sultana for her endless support, warm encouragement and her sacrifice during the research period. It was not possible for me to complete this research without her personal support. I would also like to thanks my lovely daughters Hridita Islam, Ambreen Islam and my lovely son Ajwad Raid for their warm encouragement.

Finally, I would like to dedicate this thesis to my parents, Md. Joynal Abedin and Mrs Rahima Khatun

Chapter 1: Introduction

1.1 Research background

High-performance polymer matrix composites offer excellent mechanical properties with high specific strength and stiffness. Composite structure and properties can be customised to particular applications and additional functionality can be incorporated, *e.g:* sensing, self-healing, morphing or energy storage. Therefore, the application of high-performance composite materials has been increasing progressively in a wide range of areas such as aerospace, automobile, marine, wind turbine blades, civil construction, sporting goods and other industries. The global market value of high-performance composites was at USD 23.50 Billion in 2016 and it is predicted to reach USD 33.33 Billion by 2022 [1]. In addition, the flexibility in textile architectures has widened the opportunity to use these composites from non-load bearing applications to primary load-bearing applications. Despite this progress, inherent brittleness is considered one of the major limitations of composites. The composite structures under any loading conditions fail suddenly and catastrophically with little or no warning. Whereas traditional metal or polymer structures fail progressively with ductile deformation beyond the elastic limit before failure. The lack of warning before failure leads to safety concerns which can limit their applications due to the unpredictable failure behaviour. Hence, the development of composites with the inherent ductile property which can improve the safety concerns for certain applications is of significant interest.

The ductile and pseudo-ductile properties of fibre-reinforced polymer composites have been a highly active research area over the last decade. A significant amount of research has been done to improve the ductility or pseudo-ductility of the composite laminates without sacrificing specific strength and stiffness. Various material systems and manufacturing processes have been proposed to make composites more resistant to damage and improve their ductility. One of the approaches to introduce ductility in fibre reinforced composites is to replace brittle fibre with ductile fibre. In this respect, low diameter stainless steel fibres with brittle and ductile matrix have been studied and a higher failure strain with plastic deformation was achieved [2]. However, these

composites, compared to carbon/epoxy laminates have a higher density which limits their application in lightweight structures.

In a recent review article, Swolfs *et al.* [3] indicated that appropriate hybrid architecture can lead to improve the composites inherent ductile properties and also change the damage propagation mechanisms leading to ultimate failure. The hybridisation of fibres is an established approach where two or more different types of fibres are typically combined to achieve unique properties of the resulting material. Often these fibres are combinations of low strain (LS) and high strain (HS) that improves the ductility of composites. During loading, these two components fail at different stages. One of the main disadvantages of these composites is that under tensile loading a major load drop is observed after the LS component failure. This phenomenon of significant load drop was investigated in several studies recently. These studies show that the strength, stiffness, volume of HS and LS constituents, fibre distribution, the layup sequence as well as ply thickness play a significant role in the initiation and propagation of damage after initial failure [4], [5]. Although, achieving the ductility or pseudo-ductility (progressive failure) in composites can be challenging the design of inherent ductile hybrid architecture is very important. In this research, several studies have been carried out to investigate the manufacturing methods of hybrid composite materials using different dry fibres architecture and how to achieve progressive failure under certain loading conditions.

The design of pseudo-ductile composite mainly depends on the design of the reinforcing hybrid fibres. The architecture of hybrid fibres requires inherent ductile properties to achieve pseudo ductility. Several studies have been proposed in literature like creating pseudo-ductility in a composite via incorporating ductile fibres through hybrid or commingling yarn or tow [6], [7], fibre reorientation via using excess length [8], thin ply angle-ply laminates [9], thin-ply spread tow hybrid UD laminates [4], [5], [10]–[12] and core-shell design [13]. In fact, the thin ply spread tow technology has attracted more and more attention for pseudo-ductile composites in recent years. In this composite, LS thin ply is used to reduce the energy release rate during the delamination of the plies which is sandwiched by HS thick plies is considered as one of the key design criteria for manufacturing pseudo-ductile composites. These studies recommended that the outer HS material layers should be thick and strong enough to take the load after LS material failure. Thin ply angle-ply laminates also have shown pseudo-ductile response through fibre rotation and matrix plasticity [9]. The main limitation of these composites is the

poor drapability and higher manufacturing cost to produce decent thick laminates. On the other hand, core-shell design of carbon/glass hybrid rod demonstrated some degree of pseudo-ductility compared to randomly dispersed hybrid architecture [13]. But the main problem is a big stress drop observed in the stress-strain diagram during the transition phase. This core-shell approach showed an interesting result in comparison to randomly dispersed structure.

Therefore, it is necessary to design and develop a new process for inherent ductile dry fibre architecture to demonstrate low-cost alternatives to expensive thin-ply concepts which can be used as a textile preform for achieving ductility in composites.

1.2 Research Aims and Objectives

This research aims to improve the ductility or pseudo-ductility of the high-performance composites. The main aim of this research is to design and develop novel dry fibre architectures to produce low-cost textile perform alternatives to expensive thin-ply concepts for achieving ductility in composites while maintaining strength and stiffness. To achieve this aim, the following objectives have been considered.

- To design and develop new processes for dry fibre architecture to produce low-cost hybrid preform through the combination of thin-ply, angle-ply and core-shell design concept.
- Study the effect of new dry fibre architectures on the tensile properties at dry fibre state and compare with conventional hybrid architecture.
- To investigate the effect of dry fibre architecture on the ductile and pseudo-ductile properties of mesoscale composites.
- To develop textile preform using the prepared new hybrid tows.
- To investigate the effect of new fibre architectures on the ductile and pseudo-ductile properties at the laminate stage and compare with conventional hybrid composites.
- Study the effect of resin properties on the ductility of the new hybrid tow composites.
- Study the effect of fibre orientation of new hybrid tow in the ductile or pseudo-ductile properties of the composites.

1.3 Outline of the Thesis

Each of the objectives have been elaborated into individual chapters. The respective methodology, experiments, results, analysis and summary of key findings of a particular configuration were included in each of these chapters. The overall summary was presented in the conclusion chapter

In Chapter 1 a short introduction to the application of composite laminates in a different sector and their key limitation due to lack of ductility was provided. Different techniques that are used to enhance the ductility of the composites have been identified. The aims and objectives of this study are also presented in this chapter.

In Chapter 2 a literature review relevant to the studies in this research has been presented. A brief idea about composite materials and detailed background and fundamental knowledge about ductility and pseudo ductility have been discussed. Reviews of different techniques that have been used to improve the ductility or pseudo-ductility of the composite laminates have been presented to justify the research.

In Chapter 3 a process development for preparing the hybrid preforms for ductile composites has been discussed. Preparation of intra-tow hybrid preform by spreading and commingling process has been illustrated. The fabrication of thermoset composite laminates from hybrid and non-hybrid tow and their mechanical properties were also studied.

In Chapter 4 a novel process development for micro-wrapped hybrid dry fibre architecture for improving the ductility of high-performance composites has been presented. Lab-scale machine designs and set up were illustrated. Structural and mechanical properties of different dry hybrid tows were studied. In addition, the manufacturing method of micro-wrapped and side by side hybrid tow composites rods have been discussed. Tensile properties of the composite rods were also studied.

In Chapter 5 preparation of unidirectional fabric by using micro-wrapped hybrid tow has been presented. Fabrications of unidirectional and unidirectional woven composite panels from different micro-wrapped and side by side hybrid tow with epoxy resin were discussed. Tensile properties of the composite with different hybrid configurations were studied.

In Chapter 6 the influence of two epoxy resin systems on the composite laminate ductility has been investigated.

In Chapter 7 the effect of wrapping directions (such as single and double helix wrapping) in the composite mechanical properties has been discussed.

In Chapter 8 a brief summary of the findings has been presented with proposed future work.

References

[1] M. Rohan, "High-Performance Composites Market Worth 33.33 Billion USD by 2022," *MarketsandMarkets*. [Online]. Available:

[2] M. G. Callens, L. Gorbatikh, and I. Verpoest, "Ductile steel fibre composites with brittle and ductile matrices," *Compos. Part A Appl. Sci. Manuf.*, vol. 61, pp. 235–244, Jun. 2014.

[3] Y. Swolfs, I. Verpoest, and L. Gorbatikh, "Recent advances in fibre-hybrid composites: materials selection, opportunities and applications," *Int. Mater. Rev.*, pp. 1–35, Apr. 2018.

[4] M. Jalalvand, G. Czél, and M. R. Wisnom, "Damage analysis of pseudo-ductile thin-ply UD hybrid composites – A new analytical method," *Compos. Part A Appl. Sci. Manuf.*, vol. 69, pp. 83–93, Feb. 2015.

[5] M. R. Wisnom, G. Czél, Y. Swolfs, M. Jalalvand, L. Gorbatikh, and I. Verpoest, "Hybrid effects in thin ply carbon/glass unidirectional laminates: accurate experimental determination and prediction," *Compos. Part A Appl. Sci. Manuf.*, vol. 88, pp. 131–139, Apr. 2016.

[6] W. M. Diao H, Bismarck A, Robinson P, "Pseudo-ductile behaviour of unidirectional fibre reinforced polyamide-12 composite by intra-tow hybridization," in *Proceedings of ECCM 15 Conference*, 2012, no. June, pp. 24–28.

[7] E. Selver, P. Potluri, C. Soutis, and P. Hogg, "Healing potential of hybrid

materials for structural composites," *Compos. Struct.*, vol. 122, pp. 57–66, Apr. 2015.

[8] S. Pimenta and P. Robinson, "Wavy-ply sandwich with composite skins and crushable core for ductility and energy absorption," *Compos. Struct.*, vol. 116, pp. 364–376, Sep. 2014.

[9] J. D. Fuller and M. R. Wisnom, "Pseudo-ductility and damage suppression in thin ply CFRP angle-ply laminates," *Compos. Part A Appl. Sci. Manuf.*, vol. 69, pp. 64–71, Feb. 2015.

[10] G. Czél, M. Jalalvand, and M. R. Wisnom, "Design and characterisation of advanced pseudo-ductile unidirectional thin-ply carbon/epoxy– glass/epoxy hybrid composites," *Compos. Struct.*, vol. 143, pp. 362–370, Feb. 2016.

[11] G. Czél, M. Jalalvand, M. R. Wisnom, and T. Czigány, "Design and characterisation of high performance, pseudo-ductile all-carbon/epoxy unidirectional hybrid composites," *Compos. Part B Eng.*, vol. 111, pp. 348–356, Feb. 2017.

[12] G. Czél and M. R. Wisnom, "Demonstration of pseudo-ductility in high performance glass/epoxy composites by hybridisation with thin-ply carbon prepreg," *Compos. Part A Appl. Sci. Manuf.*, vol. 52, pp. 23–30, Sep. 2013.

[13] Y. Liang, C. Sun, and F. Ansari, "Acoustic Emission Characterization of Damage in Hybrid Fiber-Reinforced Polymer Rods," *J. Compos. Constr.*, vol. 8, no. 1, pp. 70–78, Feb. 2004.

Chapter 2: Literature Review

2.1 Introduction

This research aims to improve the ductility or pseudo-ductility of high-performance composites to overcome the foremost limitation of conventional composites. The purpose of this chapter is to describe the recent developments regarding ductility or pseudo-ductility in high-performance composites, which is of interest in the automotive and airframe industries. Researchers have been using different techniques for creating ductility in a composite such as fibre reorientation, material architecture, and incorporate ductile fibres, hybrid or commingling yarn or tow. However, to create ductility or pseudo-ductility in the high-performance composites by hybridisation of filaments with different strain to failure at tow scale is a challenging topic in the composite world. The architecture of the hybrid preforms has a direct effect on the properties of the composites. In this chapter, the work related with the improvement of ductility and pseudo-ductility such as the development of new machinery, process, material architecture and characterisation of such new techniques and the potential benefits of using such technologies in composites industries is discussed.

2.2 High-performance composites

Composites are one of the engineering materials in which two or more distinct materials are combined resulting in a third useful material with superior properties than those of the individual constituent materials acting independently [1], [2]. In general, composites represent to materials having strong reinforcement, i.e. continuous or discontinuous fibres or particles, bonded by a weaker matrix material. However, high-performance composites are specifically high-performance fibre (such as carbon, glass, aramid, etc.) structure reinforced polymer matrix composites. An ideal reinforced fibre for high-performance composites must have higher strength and stiffness, low specific weight, good heat and chemical resistance and excellent adhesion to the matrix materials. Therefore, the applications of the high-performance composites are increasing day by day because of their outstanding mechanical properties such as high specific strength, stiffness, corrosion resistance, impact strength and thermal conductivity and so on.

Despite this progress, an important limitation of the current composite is their inherent brittleness which caused a sudden and catastrophic failure without plastic deformation. This behaviour limits their uses for structural and high volume applications. So, it is a big challenge to prepare high-performance composites with inherent ductile properties which will allow them to go plastic deformation during the failure.

2.3 Ductility and pseudo-ductility

2.3.1 Ductility

Ductility is the capacity of a material or a structure to tolerate non-recoverable deformation. In material science, ductility is the ability of a solid material to deformer in a plastic manner during the tensile loading [3]. In practice, this appears in a load-displacement curve as irreversible inelastic displacement and equates to the growth of plasticity, and in a creaking body, the growth of a creak in a stable manner. The vital role of the ductility is that it consumes energy, and this energy cannot be released on a fracture. Low ductility indicates that a material is brittle and will break without noticeable plastic deformation under a tensile load. Higher ductility indicates that material will go plastic deformation before the break when a tensile load is applied. A schematic illustration of the stress-strain curves of brittle and ductile materials are shown in Figure 2.1

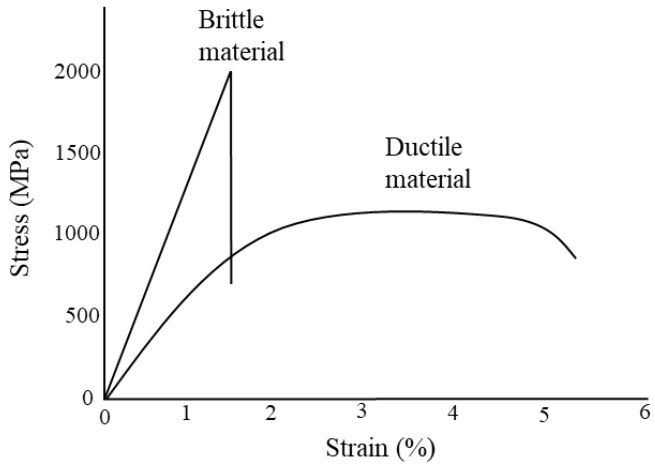

Figure 2.1: Schematic illustration of the stress-strain curves of brittle and ductile materials.

2.3.2 Pseudo-ductility

Different technologies have been used for creating inherent ductility in composites that will allow a gradual failure while the composite retains the high strength and specific stiffness. This behaviour is termed pseudo-ductility as it appears like the ductile behaviour which is found in metals. The term pseudo-ductility has been around more than twenty years [4], [5], but in recent years, it has exposed a strong revitalisation [6]–[14]. There is no clear definition for pseudo-ductility but it can be measured using pseudo-ductile strain. Wisnom *et al.* [15] have defined the pseudo-ductile strain as the difference between the final failure strain, and the elastic strain at the same stress (Figure 2.2). Jalalvand *et al.* [16] explained the pseudo-ductile strain in the following way.

When a tensile load is applied in hybrid composites, the damage initiates and develops gradually and the stress-strain response deviates from the initial linear elastic straight line. Usually, two types of nonlinear stress-strain responses are observed. If the extra stress-strain obtains after initial failure without stress drop due to gradual failure then the pseudo-ductile strain can achieve. The pseudo-ductile strain is the extra strain between the ultimate failure strain and the initial slope line at the failure stress level as shown in (Figure 2.2 a). In contrast, if the stress drop occurs as the first nonlinearity in the stress-strain graph before ultimate failure which includes loss of integrity, then it is called brittle failure where pseudo-ductile strain is considered zero (Figure 2.2 b).

Carbon fibre composite materials fail catastrophically without warning. This sudden failure of composites leads to high safety factor which leads to hampering the full exploitation of their mechanical properties [17]. Conventional hybrid composites usually exhibit a major vertical load drop on their stress-strain graph after low strain fibre failure. Such kind of load drop is restricting the composite materials in certain applications. Therefore pseudo-ductility would be needed for the progressive failure of the composites which can show a warning sign earlier than the final failure.

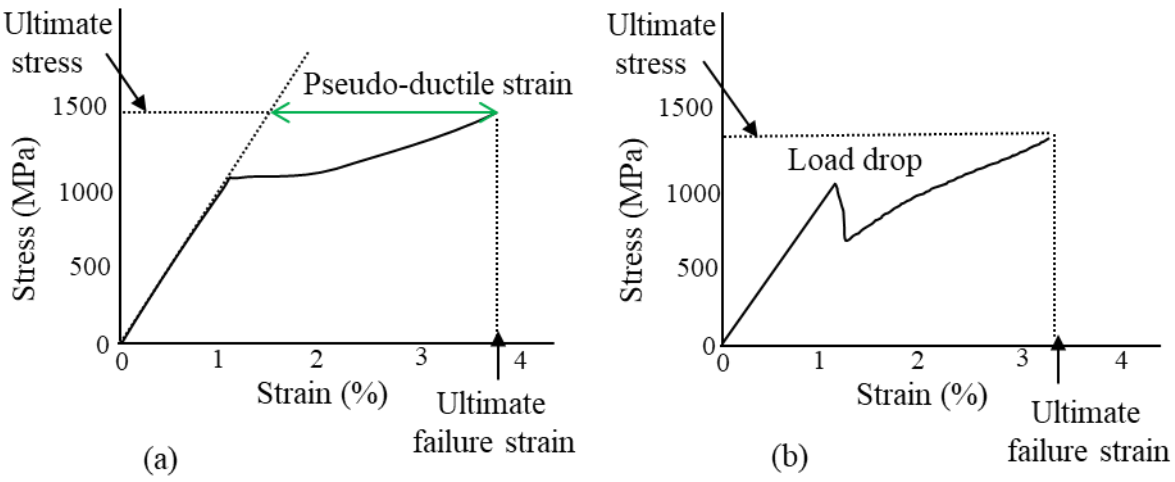

Figure 2.2: Schematic of (a) a nonlinear stress-strain curve of pseudo-ductile composite with gradual damage process and (b) a nonlinear stress-strain curve of brittle failure of composite with loss of integrity and load drop before ultimate failure process.

The research on pseudo ductile materials is progressively increasing. Different technologies are being used to achieve pseudo ductility in composites such as hybridisation: incorporating ductile fibres through hybrid or commingling yarn or tow [18]–[22], material architecture by fragmentation in thin ply spread tow [9], [12], [15]–[17], [23]–[27], fibre re-orientation via using excess length (angle plies and waviness) [6], [8], [20], [28], [29], braiding [30]–[32], incorporating ductile constituents [33], [34] and controlling the damage mechanism in non-hybrid composites [35]. But a review published by Swolfs *et al.* [36] pointed out that most of the researcher have been focusing on hybrid composites.

2.4 Hybrid composites

The failure strain and toughness of the composites can be increased by replacing the brittle fibres with ductile fibres. In this case, metal fibres have high stiffness and large strain to failure but the problem is their weight (high densities). On the other hand, some fibres do have low densities and with high ductility but the problem is their stiffness and limited temperature resistance. One of the promising mechanisms for improving the toughness is incorporating nano-sized organic and inorganic particles with epoxy resin. Since the problem of these toughening strategies, researchers are given emphasised in hybridisation to make a strong lightweight material with improved toughness by combining fibres with different stiffness and failure strains. Hybrid composites deliver

improve mechanical properties such as tensile modulus, compressive strength, ductility and impact strength which cannot be realised in non-hybrid composite materials. The literature review [18], [22], [36]–[39] shown that the study of the novel application of hybrid composite is challenging research to the researchers for many years.

2.4.1 Definition of hybrid composite

The term hybrid is usually used to represent the combination of two different types of fibre into one single matrix. In principle, different types of fibres may be incorporated into a hybrid, but it is more likely that a combination of only two types of fibres would be most preferable. The purpose of hybridisation is to fabricate new materials which will be balancing the inherent advantages and disadvantages of its constituents. Hybrid composites which are fabricated by combining two or more fibre types give better balance in mechanical properties than non-hybrid composites. The two fibre types naturally referred to as low strain (LS) and high strain (HS) fibres. In many earlier researchers, carbon and glass fibre layers were used as the constituents [19], [36], [40], [41].

2.4.2 Types of hybrid composite

According to the arrangement of reinforced materials in the composite, hybrid composites can be categorised into three major types [36], [42], [43].

(a) Interlaminated hybrids: where the hybridisation is achieved at the laminate level by stacking plies of different constituents layer by layer [18], [44]–[46] (Figure 2.3a). This is the easiest and cheapest method for producing a hybrid composite and well used.

(b) Intra-ply or intra-yarn hybrids: where different bundles are mixed within the layers by the parallel winding of different tows, yarns and filament bundles [47]–[49] or co-weaving of different tows or filaments [50], [51] (Figure 2.3b)

(c) Intermingled hybrids: where different types of fibres are intimately mixed within the ply and the hybridisation is achieved. Intermingling hybridisation has been done by commingling [52]–[55] or wrapping process (Figure 2.3c).

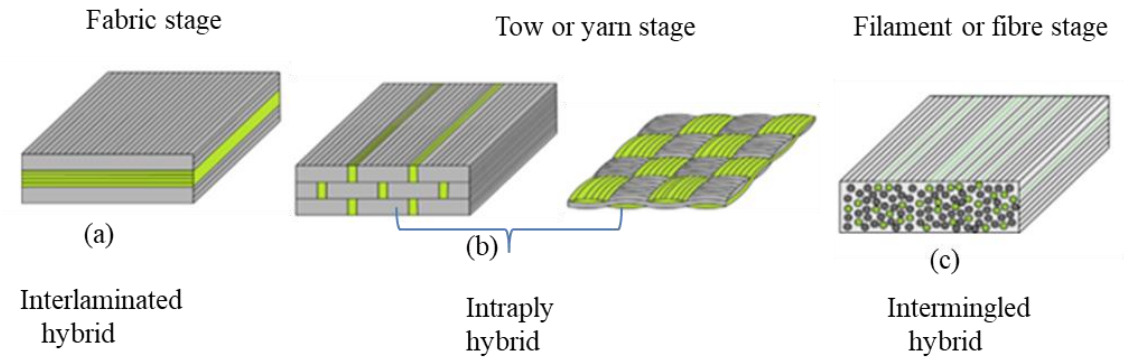

Figure 2.3: Hybrid configurations for continuous fibre reinforced composites [43]

2.4.3 Damage mode of UD hybrid composites

Jalalvand *et al.* [9] presented an analytical method for prediction all possible damage modes of UD hybrid composites and their stress-strain response during the tensile loading. They demonstrated four different scenarios of the damage mode in UD hybrid composites under tensile loading when the first crack initiation happened in the low strain materials are shown in Figure 2.4.

1. Premature failure of the high strain material because high strain material fails earlier than low strain material fragmentation caused catastrophic failure of the laminate.
2. Catastrophic delamination, in this case, low strain material fails after the delamination and followed by high strain material failure.
3. In this case, fragmentation has happened in the low strain material and after that high strain material failure happened.
4. Initially, fragmentation has occurred in the low strain material followed by dispersed delamination and finally high strain material failed.

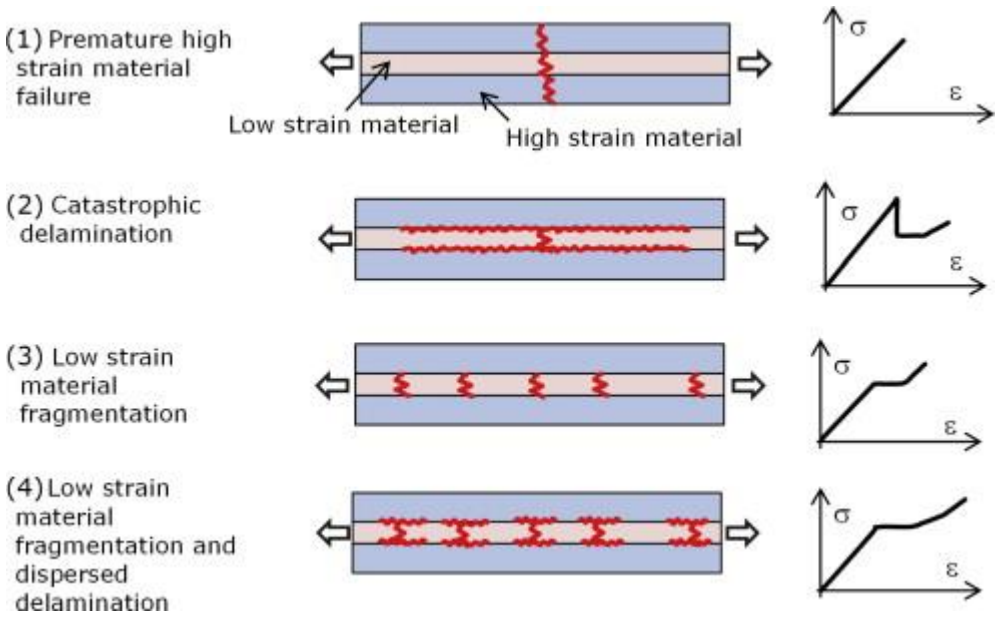

Figure 2.4: Different damage scenarios of UD hybrid laminates. Stress-strain responses of four possible damage scenarios are shown on the right-side [9]

The above study clearly demonstrates that low strain material fragmentation and dispersed delamination is very important to achieve the ductile or pseudo-ductile behaviour of the composites. To achieve the low strain material fragmentation and dispersed delamination, hybrid architecture and proportion of low and high strain material play a significant role [16], [24], [56]. Aveston *et al.* [56] studied the importance of the constituents` fraction in hybrid composites and shown that there is an upper limit for the volume fraction of LS material to HS material for overcoming the complete fracture of LS material. They concluded that using less portion of LS material than this critical fraction leads to multiple fracture or fragmentation of the low strain material. Jalalvand *et al.* [24] established the concept of damage mode maps as a function of carbon layer thickness and relative volume fraction of carbon. A schematic illustration of their damage mode map is shown in Figure 2.5 where four quadrants represent a different failure behaviour of the hybrid composite. The maximum thickness of the carbon layer and relative volume fraction of carbon for a UD thin-ply carbon-glass hybrid composite can be predicted from their damage modes map for pseudo-ductile composites. Hence, to attain a gradual failure process during the tensile loading, it is necessary to select an appropriate configuration to combine different types of low strain and high strain fibres with appropriate volume fraction.

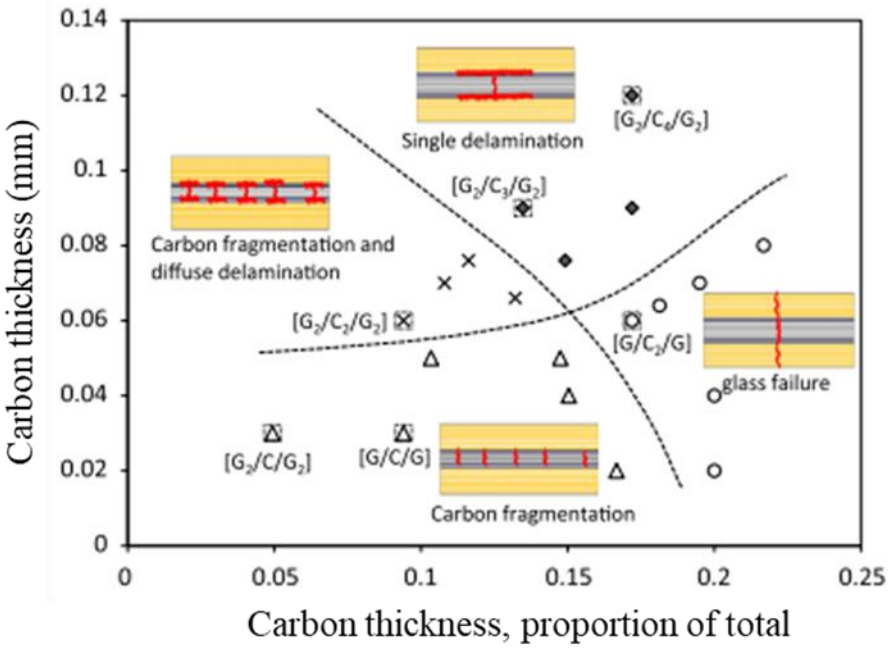

Figure 2.5: Damage modes map for carbon/glass hybrid composites as a function of the absolute and relative thickness of carbon layers [24].

2.4.4 The hybrid effect

The hybrid effect can be defined as the improvement of apparent failure strain of the low elongation fibre in a hybrid composite compared to the failure strain of low elongation fibre reinforced in non-hybrid composite (Figure 2.6a). The hybrid effect is also defined as the deviation between the properties of the hybrid composites and the properties predicted from the simple role of mixtures (ROM) based on the properties of the composites containing one fibre type (Figure 2.6b) [57]. A positive or negative hybrid effect in hybrid composites is defined as a positive or negative deviation of certain mechanical property from the role of mixtures behaviour [57]. The hybrid effect was first published by Hayashi in 1972 [18] for UD GF/CF hybrid composites. He reported that the failure strain of the carbon fibre layers in a GF/CF hybrid composite was 40% higher compared to those measured in the single carbon fibre composite. Swolfs *et.al*. [58] schematically defined (Figure 2.6) the hybrid effect corresponding to Hayashi`s [18] and Marom et.al [57] observations.

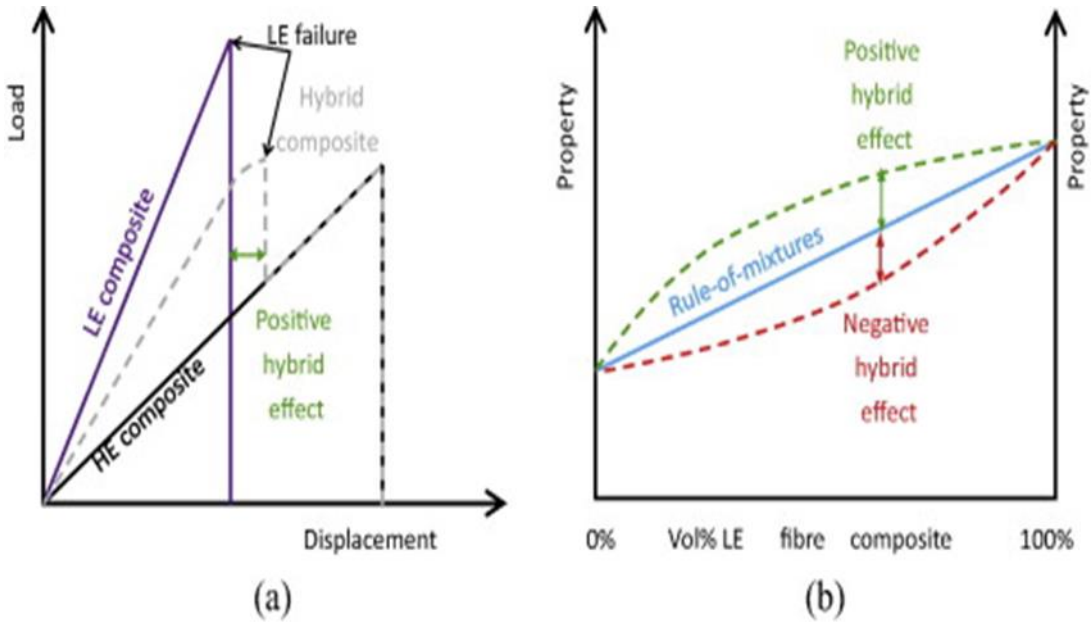

Figure 2.6: Illustration of the hybrid effect: (a) the apparent failure strain enhancement of the low elongation fibres, under the assumption that relative volume fraction is 50/50 and that the hybrid composite is twice as thick as the reference composites and (b) a deviation from the rule of mixtures [58].

2.4.5 Strain to failure of hybrid composites

Carbon fibre reinforced composites have excellent mechanical properties but a major drawback is the lack of toughness and low failure strain. It is a challenging task for the researcher to increase the failure strain. Many approaches have been taken to improve the failure strain of carbon fibre composites. Incorporating ductile fibre, such as metal can improve failure strain but the problem is their specific strength. One of the most suitable methods to improve the failure strain is fibre hybridisation to maintain high stiffness and strength [19], [40], [51]. A recent literature review [36] showed that the most popular hybridisation for carbon fibre composites is glass fibre because glass fibre has good mechanical properties, higher elongation and cheaper than carbon fibre which can play an important role to reduce the cost than all carbon fibre composite. Kretsis [59] clearly demonstrated in his review paper that with decreasing the LS fibre content hybrid effect is increased. It has been reported a +36% to +90% hybrid effect by Pandya *et.al* [60] in a carbon/glass fibre composite, where relative content of carbon fibre was 47%. Furthermore, a hybrid effect has increased by arranging the carbon fibre layer as an inner pile rather than outer piles. You *et.al* [61] reported maximum hybrid effect was attained when the carbon and glass fibres were well dispersed and they achieved

33% hybrid effect in UD composite. Wisnom *et al*. [45] experimentally studied the thin and thick ply carbon/glass UD interlayer hybrid composites. The magnitude of the hybrid effect depends on ply thickness and maximum 20% of the hybrid effect was found in thin ply hybrid composite. A brief outline of the hybrid effect reported in the literature is summarised in Table 2.1. The hybrid effect was calculated as the relative failure strain improvement of the carbon fibres in the hybrid composites compared to their failure strain in an all-carbon fibre composite.

Table 2.1: Overview of the hybrid effect for failure strain of UD hybrid composites

Author(s)/References	Materials	Hybrid type	Volume ratio (LE/HE)	Hybrid effect (%)	Comments
Hayashi [18]	CF/GF	Interlayer	25/75	+45	UD
Bunsell and Harris [19]	CF/GF	Interlayer	33/67 50/50	+42 +84	UD
Manders and Bader [40]	CF/GF	Interlayer Interlayer	5/95 to 50/50 6/94 to 0.4/99.6	+6 to 46 +30 to+52	UD
Zweben [38]	CF/Kevlar	Interlayer Interlayer	50/50 50/50	+4 +32	UD MD
You et.al [61]	CF/GF	Intralayer	47/53	+9 to +33	UD
Pandya et.al [60]	CF/GF	Interlayer	45/55	+36 to +90	MD
Diao et.al [62]	CF/GF	Intermingled	60/40	+14	UD
Wisnom et.al [45]	CF/GF	Interlayer	-	+20	UD

UD = Unidirectional and MD = Multidirectional

Most of these studies have paid attention to the primary failure strain compared to the ultimate failure strain. The published researches indicate that the ultimate failure strain of UD hybrid composites is lower than the failure strain of single fibre composites

comprising only the high elongation fibres but it is higher than that of composites comprising only the low elongation fibres [17]–[19].

2.4.6 Tensile strength of hybrid composites

According to many published studies the hybrid effect for tensile strength of UD hybrid composites is based on a bilinear rule of mixtures dependent on the volume fraction of low strain fibre in the total fibres [36], [39], [40], [56]. The relative volume fraction of the LS and HS fibre types will determine whether the failure of the LS or the HS bundles corresponds to the ultimate failure strength of the hybrid composite. If the tensile strain of the hybrid composite is less than the failure strain of the LS fibre then the LS and HS fibre carries the tensile stress and failed together. If the tensile strain of the composite exceeds the failure strain of the LS fibre, LS fibres fail first and stop carrying the tensile stress followed by the HS fibres and ultimate failure occurred. The stress carrying capacity of the HS material depends on the volume fraction of HS fibre in the composite. In this case, the strength of the hybrid composite is either the stress in the hybrid when LS fibres fail or the stress in the hybrid when HS fibres fail, depending on which one has a maximum value.

However, deviations from the theoretical tensile strength of hybrid composites have been observed in the experimental studies. Some researchers found a positive deviation [40], [49], [61] while researchers found negative deviation [48], [63]. This deviation can occur due to different reasons. Initial failure strain (LS fibre failure) actually increases in fibre hybrid composites compared to the composites with only LS fibres; this would lead to positive deviation. On the other hand, the strength of the HS fibres can be lower due to damage introduced when the LS fibres fail which would lead to negative deviation.

2.5 Techniques and mechanisms for creating ductility and pseudo-ductility

The techniques and mechanisms which have used to introduce ductility and pseudo ductility in the composites are stated below:

2.5.1 Ductility via thin-ply technology

In recent years, there has been an increasing interest in spread tow technology in automotive, aerospace, marine and wind turbine industries due to weight saving and

enhanced performance in mechanical properties. The spread tow UD tapes are ultra-lightweight thinner ply than the conventional carbon fibre tapes, where filaments are evenly spread with greater filament straightening. As a result, more materials are packed in the same area which gives superior mechanical properties. The images of spread tow carbon tape and regular tow carbon tape are shown in Figure 2. 7. The spread tow reinforcement idea was first introduced in 2004 since then the uses of this reinforcement have speedily increased. Continuous fibres reinforcements to manufacture composite is available in different forms such as UD tapes, non-crimp fabrics (NCF) and woven fabrics [64]. UD tapes consist of highly orientated fibre and are available in a wide range of areal weights. The advantages of the spread UD tape and NCF are very thin, lightweight and an almost even surface and small weaving angle. They have a superior resin impregnation property and less delamination. In the laminates made of carbon fibre spread tow UD tape and woven fabric, resin and carbon fibres are dispersed uniformly leading to an increased in the mechanical properties. Spread tow reinforced composites have higher strength and strain to failure compared to those from standard prepregs because they delayed the starting of matrix cracking and delamination [65]–[69].

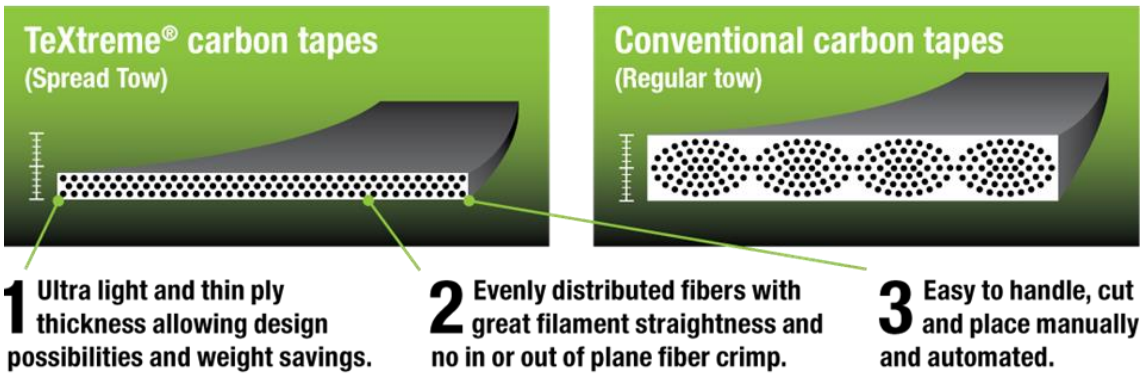

Figure 2. 7: Comparison between spread tow tape and conventional carbon fibre tapes [64]

Recently, researchers have shown an increased interest in thin ply hybrid composite to improve the ductility or pseudo ductility [9], [15]–[17], [23], [24], [26], [45], [70], [71]. Thin-ply interlayer hybrid composites represent a promising approach to achieve a favourable ductile behaviour in the composites. The failure mechanism of fragmentation

in a thin ply carbon/glass hybrid composites has been studied by Czel *et al.* [17] and reported that the central carbon layer thickness plays a significant role for carbon layer fragmentation and diffuse delamination. A hybrid composite with a thin high strength carbon layer (29 to 58 μm) between the E-glass layers showed a favourable pseudo-ductile behaviour without significant stress drop. On the other hand, hybrid composite with a thick carbon layer between the glass layers showed conventional hybrid failure behaviour with a significant drop in stress after carbon layer fail. However, with this hybrid architecture, they did not get any increase of the stress value after pseudo-yielding. They also have done another study [23] where S-glass used as a high strain material and a variety of thin ply carbon prepregs were used as a low strain material. Favourable pseudo-ductile behaviour has been observed with a smooth transition of the load after low strain material failure. Another study of interlayer thin-ply hybrid composites has been done with different grades of carbon fibres [70]. The high modulus thin-ply carbon fibre sandwiched with high tenacity thick-ply carbon fibre. A metal like stress-strain responses observed during the tensile loading. The central high modulus carbon plies fragmented and delaminated stably from central to the outer high strength carbon layers under uniaxial tensile loading. The stress-strain response of the M55/T1000 thin-ply hybrid configuration is shown in Figure 2.8. To clarify this phenomenon an FEA damage mode in tensile loading was proposed by Jalalvand *et al.* [24] for the thin-ply carbon/glass UD hybrid laminate. The damage mode maps as a function of the absolute and relative thickness of carbon layers are shown in Figure 2.5. The damage mode maps clearly stated how the maximum stiffness and desire diffuse delamination of the hybrid composite can be achieved by controlling the amount and thickness of the carbon fibres. There damage mode map is a very useful tool for designing the hybrid configuration for suitable ductile composite materials.

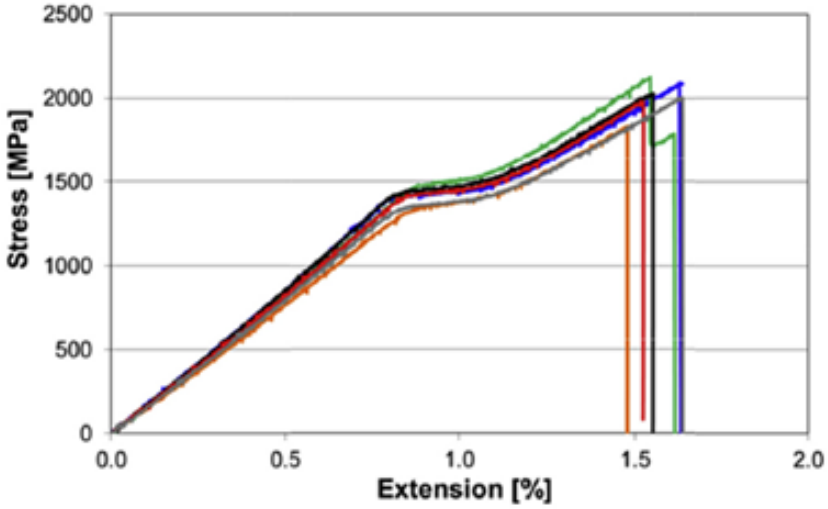

Figure 2.8: Tensile response of the M55/T1000 thin-ply hybrid composite [70].

The loading-unloading-reloading response of thin-ply and angle-ply laminate has been studied by Wisnom *et al*. [72]. Their study shows that a reduction of initial modulus happened in the composites due to the damage during the loading-unloading-reloading test. So these results indicate that these laminates are pseudo-ductile rather than truly ductile. Recently, Fotouhi *et al.* [12], who studied carbon/glass quasi-isotropic (QI) thin-ply hybrid composites, reported that the QI hybrid laminate showed the expected pseudo-ductility during tensile loading that avoids catastrophic failure. The problem of these reinforced composites is that it is difficult to make complex geometries from UD tape because the UD sheet tends to split, wrinkle and fold, creating uneven fibre distribution in the composite. The manufacturing cost also is very high.

2.5.2 Ductility via aligned discontinuous fibres

Discontinuous fibre reinforced composites have some advantages over continuous fibre reinforced composites as it is easy to produce a complex structure with discontinuous fibres due to their superior formability [73]. A number of studies have been done on highly aligned discontinuous fibre reinforced composites and it has been reported that ductility can be introduced in high-performance composites using aligned discontinuous fibres [14], [74]–[77]. Researchers have been used the High-Performance Discontinuous Fibre (HiPerDiF) technology to produce highly aligned discontinuous fibre architecture [76]. HiPerDiF method is suitable for producing highly aligned short fibre reinforcement as tow and tape form. Bristol University achieved 65% of the fibres to be

within ±3 of the main axis which allowed them to achieve up to 55% fibre volume fraction in the composites [35], [43], [78]. The effect of relative carbon volume ratios on pseudo-ductility in intermingled carbon/glass hybrid composites with highly aligned discontinuous fibres under loading condition reported by Yu *et al*.[7]. Two different short fibre hybrid composites, high strength carbon/E-glass and high modulus carbon/E-glass, have been studied. The study demonstrated that high strength carbon/E-glass aligned short fibre hybrid composite did not exhibit pseudo-ductility but high modulus carbon/E-glass aligned short fibre hybrid composite shows the pseudo-ductility. The study also shows that 0.25 relative high modulus carbon volume ratio with E-glass fibre composite yield the maximum pseudo-ductile strain. However, in comparing with continuous filament UD composite the discontinuous fibre reinforced composite exhibited low longitudinal tensile strength [79]. This low strength of the composite limited their uses in a load-bearing application.

2.5.3 Ductility via fibre reorientation

The orientational sequence of the reinforced material in the composite influence the mechanical properties of the composites. Another technique of creating additional strain and pseudo-ductility is to use an angle-ply laminate where the piles are oriented at an angle to the loading direction which allowed the fibres to rotate under tensile loading [29], [80]–[84]. Ogihara and Nakatani [81] studied the effect of ply thickness on carbon/epoxy angle-ply laminates. Specimen of ±45º angle-ply laminates with a ply thickness of 0.05 mm [(±Q)12]s (48-ply) exhibited higher tensile stress and strain compared to 0.15 mm $[(+Q)4/(-Q)4]_s$ (16-ply) thickness angle-ply laminates. A recent study has shown that thin CFRP angle-ply laminates containing symmetric pairs of ±26º piles with 0° layer on the midplane have shown good pseudo-ductile performance with a strain of 2.22% under quasi-statically loaded tension [6]. Analytical modelling of thin ply angle-ply composites have been studied by Fuller and Wisnom [8] and shown that higher failure strains have been achieved with angle-ply than those of UD hybrid composites. The study has shown that a specific fibre angle (±26 and ±27) exhibited maximum stress and strain value with a promising pseudo-ductile strain. These types of laminates have demonstrated the higher failure strain but sometimes free-edge delamination happened and premature failure occurred. The alternative approach of introducing the ductility in the composite is fibre waviness to provide excess length which permits additional extension during tensile loading due to fibre re-orientation

[20], [29], [85]–[89]. Pimenta and Robinson [29] studied the sandwich structure symmetrical-wavy composite with carbon-epoxy skin and a crushable foam core. They found that the wavy-ply sandwich structure laminate provides large deformations about 8.6% and high energy absorption during the tensile loading. Unidirectional wavy carbon fibre reinforced polyamide-12 (PA-12) composites was studied by Diao *et al*. [20]. The fibre waviness in the UD carbon fibre reinforced polyamide-12 introduced by gas-texturing and non-constrained annealing methods. Wavy carbon fibre reinforced PA-12 composites, instead of catastrophic failure, displayed gradual failure during tensile loading. Gas-textured carbon fibre/PA-12 composites did not exhibit any additional strain but the tensile strength of the composites have been reduced compared to the control composite due to fibre damage happened during the gas-texturing process. Though non-constrained annealed carbon fibre/PA-12 shown higher ultimate failure strain compared to the control composites, a significant stress drop observed. Figure 2.9 shows the schematic illustration of how the wavy fibres provide the deformation over a range of angles.

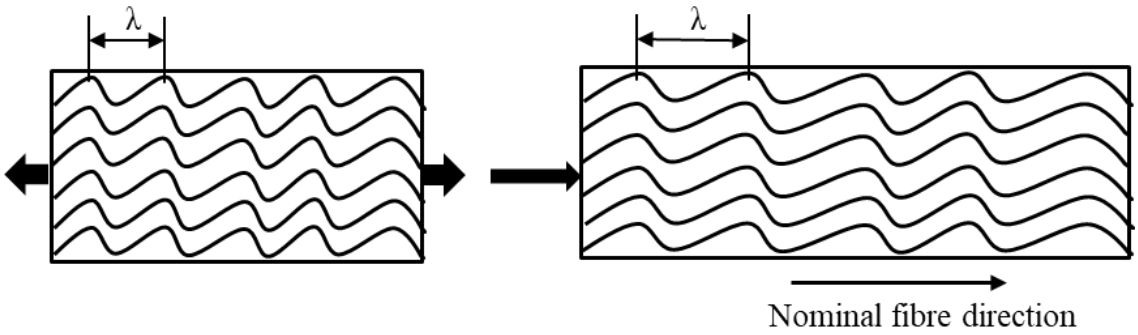

Figure 2.9: Schematic of non-straight or wavy fibres to provide deformation under loading over a range of angles.

2.5.4 Ductility via braided architecture

Braiding is a branch of textile that involves inter-twining of three of more stands of material. The braid structure can be two-dimensional (2D) or three-dimensional (3D). The 2D braided structure can be either biaxial or triaxial. In the biaxial braid, two sets of yarn intertwine in the opposite direction, where one set of yarns in one direction is passing under and over the other. The triaxial braid contains an additional set of

longitudinal yarns to the biaxial intertwining yarn which plays a significant role in the overall performance of the braid. Braided composites have been using in a wide range of applications such as automotive, medical and aerospace industries [90]. Braided composites often show higher energy absorption properties due to its multiple fibre breakage generated during the loading process [91], [92]. The energy absorption of the braided composites can be controlled by altering the off-axis braiding angles. A large braiding angle contributes to higher strain to failure and energy absorption of the composite but decreases the stiffness and yield strength [91], [93]. Researchers have been used braided preforms to create ductility in the composites [30]–[32], [94]–[96]. Nanni *et al.*[96] found the bilinear stress-strain response in a braided composite which has been fabricated from epoxy-impregnated aramid fibre skin with a steel core. A study by Harry *et al*. [94] has shown that a Kevlar-carbon hybrid fibre reinforced polymer rebars fabricated using a braining-pultrusion process exhibit bilinear ductile stress-strain behaviour similar to that of conventional steel rebars. Rosso et al. [31] investigated the mechanical properties of dry microbraids and microbraid reinforced polymer composites (mBRPC). The mBRPC showed progressive failure during tensile testing. Flexural and torsional behaviour of biaxial and triaxial braided composite studied by Potluri *et al*. and higher torsional stiffness observed with ±65° braid angle. Gautam *et al*. [32] studied the stress-strain behaviour of carbon-epoxy biaxial and triaxial braided composites under tensile loading for different braid angles. Tubular braided perform flattened before resin infusion and fabricated the composites. Biaxial braided specimens with ±35°, ±45° and ±55° braiding angles exhibit pseudo-ductile behaviour under uniaxial tensile loading and pseudo-ductility were increased with braid angle. It was also observed that the initial modulus and yield strength reduced sharply with increasing braid angle. Subsequently, triaxial braid with a limited amount of axial insertion can improve the modulus and tensile strength of the composites while retaining the significant pseudo-ductility. The problem of this kind of composites is their low stress and modulus compared to unidirectional composites and after the initial failure, there are no extended stress values.

2.5.5 Ductility via wrapping process

2.5.5.1 Wrapped yarn

Typically a wrapped yarn is composed of a straight core of short fibre bundle, filaments or tow which is wrapped with covering filaments, yarns or tows. The wrapping of the core can be done by in different ways such as single wrapping, double wrapping and X-wrapping. Wrapping can be done in either a clockwise direction (S-wrap) or anticlockwise direction (Z-wrap). Wrapping can also be applied in both directions (S and Z) in the same yarn and produced an X-wrap or double wrap yarn [97], [98]. The wrapping filaments or tow can be matrix-forming filament for thermoplastic composites or they can be any other filament or tow which remains in the final composite in their unique form. The wrapped yarn has specific features that are different from those of traditional spun yarns. Louis and Salaun [97] studied the filament wrapped short fibre yarn with different wrapping directions and found that the double wrapped yarn had higher strength and elongation than the single wrap yarn. On the other hand, the wrapping angle and density play a significant role in the tensile properties of the wrapped yarn. Behery *et al*. [99] investigated the properties of the wrapped yarns which have been spun from polyester staple fibre wrapped with different continuous filament yarn. The study showed that the wrapped yarn with a higher wrapping density and higher linear density of the wrapping continuous filament yarn had higher strength. The effect of twist and filament fineness on tensile behaviour of high-performance multifilament yarn has been studied by researchers [100], [101]. The experimental results revealed that the yarn strength increased up to a certain range of twist and a significant yarn performance was achieved for twist levels up to 20 turns /m [100]. The effect of the degree of a twist on the yarn mechanical properties, such as the yarn strength and strain to break published by Rao and Farris [101] shown in Figure 2.10. Their study suggested that there is an optimal twist angle of around 7° at which the filament yarn has shown maximum tensile strength but the strain to failure of the twisted filament yarn increased with the increase of twist angle. Mirdehghan *et al.* [102] investigated the structural and tensile properties of glass/polyester co-wrapped and side by side hybrid yarn. The study showed that co-wrapped hybrid yarn has a higher breaking load compared to the side by side hybrid and single glass yarns. Therefore, it is very important to select the proper process parameters to manufacture the ideal wrapped yarn for the respective application.

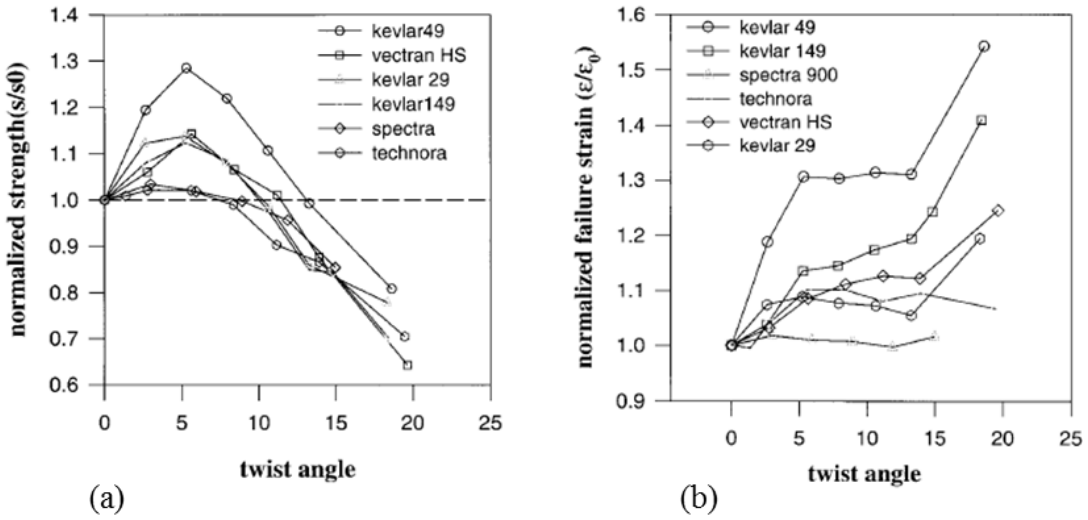

Figure 2.10: Properties of high-performance continuous fibre yarn with different twist angles (a) normalised strength and (b) normalised failure strain [101]

2.5.5.2 Wrapped Yarn Composites

There are a few studies [103] that have been done for wrapped yarn thermoplastic composites but so far there is no research that has been found on micro-wrapped hybrid tow high-performance thermoset composites. Merter *et al*. [98] studied the effect of wrapping direction on glass and polypropylene hybrid thermoplastic composites where polypropylene and glass fibre are used as a matrix and reinforcement constituent respectively. The co-wrapped hybrid yarns produced by twisting of polypropylene fibre around the glass fibre by single wrap (S shape) and double wrap (S and Z shapes) techniques. The study showed that mechanical properties of the single wrapped hybrid yarn were better than double wrapped hybrid yarn composite. The problem of these kinds of composites is the inhomogeneous distribution of the reinforcement and matrix fibre may cause inhomogeneity of the reinforced and matrix material in the composites. On the other hand, researchers have been using the core-shell technique to improve the flexural and ductile properties of the composites. Abbott and Freischmidt [104], [105] have been investigated the flexural properties of the composites manufactured from helically wrapped yarns. The yarn made by wrapping high strength paper tape around the glass fibre and other types of continuous filament. They reported that the wrapped

yarn composites bent in a ductile manner with a specific bending stiffness similar to those of steel and aluminium.

Liang *et al*. [106] investigated pseudo-ductility of carbon/glass pultruded hybrid rods in two different hybrid form, randomly distribution and core-shell design. Randomly dispersed rods break at the failure strain of carbon fibre. Some degree of pseudo-ductility was claimed with the core-shell approach, but the stress-strain diagram showed a big stress drop during the transitional phase. The study used lower strain (higher modulus) material as the sheath and higher strain (lower modulus) material as the core. This core-shell approach showed interesting results, some degree of ductility was observed in the core-shell configuration in comparison to randomly dispersed structure. However, their observation has indicated that there is an opportunity to achieve pseudo-ductility through core-shell approach with proper design and fraction of LS and HS material.

2.5.6 Ductility via other mechanisms

Carbon nanotube [107] and regenerated cellulose [108] are some of the promising ductile fibres that could be used for making ductile composites. Carbon nanotube fibre has shown high strain to failure which can create the ductility in the composites [107]. However, endorsement and commercialisation of this material for a macroscale structural application is a challenging and lengthy process. Some studies reported that the addition of graphene in the matrix could increase the toughness of the matrix and improve the interfacial properties of the graphene-based composites [109]–[113]. The studies suggested that graphene and GO could prevent the delamination of the fibres and can delay the crack propagation at the interphase by redistributing the stress around fibres, where the cracks started to generate. A summary of the different techniques are presented in Table 2. 2

Table 2. 2: Summary of the different techniques and mechanism for creating ductility or pseudo-ductility

Techniques and mechanism	Findings	Comments
Incorporating ductile fibre	Excellent ductility	Higher density compared to carbon fibre composites.
Thin ply hybrid spread tow	Excellent ductility or pseudo-ductility	Higher manufacturing cost and poor drapability.
Aligned discontinuous short fibres hybrid	Good ductility or pseudo-ductility	Low longitudinal tensile strength compared to continuous filament UD composite.
Thin-ply angle-ply	Excellent ductility or pseudo-ductility	Sometimes free-edge delamination happened and premature failure occurred.
Braided architecture	Excellent ductility	Low stress and modulus compared to unidirectional composites.
Carbon nano-fibre	Higher strain to failure	Commercialisation is challenging work.

2.6 Matrix selection for high-performance composites

In high-performance composites, the reinforced material is the main constituent which contributes the main properties of the composite. However, the resin system also plays a significant role in the mechanical properties of the composites [114]–[117]. The fracture behaviour of the composites depends on the strength of the fibre-matrix interface. A strong interface provides high strength and stiffness but low resistance to fracture which caused a brittle failure. Alternatively, the weak interface offers low strength and stiffness but high resistance to fracture [118]. In the manufacturing of high-performance composites, thermoset epoxy resins are the best matrix material. Epoxy resin is a low viscosity reactive liquid which has good wettability. Composites manufactured with epoxy matrix provides exceptional mechanical properties and a wide range of environmental stability. The epoxy matrix is most prevalent to the manufacture of

thermoset composite for aircraft application [114], [119]. However, cured epoxies have poor resistance to crack initiation and growth due to their lack of plastic deformation and they are not as damage tolerance as a thermoplastic matrix. Nowadays, there are different types of epoxy resin available in the market such as room temperature curing and high temperature curing epoxy resin. As the resin systems have a significant effect on the mechanical properties of the composites. It is, therefore, necessary to select the best epoxy resin system which will give the best mechanical properties of the composites for a particular application. As mentioned above, thermoset resins provide excellent mechanical properties in composites; in this research, room temperature and high temperature curing epoxy resin have been used to manufacture the composites.

2.7 Summary

The objective of this research is to design new dry fibre architectures to prepare low-cost preform for ductile or pseudo-ductile composites. To achieve the objective, the problems of conventional composites, the importance of ductility, effect of fibre hybridisation, the effect of fibre architectures, mechanism of creating ductility and pseudo-ductility in the high-performance composites were comprehensively reviewed. The literature clearly indicates that the fundamental limitation of current composites is their inherent brittleness which limits their application for high volume structural applications. However, different techniques and mechanisms have been used for creating inherent ductility in the composites. Among them, fibre hybridisation is a promising method to create inherent ductility in the composites. However, hybridisation of different strain to failure filament at tow scale is a challenging topic in the composite world. On the other hand, the thin-ply laminate show potential advantages such as less resin-rich areas, smaller crimp angle in woven, higher strength, higher delamination resistance and suppression of micro-cracking before failure. Thin-ply hybrid composites also demonstrated good pseudo-ductility with high stiffness where the relative volume fraction and thickness of the low strain material is an important parameter. The limitation of this kind of composites is the higher manufacturing cost (to produce thicker panels) and poor drapability. However, the interesting finding of these studies is that the outer high strain material layers should be thick and strong enough to take the load after low strain material failure. The previous study suggested that the core-shell

approach displayed exciting results on ductility on pultruded hybrid rods therefore, core-shell dry fibre hybrid architecture can be performed for making reinforcement material for high-performance composites. On the other hand, studies on high-performance filament yarn have been shown that the maximum mechanical properties at an optimal twist angle of around 7° have been achieved. Other study suggested that co-wrapped hybrid yarn has a higher breaking load and elongation compared to the side by side hybrid yarns. Hence, it is also an important factor for considering the preparation of reinforcement materials for ductile composites.

Therefore, considering the different research outcomes, the author aims to develop novel processes for dry fibre architectures and prepared low cost reinforced materials for high-performance composites which demonstrates a significant plastic deformation (ductility) under loading condition and overcomes the sudden and catastrophic failure. Two different approaches have been considered. One is spreading and commingling of low strain and high strain filament tow and prepared intro-tow hybrid reinforcement material for UD composites. To take the advantages from wrap yarn, thin ply angle-ply laminate and core-shell hybrid technology, the author considered another approach of micro-wrapped dry fibre architecture to make hybrid tow for ductile composites. Details of these two approaches will be studied extensively in this thesis.

References

[1] F. Campbell, *Structural Composite Materials. ASM International.* ASM International, 2010.

[2] I. M. Daniel and O. Ishai, *Engineering Mechanics of Composite Materials Isaac M. Daniel, Ori Ishai*. 1994.

[3] H. E. Davis, G. E. Troxell, and G. F. W. Hauck, *The testing of engineering materials*. McGraw-Hill, 1982.

[4] F. Lamouroux, M. Steen, and J. L. Vallés, “Uniaxial tensile and creep behaviour of an alumina fibre-reinforced ceramic matrix composite: I. Experimental study,” *J. Eur. Ceram. Soc.*, vol. 14, no. 6, pp. 529–537, Jan. 1994.

[5] D. Sherman, J. Lemaitre, and F. A. Leckie, “The mechanical behavior of an alumina carbon/epoxy laminate,” *Acta Metall. Mater.*, vol. 43, no. 12, pp. 4483–

4493, Dec. 1995.

[6] J. D. Fuller, M. Jalalvand, and M. R. R. Wisnom, “Pseudo-ductility by fragmentation of central unidirectional plies in thin CFRP angle-ply laminates,” *ECCM-16th Eur. Conf. Compos. Mater.*, no. June, pp. 22–26, 2014.

[7] H. Yu, M. L. Longana, M. Jalalvand, M. R. Wisnom, and K. D. Potter, “Pseudo-ductility in intermingled carbon/glass hybrid composites with highly aligned discontinuous fibres,” *Compos. Part A Appl. Sci. Manuf.*, vol. 73, pp. 35–44, Jun. 2015.

[8] J. D. Fuller and M. R. Wisnom, “Pseudo-ductility and damage suppression in thin ply CFRP angle-ply laminates,” *Compos. Part A Appl. Sci. Manuf.*, vol. 69, pp. 64–71, Feb. 2015.

[9] M. Jalalvand, G. Czél, and M. R. Wisnom, “Damage analysis of pseudo-ductile thin-ply UD hybrid composites – A new analytical method,” *Compos. Part A Appl. Sci. Manuf.*, vol. 69, pp. 83–93, Feb. 2015.

[10] R. Malkin, M. Yasaee, R. S. Trask, and I. P. Bond, “Bio-inspired laminate design exhibiting pseudo-ductile (graceful) failure during flexural loading,” *Compos. Part A Appl. Sci. Manuf.*, vol. 54, pp. 107–116, Nov. 2013.

[11] Y. Yuan, S. Wang, H. Yang, X. Yao, and B. Liu, “Analysis of pseudo-ductility in thin-ply carbon fiber angle-ply laminates,” *Compos. Struct.*, vol. 180, pp. 876–882, Nov. 2017.

[12] M. Fotouhi, M. Jalalvand, and M. R. Wisnom, “High performance quasi-isotropic thin-ply carbon/glass hybrid composites with pseudo-ductile behaviour in all fibre orientations,” *Compos. Sci. Technol.*, vol. 152, pp. 101–110, Nov. 2017.

[13] W. M. Diao H, Bismarck A, Robinson P, “Pseudo-ductile behaviour of unidirectional fibre reinforced polyamide-12 composite by intra-tow hybridization,” in *Proceedings of ECCM 15 Conference*, 2012, no. June, pp. 24–28.

[14] J. M. Finley, H. Yu, M. L. Longana, S. Pimenta, M. S. P. Shaffer, and K. D. Potter, “Exploring the pseudo-ductility of aligned hybrid discontinuous

composites using controlled fibre-type arrangements," *Compos. Part A Appl. Sci. Manuf.*, vol. 107, pp. 592–606, Apr. 2018.

[15] M. R. Wisnom, G. Czél, J. D. Fuller, and M. Jalalvand, "High performance pseudo-ductile composites," *20th Int. Conf. Compos. Mater. Copenhagen,* no. July, pp. 3–7, 2015.

[16] M. Jalalvand, G. Czél, and M. R. Wisnom, "Parametric study of failure mechanisms and optimal configurations of pseudo-ductile thin-ply UD hybrid composites," *Compos. Part A Appl. Sci. Manuf.,* vol. 74, pp. 123–131, Jul. 2015.

[17] G. Czél and M. R. Wisnom, "Demonstration of pseudo-ductility in high performance glass/epoxy composites by hybridisation with thin-ply carbon prepreg," *Compos. Part A Appl. Sci. Manuf.,* vol. 52, pp. 23–30, Sep. 2013.

[18] T. Hayashi, "On the improvement of mechanical properties of composites by hybrid composition," in *8th International Reinforced Plastics Conference, Brighton, UK*, 1972, pp. 149–152.

[19] A. R. Bunsell and B. Harris, "Hybrid carbon and glass fibre composites," *Composites*, vol. 5, no. 4, pp. 157–164, Jul. 1974.

[20] H. Diao, P. Robinson, M. R. Wisnom, and A. Bismarck, "Unidirectional carbon fibre reinforced polyamide-12 composites with enhanced strain to tensile failure by introducing fibre waviness," *Compos. Part A Appl. Sci. Manuf.,* vol. 87, pp. 186–193, Aug. 2016.

[21] E. Selver, P. Potluri, C. Soutis, and P. Hogg, "Healing potential of hybrid materials for structural composites," *Compos. Struct.,* vol. 122, pp. 57–66, Apr. 2015.

[22] Y. Swolfs, Y. Meerten, P. Hine, I. Ward, I. Verpoest, and L. Gorbatikh, "Introducing ductility in hybrid carbon fibre/self-reinforced composites through control of the damage mechanisms," *Compos. Struct.,* vol. 131, pp. 259–265, 2015.

[23] G. Czél, M. Jalalvand, and M. R. Wisnom, "Design and characterisation of advanced pseudo-ductile unidirectional thin-ply carbon/epoxy– glass/epoxy

hybrid composites," *Compos. Struct.*, vol. 143, pp. 362–370, Feb. 2016.

[24] M. Jalalvand, G. Czél, and M. R. Wisnom, "Numerical modelling of the damage modes in UD thin carbon/glass hybrid laminates," *Compos. Sci. Technol.*, vol. 94, pp. 39–47, 2014.

[25] G. Czél *et al.*, "Pseudo-ductility and reduced notch sensitivity in multi-directional all-carbon/epoxy thin-ply hybrid composites," *Compos. Part A Appl. Sci. Manuf.*, vol. 104, pp. 151–164, Jan. 2018.

[26] M. Fotouhi, P. Suwarta, M. Jalalvand, G. Czel, and M. R. Wisnom, "Detection of fibre fracture and ply fragmentation in thin-ply UD carbon/glass hybrid laminates using acoustic emission," *Compos. Part A Appl. Sci. Manuf.*, vol. 86, pp. 66–76, Apr. 2016.

[27] M. Jalalvand, G. Czél, M. W.-C. S. and Technology, and undefined 2014, "Numerical modelling of the damage modes in UD thin carbon/glass hybrid laminates," *Elsevier*.

[28] J. D. Fuller, M. Jalalvand, and M. R. Wisnom, "Combining fibre rotation and fragmentation to achieve pseudo-ductile CFRP laminates," *Compos. Struct.*, vol. 142, pp. 155–166, May 2016.

[29] S. Pimenta and P. Robinson, "Wavy-ply sandwich with composite skins and crushable core for ductility and energy absorption," *Compos. Struct.*, vol. 116, pp. 364–376, Sep. 2014.

[30] R. Tepfers, V. Tamužs, R. Apinis, U. Vilks, and J. Modniks, "Ductility of nonmetallic hybrid fiber composite reinforcement for concrete," *Mech. Compos. Mater.*, vol. 32, no. 2, pp. 113–121, Mar. 1996.

[31] S. Del Rosso, L. Iannucci, and P. T. Curtis, "Experimental investigation of the mechanical properties of dry microbraids and microbraid reinforced polymer composites," *Compos. Struct.*, vol. 125, pp. 509–519, Jul. 2015.

[32] M. Gautam, P. Potluri, and S. Ogin, "Necking behaviour of flattened tubular braided composites (PDF Download Available)," in *20th International Conference on Composite Materials Copenhagen, 19-24th July 2015*.

[33] K. Allaer, I. De Baere, P. Lava, W. Van Paepegem, and J. Degrieck, “On the in-plane mechanical properties of stainless steel fibre reinforced ductile composites,” *Compos. Sci. Technol.*, vol. 100, pp. 34–43, Aug. 2014.

[34] M. G. Callens, L. Gorbatikh, and I. Verpoest, “Ductile steel fibre composites with brittle and ductile matrices,” *Compos. Part A Appl. Sci. Manuf.*, vol. 61, pp. 235–244, Jun. 2014.

[35] M. L. Longana, H. Yu, M. Jalavand, M. R. Wisnom, and K. D. Potter, “Aligned discontinuous intermingled reclaimed/virgin carbon fibre composites for high performance and pseudo-ductile behaviour in interlaminated carbon-glass hybrids,” *Compos. Sci. Technol.*, vol. 143, pp. 13–21, May 2017.

[36] Yentl Swolfs, Larissa Gorbatikh, and Ignaas Verpoest, “Fibre hybridisation in polymer composites: A review,” *Compos. Part A Appl. Sci. Manuf.*, vol. 67, pp. 181–200, 2014.

[37] D. F. ADAMS, “High-performance composite material airframe weight and cost estimating relations,” *J. Aircr.*, vol. 11, no. 12, pp. 751–757, Dec. 1974.

[38] C. Zweben, “Tensile strength of hybrid composites,” *J. Mater. Sci.*, vol. 12, no. 7, pp. 1325–1337, Jul. 1977.

[39] Y. Swolfs, I. Verpoest, and L. Gorbatikh, “Recent advances in fibre-hybrid composites: materials selection, opportunities and applications,” *Int. Mater. Rev.*, pp. 1–35, Apr. 2018.

[40] P. W. Manders and M. G. Bader, “The strength of hybrid glass/carbon fibre composites,” *J. Mater. Sci.*, vol. 16, no. 8, pp. 2233–2245, Aug. 1981.

[41] J. Aveston and J. M. Sillwood, “Synergistic fibre strengthening in hybrid composites,” *J. Mater. Sci.*, vol. 11, no. 10, pp. 1877–1883, Oct. 1976.

[42] P. D. Bradley and S. J. Harris, “Strategic reinforcement of hybrid carbon fibre-reinforced polymer composites,” *J. Mater. Sci.*, vol. 12, no. 12, pp. 2401–2410, Dec. 1977.

[43] H. Yu, M. L. Longana, M. Jalalvand, M. R. Wisnom, and K. D. Potter, “Pseudo-ductility in intermingled carbon/glass hybrid composites with highly aligned

discontinuous fibres," *Compos. Part A Appl. Sci. Manuf.*, vol. 73, pp. 35–44, 2015.

[44] I. Taketa, J. Ustarroz, L. Gorbatikh, S. V. Lomov, and I. Verpoest, "Interply hybrid composites with carbon fiber reinforced polypropylene and self-reinforced polypropylene," *Compos. Part A Appl. Sci. Manuf.*, vol. 41, no. 8, pp. 927–932, Aug. 2010.

[45] M. R. Wisnom, G. Czél, Y. Swolfs, M. Jalalvand, L. Gorbatikh, and I. Verpoest, "Hybrid effects in thin ply carbon/glass unidirectional laminates: accurate experimental determination and prediction," *Compos. Part A Appl. Sci. Manuf.*, vol. 88, pp. 131–139, Apr. 2016.

[46] C. Dong, J. Duong, and I. J. Davies, "Flexural properties of S-2 glass and TR30S carbon fiber-reinforced epoxy hybrid composites," *Polym. Compos.*, vol. 33, no. 5, pp. 773–781, May 2012.

[47] A. A. J. M. Peijs and J. M. M. de Kok, "Hybrid composites based on polyethylene and carbon fibres. Part 6: Tensile and fatigue behaviour," *Composites*, vol. 24, no. 1, pp. 19–32, Jan. 1993.

[48] P. Ren *et al.*, "Hybrid effect on mechanical properties of M40-T300 carbon fiber reinforced Bisphenol A Dicyanate ester composites," *Polym. Compos.*, vol. 31, no. 12, pp. 2129–2137, Dec. 2010.

[49] A. A. J. M. Peijs, P. Catsman, L. E. Govaert, and P. J. Lemstra, "Hybrid composites based on polyethylene and carbon fibres Part 2: influence of composition and adhesion level of polyethylene fibres on mechanical properties," *Composites*, vol. 21, no. 6, pp. 513–521, Nov. 1990.

[50] A. Pegoretti, E. Fabbri, C. Migliaresi, and F. Pilati, "Intraply and interply hybrid composites based on E-glass and poly(vinyl alcohol) woven fabrics: tensile and impact properties," *Polym. Int.*, vol. 53, no. 9, pp. 1290–1297, Sep. 2004.

[51] Y. Swolfs *et al.*, "Tensile behaviour of intralayer hybrid composites of carbon fibre and self-reinforced polypropylene," *Compos. Part A Appl. Sci. Manuf.*, vol. 59, pp. 78–84, Apr. 2014.

[52] R. Alagirusamy, V. Ogale, A. Vaidya, and P. M. V Subbarao, “Effect of jet design on commingling of glass/nylon filaments,” *J. Thermoplast. Compos. Mater.*, vol. 18, no. 3, pp. 255–268, 2005.

[53] M. Golzar, H. Brünig, and E. Mäder, “Commingled Hybrid Yarn Diameter Ratio in Continuous Fiber-reinforced Thermoplastic Composites,” *J. Thermoplast. Compos. Mater.*, vol. 20, no. 1, pp. 17–26, Jan. 2007.

[54] L. Ye, K. Friedrich, J. Kästel, and Y.-W. Mai, “Consolidation of unidirectional CF/PEEK composites from commingled yarn prepreg,” *Compos. Sci. Technol.*, vol. 54, no. 4, pp. 349–358, Jan. 1995.

[55] N. Svensson, R. Shishoo, and M. Gilchrist, “Manufacturing of Thermoplastic Composites from Commingled Yarns-A Review,” *J. Thermoplast. Compos. Mater.*, vol. 11, no. 1, pp. 22–56, Jan. 1998.

[56] J. Aveston and A. Kelly, “Tensile First Cracking Strain and Strength of Hybrid Composites and Laminates,” *Philos. Trans. R. Soc. A Math. Phys. Eng. Sci.*, vol. 294, no. 1411, pp. 519–534, Jan. 1980.

[57] G. Marom, S. Fischer, F. R. Tuler, and H. D. Wagner, “Hybrid effects in composites: conditions for positive or negative effects versus rule-of-mixtures behaviour,” *J. Mater. Sci.*, vol. 13, no. 7, pp. 1419–1426, Jul. 1978.

[58] Y. Swolfs, L. Gorbatikh, and I. Verpoest, “Fibre hybridisation in polymer composites: A review,” *Compos. Part A Appl. Sci. Manuf.*, vol. 67, pp. 181–200, Dec. 2014.

[59] G. Kretsis, “A review of the tensile, compressive, flexural and shear properties of hybrid fibre-reinforced plastics,” *Composites*, vol. 18, no. 1, pp. 13–23, Jan. 1987.

[60] K. S. Pandya, C. Veerraju, and N. K. Naik, “Hybrid composites made of carbon and glass woven fabrics under quasi-static loading,” *Mater. Des.*, vol. 32, no. 7, pp. 4094–4099, Aug. 2011.

[61] Y. J. You, Y. H. Park, H. Y. Kim, and J. S. Park, “Hybrid effect on tensile properties of FRP rods with various material compositions,” *Compos. Struct.*,

vol. 80, no. 1, pp. 117–122, 2007.

[62] H. Diao, A. Bismarck, P. Robinson, and M. R. Wisnom, “Production of continuous intermingled CF/GF hybrid composite via fibre tow spreading technology,” *Eccm16 - 16Th Eur. Conf. Compos. Mater.*, no. June 2014, p. 8, 2014.

[63] C. E. Bakis, A. Nanni, J. A. Terosky, and S. W. Koehler, “Self-monitoring, pseudo-ductile, hybrid FRP reinforcement rods for concrete applications,” *Compos. Sci. Technol.*, vol. 61, no. 6, pp. 815–823, May 2001.

[64] C. Borg, “An introduction to spread tow reinforcements: Part 1 – Manufacture and properties,” *Reinf. Plast.*, vol. 59, no. 4, pp. 194–198, Jul. 2015.

[65] S. T. S Sihn, RY Kim, K Kawabe, “Experimental studies of thin-ply laminated composites,” *Compos. Sci. Technol.*, vol. 67, no. 6, pp. 996–1008, May 2007.

[66] T. Yokozeki, T. Aoki, T. Ogasawara, and T. Ishikawa, “Effects of layup angle and ply thickness on matrix crack interaction in contiguous plies of composite laminates,” *Compos. Part A Appl. Sci. Manuf.*, vol. 36, no. 9, pp. 1229–1235, Sep. 2005.

[67] T. Yokozeki, Y. Aoki, and T. Ogasawara, “Experimental characterization of strength and damage resistance properties of thin-ply carbon fiber/toughened epoxy laminates,” *Compos. Struct.*, vol. 82, no. 3, pp. 382–389, Feb. 2008.

[68] A. Arteiro, G. Catalanotti, J. Xavier, and P. P. Camanho, “Large damage capability of non-crimp fabric thin-ply laminates,” *Compos. Part A Appl. Sci. Manuf.*, vol. 63, pp. 110–122, Aug. 2014.

[69] J. Cugnoni *et al.*, “Towards aerospace grade thin-ply composites: Effect of ply thickness, fibre, matrix and interlayer toughening on strength and damage tolerance,” *Compos. Sci. Technol.*, vol. 168, pp. 467–477, Nov. 2018.

[70] G. Czél, M. Jalalvand, M. R. Wisnom, and T. Czigány, “Design and characterisation of high performance, pseudo-ductile all-carbon/epoxy unidirectional hybrid composites,” *Compos. Part B Eng.*, vol. 111, pp. 348–356, Feb. 2017.

[71] G. Czél, S. Pimenta, M. R. Wisnom, and P. Robinson, “Demonstration of pseudo-ductility in unidirectional discontinuous carbon fibre/epoxy prepreg composites,” *Compos. Sci. Technol.*, vol. 106, pp. 110–119, Jan. 2015.

[72] M. R. Wisnom, J. Fuller, P. Suwarta, and G. Czel, “Repeated tensile loading of thin-ply pseudo-ductile laminates,” *ASC proceeding 2015*, pp. 2–9, 2015.

[73] M. SUCH, C. WARD, and K. POTTER, “Aligned Discontinuous Fibre Composites: A Short History,” *J. Multifunct. Compos.*, vol. 2, no. 3, 2014.

[74] M. Hashimoto, T. Okabe, T. Sasayama, H. Matsutani, and M. Nishikawa, “Prediction of tensile strength of discontinuous carbon fiber/polypropylene composite with fiber orientation distribution,” in *Composites Part A: Applied Science and Manufacturing*, 2012, vol. 43, no. 10, pp. 1791–1799.

[75] S. Pimenta and P. Robinson, “An analytical model for the mechanical response of discontinuous composites,” in *19th International Conference on Composite Materials*, 2013.

[76] H. Yu, K. D. Potter, and M. R. Wisnom, “A novel manufacturing method for aligned discontinuous fibre composites (High Performance-Discontinuous Fibre method),” *Compos. Part A Appl. Sci. Manuf.*, vol. 65, pp. 175–185, Oct. 2014.

[77] H. Yu, M. L. Longana, M. Jalalvand, M. R. Wisnom, and K. D. Potter, “Hierarchical pseudo-ductile hybrid composites combining continuous and highly aligned discontinuous fibres,” *Compos. Part A Appl. Sci. Manuf.*, vol. 105, pp. 40–56, Feb. 2018.

[78] H. Yu, K. D. Potter, and M. R. Wisnom, “A novel manufacturing method for aligned discontinuous fibre composites (High Performance-Discontinuous Fibre method),” *Compos. Part A Appl. Sci. Manuf.*, vol. 65, pp. 175–185, Oct. 2014.

[79] Y. Li and S. Pimenta, “Development and assessment of modelling strategies to predict failure in tow-based discontinuous composites,” *Compos. Struct.*, vol. 209, pp. 1005–1021, Feb. 2019.

[80] C. T. Herakovich, “Influence of Layer Thickness on the Strength of Angle-Ply Laminates,” *J. Compos. Mater.*, vol. 16, no. 3, pp. 216–227, May 1982.

[81] S. Ogihara and H. Nakatani, “Effect of ply thickness on mechanical properties in CFRP angle-ply laminates,” in *Proceedings of ECCM-15*, 2012, no. June, pp. 1–6.

[82] J. D. Fuller and M. R. Wisnom, “Exploration of the potential for pseudo-ductility in thin ply CFRP angle-ply laminates via an analytical method,” *Compos. Sci. Technol.*, vol. 112, pp. 8–15, May 2015.

[83] J. D. Fuller, M. Jalalvand, and M. R. Wisnom, “Combining fibre rotation and fragmentation to achieve pseudo-ductile CFRP laminates,” *Compos. Struct.*, vol. 142, pp. 155–166, 2016.

[84] J. D. Fuller and M. R. Wisnom, “Exploration of the potential for pseudo-ductility in thin ply CFRP angle-ply laminates via an analytical method,” *Compos. Sci. Technol.*, vol. 112, pp. 8–15, May 2015.

[85] J. Wang, K. D. Potter, M. R. Wisnom, and K. Hazra, “Failure mechanisms under compression loading in composites with designed out-of-plane fibre waviness,” *Plast. Rubber Compos.*, vol. 42, no. 6, pp. 231–238, 2013.

[86] H. J. Chun, J. Y. Shin, and I. M. Daniel, “Effects of material and geometric nonlinearities on the tensile and compressive behavior of composite materials with fiber waviness,” *Compos. Sci. Technol.*, vol. 61, no. 1, pp. 125–134, 2001.

[87] H. Khatam and M.-J. Pindera, “Microstructural scale effects in the nonlinear elastic response of bio-inspired wavy multilayers undergoing finite deformation,” *Compos. Part B Eng.*, vol. 43, no. 3, pp. 869–884, Apr. 2012.

[88] M. R. Piggott, “The effect of fibre waviness on the mechanical properties of unidirectional fibre composites: A review,” *Composites Science and Technology*, vol. 53, no. 2. pp. 201–205, 1995.

[89] C.-M. Kuo, K. Takahashi, and T.-W. Chou, “Effect of Fiber Waviness on the Nonlinear Elastic Behavior of Flexible Composites,” *J. Compos. Mater.*, vol. 22, no. 11, pp. 1004–1025, Nov. 1988.

[90] C. Ayranci and J. Carey, “2D braided composites: A review for stiffness critical applications,” *Compos. Struct.*, vol. 85, no. 1, pp. 43–58, Sep. 2008.

[91] M. Okano, K. Sugimoto, H. Saito, A. Nakai, and H. Hamada, “Effect of the braiding angle on the energy absorption properties of a hybrid braided FRP tube,” *Proc. Inst. Mech. Eng. Part L J. Mater. Des. Appl.*, vol. 219, no. 1, pp. 59–66, Jan. 2005.

[92] V. M. Karbhari, J. E. Haller, P. K. Falzon, and I. Herszberg, “Post-impact crush of hybrid braided composite tubes,” *Int. J. Impact Eng.*, vol. 22, no. 4, pp. 419–433, Apr. 1999.

[93] A.-M. Harte and N. A. Fleck, “On the mechanics of braided composites in tension,” 2000.

[94] H. G. Harris, W. Somboonsong, and F. K. Ko, “New Ductile Hybrid FRP Reinforcing Bar for Concrete Structures,” *J. Compos. Constr.*, vol. 2, no. 1, pp. 28–37, Feb. 1998.

[95] N. F. Grace, W. F. Ragheb, and G. Abdel-Sayed, “Strengthening of Cantilever and Continuous Beams Using New Triaxially Braided Ductile Fabric,” *ACI Struct. J.*, vol. 101, no. 2, pp. 237–244, Mar. 2004.

[96] A. Nanni, M. J. Henneke, and T. Okamoto, “Tensile properties of hybrid rods for concrete reinforcement,” *Constr. Build. Mater.*, vol. 8, no. 1, pp. 27–34, Jan. 1994.

[97] G. L. Louis and H. L. Salaun, “‘X’ Direction Filament-Wrapped Yarn,” *Text. Res. J.*, vol. 56, no. 3, pp. 161–163, Mar. 1986.

[98] N. E. Merter, G. Başer, and M. Tanoğlu, “Effects of hybrid yarn preparation technique and fiber sizing on the mechanical properties of continuous glass fiber-reinforced polypropylene composites,” *J. Compos. Mater.*, vol. 50, no. 12, pp. 1697–1706, May 2016.

[99] H. M. Behery and M. F. Nunes, “33—THE STRUCTURE, TENSILE PROPERTIES, AND MORPHOLOGY OF FAILURE OF WRAPPED YARNS,” *J. Text. Inst.*, vol. 77, no. 6, pp. 386–402, Nov. 1986.

[100] R. Chudoba, M. Vo0echovský, V. Eckers, and T. Gries, “Effect of Twist, Fineness, Loading Rate and Length on Tensile Behavior of Multifilament Yarns

(A Multivariate Study)," *Text. Res. J. Artic. Text. Res. J.*, vol. 77, no. 11, pp. 880–891, 2007.

[101] Y. Rao and R. J. Farris, "A modeling and experimental study of the influence of twist on the mechanical properties of high-performance fiber yarns," *J. Appl. Polym. Sci.*, vol. 77, no. 9, pp. 1938–1949, Aug. 2000.

[102] A. Mirdehghan, H. Nosraty, M. M. Shokrieh, and M. Akhbari, "The structural and tensile properties of glass/polyester co-wrapped hybrid yarns," *J. Ind. Text.*, vol. 47, no. 8, pp. 1979–1997, May 2018.

[103] B. Baghaei, M. Skrifvars, and L. Berglin, "Manufacture and characterisation of thermoplastic composites made from PLA/hemp co-wrapped hybrid yarn prepregs," *Compos. Part A Appl. Sci. Manuf.*, vol. 50, pp. 93–101, Jul. 2013.

[104] G. M. Abbott, "Wrapped-yarn reinforced composites: Part I-yarn properties," *Compos. Sci. Technol.*, vol. 24, no. 2, pp. 147–158, Jan. 1985.

[105] G. M. Abbott and G. Freischmidt, "Wrapped-yarn reinforced composites: Part II—composite properties," *Compos. Sci. Technol.*, vol. 24, no. 4, pp. 299–312, Jan. 1985.

[106] Y. Liang, C. Sun, and F. Ansari, "Acoustic Emission Characterization of Damage in Hybrid Fiber-Reinforced Polymer Rods," *J. Compos. Constr.*, vol. 8, no. 1, pp. 70–78, Feb. 2004.

[107] S. Boncel, R. Sundaram, and A. Windle, "Enhancement of the Mechanical Properties of Directly Spun CNT Fibres by Chemical Treatment," *ACS Nano*, vol. 5, no. 12, pp. 9339–9344, 2011.

[108] S.-R. Shamsuddin, K.-Y. Lee, and A. Bismarck, "Ductile unidirectional continuous rayon fibre-reinforced hierarchical composites," *Compos. Part A Appl. Sci. Manuf.*, vol. 90, pp. 633–641, Nov. 2016.

[109] T. Kuilla, S. Bhadra, D. Yao, N. H. Kim, S. Bose, and J. H. Lee, "Recent advances in graphene based polymer composites," *Progress in Polymer Science (Oxford)*, vol. 35, no. 11. Elsevier Ltd, pp. 1350–1375, 2010.

[110] Y. J. Wan *et al.*, "Grafting of epoxy chains onto graphene oxide for epoxy

composites with improved mechanical and thermal properties," *Carbon N. Y.*, vol. 69, pp. 467–480, Apr. 2014.

[111] L. C. Tang *et al.*, "The effect of graphene dispersion on the mechanical properties of graphene/epoxy composites," *Carbon N. Y.*, vol. 60, pp. 16–27, Aug. 2013.

[112] M. A. Rafiee, J. Rafiee, Z. Wang, H. Song, Z. Z. Yu, and N. Koratkar, "Enhanced mechanical properties of nanocomposites at low graphene content," *ACS Nano*, vol. 3, no. 12, pp. 3884–3890, Dec. 2009.

[113] F. Yavari, M. A. Rafiee, J. Rafiee, Z. Z. Yu, and N. Koratkar, "Dramatic increase in fatigue life in hierarchical graphene composites," *ACS Appl. Mater. Interfaces*, vol. 2, no. 10, pp. 2738–2743, Oct. 2010.

[114] C. Soutis, "Carbon fiber reinforced plastics in aircraft construction," *Mater. Sci. Eng. A*, vol. 412, no. 1–2, pp. 171–176, Dec. 2005.

[115] M. G. Callens, L. Gorbatikh, and I. Verpoest, "Ductile steel fibre composites with brittle and ductile matrices," *Compos. Part A Appl. Sci. Manuf.*, vol. 61, pp. 235–244, Jun. 2014.

[116] K. W. Garrett and J. E. Bailey, "The effect of resin failure strain on the tensile properties of glass fibre-reinforced polyester cross-ply laminates," *J. Mater. Sci.*, vol. 12, no. 11, pp. 2189–2194, Nov. 1977.

[117] A. Gopinath, M. S. Kumar, and A. Elayaperumal, "Experimental Investigations on Mechanical Properties Of Jute Fiber Reinforced Composites with Polyester and Epoxy Resin Matrices," *Procedia Eng.*, vol. 97, pp. 2052–2063, Jan. 2014.

[118] A. C. Garg and Y.-W. Mai, "Failure mechanisms in toughened epoxy resins—A review," *Compos. Sci. Technol.*, vol. 31, no. 3, pp. 179–223, Jan. 1988.

[119] J. D. Muzzy and A. O. Kays, "Thermoplastic vs. thermosetting structural composites," *Polym. Compos.*, vol. 5, no. 3, pp. 169–172, Jul. 1984.

Chapter 3: Spread and Commingled Carbon/Glass Hybrid Composites for Ductility

Fibre hybridisation is a favourable approach to create ductility in the high-performance composites. The hybridisation of different filaments at tow scale is a challenging topic in the composite world. The main aim of this study is to develop a new dry fibre architecture for the manufacturing of hybrid preform. A novel technique of pneumatic spreading and commingling process was developed to produce carbon and glass fibre intra-tow commingled preform to improve the ductility of the high-performance composites.

3.1 Introduction

In recent years, there has been an increasing interest in spread tow technology in automotive, aerospace, marine and wind turbine industries due to weight saving and excellent mechanical properties [1], [2]. The spread tow UD tapes manufactured are ultra-lightweight ply which is thinner than conventional carbon fibre tapes, where filaments are evenly spread with great filament straightness. As a result, more materials are packed in the same area which gives superior mechanical properties to the composite. Different techniques have been used for spreading carbon and glass fibre tow to prepare thin-ply spread tows such as mechanical [3], vibration/acoustic [4] and pneumatic [1]. Mechanical spreading is a simple and easy method, but excessive angles or contact points; pins can cause fibre damage during the spreading process. However, the pneumatic spreading method is the best among them because during pneumatic spreading airflow does not damage the filaments. The principle of the pneumatic spreading method is; when airflow continuously passes through the fibre tow in a low tension or a tension-free state, the tow spread is stable [1]. Under this circumstance, the space between the filaments is increased which allows the other filament to be interleaved into the increased space to form wider spread tow. Schematic of tow spreading process with a pneumatic method is shown in Figure 3.1

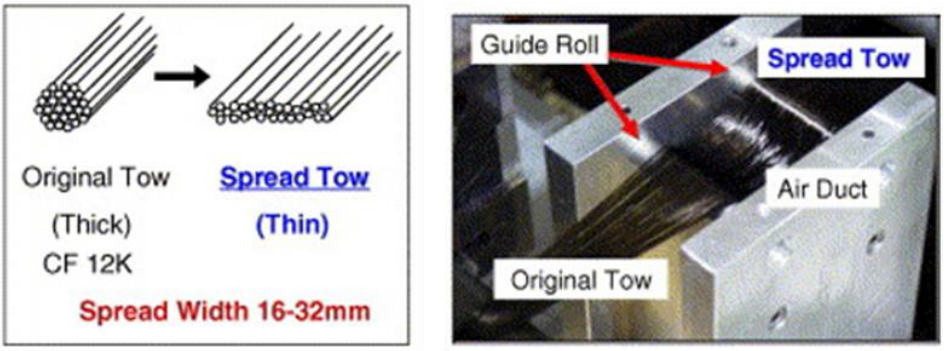

Figure 3.1: Schematic of the tow-spreading technique with a pneumatic method [1].

On the other hand, thin ply spread tow hybrid technology has been used for creating ductility or improving the strain to failure of the carbon fibre composites to overcome the limitation of conventional carbon fibre composites [5]. There are also other techniques that can be used for introducing ductility in composites such as fibre reorientation [6] and incorporation of ductile fibres with brittle fibres, e.g. hybrid or commingling yarn [7]. In order to increase the strain to failure of carbon composites, higher strain to failure fibre such as glass fibres have been used with a low strain to failure carbon fibre to manufacture a hybrid composite [5], [8]–[10]. The purpose of fabricating hybrid composites is to achieve the advantages of both fibres to attain the desired mechanical properties of the composites. Ideally, the carbon fibres offer the tensile stiffness in the initial loading, while the glass fibres contribute in a higher strain to failure of the hybrid composite. The low strain (LS) to failure and high strain (HS) to failure fibres can be hybridised in different configurations. According to the distribution of the fibres in hybrid composite laminates, they can classify into, interlayer hybrid [10]–[13], where layers of two different fibres are stacked onto each other, intra-layer hybrid [13], [14], where the two fibres are mixed together in one layer and intermingled hybrids, where two fibres are mixed within the tow or yarn [15]–[18]. In the intermingled hybrid composite, the dispersion of the two fibre types plays an important role to contribute to the hybrid effect. When the two fibre types are entirely randomly distributed then it is possible to get the good dispersion. However, previous researchers have shown that the mechanical properties of hybrid composites are affected by the level of hybridisation [16], [17], [19]–[21]. Peijs et al. [22] studied the mechanical properties of the carbon and high-performance polyethylene (HPPE) UD hybrid

composites for two different configurations. Their results show that tow-to-tow carbon/HPPE intermingled hybrid epoxy composites had a higher strain to failure than control carbon fibre epoxy composite, though the strain to failure of sandwich carbon/HPPE hybrid composite did not increase. You et al. [20] reported maximum hybrid effect was attained when the carbon and glass fibres were well dispersed and they achieved a 33% hybrid effect in UD composite. Mishnaevsky and Dia [23] reported that a finer dispersion leads to slower development of internal damage.

Therefore, uniform random distribution of two different fibres in the hybrid preform is very important to achieve a higher strain to failure in high-performance hybrid composites. This can be possible if two fibres are completely hybridised at the filament stage before preparing the preform for hybrid composites. It is easy to achieve uniform random distribution in discontinuous fibre [24], [25] but very difficult to achieve for continuous filament. Some researchers hybridised the two different fibres at the filament level by using simultaneous filament winding [26], [27] and commingling [7] process to fabricate hybrid composites. There are few studies [28], [29] that have been carried out to prepare the intermingled commingling spread tow preform for high-performance hybrid composites to improve the ductility, it leaves scope for further investigation.

In this study, an air-assisted spreading process was developed for spreading and commingling of carbon and glass fibre tow to make a thin-ply spread tow tape. The commingled tow was used for the manufacturing of a carbon/glass fibre reinforced epoxy hybrid composite via vacuum bag resin infusion. Layer by layer carbon/glass fibre spread tow hybrid composite was also manufactured. Finally, the tensile behaviour of these hybrid composites was investigated.

3.2 Materials and methods

3.2.1 Materials

The continuous E-glass fibre tow (Hybon, type 2002, 2400 Tex) and the continuous carbon fibre tow (Torayca T700 60E, 12K) were used for spreading and commingling. The carbon fibre that was used here was an untwisted tow, low in size content. The sizing amount on the fibre was 0.3% and it helps to easily spread the tow. E-glass fibre was also untwisted. Details of the fibre properties are summarised in Table 3.1.

Table 3.1: Properties of carbon [30] and E-glass fibres [31]

Fibre Type	Carbon T700 60E	E-glass 2002
Manufacturer	Torayca	Hybon
Tensile strength (MPa)	4900	2290
Tensile Modulus (GPa)	230	75
Tensile strain (%)	2.1	4.8
Filament Diameter (µm)	7	17
Density (g/cm^3)	1.80	2.58
Tex (g/1000m)	800	2400

Araldite ® LY 564, a low molar mass diglycidyl ether of bisphenol A (DGEBA)/ butane diol-diglycidyl ether resin and Aradur ® 2954 (2, 2′-dimethyl-4.4′-methylene bis (cyclohexylamine) hardener (both Huntsman Advanced materials) were used as a matrix. Details of matrix properties are shown in Table 3.2.

Table 3.2: Properties of resin [32]

Resin & Hardener	Curing Temp. and time	Post curing Temp. and time	Tensile Strength (MPa)	Elongation at Break (%)	Tensile Modulus (GPa)	T_G (°C)
Araldite LY564 and Aradur 2954	80 °C 2 h	140 °C 6-8 h	71-77	4.5-5.5	2.5-2.6	123-130

3.2.2 Machine description

To develop a manufacturing process for spreading the carbon and E-glass fibre tow into a ribbon of filament, the experiments were carried out in a web processing machine. The commingling of the carbon and E-glass fibre tow was also carried out in this machine. Some modifications have been done in this machine to carry out the spreading experiments. The web processing machine consists of seven sequential zones namely;

let-off, sizing, spreading, printing, drying, cooling and winding. Figure 3.2 shows the material flow path through various zones of the web processing machine.

It was found from a previous research [33] that the carbon fibre tow passes through the size bath as a rectangular cross-section however on leaving the size bath, the tow takes a tubular geometry which is difficult to spread at the desired width. On the other hand, in this study, it was not necessary to introduce a metallic component. Hence, to avoid this difficulty, experiments were carried out to spread the dry fibre tow bypassing the sizing and printing unit. The tow spreading and commingling machine consists of these zones namely; let-off, pneumatic spreading, sizing, drying, cooling and winding. The material flow path of the modified spreading machine is shown in Figure 3.3.

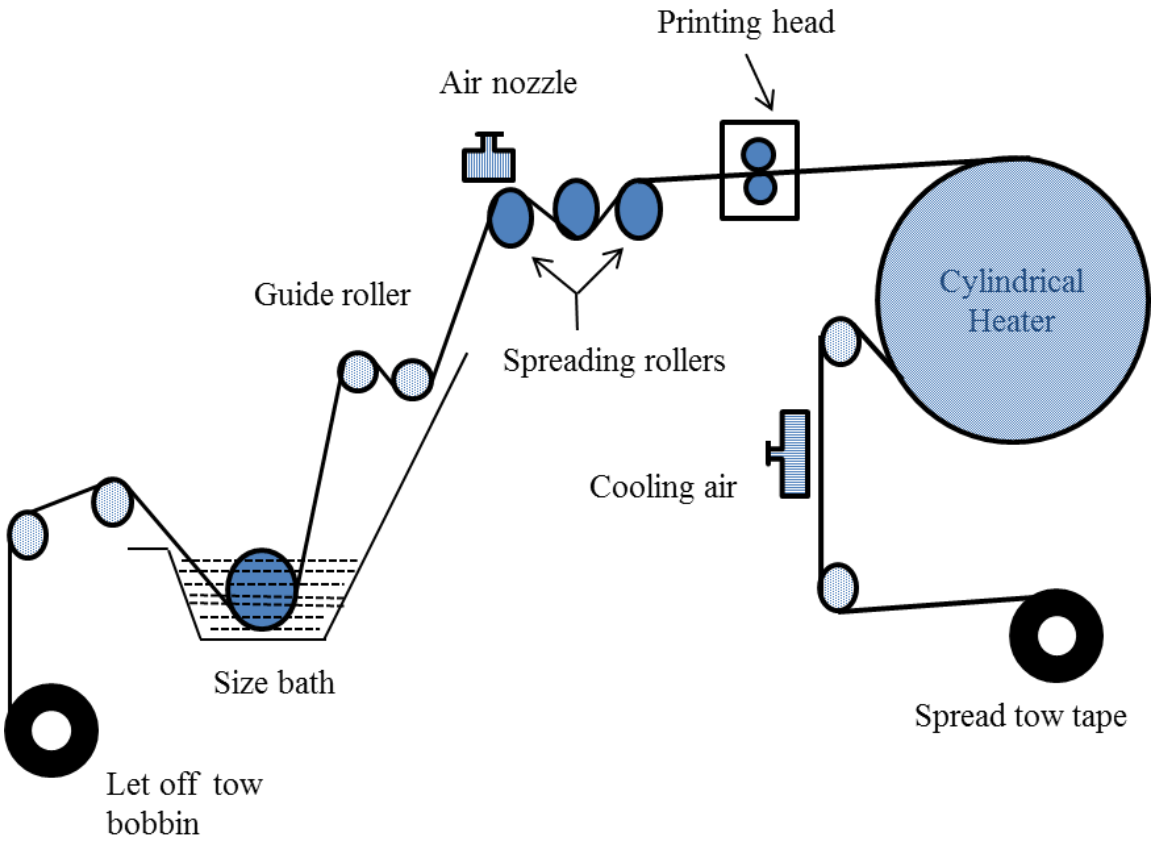

Figure 3.2: Schematic diagram of the tow (web) processing machine.

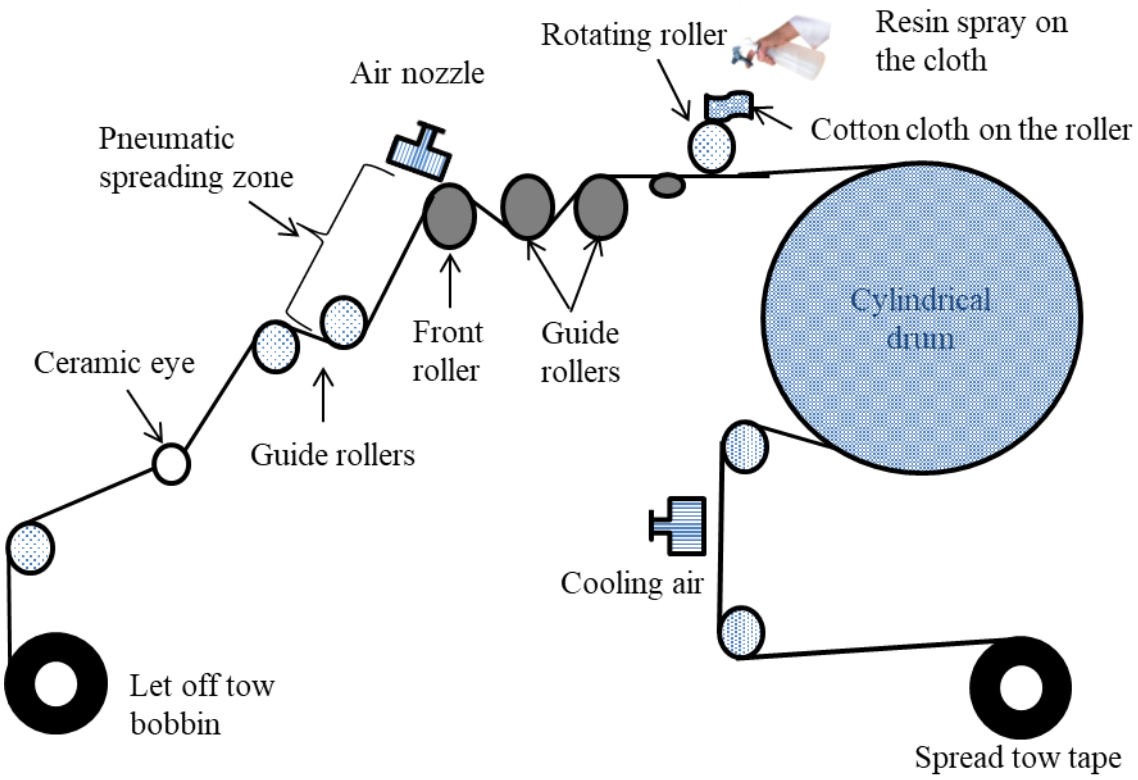

Figure 3.3: Schematic diagram of the tow spreading machine.

3.2.3 Spreading of carbon fibre tow

Figure 3.3 shows the material flow path through various zones of carbon fibre tow spreading machine which is used for this experiment. The carbon tow bobbin was placed in the let-off unit where tension was controlled by back tension through negative feeding. The tow was unwound in a direction perpendicular to the axis of rotation of the bobbin to ensure that tow receives no twist during the let-off stage. At first, the tow passed through the guide roller, ceramic eyelet and another guide roller. Then the tow passed through the air-assisted spreading zone where filaments spreading happened. When the tow passed through the guide and front rollers, a 4 bar pressure was applied by regular ambient temperature air blowing at 35-degree angle on the tow. It was observed that tow tension, airflow rate and angle of airflow are very important factors for spreading the tow. When the tension on the tow was low, it was easy to spread the tow. Figure 3.4 shows the air-assisted spreading zone. In this Figure, it is clearly shown that the tow was spread more than 20 mm and passing over guide rollers for even spreading.

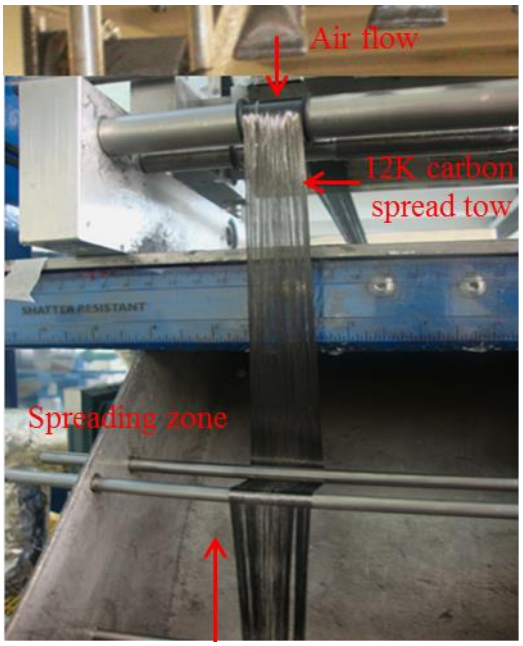

Figure 3.4: Air-assisted spreading of carbon fibre tow.

After spreading, the tow passed through on the contact of a rotating roller for sizing the spread tow. As shown in Figure 3.3, a piece of cotton cloth was placed on the top of the rotating roller and resin was sprayed on this cloth in order to control the gradual application of the resin on the spread tow. When the spread tow passes under the rotating roller, the resin was transferred from the rotating roller to the spread tow. Thereafter the tow was passed over the cylindrical drum which was heated to 115°C, in order to dry the size coating on the spread tow. After that, the dried tow was air-cooled using a blast of ambient temperature air. Finally, the tow was wound on a bobbin as a tape, which was used for manufacturing 100% carbon fibre spread tow composites. Similarly, carbon fibre spread tow was also separately prepared for a commingling process, without sizing, and was wound onto a bobbin as a tape.

3.2.4 Spreading of E-glass fibre tow

At first 2400 tex glass fibre tow was unwound from the bigger package and wound on a bobbin. During this process, great care was taken so no twisting of the tow occured during winding. As the glass fibre tow has higher size contents so it was difficult to spread the glass fibre tow in the air-assisted spreading process. For this reason, initially, the glass fibre tow was partially spread using the roller spreading process. Figure 3.5

shows the photograph of the roller spreading process where the glass fibre tow passed through the different spreading rollers and finally tow was wound on a bobbin. This partially spread tow was spread again with air-assisted spreading process.

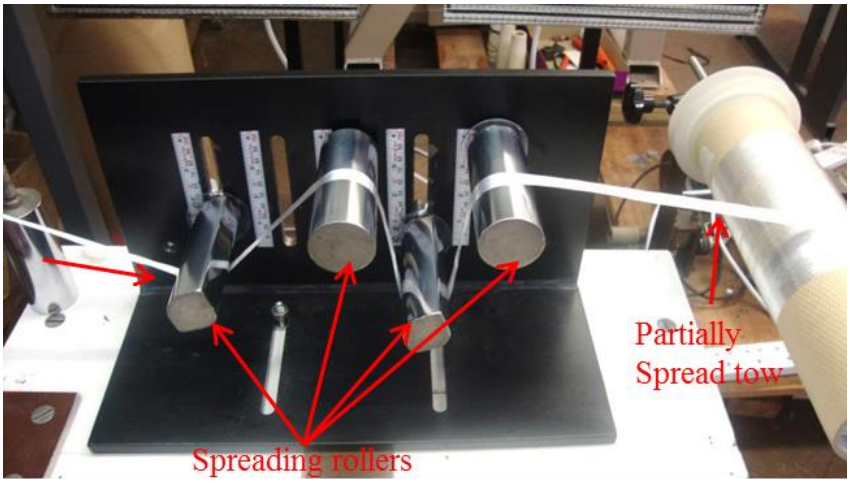

Figure 3.5: Photograph of roller spreading process.

.

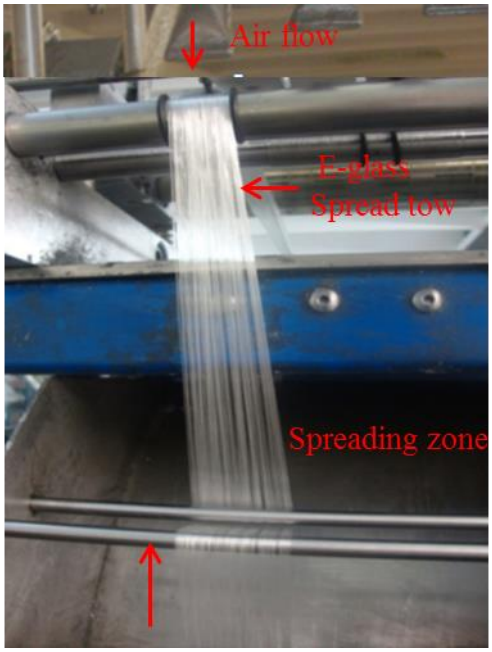

Figure 3.6: Air-assisted spreading of E-glass fibre tow.

The partially spread glass fibre tow was fed in the let-off unit of the tow spreading machine (Figure 3.6) and was passed through the air-assisted spreading system for further spreading. Figure 3.6 shows the photograph of the air-assisted spreading zone

where glass fibre tow was spread. After spreading, the tow passed over the cylindrical drum and finally wound on a bobbin as a tape form without sizing. The width of the carbon and glass fibre spread tows was 20 mm. Carbon and glass fibre spread tow tapes are shown in Figure 3.7a and b respectively.

Figure 3.7: Spread tows (a) 12 K carbon fibre and (b) 2400 tex E-glass fibre.

3.2.5 Commingling of carbon and E-glass fibre tow

The aim of this study was to prepare carbon and glass fibre commingled UD tape for fabricating the ductile composites. In the literature review [34], it was found that 0.10 to 0.25 relative carbon ratio was suitable to achieve the better ductility in intermingled carbon-glass hybrid composites with highly aligned discontinuous fibre. Therefore, the fibre volume fraction of carbon and glass fibre in the commingled tape was kept around 20 and 80% respectively.

In order to prepare the carbon/glass fibre commingled tape, the carbon and glass fibre spread tow bobbins were fed from a tension control creel as a sandwich form. Two E-glass and one carbon fibre spread tows were used. The carbon fibre spread tow was placed in the middle and glass fibre spread tows were placed on top and bottom of the carbon fibre spread tow and passed through the air-assisted spreading zone for spreading and commingling. Special care was taken to overlap the carbon and E-glass fibre tow before entering the commingling zone. When carbon and glass spread tows passed through the air-assisted commingling unit the air blow generated the space and the carbon and glass filament commingled and produced a commingled tow. After that, the partially commingled tow passed through the cylindrical drum without sizing and wound on a bobbin as a tape form. To get a higher degree of dispersion, the partially commingled tow was fed in the tow processing machine and passed through the air-

assisted spreading and commingling zone for further commingling. During this process, further commingling of the carbon and glass filaments was observed, which increased the degree of hybridisation. After commingling, the tow passed through the spray sizing zone. A 2% aqueous dispersion of a solid diglycidyl ether of bis-phenol (DGEBA) epoxy resin EPI-REZ™ 3522-W-60 (Hexion) was used for sizing the commingled tow. Then the tow passed over the 115°c heated drum for drying the size. After that, the dried tow was cooled and wound on a bobbin as a tape form. Air assisted commingling unit and carbon and glass fibre commingled tape bobbin is shown in Figure 3.8. The schematic illustration of the principle of the air-assisted commingling process is shown in Figure 3.9.

Figure 3.8: Air-assisted commingling unit and commingled tape (a) during the first passage, (b) during the second passage and (c) carbon/E-glass commingled tape.

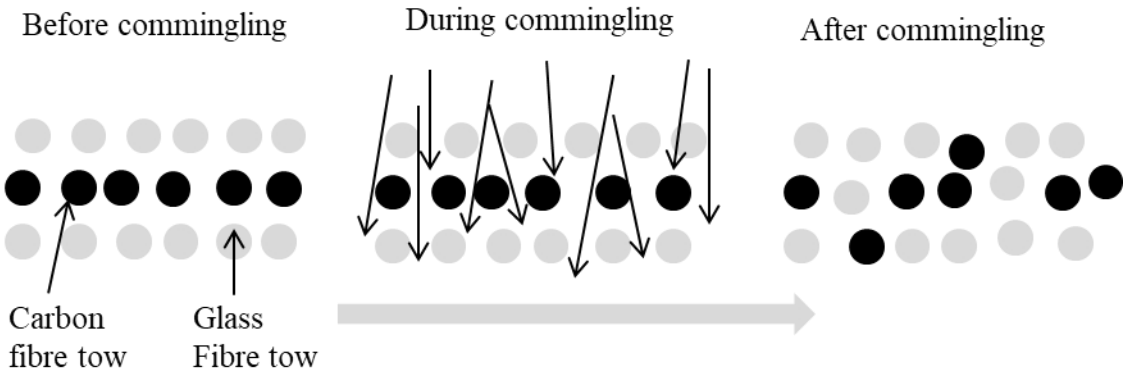

Figure 3.9: Schematic illustration of the air-assisted commingling process.

3.2.6 Fabrication of UD composite laminates

Four different types of UD composite panels were manufactured by vacuum-assisted resin infusion process.

(a) Panel 1 was manufactured from carbon fibre spread tow tape.
(b) Panel 2 was manufactured from E-glass fibre spread tow tape.
(c) Panel 3 was manufactured from carbon and E-glass fibre thin-ply spread tow, layer by layer hybrid process
(d) Panel 4 was manufactured from carbon/E-glass commingled spread tow.

At first, the mould surface was cleaned with Sika mould cleaner to remove any contaminants such as grease, oil and wax on the surface. After cleaning the mould, a universal chemical release agent was applied on the surface of the mould to avoid the resin to stick. Release agent was applied several times and after every application the release agent was allowed to dry on the mould surface. Four different panels were prepared with different materials.

3.2.6.1 Lay-up sequence of panel 1 and 2

UD laminate panel 1 was prepared from carbon fibre spread tow. Tow parameters are given in Table 3. 4. Carbon fibre spread tow was cut a length of 30 cm and carefully laid-up them on the mould layer by layer. Five pieces of tow were placed side by side and special care was taken to avoid the gap between the tows. Six layers of carbon tow were laid up under tension to maintain the fibre alignment. At both sides gum tape was used to hold the filaments and the prepared panel is shown in Figure 3.11(a). Panel 2 was prepared the same way and E-glass fibre spread tow was used instead of carbon fibre spread tow Figure 3.11(b).

3.2.6.2 Lay-up sequence of panel 3

UD laminate panel 3 was prepared from carbon and E-glass fibre spread tow. Carbon and E-glass fibre spread tows were laid-up on the mould layer by layer by following the sequences glass/carbon/glass. Three layers of carbon and six layers of E-glass fibre tows were laid up under tension to maintain the fibre alignment. The layup sequence of carbon and glass fibre spread tow is shown in Figure 3.10 and the prepared panel is shown in Figure 3.11(c). The resultant volume fraction of carbon and E-glass fibre in the panel was 20 and 80% respectively.

Figure 3.10: Lay-up sequence of carbon and E-glass fibre thin-ply spread tow.

3.2.6.3 Lay-up sequence of panel 4

UD laminate panel 4 was prepared from carbon/E-glass commingled tow. The width and thickness of the commingled tow were 22 mm and 0.195 mm respectively and volume fraction of carbon and glass fibre was 20 and 80% respectively. Carbon/E-glass commingled tow was cut a length of 30 cm and carefully laid up on the mould layer by layer. Four layers of commingled tape were laid up under tension to maintain the fibre alignment. Both side gum tape was used to hold the filaments and the prepared panel is shown in Figure 3.11(d).

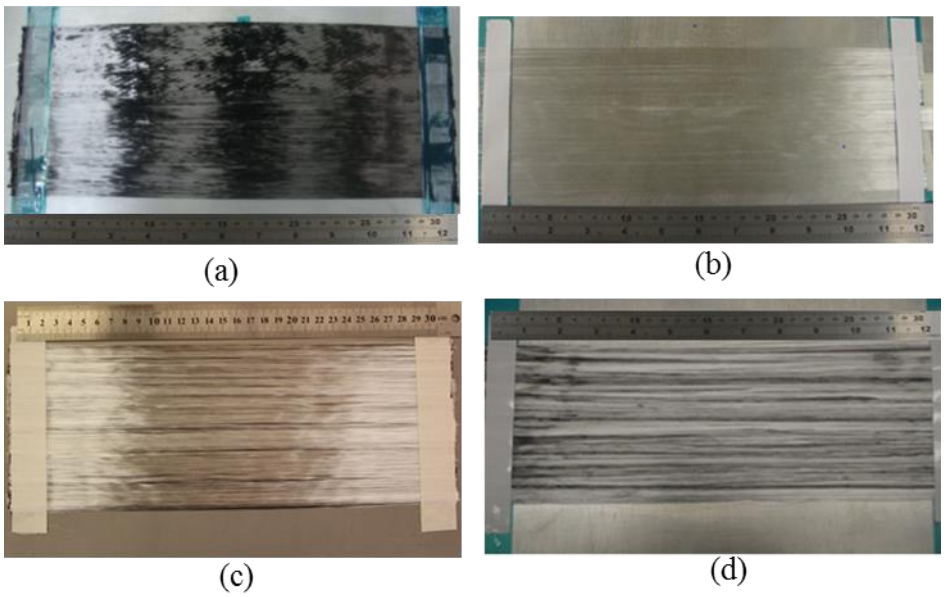

Figure 3.11: Photographs of the different UD composite panels (a) Carbon fibre spread tow, (b) E-glass fibre spread tow, (c) carbon/E-glass spread tow layer-by-layer hybrid and (d) carbon/E-glass commingled hybrid.

A piece of peel-ply was laid-up on the top of each panel that would not stick with layup tows but allows the resin to seep through. Then a layer of breather cloth (nylon mesh) laid-up on the top of the peel ply which absorbed the resin and allowed the resin to be passed uniformly over the surface of the layup. Then a sticky tape placed all around the laid panels. A vacuum bag is placed on the top of the layers and cover the plies and sealed to the mould with sticky tape. Inlet and outlet tubes passed through the vaccum bag seal and were connected through a spiral tube with the laid piles for resin impregnation. Then the outlet tube was connected to a vacuum pump to reduce the air pressure inside the vacuum bag. The vacuum bagging method used for the development of composite is shown in Figure 3.12.

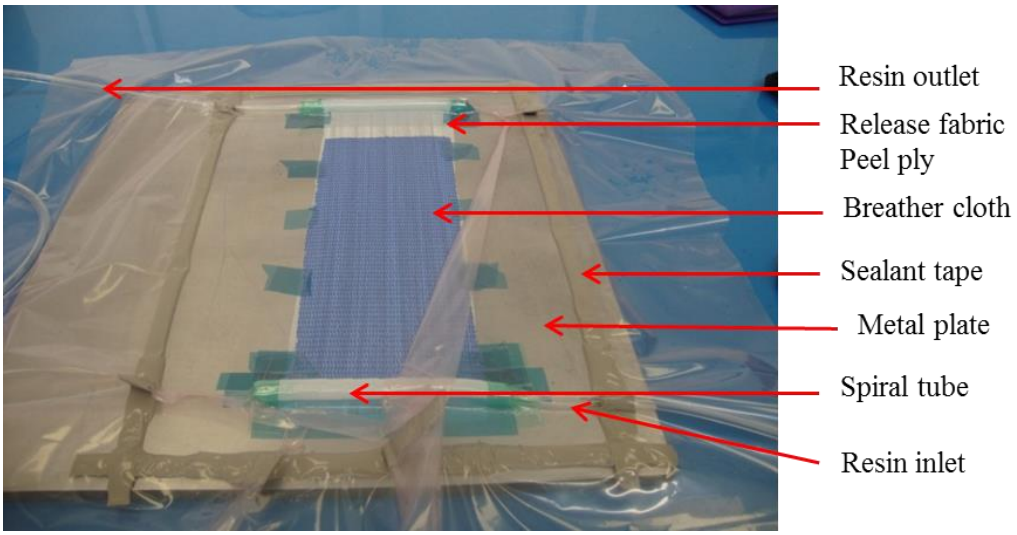

Figure 3.12: Vacuum-assisted resin infusion (VARI) process.

3.2.6.4 Resin infusion

Araldite ® LY 564 resin and Aradur ® 2954 hardener were used as a matrix. The proportions are usually given by the supplier and can be found on the containers of the hardener or resin. The mixing ratio of resin to hardener is 100:35. The mixing was performed in the mixing containers with the mixing stick and it is done slowly to avoid air bubbles in the mixer. Then the mixer was put in a degassing machine to ensure the complete removal of gas bubbles from the resin to make a void-free laminate. The inlet

tube was then submerged in the container of resin and the resin mixer was infused into the vacuum bag layer using the vacuum pump for uniform distribution of resin and also to remove the entrapped air. The resin flow was controlled manually using a clamp on the inlet tube. Once the resin infusion was completed, the complete panel was kept inside an oven chamber for curing. Curing and post-curing were carried out in an oven at 80 ºC for 1 hour and 140 ºC for 6 hours.

3.2.7 Mechanical testing of different composites

Different types of composite panels were taken out from the mould and then specimens of appropriate dimensions were prepared from the composite panel for mechanical testing according to ASTM D3039 [35] standard. End tabs made of woven glass-epoxy plates 1.50 mm thickness were cut according to the size and sandblasted. The end tabs were bonded to the specimen using Cytec MTA 240 adhesive film by hot press machine at 120 ºC for 1 hour under 2 bar pressure. Then test specimens were cut from the panel by using a diamond-tipped cutter and the tensile test specimens were prepared according to ASTM D3039. Dimensions of the tensile test specimen are shown in Figure 3.13. Tensile tests were done on an electromechanical testing machine (Instron 5982) with a cross-head displacement speed of 2 mm/min. The load was measured with a 100 kN load cell. The strain was measured by using an Imetrum video extensometer. White speckled patterns were created on the specimen surfaces, using white marking pigments, to measure the strain in the composite. The gauge length of the strain measurement was 50 mm.

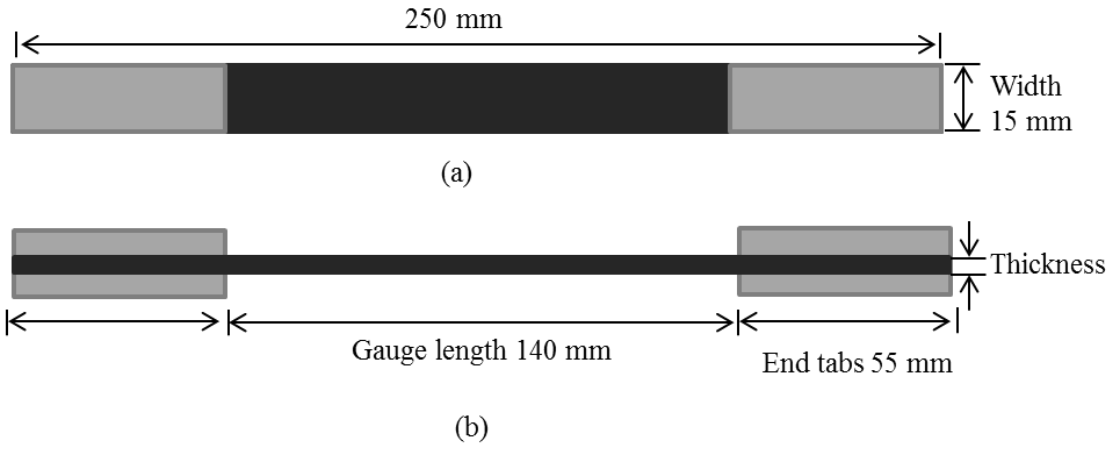

Figure 3.13: Dimension of the test specimen used for tensile testing (a) top view and (b) side view.

3.2.8 Volume fraction and density measurement

Fibre volume fraction (FVF), matrix volume fraction (MVF) and void volume fraction (VVF) of composite laminates were calculated using the following equations

Fibre volume fraction for single constituent and matrix

$$V_f = \frac{\frac{w_f}{\rho_f}}{\frac{w_f}{\rho_f} + \frac{w_m}{\rho_m}} \tag{3-1}$$

Fibre volume fraction for hybrid constituent and matrix

$$V_f = \frac{\frac{w_g}{\rho_g} + \frac{w_c}{\rho_c}}{\frac{w_g}{\rho_g} + \frac{w_c}{\rho_c} + \frac{w_m}{\rho_m}} \tag{3-2}$$

Matrix volume fraction of hybrid composite

$$V_m = \frac{\frac{w_m}{\rho_m}}{\frac{w_g}{\rho_g} + \frac{w_c}{\rho_c} + \frac{w_m}{\rho_m}} \tag{3-3}$$

Voids in the laminate

$$V_v = 1 - \frac{\rho_{exp}}{\rho_{th}} \tag{3-4}$$

Where, V_f is the fibre volume fraction, V_m is the matrix volume fraction, w_f is the weight of the fibre, ρ_f is the density of the fibre, w_m is the weight of the matrix, ρ_m is the density of the matrix, w_g and w_c are the weight of glass and carbon fibre and ρ_g and ρ_c are the density of glass and carbon fibre, V_v is the void content in the composites, ρ_{exp} and ρ_{th} are the practical and the theoretical density of the composites.

The density of the composites was measured according to ASTM D792 [36] in an AL50L (Mettler Toledo, UK) analytical balance using deionised water. In this method,

the composite specimens were weighted in the air followed by carefully immersing in distilled water at a specific temperature. The density of the specimen was generated by the balance electronically once the masses were measured from the following equation:

$$\rho_c = \frac{w_1}{w_1 - w_2}(\rho_0 - \rho_L) + \rho_L \quad (3\text{-}5)$$

Here, ρ_c is the density of composite, w_1 and w_2 is the weight of the specimen in air and water, ρ_0 is the density of the water, ρ_L is the density of the air (0.0012 g/cm3).

The theoretical density of the composites was measured using the following equation

$$\rho_{th} = V_f\rho_f + V_v\rho_m \quad (3\text{-}6)$$

Where, V_f and V_m are the volume fraction of fibre and matrix, ρ_f and ρ_m are the density of the fibre and matrix respectively.

The summary of the data of the four different types of composite laminates is presented in Table 3.3.

Table 3.3: Summary of physical properties of the different composites

Specimen type	Volume fraction, Carbon (%)	Volume fraction E-glass (%)	Density (g/cm^3)	Void (%)
Carbon Spread tow	56.51±0.15	-	1.51±0.01	0.61±0.02
E-glass Spread tow	-	55.42±0.24	1.93±0.01	0.91±0.03
CF/E-G Layer by layer	10.95±0.22	45.48 ±0.32	1.87±0.01	0.66±0.04
CF/E-G commingling	10.30±0.31	42.82±0.25	1.82±0.01	0.85±0.02

3.2.9 Microscopic analysis of hybrid composites

In order to analyse the distribution of carbon and glass fibre in the hybrid composites, the cross-section of the laminates were fixed into a transparent Araldite epoxy resin and hardener. The epoxy resin was cured at room temperature for 48 hours. Then the samples were ground by P400, P800, and P1200 sandpapers to get the flat surfaces. Finally, the samples were polished by using 6 µm, and 1 µm diamond paste to achieve a mirror finish. Then the samples were coated with a thin layer of gold and platinum using Quorum Q150T ES machine to develop their conductivity and prevent the

accumulation of charges. A Philips model XL 30 Screening Electron Microscope (SEM) was used to observe the cross-section of the composites.

3.3 Results and Discussion

3.3.1 Spreading and commingling of carbon and glass fibre tows

As the quality of spread tow affects the commingling process of the carbon and E-glass fibres tows therefore, it was important to spread the carbon and E-glass fibre tow to a suitable width for commingling. The air-assisted spreading process allows spreading the carbon and E-glass fibre tows without noticeable damage to the filament by 4-5 times. It was observed that tow tension, airflow rate, amount of size in the tow and angle of airflow were very important factors for spreading the tow. During the spreading process, it was also observed that twist and fibre entanglements within the tow affected the quality of the spread tows. It was difficult to maintain the spread tow width if there were twist and entanglements within the tow. Although it was mentioned in the Torayca technical data sheet that carbon T700 60E is twist free tow but unfortunately during processing, some entanglement or twist was observed in the tow which was unpredictable. Figure 3.14 shows the photograph of the spreading process of carbon tow with and without a twist. The tow is easily spread by the air-assisted spreading process when there was no twist (Figure 3.14a) but the spreading process was obstructed if there was any twist in the tow (Figure 3.14b).

The photograph of the carbon and E-glass fibre as received fibre bundle, spread tows and carbon/E-glass commingled tape are shown in Figure 3.15. The average width of the as-received 12K carbon and 2400 tex E-glass bundle was around 5 and 4.5 mm respectively. The width of the 12K carbon and 2400 tex glass fibre tows were spread to increase their width four times. Summary of the tow parameters such as width, thickness and mass per unit area of the carbon fibre, E-glass fibre spread tow and carbon/E-glass fibre commingled tow are given in Table 3. 4.

(a) (b)

Figure 3.14: Effect of tow twist on spreading process; (a) tow without twist and (b) tow containing twist.

Table 3. 4: Summary of the spread tow and commingled tape parametres

Specimen name	Original tow width (mm)±SD	Spread tow width (mm)±SD	Thickness (mm)±SD	Areal density (g/m^2) ± SD	Volume fraction (%)
12K Carbon	5.5 ± 0.50	20 ± 1.01	0.0432 ± 0.002	40.35 ± 2.04	100% CF
2400 tex E-glass	5 ± 0.50	21 ± 1.12	0.0813 ±0.005	120 ± 4.50	100% GF
Carbon/E-glass commingled	-	22 ± 1.05	0.195 ±0.006	255 ± 6.54	20% C and 80% G

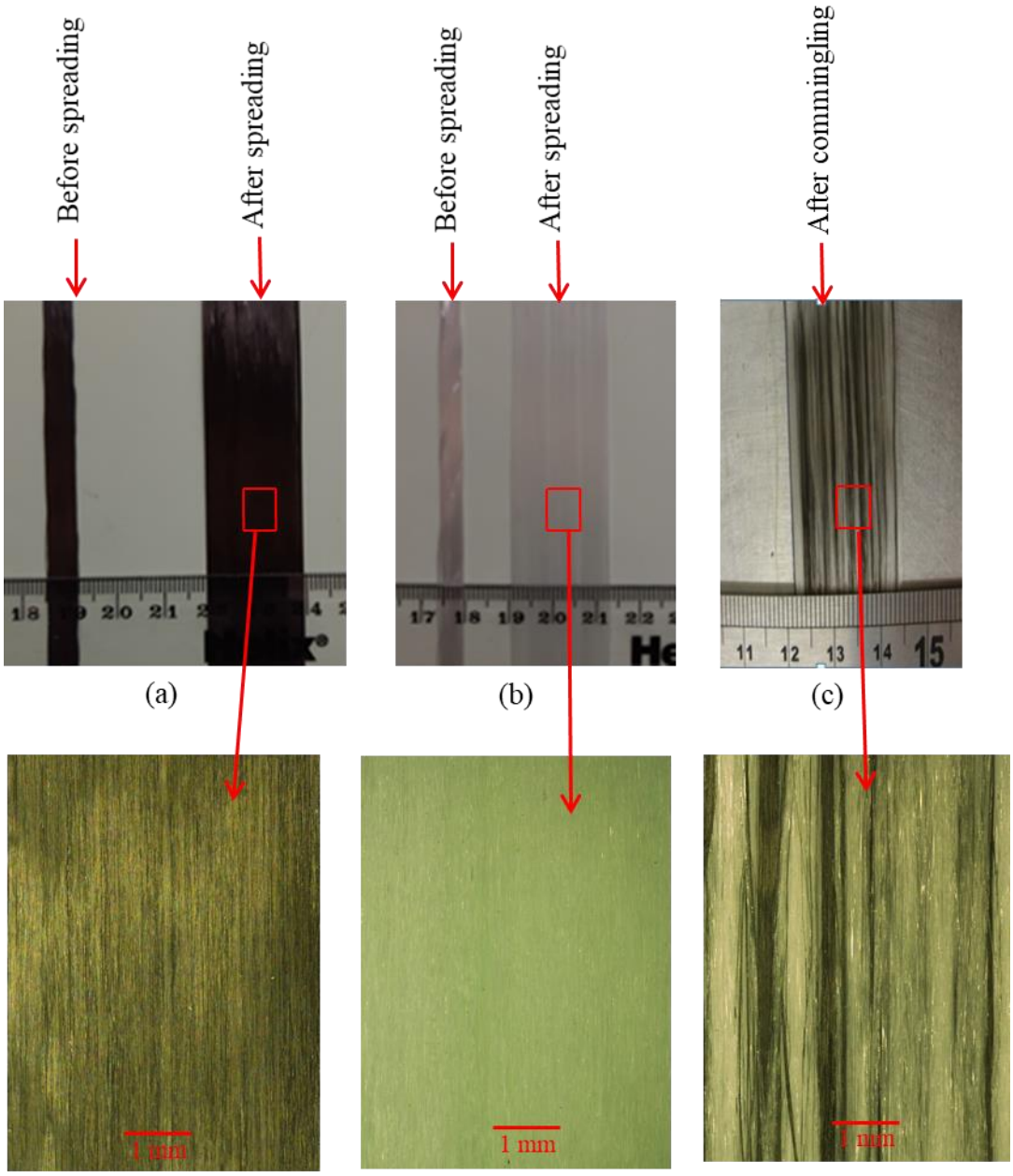

Figure 3.15: Photograph of different spread and commingled tow; (a) 12K carbon fibre, (b) 2400 tex E-glass and (c) carbon/E-glass commingled tape.

3.3.2 Cross-section images of composites

The distribution of carbon and E-glass in the hybrid composites were analysed by scanning electron microscopic (SEM). Cross-sectional images of carbon/E-glass layer-by-layer and commingled hybrid UD composites are shown in Figure 3.16. The images clearly show that in the carbon/E-glass fibre inter-layer hybrid composite, carbon and E-glass fibre stay layer by layer but some carbon fibres entered between the glass filaments. As the carbon and glass fibre spread tow were dry and partially sized, so

during the vacuum resin infusion process, some fibre migrated from one layer to another layer (Figure 3.16a). On the other hand, carbon fibres were distributed in the commingled tow as a bundle form (Figure 3.16b). Carbon and E-glass fibre did not evenly distribute during the commingling process but some degree of hybridisation was achieved in the commingling process at tow level.

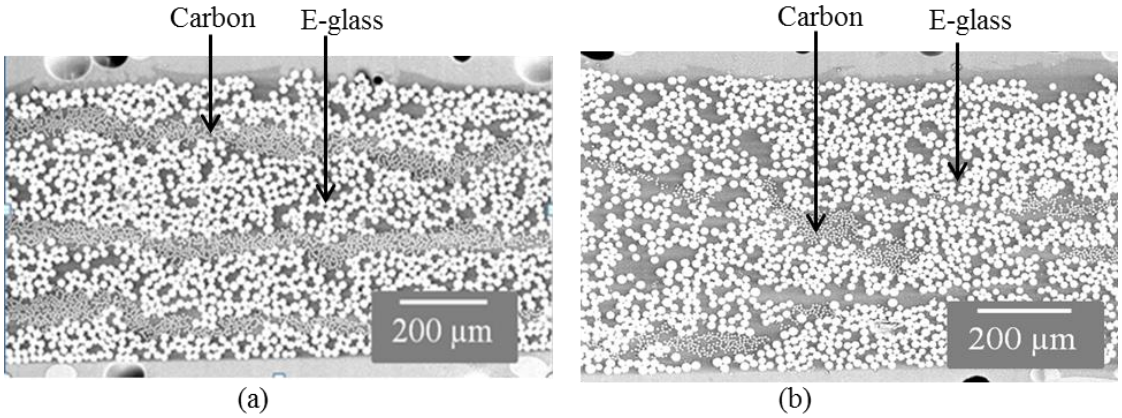

Figure 3.16: Cross-sectional images of spread tow hybrid UD composites: (a) layer-by-layer hybrid and (b) commingling.

3.3.3 Tensile properties of carbon and E-glass fibre spread tow composites

To study the effect of layer by layer (inter-tow) and commingled (intra-tow) hybridisation, four different types of composites were manufactured and tested. Normalised tensile test results of different composites are presented in Table 3.5. All the data was normalised at 55% fibre volume fraction. Control carbon and glass fibre epoxy composites were manufactured from carbon and E-glass fibre spread tow. The stress-strain graph of control spread tow carbon fibre and E-glass fibre composites are shown in Figure 3.17a and b respectively. The ultimate failure strain of the 100% (control) carbon fibre and E-glass fibre composite was 1.63% and 2.74% respectively. Tensile modulus of the 100% carbon and E-glass fibre spread tow composite was 104.6 and 34.5 GPa respectively. The maximum stress of carbon and E-glass fibre spread tow composite was 1750 and 787 MPa respectively.

Table 3.5: Summary of normalised tensile properties of different composites

Type of Laminate	Max. Stress (MPa) ± SD	Initial Modulus (GPa) ± SD	Initial failure strain (%) ± SD	Ultimate failure strain (%) ± SD
CF Spread tow	1750 ± 94	104.6 ± 3.64	1.63 ± 0.04	1.63 ± 0.04
E-glass	787 ± 44	34.8 ± 1.40	2.59 ± 0.10	2.74 ± 0.13
CF/E-G Layer by layer	989± 59	50.4 ± 1.35	1.73 ± 0.13	2.06± 0.06
CF/E-G commingling	976 ± 58	49.5 ± 1.32	1.66 ± 0.03	2.03± 0.03

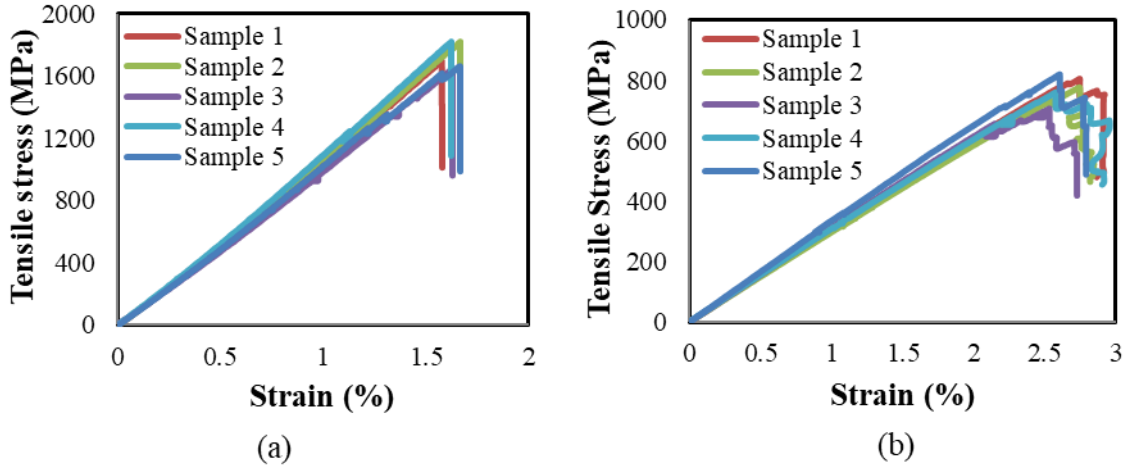

Figure 3.17: Tensile stress-strain graph of (a) 100% carbon fibre/epoxy and (b) 100% E-glass fibre/epoxy composite.

3.3.4 Tensile properties of carbon/E-glass layer by layer and commingled hybrid composites

Figure 3.18 and Figure 3.19 shows the tensile stress-strain curves of carbon/E-glass layer by layer and commingled hybrid composites. The pristine and failed images of the specimen are shown in (Figure A1, Appendix A). Both stress-strain graphs clearly show that the hybrid composites failed more progressively than the spread tow 100% carbon fibre composite. It is interesting to note that the nonlinearity of the stress-strain graph was observed in both graphs. Most of the specimens showed multiple breaks in the stress-strain graph. As the strain to failure of the carbon fibre is less than E-glass fibre, therefore carbon fibre failed first and E-glass fibre carried the load and final failure

happened. The ultimate strain to failure of the layer by layer and commingled hybrid composites were 2.06% and 2.03% respectively which was about 27% higher than that of control carbon fibre composite and about 25% lower than that of control E-glass fibre composite. The average initial failure strain of the layer by layer hybrid composite was higher than commingled hybrid one. In the commingled hybrid composite, the initial failure occurred earlier than the layer by layer hybrid composite. These results indicate that there was an effect of hybrid techniques on the failure process of the composites. The thin layer hybrid configuration enhances the initial failure process compared to that of the commingled process. The difference between ultimate and initial strain to failure was higher in commingled hybrid composites than the layer by layer one. The enhancement of ultimate strain to failure and the different failure mode among the hybrid composites and control carbon composite could be related to a different reason. The main possible failure mechanism of the hybrid composite is that: when carbon fibres failed, the first non-linearity in the stress-strain curves was observed. Then the load was redistributed to nearby glass fibres or unbroken carbon fibres and delays the crack propagation which was initiated by carbon fibre failure and allowed the hybrid composites to more progressive failure. Finally, with the increase of load, more fibres in the hybrid composite failed which lead to the ultimate failure of the composites. The stress concentration generated by the failure of carbon fibre leads to an increased failure probability in the surrounding fibres which leads to the development of clusters of broken fibres. Therefore, the stress concentration produced by the failure of carbon fibre results in the early failure of the E-glass fibre in the hybrid composite compared to control E-glass fibre composite. For this reason, the ultimate failure strain of the carbon/E-glass hybrid composite was lower than that of control E-glass fibre composite. The enhancement in the ultimate strain to failure of UD hybrid composite is affected by many factors, such as distribution and volume ratio of low elongation and high elongation fibres. A recent study [5] shows that thin-ply spread tow hybrid composite demonstrated better ductility compared to thick-ply hybrid composite. On the other hand, some researchers [18], [21], [37] have claimed that higher dispersion of the low and high strain fibres contributed higher strain to failure of the composites compared to lower dispersion hybrid composites. Diao et al. [38] studied the carbon and E-glass fibre commingled hybrid composite and found a 14% increase in ultimate strain to failure compared to that of the control carbon fibre composite. The ultimate strain to failure of the commingled hybrid composite was 1.52 % with the similar type of carbon and glass

fibre used in this study. However, a significant (27%) improvement of the ultimate strain to failure compared to their study was observed in this research.

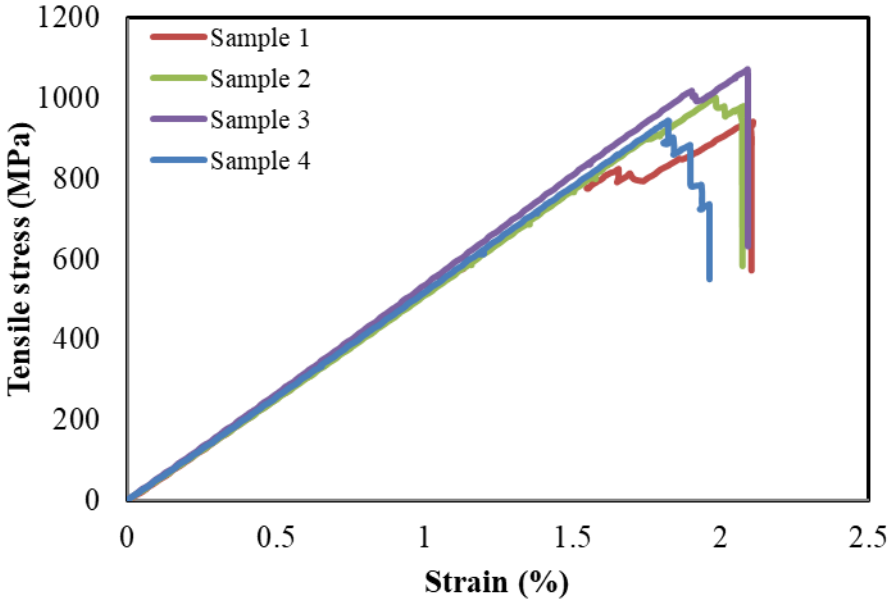

Figure 3.18: Tensile stress-strain graph of carbon/E-glass fibre layer by layer (inter-tow) hybrid composite.

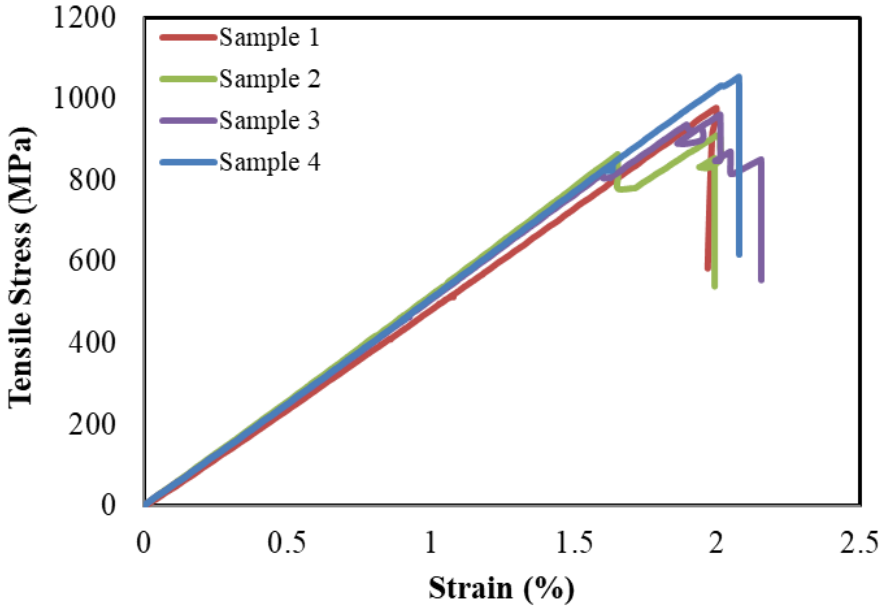

Figure 3.19: Tensile stress-strain graph of carbon/E-glass fibre commingled (intra-tow) hybrid composite.

Maximum tensile strength of the layer by layer and commingled hybrid composites was 989 and 976 MPa respectively. A slight lower value was observed in commingled

hybrid composite compared to layer by layer hybrid. It might happen due to the additional process for commingling tow which could create internal damage to the filament. The tensile strength value calculated according to the rule of the mixture was 1640 MPa which is different compared to experimental results. However, it is difficult to predicate the tensile strength and strain to failure of the hybrid composites because the hybrid architecture affects the load redistribution after the failure of low strain fibres.

The tensile modulus of the layer by layer and commingled hybrid composites were almost similar (50.4 and 49.5 GPa) respectively. According to the rule of mixture, the calculated value of the modulus was 57.5 GPa which is close to the experimental results. These results indicate that thin ply layer by layer and commingled hybrid architecture can be designed according to the rule of mixture for desired stiffness of the composites. Tensile modulus was increased by about 44% for the hybrid composites when compared with control glass fibre composite. There was no significant difference in the tensile test results between two hybrid architecture composites. Therefore, the air-assisted spreading and commingling process delivered a latent carbon/E-glass hybrid preform manufacturing route for hybrid composites which improved the ductility and ultimate strain to failure compared to control carbon fibre composite. A typical normalised stress-strain graph of CF spread tow, E-G spread tow, CF/E-G layer by layer and CF/E-G commingled hybrid spread tow composites are presented in Figure 3.20.

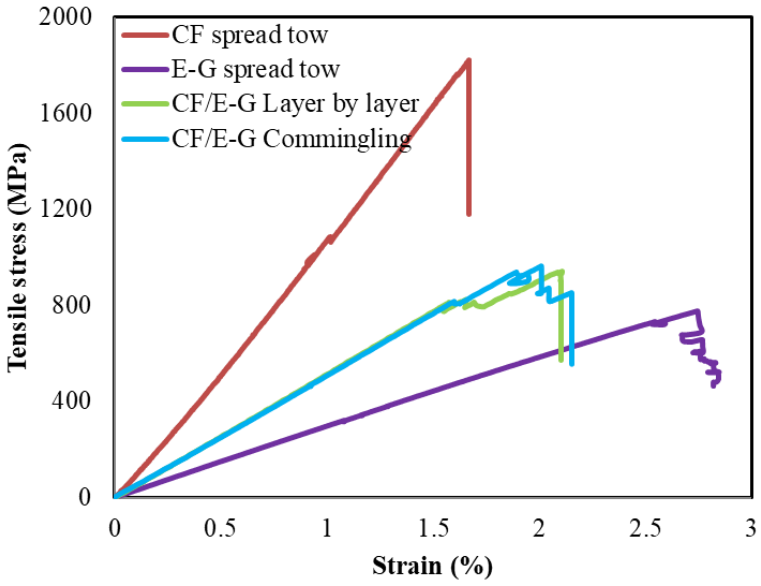

Figure 3.20: Typical normalise stress-strain graphs of different composites.

3.4 Summary

A process for spreading and commingling of carbon and glass fibre tows to make a commingled tow was described in this chapter. In this process, by the help of airflow, the thick filament tows were spread about 4-5 times without noticeable filament damage. A regular ambient temperature compressed air was used for this experiment. During these experimental studies, it was found that tow tension, airflow rate and angle of airflow are very important factors for spreading the tow. Carbon and glass fibre spread tows were prepared which were used to prepare commingled tape. A commingled tape was prepared from carbon and glass fibre spread tow using air-assisted spreading and commingling process where carbon and glass fibres were partially hybridised at the tow level.

A comparative study of the tensile properties of the layer by layer and commingled hybrid composites with epoxy resin were carried out. Both hybrid composites exhibited more gradual and improved tensile failure strain compared to 100% carbon fibre spread composite. The ultimate strain to failure of the hybrid composites was about 26% higher than control carbon fibre composite but it was 25% lower than that of control E-glass fibre composite. There was no significant difference observed in the tensile test results between the two-hybrid architectures.

References

[1] S. T. S Sihn, RY Kim, K Kawabe, "Experimental studies of thin-ply laminated composites," *Compos. Sci. Technol.*, vol. 67, no. 6, pp. 996–1008, May 2007.

[2] T. Yokozeki, Y. Aoki, and T. Ogasawara, "Experimental characterization of strength and damage resistance properties of thin-ply carbon fiber/toughened epoxy laminates," *Compos. Struct.*, vol. 82, no. 3, pp. 382–389, Feb. 2008.

[3] M. S. Irfan *et al.*, "Lateral spreading of a fiber bundle via mechanical means," *J. Compos. Mater.*, vol. 46, no. 3, pp. 311–330, Nov. 2011.

[4] S. Iyer and L. T. Drzal, "Method and system for spreading a tow of fibers," *US Pat. 5,042,111*, Aug. 1991.

[5] G. Czél and M. R. Wisnom, "Demonstration of pseudo-ductility in high

performance glass/epoxy composites by hybridisation with thin-ply carbon prepreg," *Compos. Part A Appl. Sci. Manuf.*, vol. 52, pp. 23–30, Sep. 2013.

[6] J. D. Fuller and M. R. Wisnom, "Exploration of the potential for pseudo-ductility in thin ply CFRP angle-ply laminates via an analytical method," *Compos. Sci. Technol.*, vol. 112, pp. 8–15, May 2015.

[7] E. Selver, P. Potluri, C. Soutis, and P. Hogg, "Healing potential of hybrid materials for structural composites," *Compos. Struct.*, vol. 122, pp. 57–66, Apr. 2015.

[8] T. Hayashi, "On the improvement of mechanical properties of composites by hybrid composition," in *8th International Reinforced Plastics Conference, Brighton, UK*, 1972, pp. 149–152.

[9] A. R. Bunsell and B. Harris, "Hybrid carbon and glass fibre composites," *Composites*, vol. 5, no. 4, pp. 157–164, Jul. 1974.

[10] P. W. Manders and M. G. Bader, "The strength of hybrid glass/carbon fibre composites," *J. Mater. Sci.*, vol. 16, no. 8, pp. 2233–2245, Aug. 1981.

[11] M. R. Wisnom, G. Czél, Y. Swolfs, M. Jalalvand, L. Gorbatikh, and I. Verpoest, "Hybrid effects in thin ply carbon/glass unidirectional laminates: accurate experimental determination and prediction," *Compos. Part A Appl. Sci. Manuf.*, vol. 88, pp. 131–139, Apr. 2016.

[12] N. Saha, A. N. Banerjee, and B. C. Mitra, "Tensile behaviour of unidirectional polyethylene-glass fibres/PMMA hybrid composite laminates," *Polymer (Guildf).*, vol. 37, no. 4, pp. 699–701, Jan. 1996.

[13] P. J. Hine, M. J. Bonner, I. M. Ward, Y. Swolfs, and I. Verpoest, "The influence of the hybridisation configuration on the mechanical properties of hybrid self reinforced polyamide 12/carbon fibre composites," *Compos. Part A Appl. Sci. Manuf.*, vol. 95, pp. 141–151, Apr. 2017.

[14] H. Ikbal, Q. Wang, A. Azzam, and W. Li, "Effect of hybrid ratio and laminate geometry on compressive properties of carbon/glass hybrid composites," *Fibers Polym.*, vol. 17, no. 1, pp. 117–129, Jan. 2016.

[15] C. N. Herath, B. B. Hwang, B. S. Ham, J. M. Seo, and B. C. Kang, “An Analysis on the Tensile Strength of Hybridized Reinforcement Filament Yarns by Commingling Process,” *Mater. Sci. Forum*, vol. 539–543, pp. 974–978, Mar. 2007.

[16] B. Lauke, U. Bunzel, and K. Schneider, “Effect of hybrid yarn structure on the delamination behaviour of thermoplastic composites,” *Compos. Part A Appl. Sci. Manuf.*, vol. 29, no. 11, pp. 1397–1409, Nov. 1998.

[17] E. Mäder, C. Rothe, and S.-L. Gao, “Commingled yarns of surface nanostructured glass and polypropylene filaments for effective composite properties,” *J. Mater. Sci.*, vol. 42, no. 19, pp. 8062–8070, Oct. 2007.

[18] H. Fukunaga, T.-W. Chou, and H. Fukuda, “Strength of Intermingled Hybrid Composites,” *J. Reinf. Plast. Compos.*, vol. 3, no. 2, pp. 145–160, Apr. 1984.

[19] C. E. Bakis, A. Nanni, J. A. Terosky, and S. W. Koehler, “Self-monitoring, pseudo-ductile, hybrid FRP reinforcement rods for concrete applications,” *Compos. Sci. Technol.*, vol. 61, no. 6, pp. 815–823, May 2001.

[20] Y. J. You, Y. H. Park, H. Y. Kim, and J. S. Park, “Hybrid effect on tensile properties of FRP rods with various material compositions,” *Compos. Struct.*, vol. 80, no. 1, pp. 117–122, 2007.

[21] S. Pimenta and P. Robinson, “Modelling the tensile response of unidirectional hybrid composites,” *ECCM-16TH Eur. Conf. Compos. Mater. Seville, Spain*, no. June, pp. 22–26, 2014.

[22] A. A. J. M. Peijs and J. M. M. de Kok, “Hybrid composites based on polyethylene and carbon fibres. Part 6: Tensile and fatigue behaviour,” *Composites*, vol. 24, no. 1, pp. 19–32, Jan. 1993.

[23] L. Mishnaevsky and G. Dai, “Hybrid carbon/glass fiber composites: Micromechanical analysis of structure–damage resistance relationships,” *Comput. Mater. Sci.*, vol. 81, pp. 630–640, Jan. 2014.

[24] H. Yu, K. D. Potter, and M. R. Wisnom, “A novel manufacturing method for aligned discontinuous fibre composites (High Performance-Discontinuous Fibre

method)," *Compos. Part A Appl. Sci. Manuf.*, vol. 65, pp. 175–185, Oct. 2014.

[25] J. M. Finley, H. Yu, M. L. Longana, S. Pimenta, M. S. P. Shaffer, and K. D. Potter, "Exploring the pseudo-ductility of aligned hybrid discontinuous composites using controlled fibre-type arrangements," *Compos. Part A Appl. Sci. Manuf.*, vol. 107, pp. 592–606, Apr. 2018.

[26] A. A. J. M. Peijs and R. W. Venderbosch, "Hybrid composites based on polyethylene and carbon fibres Part IV Influence of hybrid design on impact strength," 1991.

[27] G. Marom, S. Fischer, F. R. Tuler, and H. D. Wagner, "Hybrid effects in composites: conditions for positive or negative effects versus rule-of-mixtures behaviour," *J. Mater. Sci.*, vol. 13, no. 7, pp. 1419–1426, Jul. 1978.

[28] H. Diao, A. Bismarck, P. Robinson, and M. R. Wisnom, "Production of continuous intermingled CF/GF hybrid composite via fibre tow spreading technology," *Eccm16 - 16Th Eur. Conf. Compos. Mater.*, no. June 2014, p. 8, 2014.

[29] H. Diao, P. Robinson, M. R. Wisnom, and A. Bismarck, "Unidirectional carbon fibre reinforced polyamide-12 composites with enhanced strain to tensile failure by introducing fibre waviness," *Compos. Part A Appl. Sci. Manuf.*, vol. 87, pp. 186–193, Aug. 2016.

[30] "Carbon Fiber - TORAY T700SC-12000-60E." [Online]. Available: https://www.900gpa.com/en/product/fiber/CF_004D1BB2D0?u=metric. [Accessed: 03-Jun-2019].

[31] "Technical Data sheet Glass Fiber PPG HYBON 2002." [Online]. Available: https://www.900gpa.com/en/product/fiber/GF_009729965F?u=metric.

[32] "Araldite ® LY564 Aradur ® 2954 Advanced Materials Araldite ® LY 564* / Aradur ® 2954*, Technical data sheet Huntsman."

[33] V. Koncherry, P. Potluri, and A. Fernando, "Multi-Functional Carbon Fiber Flat Tape for Composites," The University of Manchester, Manchester, UK, 2013.

[34] H. Yu, M. L. Longana, M. Jalalvand, M. R. Wisnom, and K. D. Potter, "Pseudo-

ductility in intermingled carbon/glass hybrid composites with highly aligned discontinuous fibres," *Compos. Part A Appl. Sci. Manuf.*, vol. 73, pp. 35–44, Jun. 2015.

[35] "ASTM D3039 Standard Test Method for Tensile Properties of Polymer Matrix Composite Materials -D3039 2008, Annual Book of ASTM Standards."

[36] "ASTM Standard Test Methods for Density and Specific Gravity (Relative Density) of Plastics by Displacement D792-2013."

[37] M. J. Pitkethly and M. G. Bader, "Failure modes of hybrid composites consisting of carbon fibre bundles dispersed in a glass fibre epoxy resin matrix," *J. Phys. D. Appl. Phys.*, vol. 20, no. 3, pp. 315–322, Mar. 1987.

[38] H. Diao, A. Bismarck, P. Robinson, and M. R. Wisnom, "Production of continuous intermingled CF/GF hybrid composite via fibre tow spreading technology," *Eccm16 - 16Th Eur. Conf. Compos. Mater.*, no. June 2014, p. 8, 2014.

Chapter 4: Process Development and Evaluation of Micro-Wrapped Hybrid Tows

This chapter describes a novel process for dry fibre architecture to produce low-cost preforms in order to improve the ductility of high-performance composites. The hybridisation of two different dry fibres with different failure strain was carried out through a micro-wrapping process where low strain filament was kept straight in the core and high strain filament stayed as a sheath and produced a core-shell design hybrid tow. In order to compare the micro-wrapped hybridisation process to another type of hybridisation, a side-by-side parallel hybrid process was considered. The effect of micro-wrapping hybridisation on the tensile properties of dry hybrid tows and single hybrid tow composite rods was investigated.

4.1 Introduction

Composite materials, in particular, high-performance fibre reinforced composites, play a significant role in structural applications due to their high specific strength and stiffness. However, inherent brittleness and low toughness of these materials partially limit their uses. Hence, it is important to produced high-performance composite with inherent ductile properties which can increase the opportunity of its structural applications. Appropriate dry fibre hybrid architecture can improve the composites inherent ductile properties and also change the damage propagation mechanisms leading to ultimate failure [1]. Therefore, the filament stage dry fibre hybrid architecture used to prepare low-cost textile preforms for ductile composites is a challenging topic in the high-performance composite research. Tavares *et al*. [2] numerically and analytically studied the effect of fibre hybridisation on the tensile failure of a bundle of dry fibres and unidirectional composites. As the filaments and filament tows are the fundamental objects in fibre reinforced hybrid composite, it is very important to understand the interaction phenomena between the two fibres in terms of strength and strain. Their dry fibre study showed that fibre volume fraction of two different fibre (LS and HS) is

important to achieve a progressive failure of the hybrid bundle of fibres. They achieve the pseudo-ductile response with a volume fraction of 12.5 to 25% of LS fibre. So, this study aims to maintain about 20% LS fibre volume fraction during the design of the hybrid configuration.

The hybridisation can be done on a small scale (fibre, filament or tow) or on a large scale (layers, protrusions). The intra-yarn hybrid architecture can be formed by mixing different fibres by using different techniques such as side-by-side [3], [4], commingling [5], [6] and co-wrapping [7]–[10]. Conventional co-wrapped hybrid yarn such as nylon/cotton, polyester/wool and PLA/hemp have been prepared by wrapping the parallel short fibre strand with continuous multifilament yarn [11], [12]. The researchers have been using the conventional idea for the production of reinforced material for thermoplastic composites where the high elongation thermoplastic matrix filament such as nylon, polyester or polypropylene wrapped around a low elongation fibre stand such as carbon or glass. Recently, the tensile properties of glass/polyester co-wrapped hybrid yarns and side by side hybrid yarn have been studied by Mirdehghan *et al.* ([8]. They found that the breaking load was increased by 62% for the co-wrapped hybrid yarn in comparison with the side by side hybrid yarn. Previous studies also reported that the wrapping angle and density play a significant role in the tensile properties of the wrapped yarn [13]–[15]. Xu *et al.* [10] studied the tensile properties of the glass/PEEK co-wrapped hybrid yarn composites under different processing conditions and found that tensile properties of the composites vary with processing temperature. Most of the above researchers have used the co-wrapped hybrid yarn for the manufacturing of thermoplastic composites. So far, there are no published works available on the tensile behaviour study of micro-wrapped hybrid yarn in thermoset composites. Therefore, this research focused on the production of micro-wrapped hybrid tow for the manufacture of inherent ductile thermoset composites.

On the other hand, the researchers are using the core-shell technique to improve the flexural and ductile properties of the composites. Abbott and Freischmidt [16], [17] have investigated the flexural properties of the composites manufactured from helically wrapped yarn. They found that the wrapped yarn composites bent in a ductile manner with a specific bending stiffness comparable to those of steel and aluminium. Liang *et al*. [18] investigated pseudo-ductility of carbon/glass rods in two different hybrid forms, randomly distributed and core-shell design. As can be seen in Figure 4.1, randomly

dispersed rods break at the failure strain of carbon fibre, whereas some degree of pseudo-ductility was claimed with the core-shell approach, but the stress-strain diagram showed a big stress drop during the transition phase. The study used lower strain (higher modulus) material as the sheath and higher strain (lower modulus) material as the core. This core-shell approach showed interesting results as shown in Figure 4.1 some degree of ductility was observed in the core-shell configuration in comparison to randomly dispersed structure. Tepfers *et al*.[19] reported that aramid fibre braid around the unidirectional carbon fibre core in an epoxy matrix shows a ductile behaviour during the tensile loading. So far, there are no studies that investigated the effect of micro-wrapping hybridisation on the pseudo-ductility of high-performance composites.

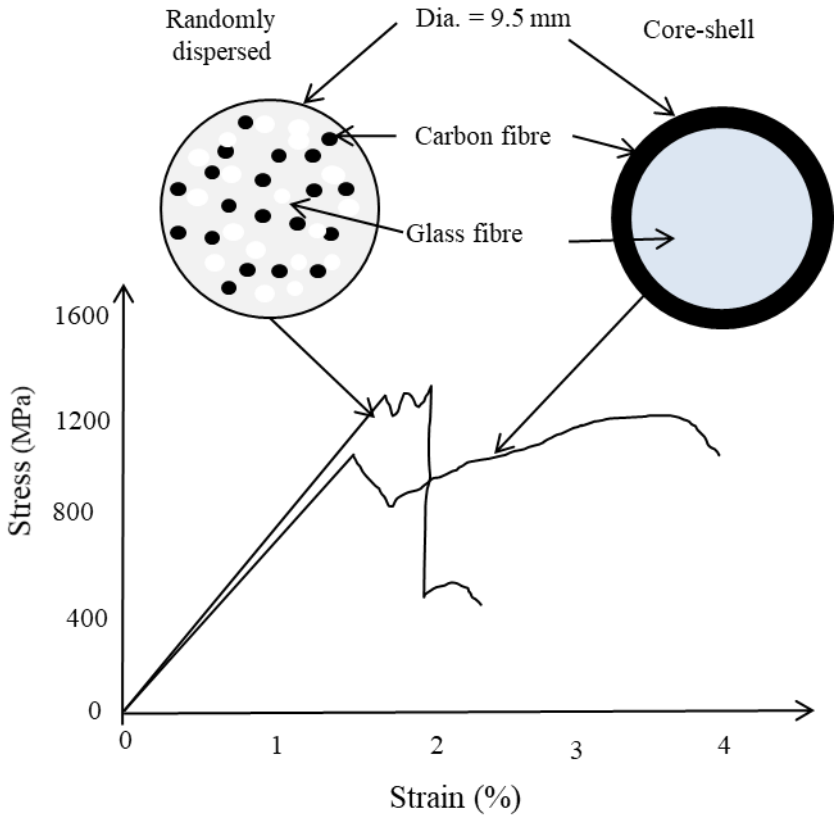

Figure 4.1: Schematic of the stress-strain graph of randomly dispersed and core-shell type composites rods [18].

Alternatively, recently researchers have shown an increased interest in thin ply technology, combining carbon and glass thin plies to achieve pseudo ductility [20]. One

of the recent studies revealed that all-carbon thin-ply hybrids composites exhibited gradual failure and demonstrated pseudo-ductility with high stiffness [21]. Thin ply angle-ply laminates also have shown pseudo-ductile response through fibre rotation and matrix plasticity [22] The limitation of this kind of composites is the higher manufacturing cost to produce the thicker panels. The interesting finding of this study is that the outer, high strain material layers should be thick and strong enough to take the load after low strain material failure.

However, it is clear from the previous studies, that appropriate design of preform hybrid architecture can delay catastrophic failure by permitting progressive breakage of low strain to failure fibre and smoothly transferring the load from broken to the undamaged high strain to failure fibres. Hence, the combination of thin ply, angle ply and core-shell design concepts provide the opportunity to develop a novel dry fibre architecture for manufacturing textile preform for pseudo-ductile composites. To achieve this, micro-wrapped hybrid architecture was chosen to produce low-cost hybrid preform for high-performance composite. The hybridisation of two different dry fibres with dissimilar failure strain was done through the micro-wrapping process. Tensile properties of the dry micro-wrapped hybrid tow and micro-wrapped hybrid tow epoxy composite rods (mesoscale) were investigated and compared with side by side hybrid architecture.

4.2 Experimental

4.2.1 Materials

Table 4.1: Properties of different carbon and glass fibres [23]–[26]

Fibre Type	Carbon T700 60E	Carbon M55J	E-glass 2002	Glass S2 (758-AB-675)
Manufacturer	Torayca	Torayca	Hybon	AGY
Tensile strength (MPa)	4900	4020	2290	3660
Tensile Modulus (GPa)	230	540	75	89
Tensile strain (%)	2.1	0.8	4.8	5.7
Filament Diameter (µm)	7	5	17	14
Density (g/cm^3)	1.80	1.91	2.59	2.49
Tex (g/1000m)	800	218	2400	735

In order to produce the micro-wrapped hybrid tow Hybon (type 2002) E-glass fibre (E-G), AGY S-glass fibre (S-G), Torayaca 6K high modulus carbon fibre tow (M55J) and Torayaca 6K and 12K high tenacity carbon fibre tow (T700 60E) were used. Details of the fibre properties are summarised in Table 4.1. Technical datasheet of Torayca, AGY and Hybon. Araldite ® LY 564, a low molar mass di-glycidyl ether of bisphenol A (DGEBA)/ butane diol di-glycidyl ether resin and Aradur ® 2954 (2, 2′-dimethyl-4.4′-methylene bis (cyclohexylamine) hardener (both Huntsman Advanced materials) were used as a matrix. Details of matrix properties were shown in chapter 3 (Table 3.2).

4.2.2 Process development

In order to produce the micro-wrapped hybrid tow, a new process was designed and assembled in the laboratory. In this process, hybridisation of two different dry fibres with different strain to failure was carried out through a micro-wrapping process where low strain filament was kept straight in the core and high strain filament wrapped the core filament by a helical path and produced a core-shell type hybrid tow. Flow chart and schematic of the micro-wrapped hybrid tow manufacturing process is shown in Figure 4.2. The machine consists of the following units; core filament let-off, sheath filament wrapping, speed control nipping roller and winding system.

4.2.2.1 Let off unit of core filament:

A let-off unit was built on the metallic stand where a bobbin holder was clamped on it. Core filament bobbin was placed on the bobbin holder. Here, the core tow from the bobbin was let-off under control back tension from the bobbin holder in order to avoid inserting twist in the core filament during the wrapping process. Then the tow passed through the eyelet to maintain the correct path to feed the wrapping unit.

4.2.2.2 Wrapping unit:

The wrapping unit was set up on a metal table. This unit consists of a hollow bobbin holder for holding the wrapper filaments bobbin and a control drive motor. The bobbin holder receives the drive from the motor through a belt. The core filament passed through the hole of the wrapper bobbin holder and the wrapper filaments wrapped around the core filaments. The number of wraps on the micro-wrapped hybrid tow was controlled by controlling the spread of the motor.

4.2.2.3 Speed control nipping roller:

After the core tow wrapped by wrapping filament tow, the wrapped tow passed through the positive drive nipping roller. The line speed was controlled by controlling the nipping roller speed.

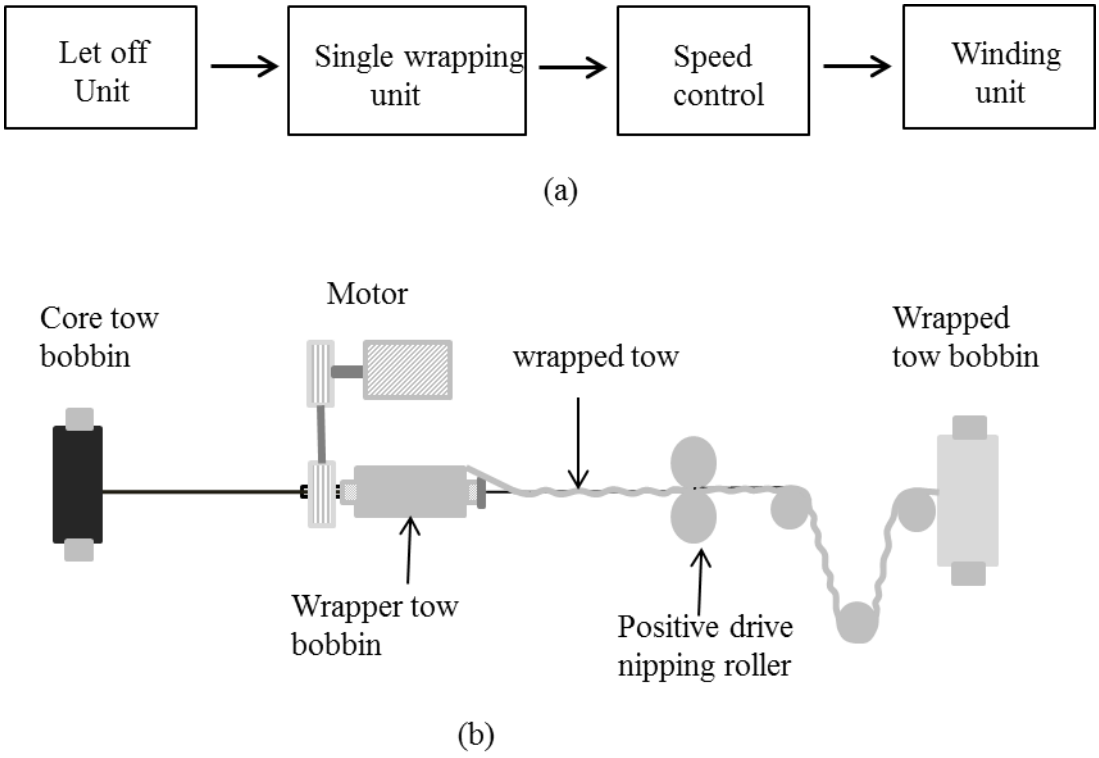

Figure 4.2: (a) Flow chart and (b) schematic of the micro-wrapped hybrid tow manufacturing process.

4.2.2.4 Winding unit:

Finally, the wrapped hybrid tow was wound on a bobbin under tension by the cross winding method.

4.2.3 Parameter selection of micro-wrapped hybrid tow

The wrapping angle and density play a significant role in the tensile properties of the wrapped yarn. Behery *et al*. [13] investigated the different wrapped yarn which was spun from polyester staple fibre with various continuous filament yarn. The study showed that the wrapped yarn with a higher wrapping density and higher linear density of the wrapping continuous filament yarn had higher strength. The effect of twist and fineness on tensile behaviour of high-performance multifilament yarn has been studied by researchers [14], [15]. The experimental results revealed that the yarn strength

increased up to a certain range of twist. A significant yarn performance was achieved for twist levels up to 20 turns /m [14]. There is an optimal twist angle of around 7° at which the filament yarn has shown maximum tensile strength [15] but the strain to failure of the twisted filament yarn increased with the increase of twist angle.

As the purpose of this research was to prepare the core and sheath type micro-wrapped hybrid tow from different high-performance filament tow, therefore low wrapping angle and lower number of wraps per metre were considered. In order to achieve the 7° wrapping angle, 27 wraps per metre were inserted over the core tow. In order to produce the micro-wrapped hybrid tow different hybrid configurations were selected. Four different types of micro-wrapped hybrid tows were prepared for this study with different hybrid configuration.

4.2.4 Preparation of micro-wrapped hybrid tow

The following types of micro-wrapped hybrid tows were produced:

4.2.4.1 Preparation of T700 and E-G micro-wrapped hybrid tow

In this process, 6K high tenacity carbon fibre (T700) tow (core) was wrapped with 2400 tex E-glass fibre (E-G) roving (sheath). T700 bobbin was placed on the bobbin holder of the let-off unit and then the tow passed through the eyelet to maintain the correct path to feed the wrapping unit. Then carbon tow passed through the hollow bobbin holder of the wrapping unit. A bobbin containing 2400 tex E-G roving was placed on a hollow bobbin holder on the wrapping unit. The bobbin holder receives the drive from the motor through a belt drive where the number of wraps per unit length was controlled. After that, the micro-wrapped hybrid tow passed through the tension and speed control roller. Finally, the hybrid tow was wound on a bobbin by a cross winding method. The core tow was helically wrapped at around 27 wraps per metre. Figure 4.3(a) shows the photograph of the micro-wrapped hybrid tow production line. Figure 4.3(b) shows that 2400 tex E-G roving was wrapping around a 6K T700 tow and the wrapped tow was wound on a bobbin by the cross winding method Figure 4.3(c). The produced micro-wrapped tow was the core-sheath type where T700 carbon tow (core) was helically surrounding by E-G (sheath). The resultant linear density of the hybrid tow was 2824 tex. The volume fraction of T700 carbon and E-G fibre in the micro-wrapped hybrid tow was 19.20 and 80.80% respectively. The hybrid tow was labelled as T700/E-G micro-wrapped hybrid tow.

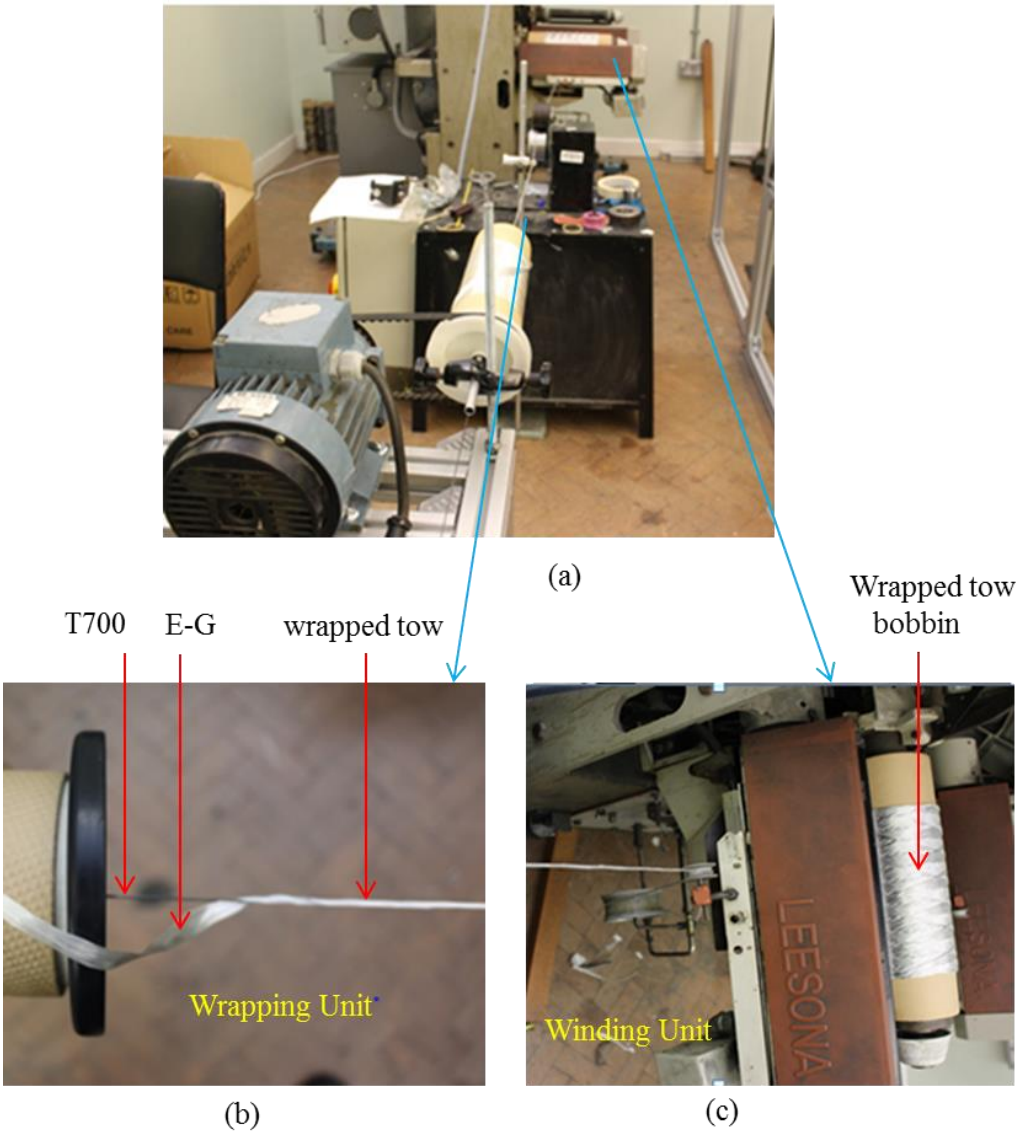

Figure 4.3: (a) Photograph of the micro-wrapped hybrid tow production line (b) 2400 tex E-G roving was wrapping around a 6K T700 carbon tow and (c) micro-wrapped tow was winding on a bobbin.

4.2.4.2 Preparation of T700 and S-G micro-wrapped hybrid tow

Three plies of 735 tex S-G roving were parallelly wound onto a bobbin without a twist with the resultant linear density of 2,205 tex. This S-G roving was then helically wrapped around the 6K T700 carbon tow at 27 wraps per metre where the T700 carbon tow stayed as core and S-G as the helical sheath. After wrapping, the hybrid tow was cross-wound onto a bobbin. The resultant linear density of the micro-wrapped tow was 2627 tex. The volume fraction of the T700 carbon and S-G fibre in the micro-wrapped

hybrid tow was 20 and 80% respectively. The hybrid tow was labelled as T700/S-G micro-wrapped hybrid tow.

4.2.4.3 Preparation of M55 and T700 micro-wrapped hybrid tow

The 6K M55 carbon tow was helically wrapped with 12K T700 carbon at 27 wraps per metre. The resultant linear density of the micro-wrapped tow was 1026 tex and the volume fraction of M55 and T700 in the hybrid tow was 20.3% and 79.7% respectively. The hybrid tow was marked as M55/T700 micro-wrapped hybrid tow.

4.2.4.4 Preparation of M55 and S-G micro-wrapped hybrid tow

Two plies of 735 tex S-G roving were parallel wound onto a bobbin without a twist with the resultant linear density of 1470 tex. This S-G roving was then helically wrapped around the 6K M55 where M55 stay as a core and S-G as a sheath. The resultant linear density of the micro-wrapped tow was 1702 tex. The volume fraction of the M55 and S-G in the micro-wrapped hybrid tow was 16 and 84% respectively. The hybrid tow was labelled as M55/S-G micro-wrapped hybrid tow.

Schematic illustration and optical microscopic images of the different micro-wrapped hybrid tows are shown in Figure 4.4. The images clearly show that the low strain to failure filament tow (core) is fully covered with high strain to failure filament tow (sheath) with a helix angle. There was no noticeable damage to the filament in the micro-wrapped hybrid tow. Parameters of the different micro-wrapped hybrid tows are presented in Table 4.2.

Table 4.2: Properties of the different micro-wrapped hybrid tows

Micro-wrapped hybrid configuration	Linear density (Tex)±SD	No of wraps (per metre) ±SD	Angle of wrap (degree) ±SD	Volume of LS fibre (%)	Volume of HS fibre (%)
T700/E-G	2824±1.84	26.84±1.61	7.63±0.99	19.20	80.80
T700/S-G	2627±1.65	27.12±1.80	7.75±0.96	20.00	80.00
M55/T700	1026±1.11	26.74±1.82	7.72±0.98	20.30	79.70
M55/S-G	1702±1.25	27.07±2.00	7.90±1.24	16.00	84.00

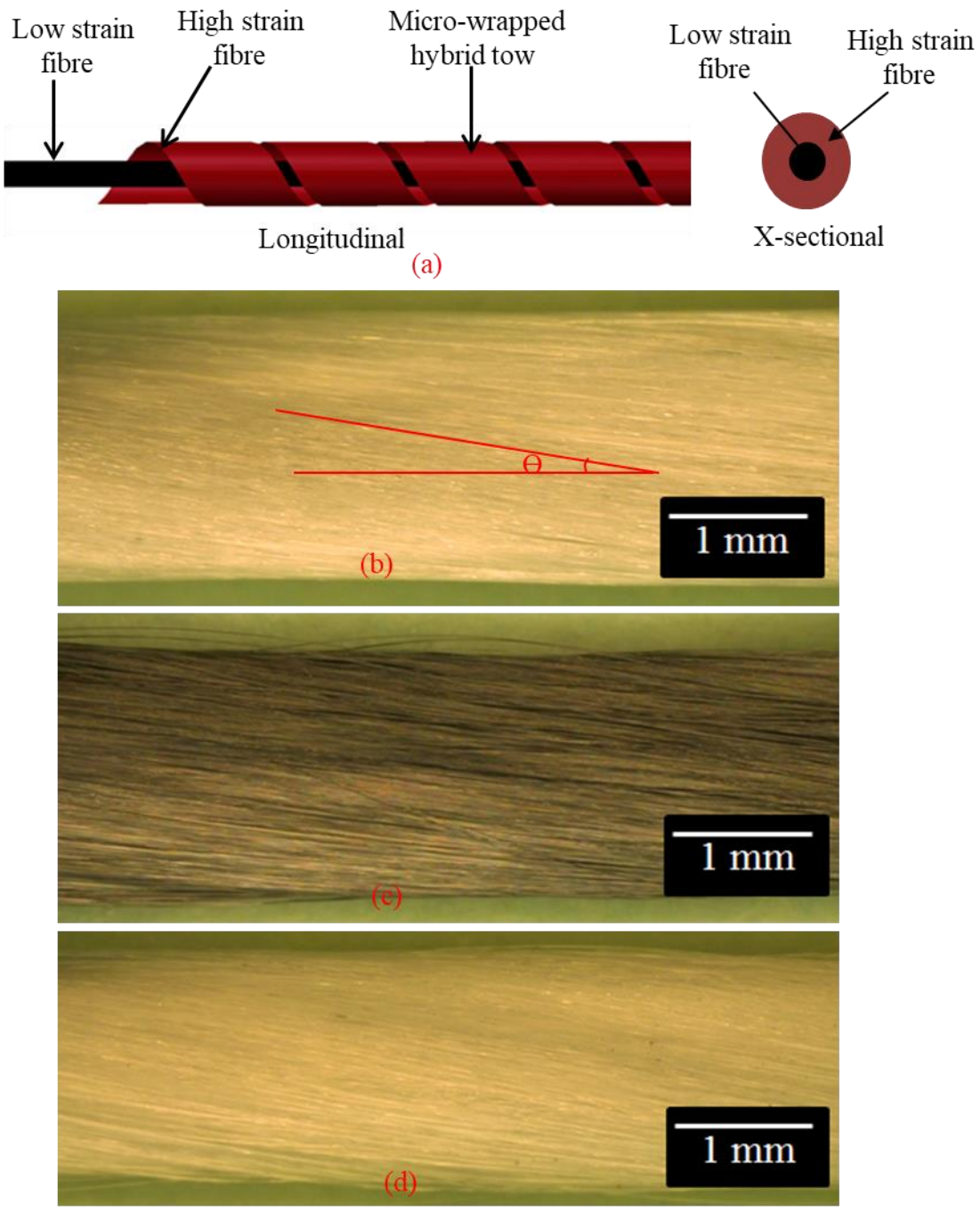

Figure 4.4: (a) Schematic illustration of micro-wrapped hybrid tow, (b), (c) and (d) typical optical microscopic images of T700/S-G, M55/T700 and M55/S-G micro-wrapped hybrid tows.

4.2.4 Preparation of side-by-side hybrid tows

In order to compare micro-wrapped hybridisation process to another type of hybridisation, a side-by-side parallel hybrid process was considered. In this process, hybrid tows were prepared by the parallel winding of low and high strain to failure

material simultaneously without wrapping or twisting. In this process, two different strain to failure materials were kept parallel to the same axial direction. Hybrid configurations similar to those of micro-wrapped tows were considered for preparing side-by-side hybrid tows. Figure 4.5 shows the schematic illustration and optical microscopic images of the different side by side hybrid tows.

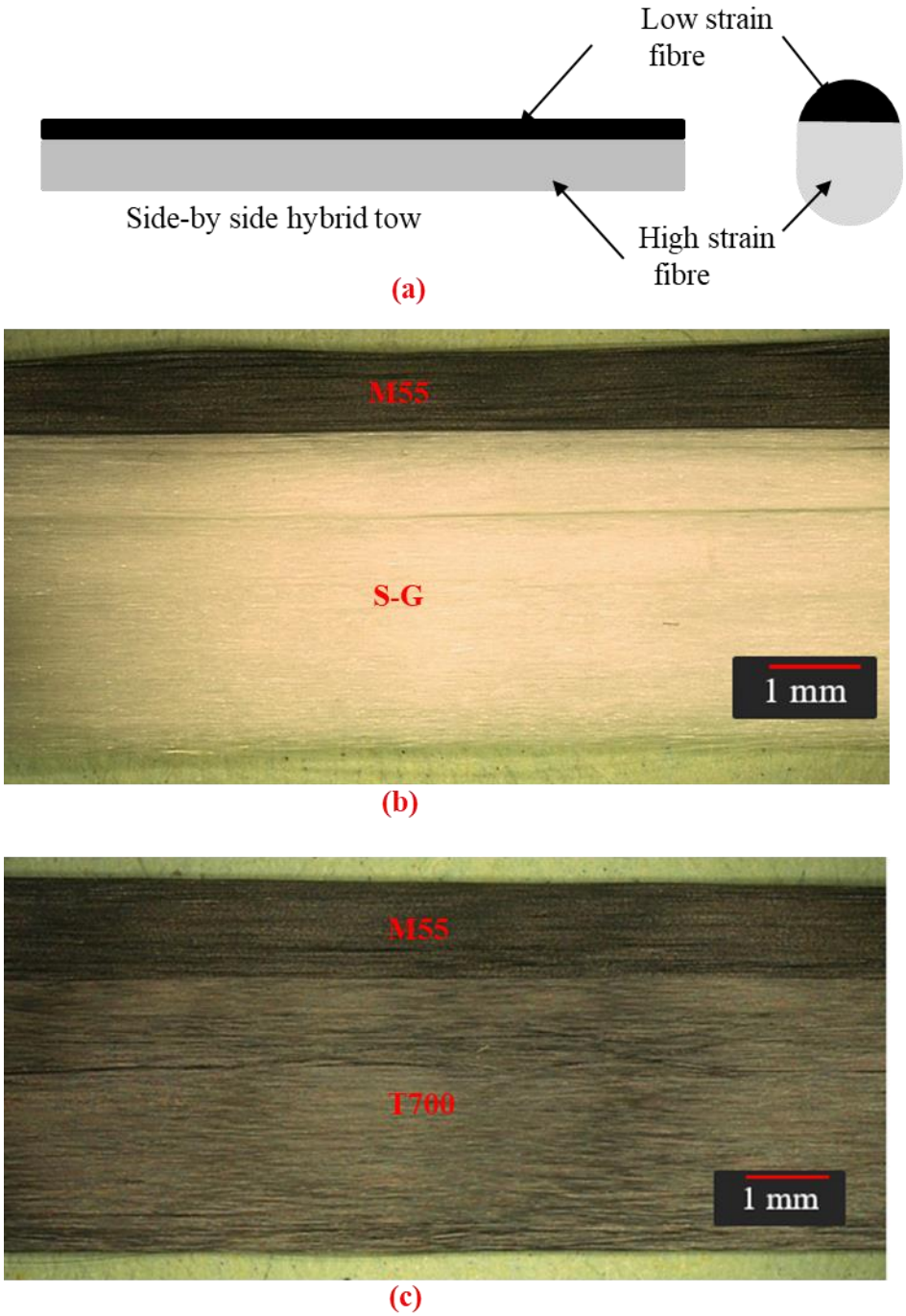

Figure 4.5: Schematic illustration of side by side hybrid tow, (b) and (c) typical optical microscopic images of M55/S-G and M55/T700 side by side hybrid tows.

4.2.5 Tensile testing of dry fibre tow

The tensile tests of hybrid tows at dry state were carried out according to ASTM D 2256 [27] using the Instron 3345 tester and the equipment had a 5kN load cell. Before closing the end grips, the ends of each tow specimen were wrapped around the 'horn' shaped jaws with slots for fibre tows. The grip pressure was 6 bars (Figure 4.6). The standards suggest test speeds up to 300 mm/min but to ensure enough data points are collected the specimens were tested at 100 mm/min with 250 mm gauge length. According to the standard 10 specimens from each group were tested. The tensile force was measured using a load cell at the upper clamp. The load value (F) was converted to nominal stress (σ) by using the following equation:

$$\sigma = \frac{F}{A} \qquad 4.1$$

Where A is the cross-sectional area of the tow calculated from the individual filament diameter and a total number of filaments per tow. This area corresponded to the total area of all filaments in tow or hybrid tow. The strain was calculated from the displacement divided by the gauge length.

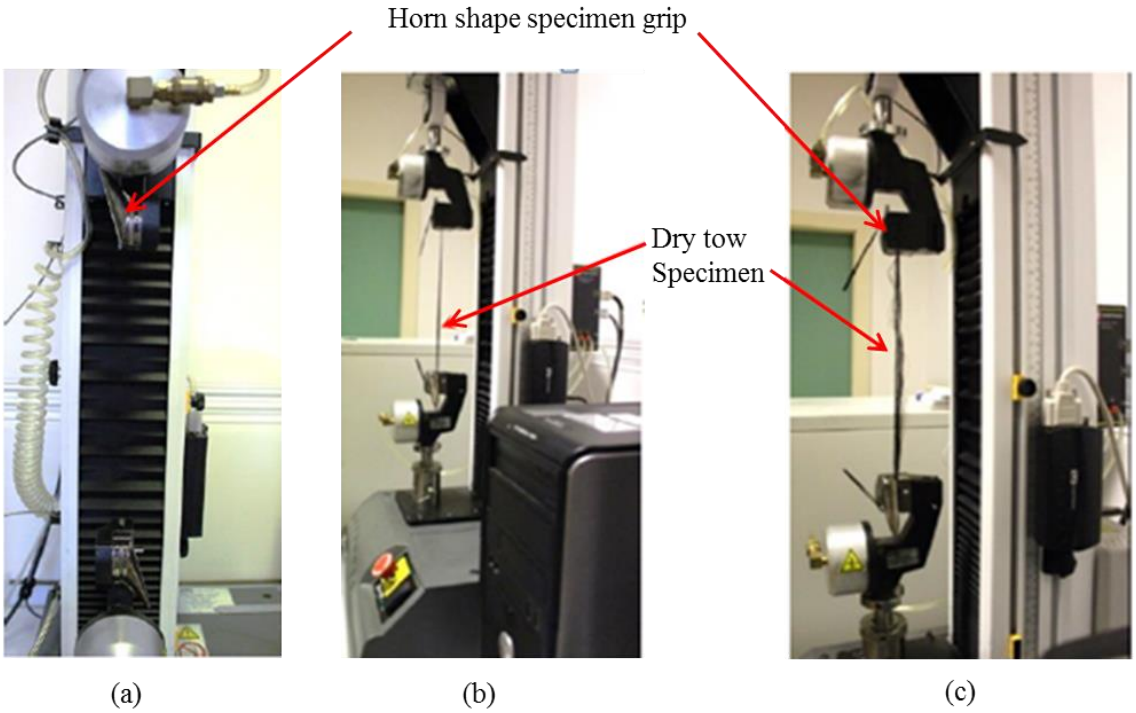

Figure 4.6: Dry tow specimen on tensile testing equipment (a) front view of the equipment; (b) tow mount on the equipment before testing and (c) tow after testing.

4.2.6 Preparation of micro-wrapped hybrid tow composite rods

To understand the tensile behaviour of micro-wrapped hybrid tow at mesoscale, single hybrid tow composite rods were fabricated by using different types of micro-wrapped and side by side hybrid tows with epoxy resin. Composite rods were manufactured using manual resin infusion process with the help of pinboard keeping the tow under tension to ensure the tow remain straight. Curing and post-curing were carried out in an oven at 80 ºC for 2 hours and 140 ºC for 6 hours. The manufacturing process of single hybrid tow composite rods is shown in Figure 4.7. List of different micro-wrapped and side by side hybrid single tow composite rods are shown in Table 4. 3.

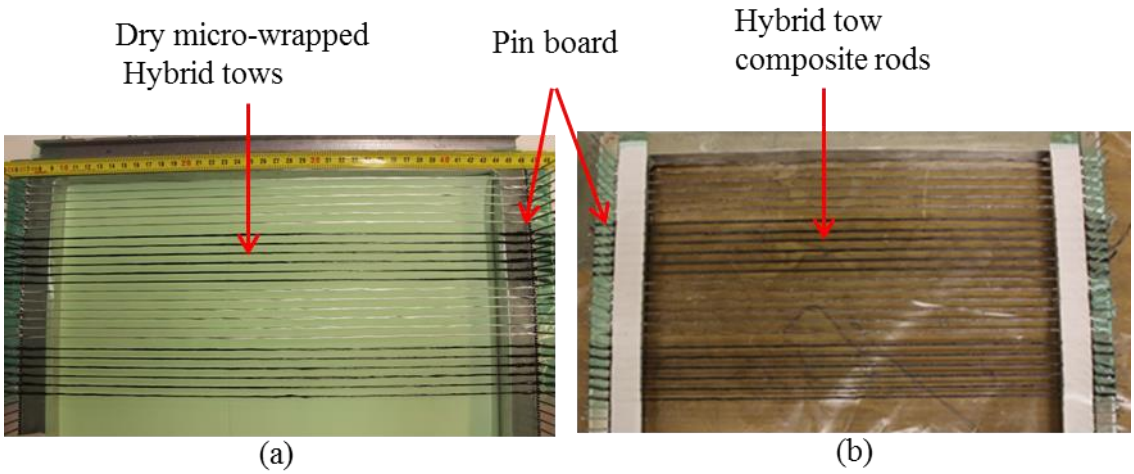

Figure 4.7: Single hybrid tow composite rod manufacturing process (a) before resin infusion (b) after resin infusion.

Table 4. 3: List of different micro-wrapped and side-by-side hybrid tow composite rods

Hybrid tow configuration	Hybrid architecture
T700/E-G	Side by side
T700/E-G	Micro-wrapped
T700/S-G	Side by side
T700/S-G	Micro-wrapped
M55/T700	Side by side
M55/T700	Micro-wrapped
M55/S-G	Side by side
M55/S-G	Micro-wrapped

4.2.7 Mechanical testing of composite rods

All the composite specimens were prepared for mechanical testing according to ASTM D 3039 [28]. End tabs made of glass fibre reinforce cross-ply plates (GFRP) with 1.60 mm thickness were bonded on the specimen using two-component Araldite 2011 A/B epoxy adhesive supplied by Huntsman. The tabbing method is shown in Figure 4.8. The two ends of the specimens were mounted inside two GFRP tabs where resin pockets were prepared with a rubber spacer (Figure 4.8a). The resin pockets were filled with Araldite 2011 A/B epoxy adhesive and closed them with another GFRP plate and binder clips (Figure 4.8b). The tabs adhesive was cured at room temperature for 48 hrs. Once the tabbing was completed, the individual samples were separated by cutting the tabbing frames using a diamond saw cutter (Figure 4.8c). Tensile tests were done under uniaxial loading on an electromechanical testing machine (Instron 5982) with a cross-head speed of 2 mm/min. The load was measured with a 100kN load cell. The strain was measured by using Imetrum Video Extensometer (IVE) with a nominal gauge length of 50 mm. The load and extension data was collected using Instron Bluehill and Imetrum Video Gauge software respectively. Five specimens were tested for each group.

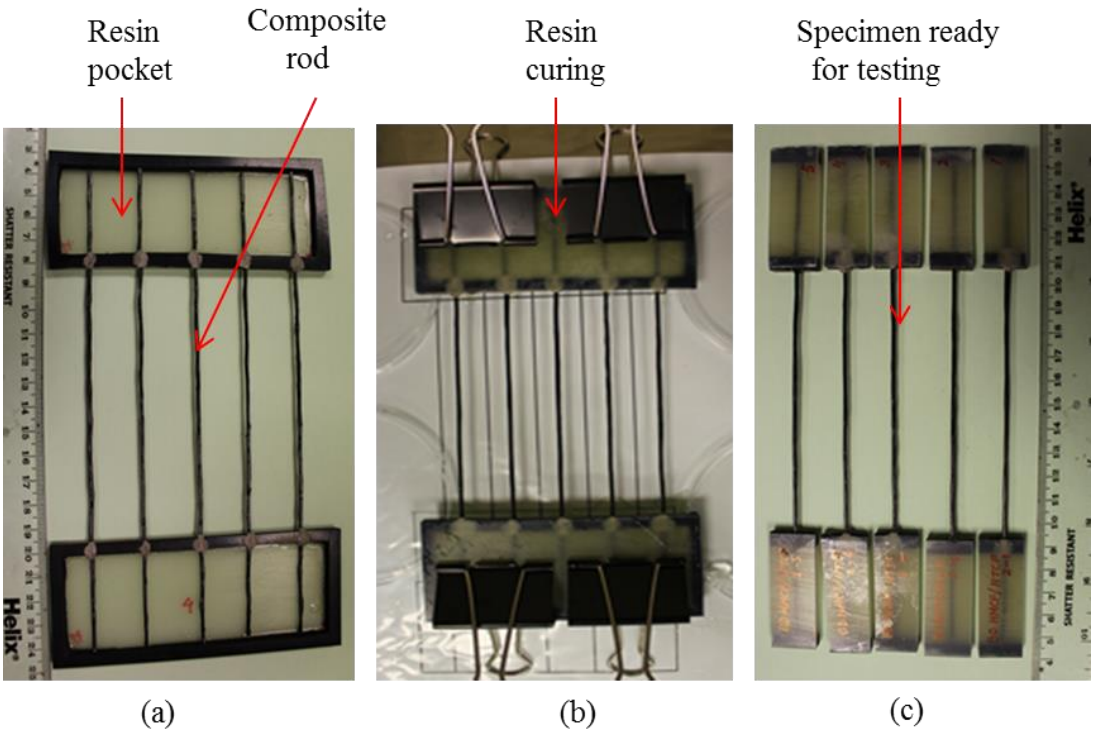

Figure 4.8: Specimen preparation for tensile testing.

4.2.8 Normalisation with fibre volume fraction

The composite samples were developed using manual resin infusion process. The cross-section area of the composites rods was not uniform along the length especially for side by side hybrid composite. Hence, only the cross-sectional area of the total number of filaments in a composite rod was used for stress calculation for all stress-strain graphs. The fibre volume fraction of different composite rods are tabulated in (Table B1, Appendix B). The data were normalised to adjust the raw test values to a single specified fibre volume fraction. An approximate 0.45 fibre volume fraction was considered.

4.2.9 Calculation of Pseudo-ductile properties:

Pseudo ductile properties of composite rods were calculated according to M. Wisnom`s definition [29]. The final modulus of the specimens was calculated by fitting lines to the straight sections of the stress-strain graph after their initial failure. Schematic of the Pseudo-ductile properties were shown in Figure 4.9.

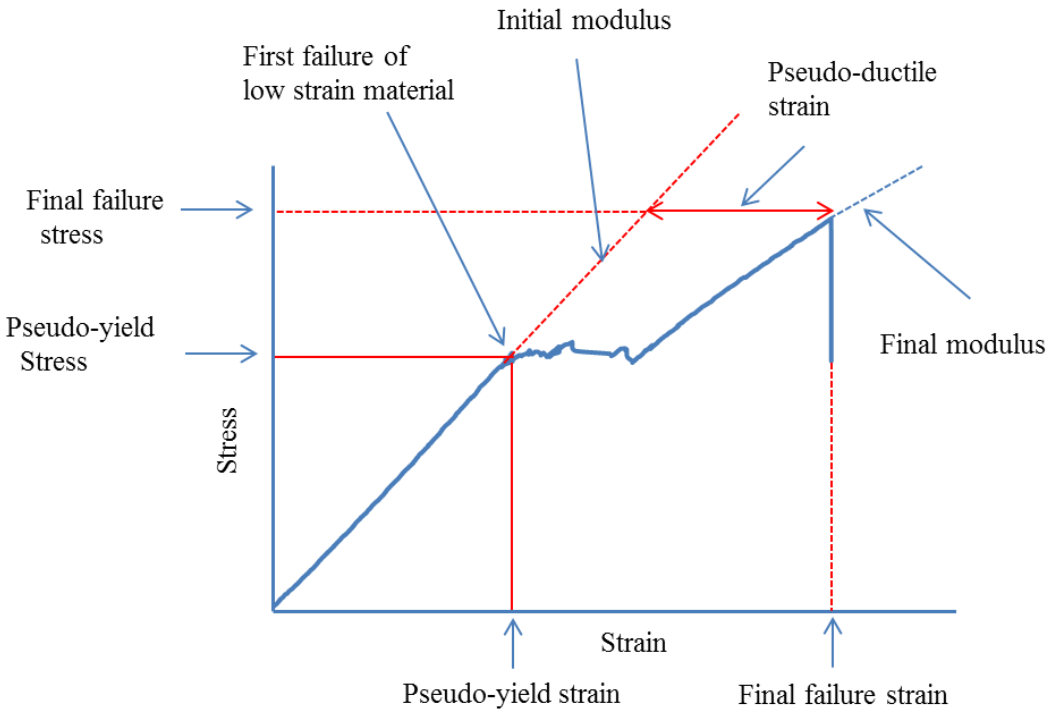

Figure 4.9: Schematic of pseudo-ductile properties.

4.3 Results and Discussion

4.3.1 Tensile behaviour of different single and hybrid dry fibre tows

In the UD composites materials, fibre and fibre tows are the important entities. The failure of the UD composites under tensile loading depends on the properties of the fibres. As the hybridisation involves the interaction between fibres that have different properties such as strength and strain, the investigation of hybrid dry fibre tows is essential to understand the interface phenomena that happened in the hybrid composites.

4.3.1.1 Tensile behaviour of different single dry fibre tows

According to the standard, ten specimens from each type of tow were tested. The average values of tensile stress and final failure strain were calculated. The summary of the tensile test results of different tows are presented in Table 4.4

Table 4.4: Summary of the tensile test of different tows

Specimen Type	T700	M55	E-G	S-G
Liner density (tex)	400	218	2400	735
Maximum Stress (MPa)	1925.1 ± 97.10	1832.3 ± 111.81	900.8±61.61	1391.4 ± 52.78
Modulus of elasticity (GPa)	156.80 ± 3.91	356.20 ± 6.90	54.28±2.46	72.02 ± 1.19
Ultimate failure strain (%)	1.89 ± 0.07	0.68 ± 0.03	2.80±0.06	3.01 ± 0.08

Tensile stress-strain curves of M55, T700, E-G and S-G single dry fibre tow are shown in Figure 4.10. The Figure clearly showed that different fibre shows different stress and strain values. T700, E-G and S-G tows filament breakage were spread over a wide range of nominal strain. These results indicate that the individual failure of filaments happened in the tow within a higher range of breaking strain. Visual observation revealed that the specimens failed with randomly breaking the filament in the tow without localisation at the same cross-section.

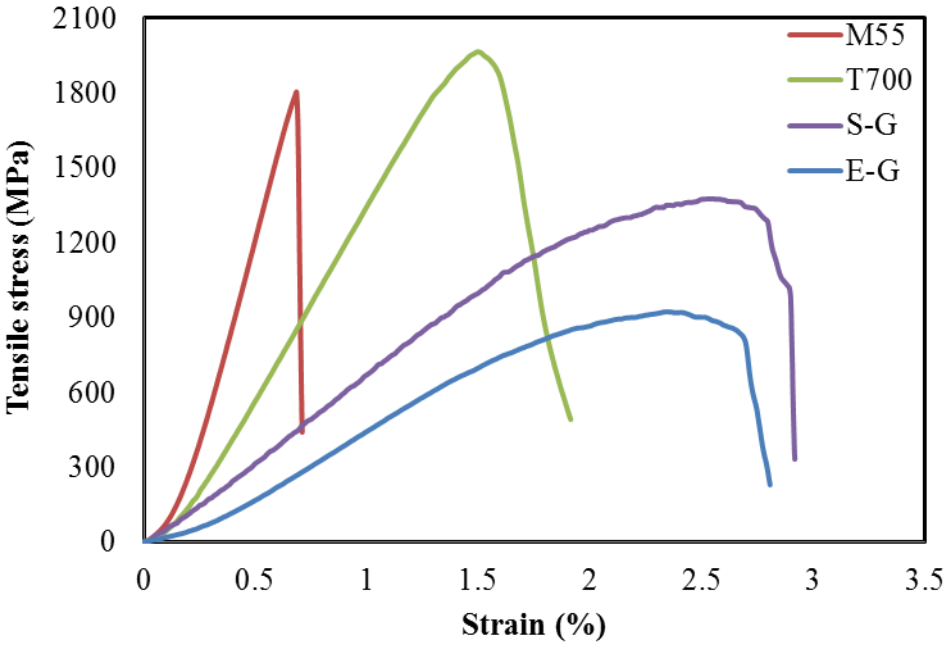

Figure 4.10: Typical stress-strain curves of different dry tows.

4.3.1.2 Tensile behaviour of T700/E-G and T700/S-G hybrid tows

Tensile stress-strain curves of the T700/E-G and T700/S-G side by side and micro-wrapped hybrid tows are shown in Figure 4.11 and Figure 4.12 respectively. The summary of the tensile tests results is presented in Table 4.5 and Table 4.6. Both hybrid configurations showed the non-linearity on their stress-strain curves. The characteristics of the initial part of the curve were similar for the side by side and micro-wrapped hybrid tows but were different after the LS filament failure. Higher stress and strain value were achieved with the micro-wrapped hybrid tows. In the T700/E-G hybrid configuration, a major load drop was observed after LS filament failure (Figure 4.11). There was less increase in the stress and strain values after initial failure. In contrast, for the T700/S-G hybrid configuration, a lower load drop was observed after LS filament failure and extended stress and strain values were observed before final failure (Figure 4.12). Higher stress drop was detected in side by side hybrid architecture than micro-wrapped one. In both configurations, higher stress and strain, values were observed with micro-wrapped hybrid tow compared to side by side hybrid tow. These results showed that there was a significant effect of the wrapping process on the hybrid tow tensile properties. The reason for the higher strength of micro-wrapped hybrid tow was that the wrapping increased the filament-filament interaction which could play an important role in filament breaking during the tensile loading and resulted in higher tow strength. The

reason for the higher failure strain of micro-wrapped hybrid tow was the helical path of the wrapper tow provided extra elongation.

Table 4.5: Summary of the tensile test results of T700/E-G hybrid tow

Specimen Type	T700/E-G SBS	T700/E-G MW
Liner density (tex)	2800±1.5	2824±1.8
Maximum stress (MPa)	1189.3±105.7	1283.2±87.5
Initial modulus (GPa)	68.8±5.3	65.5±5.3
Final modulus (GPa)	62.8±6.2	63.5±4.8
Initial failure strain (%)	2.12±0.18	2.14±0.16
Ultimate failure strain (%)	2.68±0.11	2.82±0.10

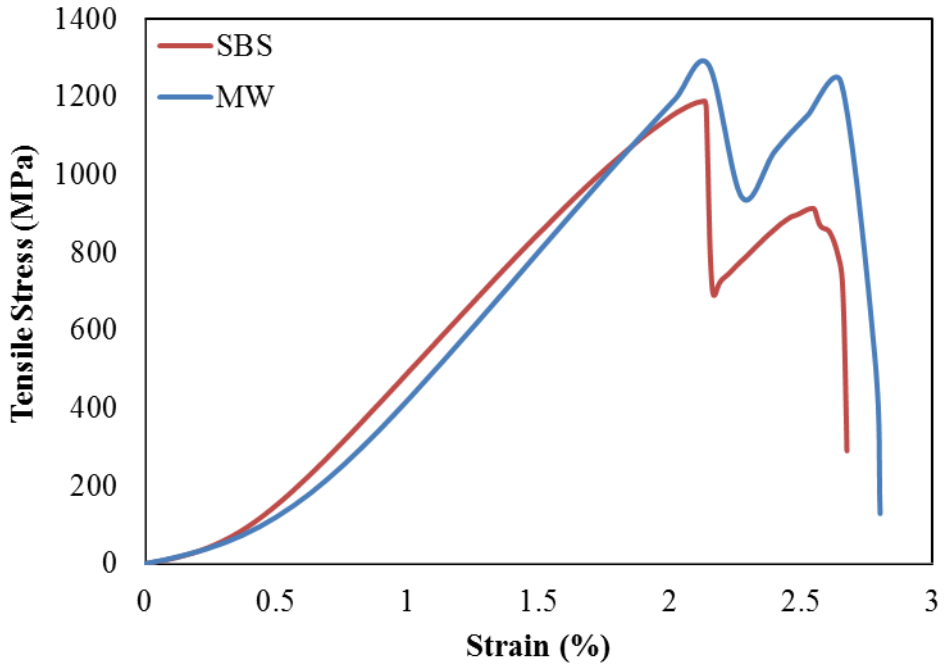

Figure 4.11: Typical stress-strain graph of T700/E-G side by side (SBS) and micro-wrapped (MW) hybrid tows.

Table 4.6: Summary of the tensile test results of T700/S-G hybrid tow

Specimen Type	T700/S-G SBS	T700/S-G MW
Liner density (tex)	2605±1.4	2627±1.65
Maximum stress (MPa)	1218.2±58.5	1392±58.62
Initial modulus (GPa)	78.5±5.6.3	75.7±2.3
Final modulus (GPa)	34.3±3.3	40.5±2.4
Initial failure strain (%)	1.75±0.18	1.82±0.12
Ultimate failure strain (%)	2.90±0.10	3.02±0.11

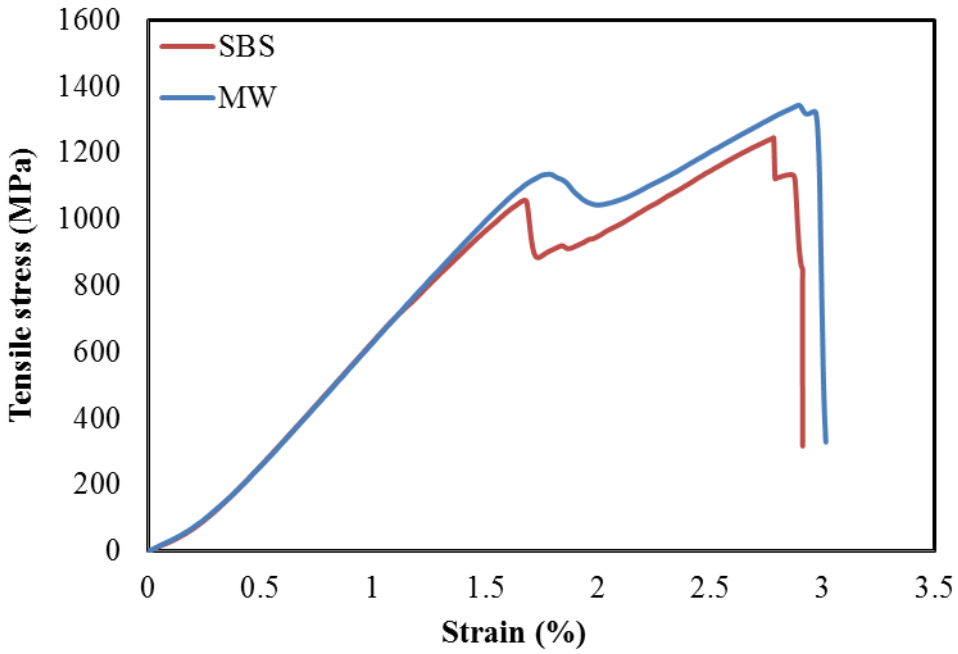

Figure 4.12: Typical stress-strain graph of T700/S-G side by side (SBS) and micro-wrapped (MW) hybrid tows.

4.3.1.3 Tensile behaviour of M55/T700 hybrid tows

To attain a higher stress and stiffness value another type of hybrid configuration was considered and studied. In this configuration, two different types of carbon fibres were selected. The M55 and T700 were used as LS and HS fibre. The summary of the tensile test results is presented in Table 4.7. Figure 4. 13 shows the stress-strain curve of M55/T700 side by side and micro-wrapped hybrid tows. A very good pseudo-ductile

response was achieved with this hybrid configuration. Both curves show the non-linearity on their stress-strain curves. There was a lower stress drop in micro-wrapped than side by side one after the failure of LS filament. The initial failure of the M55 occurred first at around 0.75% strain and then T700 carried the load and then the final failure happened. There is a significant difference in stress-strain curves between the side by side and micro-wrapped hybrid tows that were observed. Only one initial break was observed in side by side hybrid tow but multiple breaks of LS were observed in micro-wrapped hybrid tow. These results indicate that fragmentation of LS tow happened in the micro-wrapped hybrid tow. The second part of the stress-strain curve of side by side hybrid tow exhibit a similar trend to that of the T700. On the other hand, in the case of micro-wrapped hybrid tows, a sudden failure was occurred after reaching its maximum stress. Micro-wrapped hybrid tow exhibited higher stress and strain value compared to side by side hybrid tow. The initial modulus of the side by side hybrid tow was higher than the micro-wrapped hybrid tow but the final modulus was higher for micro-wrapped hybrid tow (Table 4.7). The stress-strain diagram shows that there was a larger slack for micro-wrapped tow compared to side by side which might provide the low initial modulus. It could have happened due to the extra length of the helical wrapping tow. During the production of micro-wrapped hybrid tow, some waviness could be induced that can cause large slack of the stress-strain curve of micro-wrapped hybrid tow. Failure images of M55/T700 side by side and micro-wrapped hybrid tows are shown in (Figure B1-a, Appendix B).

Table 4.7: Summary of the tensile test results of M55/T700 hybrid tows

Specimen Type	M55/T700 SBS	M55/T700 MW
Liner density (tex)	1018±1.45	1026±1.55
Ultimate stress (MPa)	1707.2±92.7	2197.3±71.5
Initial modulus (GPa)	170.2±5.7	163.08±6.3
Final modulus (GPa)	125.4±9.3	146.6±4.7
Initial failure strain (%)	0.73±0.13	0.76±0.06
Ultimate failure strain (%)	1.97±0.13	2.20±0.10

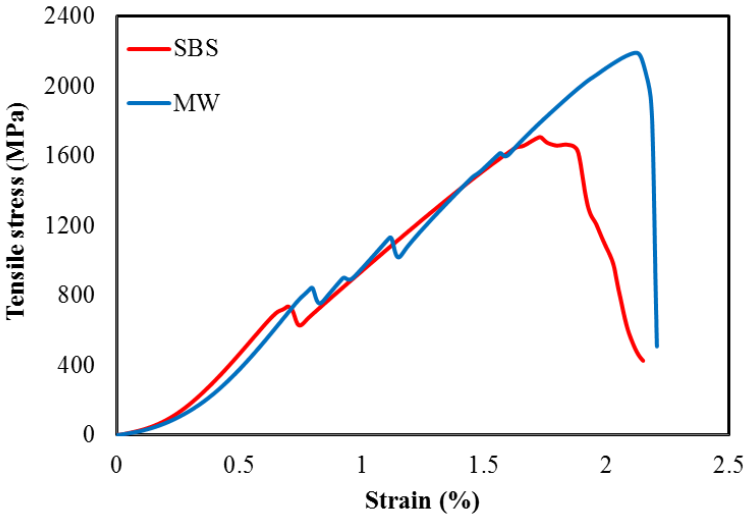

Figure 4. 13: Typical stress-strain curve of M55/T700 side by side and micro-wrapped hybrid tows.

4.3.1.4 Tensile behaviour of M55/S-G hybrid tows

To achieve the higher strain value after initial failure in hybrid composites, another hybrid configuration of M55 and S-G was also studied. The summary of the tensile test results is shown in Table 4.8. A significant difference was also observed between the side by side and micro-wrapped hybrid tow in this configuration (Figure 4.14). Higher stress and strain values were attained with micro-wrapped hybrid tow compare to the side by side hybrid tow. The initial modulus of the hybrid tow was higher than the 100% S-G tow, this increase happened due to introducing the M55. The modulus of the second part of the stress-strain curves was almost similar to that of the non-hybrid glass tow. Failure images of M55/S-G side by side and micro-wrapped hybrid tows are shown in (Figure B1-b, Appendix B).

Table 4.8: Summary of the tensile test results of M55/S-G hybrid tow

Specimen Type	M55/S-G SBS	M55/S-G MW
Liner density (tex)	1688±1.35	1702±1.60
Ultimate stress (MPa)	1317.7±112.1	1445.2±61.9
Initial modulus (GPa)	104.7±2.8	95.01±6.04
Final modulus (GPa)	59.5±2.8	69.8±3.5
Initial failure strain (%)	0.68±0.12	0.80±0.09
Ultimate failure Strain (%)	2.92±0.10	3.01±0.09

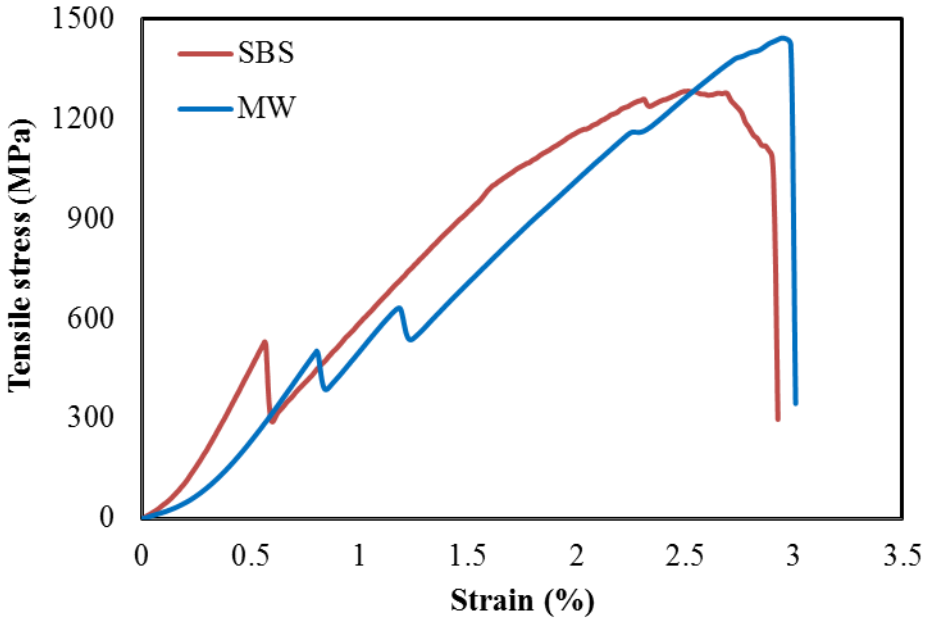

Figure 4.14: Typical stress-strain curve of M55/S-G side by side and micro-wrapped hybrid tows.

4.3.2 Tensile behaviour of hybrid tow composite rods

The dry fibre hybrid tow tensile test results showed the non-linear response of their stress-strain graphs. The results indicated that there is the opportunity to attain the pseudo-ductile behaviour in the composite with micro-wrapped hybrid architecture. To study the tensile behaviour of the micro-wrapped hybrid tow, in the mesoscale composite materials, single hybrid tow composite rods were manufactured from different types of micro-wrapped hybrid tows with epoxy resin. Side by side hybrid tow composite rods were also fabricated. Hybrid configurations similar to those of micro-wrapped tows were considered for preparing side by side hybrid tow composite rods. The list of the manufactured rods is shown in Table 4. 3. A typical example of the cross-sectional view of T700/E-G and T700/S-G micro-wrapped hybrid tow composites rods are shown in Figure 4.15. The image clearly showed that the 6K T700 core was fully wrapped with GF. Some voids were observed in the tow cross-section. The voids could have been generated during the sample preparation.

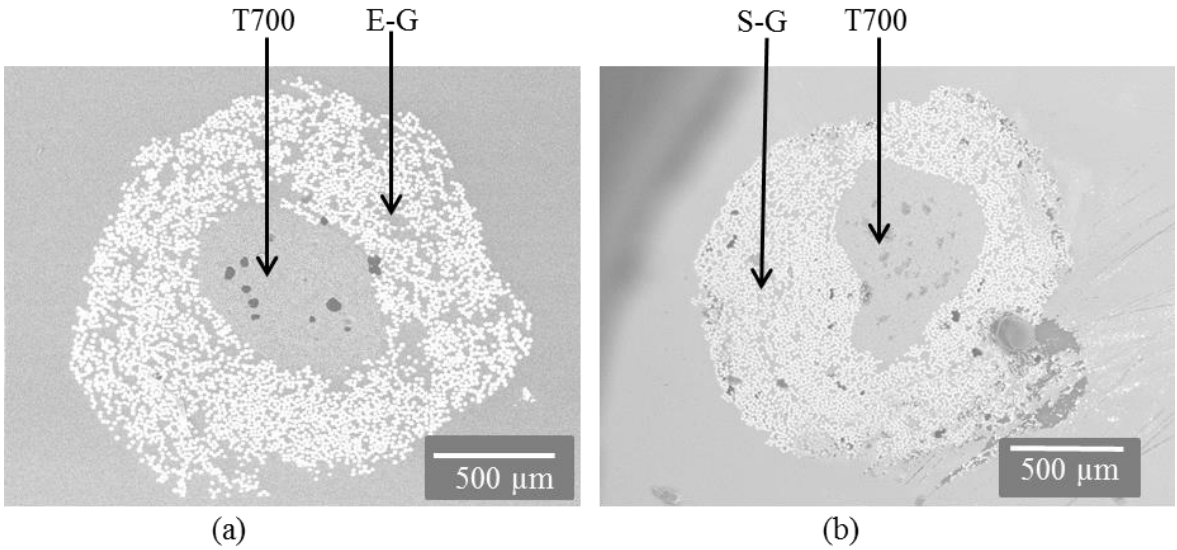

Figure 4.15: X-sectional images of micro-wrapped hybrid tow composite rods: (a) T700/E-G and (b) T700/S-G.

4.3.2.1 Tensile behaviour of T700/E-G hybrid tow composite rods

Stress-strain curves of T700/E-G side by side and micro-wrapped hybrid tow composite rods are shown in Figure 4.16a and b. Both rods of T700/E-G hybrid configuration did not demonstrate any pseudo-ductile behaviour though the dry micro-wrapped hybrid tow of this configuration demonstrated nonlinearity on their stress-strain curves. This result was not similar to the dry fibre tow but there was some hybrid effect because the final strain to failure of the composite rod was 2.09% which was higher than T700 UD composite and similar to T700/E-G spread tow hybrid UD composite (chapter 3). Tavares *et al*. [2] found similar results on their analytical and computational study of hybrid composites. They observed that the T300 carbon and alkali-resistant glass fibre hybridisation demonstrated pseudo-ductile behaviour in the tow model but did not achieve on their composite model. Their study concluded that if critical strain values of two different fibres are close to each other than this type of hybridisation did not lead to achieving the pseudo-ductile behaviour in the composites. Yu *et al.* [30] also reported similar results in their carbon/glass highly aligned discontinuous fibre composite. Their study shows that high strength carbon/E-glass hybrid composite did not show any pseudo-ductility but high modulus carbon/E-glass fibre hybrid composite show pseudo-ductile response in their stress-strain graph. The tensile test results are summarised in Table 4.9. Micro-wrapped hybrid tow composite rod show higher stress and strain value compare to the side by side hybrid tow but the modulus was higher for side by side hybrid.

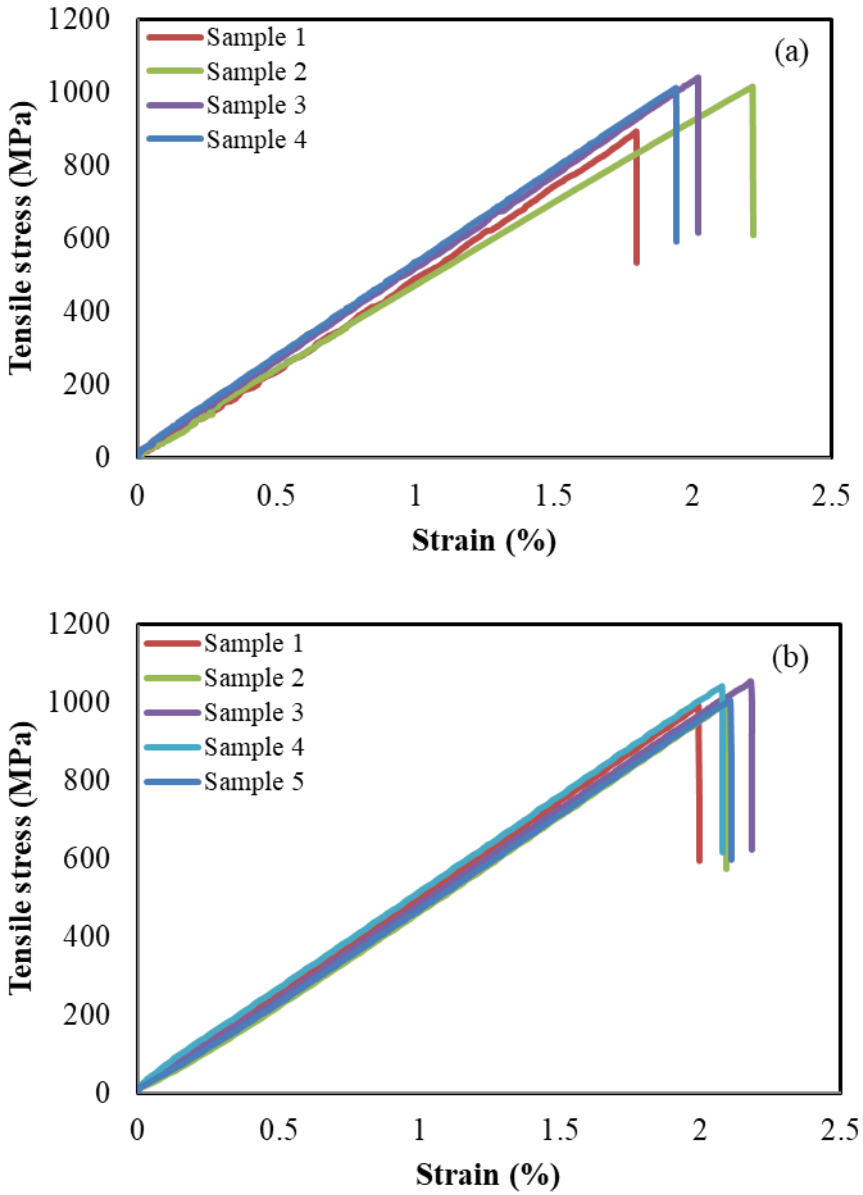

Figure 4.16: Stress-strain curves of T700/E-G (a) side by side and (b) micro-wrapped hybrid tow composite rods.

Table 4.9: Summary of the normalised tensile test results of T700/E-G hybrid tow composite rods

Specimen Type	T700/E-G SBS	T700/E-G MW
Maximum stress (MPa)	998.7±66.9	1016.5±28.3
Initial modulus (GPa)	47.9±2.90	46.54±1.33
Final failure strain (%)	2.00±0.19	2.09±0.07

4.3.2.2 Tensile behaviour of T700/S-G hybrid tow composite rods

Since the desired pseudo-ductile behaviour was not achieved with T700/E-G hybrid configuration, another hybrid configuration T700/S-G was studied. The stress-strain graphs of side by side and micro-wrapped hybrid composite rods of T700/S-G configuration are shown in Figure 4.17a and b respectively. Both graphs showed the non-linearity on their stress-strain curves during the tensile loading. Pseudo-ductile behaviour was observed with micro-wrapped hybrid tow composite rods with a little stress drop (about 12%). On the other hand, side by side hybrid did not show pseudo-ductile behaviour. A huge stress drop (about 48%) was observed after the initial failure. The Initial failure happened at a strain of 1.95% and 1.97 % for side by side and micro-wrapped hybrid rod respectively. After the initial failure glass fibre carried the load (since the S-G fibre strain to failure is higher than carbon) and final failure occurred.

Table 4.10: Summary of the normalised tensile test results of T700/S-G hybrid tow composite rods

Specimen Type	T700/S-G SBS	T700/S-G MW
Pseudo-yield Stress (MPa)	1110.35±42.96	1065.69±38.03
Stress drop (MPa)	535.55±117.38	136.66±53.15
Maximum stress (MPa)	1110.35±42.96	1134.85±50.93
Initial modulus (GPa)	52.12±3.58	50.09±1.53
Final modulus (GPa)	19.61±9.53	44.01±3.78
Pseudo-yield strain (%)	1.95±0.07	1.97±0.08
Final failure strain (%)	2.54±0.19	2.92±0.26
Difference between two failure strain (%)	0.62±0.21	0.95±0.31

In this configuration, there was no extended stress value after initial failure for side by side hybrid but some extended stress was observed for the micro-wrapped hybrid. The initial modulus of the side by side hybrid composite rod was slightly higher than micro-wrapped hybrid rod but significant difference observed in final modulus and higher value was detected on the micro-wrapped hybrid rod (Table 4.10). The original and failed images of the specimen are shown in (Figure B2-a and b, Appendix B).

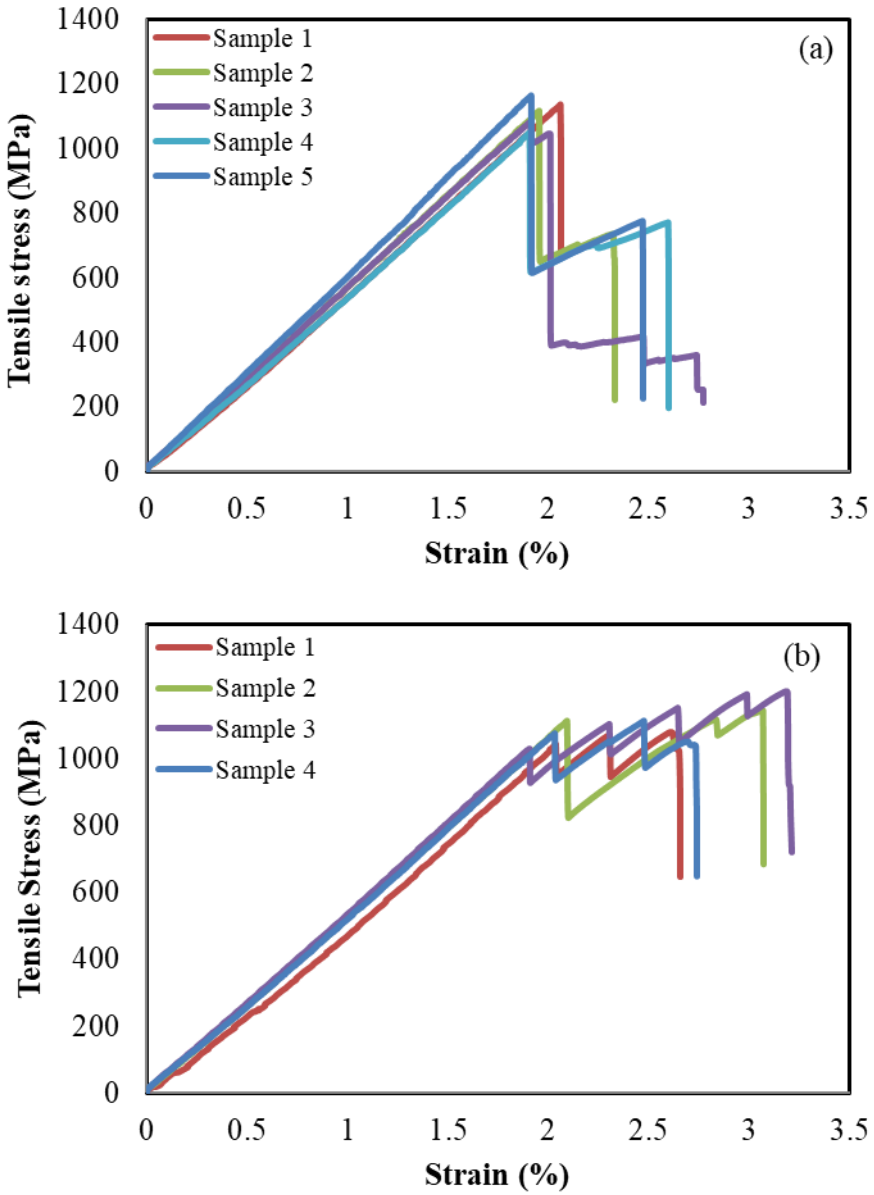

Figure 4.17: Stress-strain curves of T700/S-G (a) side by side and (b) micro-wrapped hybrid tow composite rods.

4.3.2.3 Tensile behaviour of M55/T700 hybrid tow composite rods

To obtain the higher stiffness, M55/T700 hybrid configuration was considered for preparation and testing of side by side and micro-wrapped hybrid tow composite rods. Normalised tensile test results of this hybrid composite rods are summarised in Table 4.11.

Table 4.11: Summary of the normalised tensile test results of M55/T700 hybrid tow composite rods

Specimen Type	M55/T700 SBS	M55/T700 MW
Pseudo-yield Stress (MPa)	780±98.30	934.74±73.1
Stress drop (MPa)	254.85±267.79	83.98±23.30
Maximum stress (MPa)	983.61±53.95	1530.67±73.30
Initial modulus (GPa)	125.20±1.91	128.44±4.19
Final modulus (GPa)	86.75±36.27	92.27±3.18
Pseudo-yield strain (%)	0.60±0.08	0.71±0.06
Final failure strain (%)	1.08±0.39	1.65±0.07
Difference between two failure strain (%)	0.40±0.40	0.94±0.08

Tensile stress-strain curve of M55/T700 side by side and micro-wrapped hybrid tow composite rods are shown in Figure 4.18. Side by side hybrid configuration did not show any pseudo-ductility during tensile loading. Most of the spacemen's failed after the initial failure, only two spacemen's shows non-linearity on their stress-strain graph with a huge stress drop. The reason for the early failure of the specimen might be due to high-stress drop after initial failure which caused the shaking on the specimen and resulted in the failure of the whole specimen. In contrast to the side by side hybrid rod, the micro-wrapped hybrid rod demonstrated the pseudo-ductile behaviour with little stress drop. The initial failure occurred at 0.71% strain which indicates the LS (M55) filament failure occurred first as the failure strain of the M55 is 0.80%. A flat stress plateau region was observed after initial failure. The plateau region indicated that M55 fragmented gradually and transferred the load to T700 without any catastrophic delamination. Video extensometer image shows that after initial failure (M55 break)

there was no change on the surface of the composite rod. Some matrix crack could happen adjacent to the broken filament but the surrounding T700 restricted the crack propagation and transferred the load smoothly without major load drop. The pristine and failed images of the specimen are shown in (Figure B2-c and d, Appendix B).

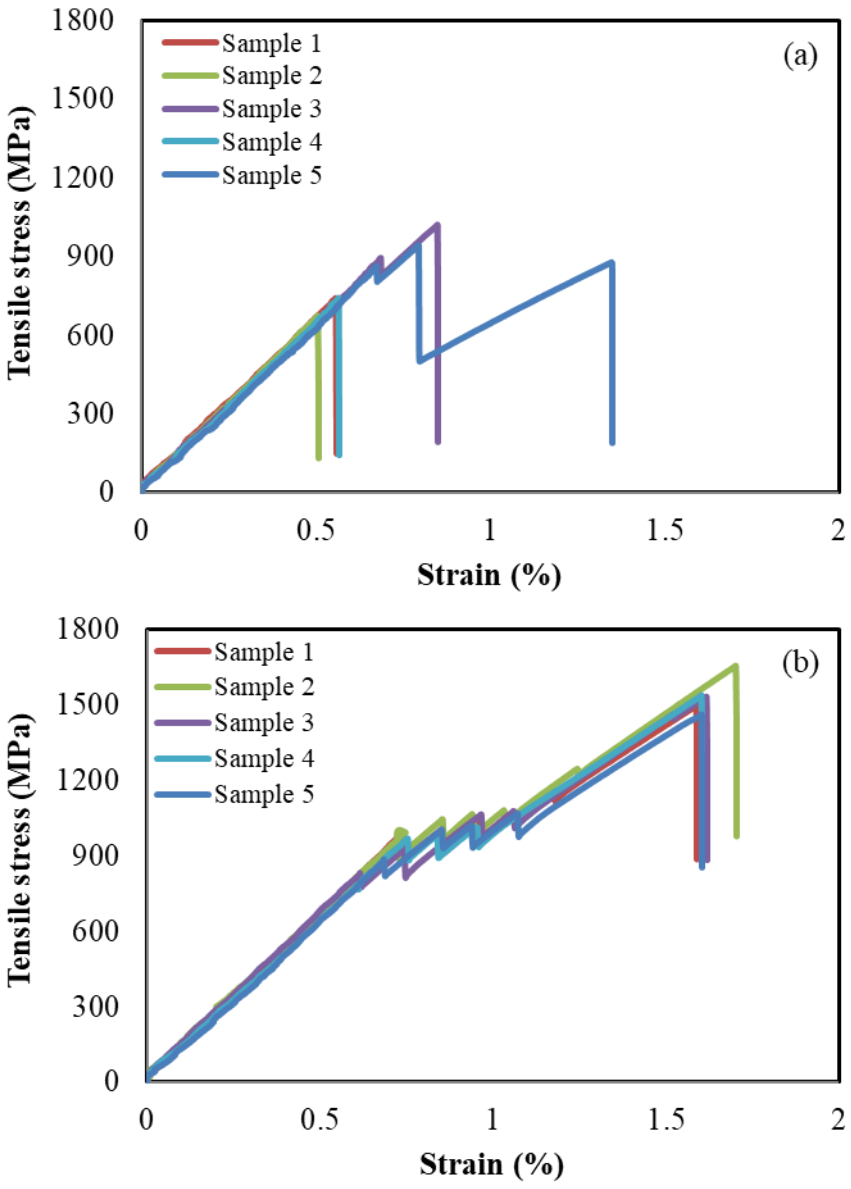

Figure 4.18: Stress-strain curves of M55/T700 (a) side by side and (b) micro-wrapped hybrid tow composite rods.

4.3.2.4 Tensile behaviour of M55/S-G hybrid tow composite rods

To observe the fragmentation in the composite rod after LS fibre breaks in hybrid composite, hybrid composite rods were manufactured from M55/S-G side by side and micro-wrapped hybrid tow and investigated. The manufactured rod was translucent and black carbon core was visible inside the glass sheath. Summary of the normalised tensile stress-strain results of these rods is presented in Table 4.12. Tensile stress-strain curves of M55/S-G side by side and micro-wrapped hybrid tow composite rods with video extensometer images at different strain level are shown in Figure 4.19. The pristine and failed images of side by side and micro-wrapped hybrid tow composite rods are presented in (Figure B2-e and f, Appendix B).

Table 4.12: Summary of the normalised tensile test results of M55/S-G hybrid tow composite rods

Specimen Type	M55/S-G SBS	M55/S-G MW
Pseudo-yield Stress (MPa)	581.17±19.12	571.43±14.35
Stress drop (MPa)	126.96±31.37	69.08±27.75
Maximum stress (MPa)	1122.32±110.50	1220.1±58.67
Initial modulus (GPa)	75.83±3.00	72.83±3.03
Final modulus (GPa)	37.35±2.29	40.25±3.45
Pseudo-yield strain (%)	0.67±0.04	0.75±0.03
Final failure strain (%)	2.91±0.19	3.02±0.13
Difference between two failure strain (%)	2.24±0.42	2.34±0.15

Both samples showed pseudo-ductile behaviour during the tensile loading. The initial failure of the M55 happened at about 0.67% strain for side by side hybrid and 0.75% strain for the micro-wrapped hybrid specimen. After initial failure, the M55 tow separated from S-G tow in the side by side hybrid rod (Figure 4.19 d) but there was no change observed in the micro-wrapped hybrid rod (Figure 4.19h) About 22% and 12% stress drop were detected for side by side and micro-wrapped hybrid rods respectively after initial failure. A flat plateau region was observed for micro-wrapped hybrid rod compare to the side by side hybrid after initial failure which indicated that the

fragmentation of the M55 fibre occurred during this period for micro-wrapped hybrid architecture. Some matrix crack could happen after initial failure adjacent to the broken filament in micro-wrapped hybrid rod but the surrounding S-G restricted the crack propagation and transferred the load smoothly without major load drop. With increasing the applied stress there was some change noticed on the specimen this indicated that matrix cracking and delamination started in the sheath material of the composite rod. The matrix delamination increased with increasing applied stress, as a result, the appearance of the composited rod was fully changed before final failure (Figure 4.19i). A schematic illustration of the failure mechanism of the M55/S-G micro-wrapped hybrid tow composite rod is shown in Figure 4.20. It has been observed by the different researchers [2], [31], [32] that when first fibre failure happened a crack in the matrix surrounding this broken fibre appeared and some stress concentration happened. The surrounding, unbroken fibres hampered the crack propagation in the matrix and reduced the stress concentration. As the composite rod was sheath and core type, these failure mechanisms might have occurred in micro-wrapped hybrid tow composites.

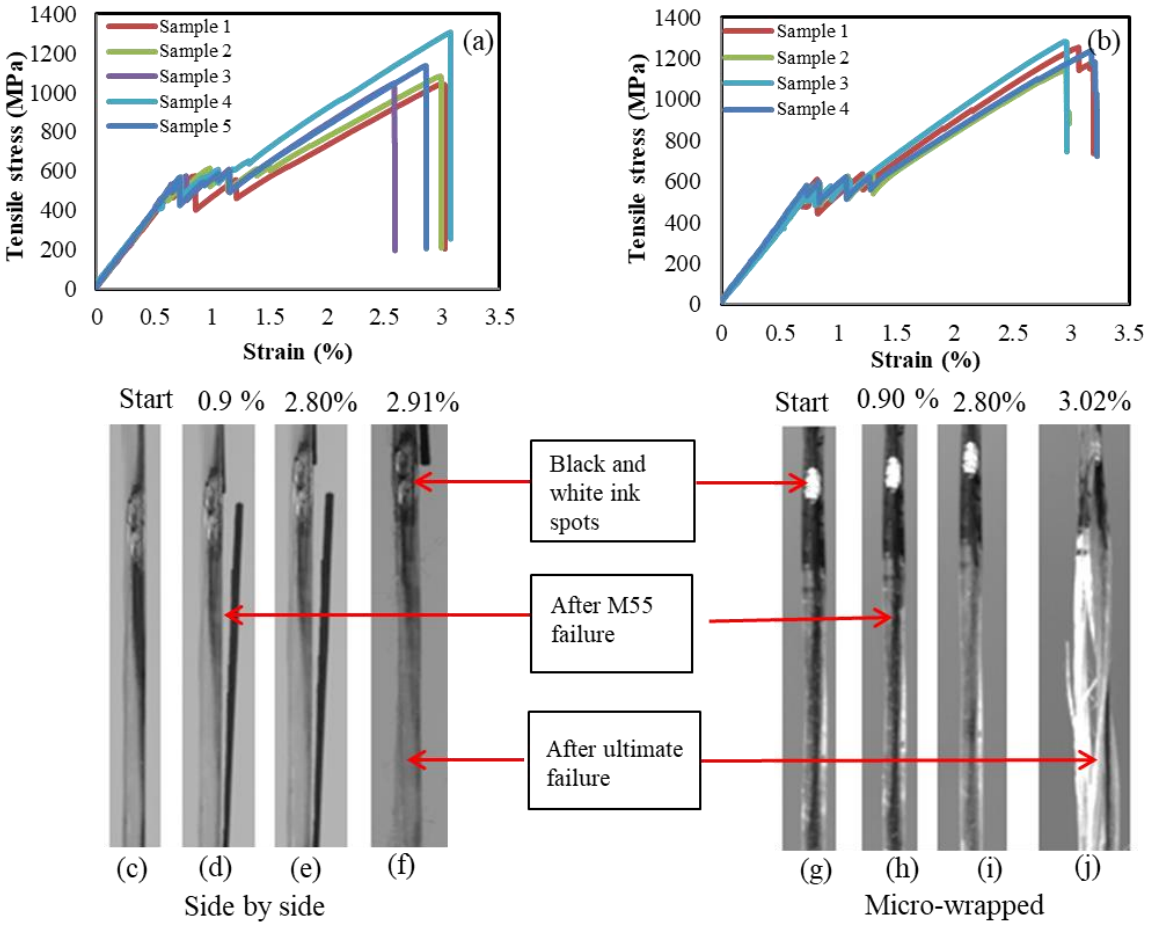

Figure 4.19: Stress-strain curves of M55/S-G (a) side by side and (b) micro-wrapped hybrid tow composite rods. Bottom video extensometer images at different strain levels.

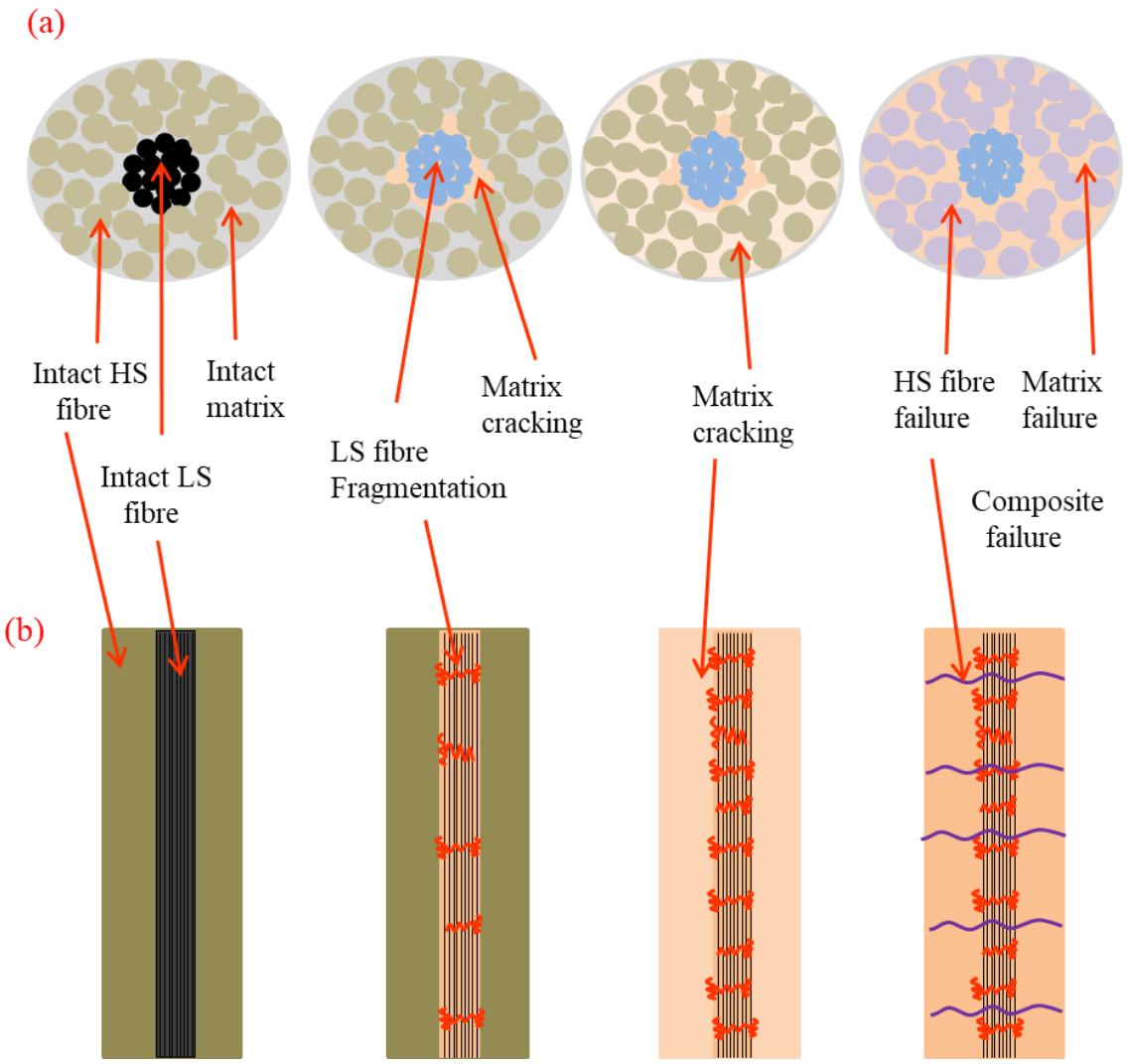

Figure 4.20: Schematic of the carbon/glass micro-wrapped hybrid tow composite rod failure mechanism; (a) cross-sectional images and (b) longitudinal images.

To observe the difference of side by side and micro-wrapped hybrid architectures at a glance a typically normalised stress-strain graph of different hybrid configurations are shown in Figure 4. 21

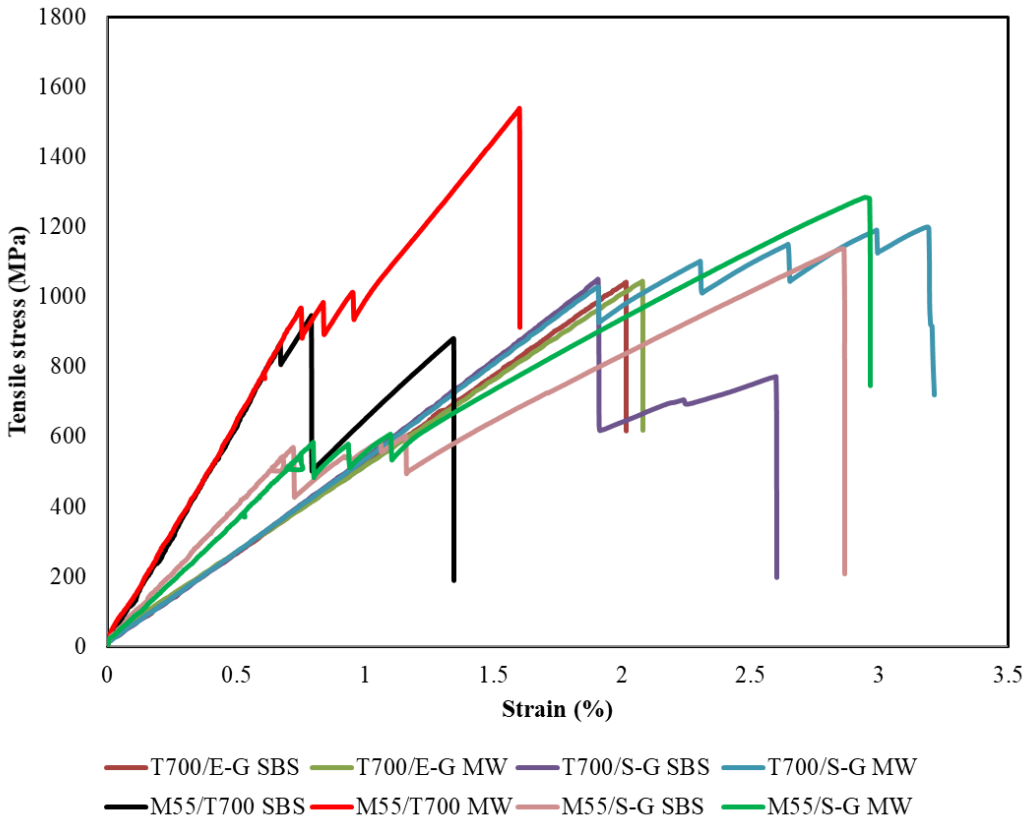

Figure 4. 21: A typical normalised stress-strain graph of different side by side and micro-wrapped hybrid tow composite rods.

4.4 Summary

Novel process development for dry fibre hybrid architecture used in manufacturing inherent ductile reinforced material for ductile or pseudo-ductile composites has been discussed in this chapter. The process is suitable for the production of core-shell type hybrid tow. Different hybrid configurations, micro-wrapped and side by side hybrid tows were prepared and their structural and tensile properties studied. Microscopic observation revealed the core-sheath architecture of micro-wrapped hybrid tow where sheath filament wrapped the core at the angle of 7-degree. Dry tow tensile test results displayed the non-linearity on their stress-strain graph. In comparison with side by side hybrid tows, the micro-wrapped hybrid tows had higher stress and strain to failure for all hybrid configurations. In the micro-wrapped hybrid tow, the wrapping increased the filament-filament interaction, which played an important role in filament breaking process during the tensile loading and resulted in higher tow strength.

Further studies were conducted to evaluate the effect of micro-wrapped hybrid architecture on the tensile behaviour in the mesoscale composites and compared with side by side hybrid architecture. Tensile test results revealed that micro-wrapped hybrid composite rods demonstrated pseudo-ductile behaviour with little stress drop after LS material failure, compared with side by side hybrid architecture. Significant stress drops were observed in side by side hybrid composite rods. However, T700/E-G configuration did not demonstrate any pseudo-ductile behaviour though the dry micro-wrapped hybrid tow of this configuration demonstrated nonlinearity on their stress-strain curve. These results indicated that the fibre-matrix interface plays a vital role in composite materials. For this reason, the composite rods results were different than dry tow test results. A flat stress plateau region was observed after the initial failure of micro-wrapped hybrid composite rods with M55/T700 and M55/S-G hybrid configuration. These results indicated that fragmentation of M55 happened and transferred the load gradually to T700 without any catastrophic delamination. Higher stress and ultimate strain to failure were observed in micro-wrapped hybrid architecture compared to side by side one in both dry fibre and composite rods tensile test. The reason of higher ultimate strain to failure of micro-wrapped hybrid tow composite was that the helical path of the wrapper tow provided 1% extra length. However, a slightly higher initial modulus was observed in side by side hybrid composite rod but final modulus was higher in micro-wrapped hybrid composite rods.

Meso-scale studies of the micro-wrapped hybrid tow composite showed that micro-wrapped hybrid architecture is an excellent technology for manufacturing of hybrid performs for pseudo-ductile composites. A detailed study of the micro-wrapped hybrid architecture in the UD composite laminates have been discussed in Chapter 5.

References

[1] Y. Swolfs, L. Gorbatikh, and I. Verpoest, “Fibre hybridisation in polymer composites: A review,” *Compos. Part A Appl. Sci. Manuf.*, vol. 67, pp. 181–200, Dec. 2014.

[2] R. P. Tavares, A. R. Melro, M. A. Bessa, A. Turon, W. K. Liu, and P. P. Camanho, “Mechanics of hybrid polymer composites: analytical and

computational study," *Comput. Mech.*, vol. 57, no. 3, pp. 405–421, 2016.

[3] B. Lauke, U. Bunzel, and K. Schneider, "Effect of hybrid yarn structure on the delamination behaviour of thermoplastic composites," *Compos. Part A Appl. Sci. Manuf.*, vol. 29, no. 11, pp. 1397–1409, Nov. 1998.

[4] A. Grozdanov and G. Bogoeva-Gaceva, "Carbon Fibers/Polyamide 6 Composites Based on Hybrid Yarns," *J. Thermoplast. Compos. Mater.*, vol. 23, no. 1, pp. 99–110, Jan. 2010.

[5] A. C. Long, C. E. Wilks, and C. D. Rudd, "Experimental characterisation of the consolidation of a commingled glass/polypropylene composite," *Compos. Sci. Technol.*, vol. 61, no. 11, pp. 1591–1603, Aug. 2001.

[6] H. Diao, A. Bismarck, P. Robinson, and M. R. Wisnom, "Production of continuous intermingled CF/GF hybrid composite via fibre tow spreading technology," *Eccm16 - 16Th Eur. Conf. Compos. Mater.*, no. June 2014, p. 8, 2014.

[7] N. E. Merter, G. Başer, and M. Tanoğlu, "Effects of hybrid yarn preparation technique and fiber sizing on the mechanical properties of continuous glass fiber-reinforced polypropylene composites," *J. Compos. Mater.*, vol. 50, no. 12, pp. 1697–1706, May 2016.

[8] A. Mirdehghan, H. Nosraty, M. M. Shokrieh, and M. Akhbari, "The structural and tensile properties of glass/polyester co-wrapped hybrid yarns," *J. Ind. Text.*, vol. 47, no. 8, pp. 1979–1997, May 2018.

[9] G. L. Louis and H. L. Salaun, "'X' Direction Filament-Wrapped Yarn," *Text. Res. J.*, vol. 56, no. 3, pp. 161–163, Mar. 1986.

[10] Z. Xu *et al.*, "Influence of processing conditions on tensile property of continuous glass fiber–reinforced PEEK composites fabricated by the co-wrapped yarn method," *High Perform. Polym.*, vol. 30, no. 4, pp. 489–499, May 2018.

[11] H. K. 1 and R. A. A. 2, "False-twister as a yarn formation factor in wrap spinning

Thermophysiological comfort in the cold View project Design of yarns and fabrics View project," *Artic. Text. Res. J.*, pp. 1926–1935, 2013.

[12] B. Baghaei, M. Skrifvars, and L. Berglin, "Manufacture and characterisation of thermoplastic composites made from PLA/hemp co-wrapped hybrid yarn prepregs," *Compos. Part A Appl. Sci. Manuf.*, vol. 50, pp. 93–101, Jul. 2013.

[13] H. M. Behery and M. F. Nunes, "33—THE STRUCTURE, TENSILE PROPERTIES, AND MORPHOLOGY OF FAILURE OF WRAPPED YARNS," *J. Text. Inst.*, vol. 77, no. 6, pp. 386–402, Nov. 1986.

[14] R. Chudoba, M. Vo0echovský, V. Eckers, and T. Gries, "Effect of Twist, Fineness, Loading Rate and Length on Tensile Behavior of Multifilament Yarns (A Multivariate Study)," *Text. Res. J. Artic. Text. Res. J.*, vol. 77, no. 11, pp. 880–891, 2007.

[15] Y. Rao and R. J. Farris, "A modeling and experimental study of the influence of twist on the mechanical properties of high-performance fiber yarns," *J. Appl. Polym. Sci.*, vol. 77, no. 9, pp. 1938–1949, Aug. 2000.

[16] G. M. Abbott, "Wrapped-yarn reinforced composites: Part I-yarn properties," *Compos. Sci. Technol.*, vol. 24, no. 2, pp. 147–158, Jan. 1985.

[17] G. M. Abbott and G. Freischmidt, "Wrapped-yarn reinforced composites: Part II—composite properties," *Compos. Sci. Technol.*, vol. 24, no. 4, pp. 299–312, Jan. 1985.

[18] Y. Liang, C. Sun, and F. Ansari, "Acoustic Emission Characterization of Damage in Hybrid Fiber-Reinforced Polymer Rods," *J. Compos. Constr.*, vol. 8, no. 1, pp. 70–78, Feb. 2004.

[19] R. Tepfers, V. Tamužs, R. Apinis, U. Vilks, and J. Modniks, "Ductility of nonmetallic hybrid fiber composite reinforcement for concrete," *Mech. Compos. Mater.*, vol. 32, no. 2, pp. 113–121, Mar. 1996.

[20] G. Czél and M. R. Wisnom, "Demonstration of pseudo-ductility in high performance glass/epoxy composites by hybridisation with thin-ply carbon

prepreg," *Compos. Part A Appl. Sci. Manuf.*, vol. 52, pp. 23–30, Sep. 2013.

[21] G. Czél, M. Jalalvand, M. R. Wisnom, and T. Czigány, "Design and characterisation of high performance, pseudo-ductile all-carbon/epoxy unidirectional hybrid composites," *Compos. Part B Eng.*, vol. 111, pp. 348–356, Feb. 2017.

[22] J. D. Fuller and M. R. Wisnom, "Pseudo-ductility and damage suppression in thin ply CFRP angle-ply laminates," *Compos. Part A Appl. Sci. Manuf.*, vol. 69, pp. 64–71, Feb. 2015.

[23] "Technical data sheet Carbon Fiber - TORAY T700SC-12000-60E." [Online]. Available: https://www.900gpa.com/en/product/fiber/CF_004D1BB2D0?u=metric.

[24] "Technical Data sheet Carbon Fiber TORAY M55J-6000-50B." [Online]. Available: https://www.900gpa.com/en/product/fiber/CF_0059DEBCC4?u=metric.

[25] "Technical Data sheet Glass Fiber PPG HYBON 2002." [Online]. Available: https://www.900gpa.com/en/product/fiber/GF_009729965F?u=metric.

[26] "Technical data sheet Glass Fiber - AGY 758-AB-675." [Online]. Available: https://www.900gpa.com/en/product/fiber/GF_0018EF5B8F?u=us.

[27] "ASTM Standard Test Method for Tensile Properties of Yarns by the Single-Strand Method D2256 - 02,Annual Book of ASTM Standards." .

[28] "ASTM D3039 Standard Test Method for Tensile Properties of Polymer Matrix Composite Materials -D3039 2008, Annual Book of ASTM Standards."

[29] M. R. Wisnom, "Mechanisms to create high performance pseudo-ductile composites," *IOP Conf. Ser. Mater. Sci. Eng.*, vol. 139, no. 1, p. 012010, Jul. 2016.

[30] H. Yu, M. L. Longana, M. Jalalvand, M. R. Wisnom, and K. D. Potter, "Pseudo-ductility in intermingled carbon/glass hybrid composites with highly aligned discontinuous fibres," *Compos. Part A Appl. Sci. Manuf.*, vol. 73, pp. 35–44, Jun.

2015.

[31] Y. Swolfs *et al.*, “Synchrotron radiation computed tomography for experimental validation of a tensile strength model for unidirectional fibre-reinforced composites,” *Compos. Part A Appl. Sci. Manuf.*, vol. 77, pp. 106–113, Oct. 2015.

[32] A. E. Scott, I. Sinclair, S. M. Spearing, A. Thionnet, and A. R. Bunsell, “Damage accumulation in a carbon/epoxy composite: Comparison between a multiscale model and computed tomography experimental results,” *Compos. Part A Appl. Sci. Manuf.*, vol. 43, no. 9, pp. 1514–1522, Sep. 2012.

Chapter 5: Investigation of Pseudo-Ductility of Different Hybrid Composites

This chapter describes the effect of micro-wrapping hybridisation on the ductile and pseudo-ductile properties of high-performance composite laminates. Four different hybrid configurations of T700/E-G, T700/S-G, M55/S-G, and M55/T700 were selected for this study. Varieties of unidirectional (UD) and UD woven hybrid composites were fabricated from different micro-wrapped hybrid tows and tested under loading in order to investigate the deformation behaviour under stress. Further study was conducted on comparing micro-wrapping hybridisation process with the conventional side by side hybridisation process on the pseudo-ductile properties using similar material combinations.

5.1 Introduction

During recent years researchers have shown a high interest in fabricating high-performance pseudo-ductile composites exhibiting a safe, progressive failure mechanism similar to yielding and strain hardening of metals with a detectable warning and a wide margin between damage initiation and final failure. A fundamental limitation of the current high-performance composites is their inherent brittleness which limits their use in many high volume and safety-critical applications. In this respect, low diameter stainless steel fibres with brittle and ductile matrix have been studied and achieved excellent ductility [1], [2]. However, the obtained composites have a relatively high density (about 3 times) compared to carbon fibre composite, which limits their application in a lightweight structure.

A modified architecture of traditional laminated composites can produce additional strain through the realignment of off-axis fibres [3]–[6] or out of plane waviness [7], [8]. These types of laminates demonstrated extra strain before final failure by allowing reorientation of the fibres. Fuller and Wisnom [4] have studied the analytical modelling of thin ply angle-ply composites and presented that higher failure strains were achieved with angle-ply than those of UD hybrid composites. The study has revealed that a

specific fibre angle (±26° and ±27°) exhibited maximum stress and strain value with a promising pseudo-ductile strain. These types of laminates have demonstrated the higher failure strain, but sometimes free-edge delamination happened and premature failure occurred.

A few recent studies also showed that thin-ply interlayer hybrid composites represent promising techniques to achieve a favourable ductile or pseudo-ductile behaviour in the composites [9]–[15]. In this hybrid architecture, pseudo-ductility was attained by overcoming the catastrophic delamination and introducing damage mechanisms of low strain material. The failure and fragmentation mechanism of the low strain material occurred through dispersed delamination followed by the failure of high strain material. However, to achieve such a failure mechanism in the thin-ply UD hybrid composite, fibre properties, volume fraction and absolute thickness of the low strain fibre plies are the important design parameters. Jalalvand *et al.* [16] established the concept of damage mode maps as a function of low strain (carbon) fibre layer thickness and relative volume fraction of low strain material. For interlayer thin-ply hybrid composite, the map predicts the maximum low strain layer thickness and relative volume fraction of low strain material that results in fragmentation and hence pseudo-ductility.

The thin-ply hybrid composites have good pseudo-ductile properties; however, higher manufacturing cost and poor preform drapability is the main barrier to make this one of the most suitable options for industrial applications. In this respect, an inherent ductile textile preform can be a good candidate to replace thin-ply technology. It is important to prepare suitable reinforcement material which will be easy to drape while fabrication is cost-effective. UD woven fabric offers a good trade-off between composite properties, cost and suitable for bulk production, making them a suitable material for the composites industries.

In a unidirectional (UD) fabric, the majority of the fibre run in the warp direction and fewer fine filaments compared to warp insert in the weft direction. The weft fibre holds the warp fibre together. Due to low interlacement, the warp fibres stay almost in the straight position and create a negligible amount of crimp in the fabric. This results in the highest possible fibre properties from a fabric in composite component construction. The UD fabric also provides structural integrity and excellent drapability, which is very important for the various composite industry to manufacture complex shapes [17]. The

schematic of the UD prepreg and UD fabric composites are shown in Figure 5.1 where the UD prepreg composite is transversely isotropic (Figure 5.1a) but UD fabric composite is orthotropic (Figure 5.1b) [18].

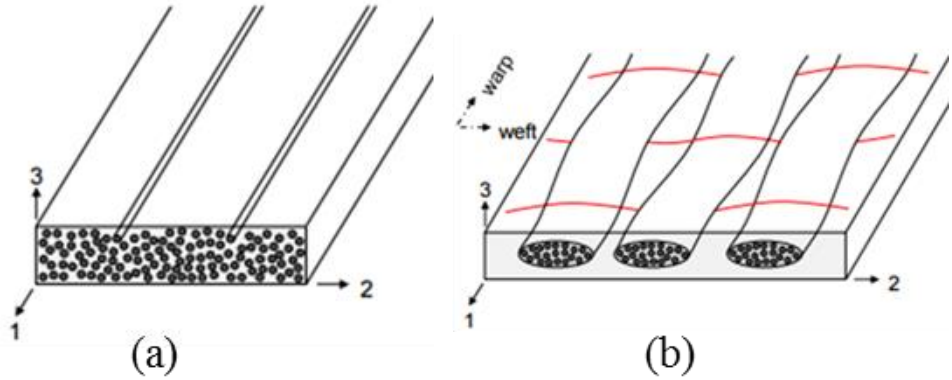

Figure 5.1: Schematic of composite: (a) unidirectional fibre composite and (b) unidirectional woven fabric composite [18].

In this chapter, the manufacturing method of micro-wrapped hybrid tow UD woven fabrics is presented. The effect of micro-wrapped hybrid architecture in the UD composite laminates tensile properties have been studied and compared with side by side hybrid architecture. Different hybrid configuration laminates were studied. Finally, the micro-wrapped hybrids tow UD and UD woven fabric composite laminate tensile properties also have been investigated.

5.2 Experimental

5.2.1 Materials

The reinforced materials used in this experiment are tow Hybon (type 2002) E-glass fibre (E-G), AGY S-glass fibre (S-G), Toray 6K high modulus carbon fibre tow (M55) and Toray 12K high tenacity carbon fibre tow (T700). Details of the fibre properties were presented in chapter 4 (Table 4.1). Two different types of resins were used. Araldite ® LY 564 resin and Aradur ® 2954 hardener were used as a matrix for high-temperature curing and post-curing resin (HTCR). EL2 epoxy resin and AT30 slow hardener were used as a matrix for room temperature curing resin (RTCR).

Four different types of micro-wrapped hybrid tows were used for this study. The manufacturing process of hybrid tows was explained in chapter 4 (section 4.3.3). Detail properties of the micro-wrapped hybrid tows are shown in Table 5.1

Table 5.1: Properties of the different micro-wrapped hybrid tows

Micro-wrapped hybrid configuration	Linear density (Tex) ±SD	No of Wrap (per metre) ±SD	Angle of wrap (degree) ±SD	Volume of LS fibre (%)±SD	Volume of HS fibre (%)±SD
T700/E-G	2824±3.5	26.84±1.61	7.63±0.99	19.20	80.80
T700/S-G	2627±3.15	27.12±1.80	7.75±0.96	20.00	80.00
M55/S-G	1702±2.45	27.07±2.00	7.90±1.24	16.00	84.00
M55/T700	1026±2.25	26.74±1.82	7.72±0.98	20.30	79.70

5.2.2 Preparation of different micro-wrapped hybrid tow UD fabric

Plain UD fabrics were manufactured with the help of a pinboard from different micro-wrapped hybrid tows. Micro-wrapped hybrid tows used as a warp and a very small amount of S-G (less than 0.50% by volume) used as a weft.

5.2.2.1 Preparation of T700/S-G micro-wrapped hybrid tow UD fabric

A UD fabric was manufactured from T700/S-G micro-wrapped hybrid tow with the help of a pinboard. T700/S-G micro-wrapped hybrid tow was used as a warp and a finer (33 tex) S-G as a weft for this fabric. The number of warp and weft per/cm was 3.6 and 0.90 respectively. The areal density of the fabric was 1010 g/m^2.

5.2.2.2 Preparation of M55/S-G micro-wrapped hybrid tow UD fabric

A plain UD woven fabric was also manufactured from M55/S-G micro-wrapped hybrid tow. M55/S-G micro-wrapped hybrid tow was used as a warp and 33 tex S-G used as a weft. Number of warp and weft per/cm was 7.1 and 0.90 respectively. The areal density of the fabric was 1210 g/m^2.

5.2.2.3 Preparation of M55/T700 micro-wrapped hybrid tow UD fabric

A plain UD fabric was manufactured on a pinboard from M55/T700 micro-wrapped hybrid tow. M55/T700 hybrid tow used as a warp and 33 tex S-G used as a weft. The number of warp and weft per/cm was 7.1 and 0.90 respectively. The areal density of the fabric was 730 g/m^2. Photographs of different micro-wrapped hybrid tow UD fabrics are shown in Figure 5.2. The Figure shows that the micro-wrapped tows in the UD fabric still have some waviness compared to UD tows. This waviness can effect some mechanical properties of the composites like kinking.

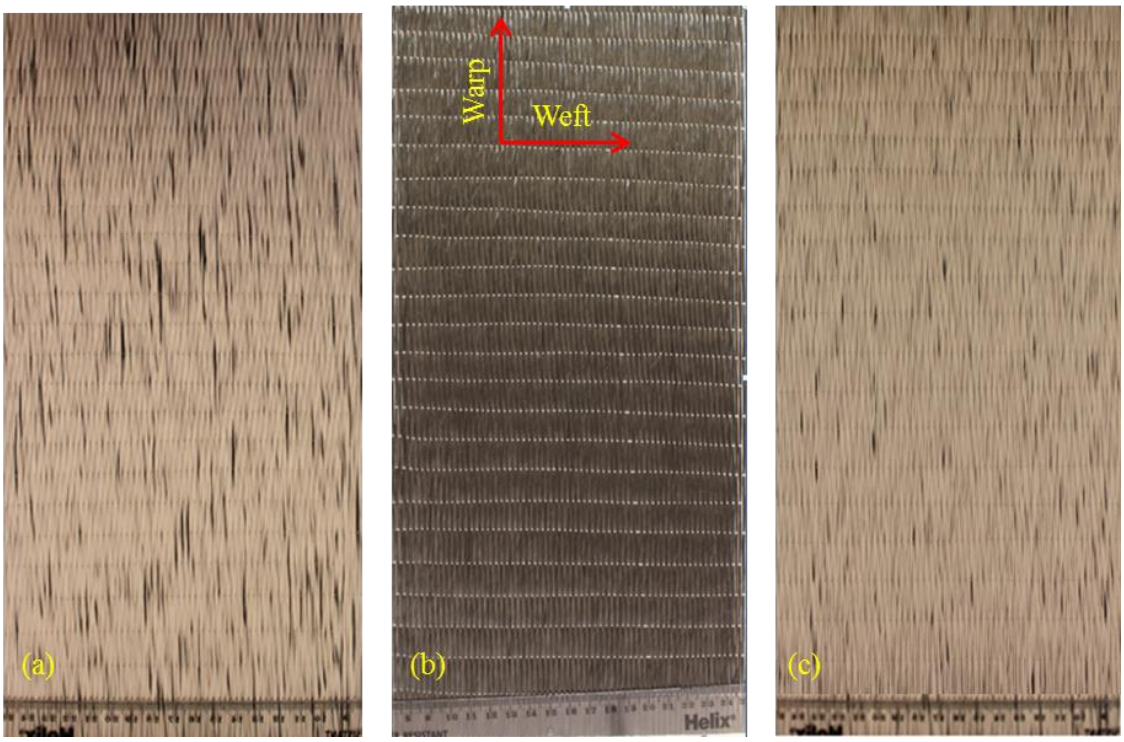

Figure 5.2: Photograph of micro-wrapped hybrid tow UD fabrics (a) T700/S-G, (b) M55/T700 and (c) M55/S-G.G.

5.2.3 Fabrication of composite laminates

5.2.3.1 Preparation of different UD and UD woven hybrid composite panels

A variety of UD and UD woven composite panels were fabricated from different micro-wrapped and side-by-side hybrid tows by vacuum-assisted resin infusion process. List

of different UD and UD woven composites manufactured from different micro-wrapped and side-by-side hybrid tows are shown in Table 5.2

Table 5.2: List of different types of hybrid composites

Panel No.	Hybrid configuration	Hybrid process	Type of specimen	Composites notation
1	T700/E-G	Micro-wrapping	UD composite	T700/E-G MWUD
2	T700/S-G	Side-by-side	UD composite	T700/S-G SBSUD
3	T700/S-G	Micro-wrapping	UD composite	T700/S-G MWUD
4	T700/S-G	Micro-wrapping	UD woven composite	T700/S-G MWUDW
5	M55/S-GF	Micro-wrapping	UD woven composite	M55/S-G MWUDW
6	M55/T700	Side-by -side	UD composite	M55/T700 SBSUD
7	M55/T700	Micro-wrapping	UD composite	M55/T700 MWUD
8	M55/T700	Micro-wrapping	UD woven composite	M55/T700 MWUDW

Panel 1, 2, 3, 6 and 7 were prepared with the help of pinboard. At first, the infusion plate was cleaned and applied a layer of release agent on the top of the plate. The hybrid tows were laid on the infusion plate with the help of the pinboard. For panel 1, 2 and 3, 3.6 tows/cm have been laid on the plate with four layers of tow laid under tension to maintain the tow alignments. But for panel 6 and 7, 7.1 tows/cm have been laid on the plate with two layers of the tows. The tail end between the infusion plate and pinboard was cut by scissors to separate from pinboard for vacuum bag resin infusion process.

Panel 4, 5 and 8 were manufactured from micro-wrapped hybrid tow UD fabric. For panel 4, four layers of T700/S-G micro-wrapped hybrid tow UD fabric was used. On the other hand, for panel 5 two layers of M55/S-G micro-wrapped hybrid tow UD fabrics and for panel 8, two layers of M55/T700 micro-wrapped hybrid tow UD fabrics were used. Figure 5.3 shows the photographs of different composites panel ready for vacuum bag resin infusion.

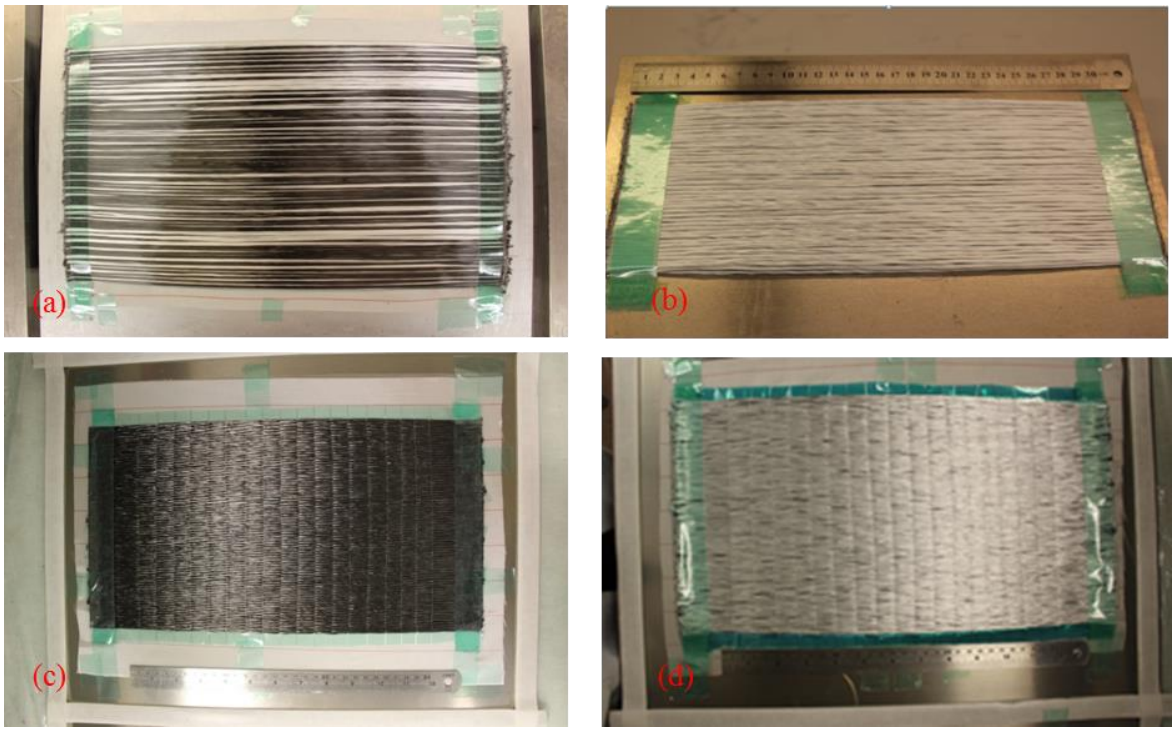

Figure 5.3: Photograph of the different UD and UD woven composite panels ready for resin infusion (a) T700/S-G side by side hybrid UD, (b) T700/S-G micro-wrapped hybrid UD (c) M55/T700 micro-wrapped hybrid UD woven and (D) M55/S-G micro-wrapped hybrid UD woven.

5.2.3.2 Vacuum bag resin infusion process

A new vacuum bag resin infusion process was used for manufacturing the composite laminates which were developed by Robotics and Textile Composites Research Group in the University of Manchester. In traditional vacuum bagging composite laminate manufacturing process, only the bottom metal plate has been used to control the flatness of the whole laminate. The thickness of the resin on the top of the panel is only controlled by the flexible bagging film. However, variation of the resin thickness on the bottom and top of the laminate often happens. In the new process, two metal plates were used on the bottom and top of the laminate to control the same surface finish on both

sides of the laminate. The prepared panel with a different preform was covered with a peel ply. A metal plate with a hole in the centre of it was placed on top of the peel ply and a PVC resin outlet tube was connected on the hole of the plate. Another end of the outlet tube was connected with a vacuum pump to extract the air from the vacuum bag and also sucked out the extra resin from the system during the resin infusion process. A PVC resin inlet tube connected with a spiral tube and the spiral tube was placed around the top plate which allowed the resin to enter the preform from all sides. Once all the required materials were placed and secured, a nylon vacuum bagging film was placed to cover the materials and the film was sealed to the bottom metal plate using sealant tape. Photograph of the typical vacuum bagging arrangement is shown in Figure 5.4

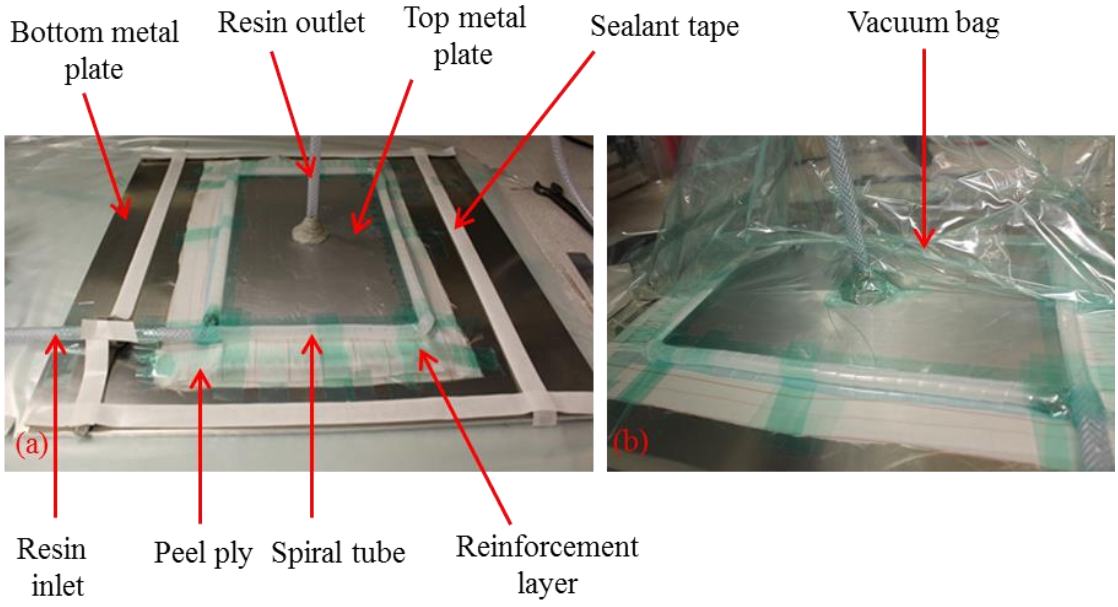

Figure 5.4: Vacuum bagging resin infusion process.

The two parts of epoxy, resin and the hardener were mixed properly in a paper container. After the mixing of two parts, the mixture was placed in a degassing chamber to completely remove the gas bubbles to make a void-free laminate. Once the degassing was completed the resin was infused into the sealant bag through the inlet tube by connecting the outlet tube with a vacuum pump. Curing and post-curing were carried out in an oven at 80ºC for 2 hours and 140ºC for 8 hours. For room temperature curing resin, curing was carried out at room temperature for 48 hours.

5.2.4 Characterisation

An optical microscope (Keyence digital microscope VHX-500F, UK) and a Philip XL-30 field emission gun scanning electron microscope (SEM) were used for analysis of the X-sectional images of the composites.

5.2.5 Mechanical testing

All the composite specimens were prepared for mechanical testing according to ASTM D3039M [19]. End tabs made of glass fibre reinforce cross-ply plates with 1.60 mm thickness were bonded on the specimen using two-component Araldite 2011 A/B epoxy adhesive supplied by Huntsman. The individual samples were cut from the composite panel with a diamond cutting wheel. Tensile tests were done under uniaxial loading on an electromechanical testing machine (Instron 5982) with a cross-head speed of 2 mm/min. The load was measured with a 100KN load cell. The strain was measured by using Imetrum video extensometer with a nominal gauge length of 50 mm. A typical photograph of the micro-wrapped hybrid tow composite specimens ready for the tensile test is shown in Figure 5.5.

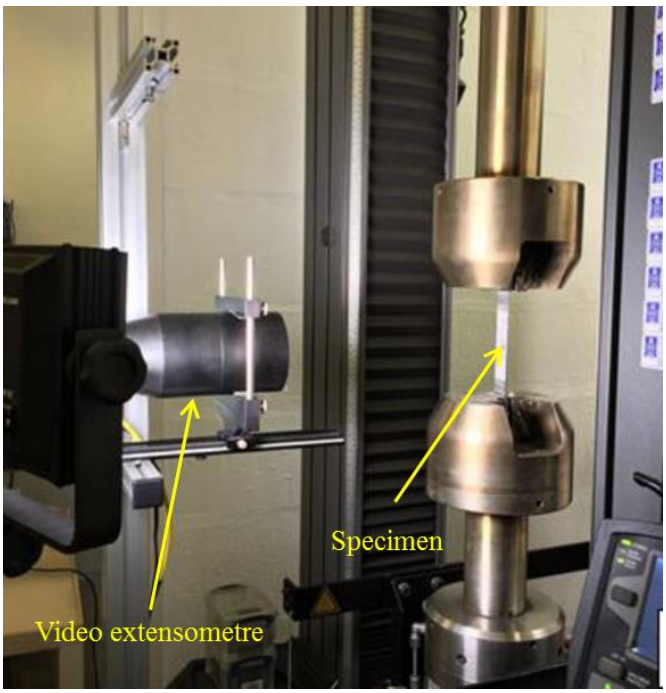

Figure 5.5: Machine set up for the tensile test of the composites.

5.2.6 Normalisation with fibre volume fraction

Fibre volume fraction differs in the composite batch to batch even if the manufacturing materials and the process is the same. Mechanical properties of the composites depend on the volume fraction of fibre in the laminate. The data were normalised to adjust the raw test values to a single specified fibre volume fraction of 55%. In a UD composite, fibre dominated properties such as strength and stiffness vary linearly with fibre volume fraction. The raw data were normalised by using the following equation [20]

$$Normalised\ Value = Test\ value \frac{FV_{normalising}}{FV_{specimen}} \quad 5.1$$

Where $FV_{normalising}$ is the chosen common fibre content (volume fraction); $FV_{specimen}$ is the actual specimen fibre content (volume fraction). The fibre volume fraction of different composite laminates are tabulated in (Table C1, Appendix C)

5.3 Results and Discussion

5.3.1 T700/E-G hybrid configuration

5.3.1.1 Microscopic analysis of composite

Cross-sectional image of T700/E-G micro-wrapped hybrid tow UD composite which was fabricated with HTCR is shown in Figure 5.6. The image clearly showed that all the T700 fully covered with a thick E-G fibre. During the micro-wrapping process, the core fibre (T700) took different shape such as round and oval inside the E-G fibre.

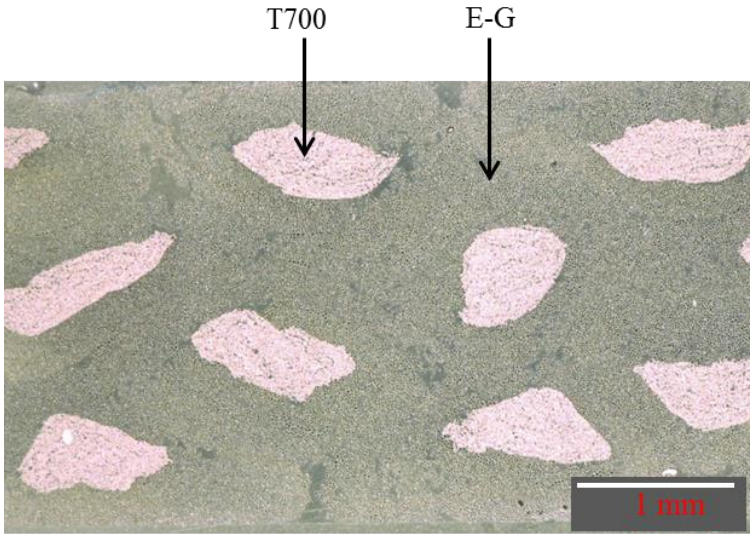

Figure 5.6: Cross-sectional image of T700/E-G micro-wrapped hybrid tow UD composite.

5.3.1.2 Tensile behaviour of T700/E-G micro-wrapped hybrid tow UD composite

The stress-strain graph of T700/E-G micro-wrapped hybrid tow UD composite is shown in Figure 5.7. The tensile test results are presented in Table 5.3. Some of the specimens show the non-linearity in their stress-strain graph and some specimens did not. The stress-strain curves are slightly different than micro-wrapped composite rods which are presented in chapter 4 (4.3.2.1). The average initial failure strain of specimens was 1.62% which is similar to T700 UD composite. After initial failure, a little stress drop was observed but there was no visual change detected on the specimen surface (Figure 5.7b). The pristine and failed images of the specimen are shown in (Figure C1-a, Appendix C). These results indicated that after the initial failure of the T700, the surrounded E-G suppressed the crack propagation and transferred the stress to E-G without major stress drop. Few fractures were observed at the edge of the sample just before ultimate failure (Figure 5.7c). When the strain reached about 1.87% the final failure happened but the failure was not explosive, like traditional high-performance single fibre type UD composites. In this configuration, the strain between initial failure and ultimate failure was only 14% of the total strain. One of the samples behaved exceptionally which did not go through initial failure. Therefore, a different hybrid configuration was considered and S-G fibres were used instead of E-G and T700/S-G micro-wrapped hybrid tow was prepared and the mechanical properties of the laminates were studied.

Table 5.3: Tensile test results of T700/E-G micro-wrapped hybrid tow UD composite

Specimen Type	T700/E-G MW UD (±SD)
Pseudo-yield Stress (MPa)	876.2±35.3
Stress drop (MPa)	23.0±16.3
Maximum stress (MPa)	918.7±35.0
Initial modulus (GPa)	52.76±0.76
Pseudo-yield strain (%)	1.62±0.06
Final failure Strain (%)	1.87±0.03
Difference between two failure strain (%)	0.25±0.04

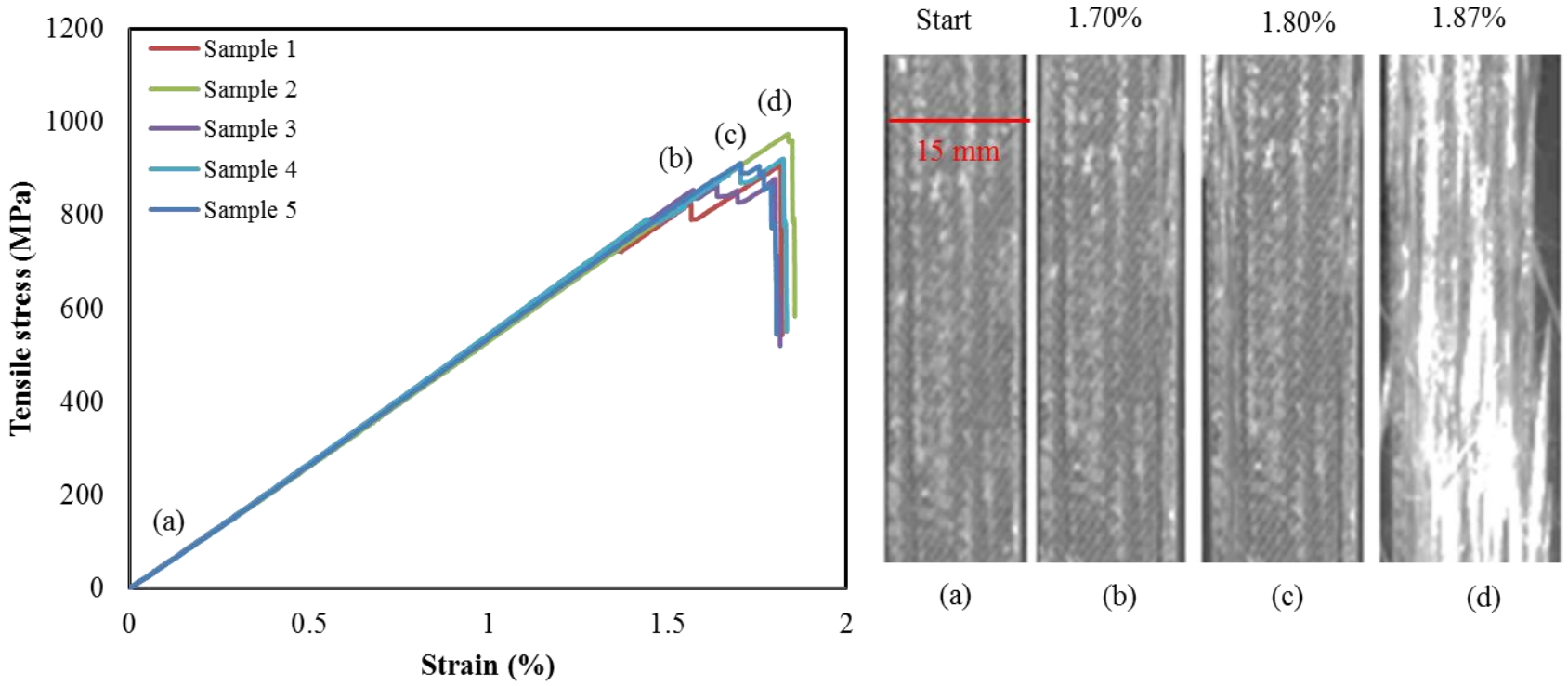

Figure 5.7: Stress-strain graph of T700/E-G micro-wrapped hybrid tow UD composite. Right side video extensometer images of the specimen at different strain levels during tensile loading; (a) start, (b) after initial failure, (c) just before ultimate failure and (d) after ultimate failure.

5.3.2 T700/S-G hybrid configuration

A previous parametric study [11] revealed that S-glass/TR30 carbon fibre hybrid provided improved pseudo-ductile strain compared to the E-glass/TR30 hybrid configuration. Therefore, T700/S-G hybrid configuration was considered to prepare micro-wrapped hybrid tow. In order to compare micro-wrapped hybridisation process to the side by side hybrid process, UD composite laminates were fabricated from T700/S-G side by side and micro-wrapped hybrid tow with high temperature curing resin (HTCR).

5.3.2.1 Microscopic analysis of composites

Figure 5.8 shows the cross-sectional images of T700/S-G side by side and micro-wrapped hybrid tow composites. As shown in Figure 5.8a side-by-side composites, T700 and S-G fibre distributed randomly inside and on the surface of the composite. On the other hand, micro-wrapped hybrid, the core tows (T700) were distributed inside the sheath tow (S-G) in the composite with different shapes but it was fully covered by a sheath (S-G) (Figure 5.8b).

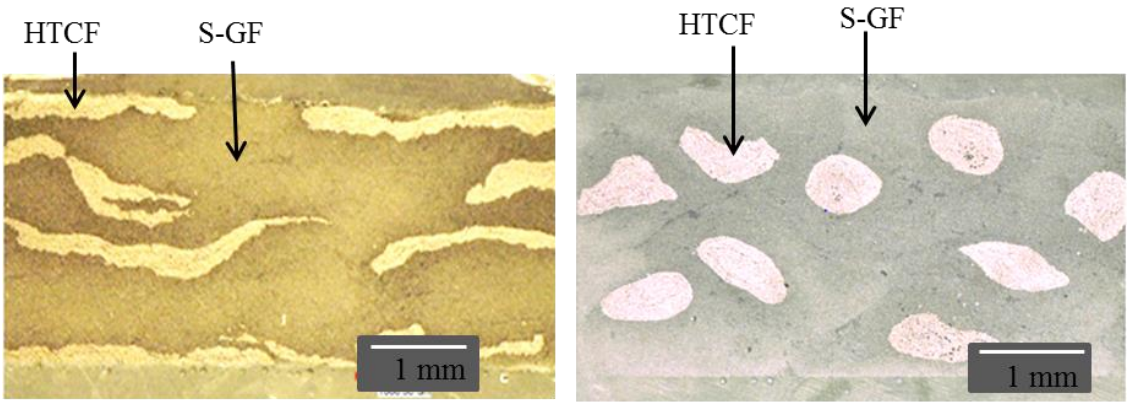

Figure 5.8: Cross-sectional images of T700/S-G UD composites: (a) side-by-side and (b) micro-wrapped hybrid.

5.3.2.2 Tensile behaviour of T700/S-G side by side hybrid UD composite

Normalised tensile test results of T700/S-G side-by-side UD, micro-wrapped UD and micro-wrapped UD woven composites are presented in Table 5.4. It was noted that after an initial failure major damage was observed on the side-by-side hybrid specimen surface and video strain measurement system lost the accuracy of the strain measurement. For this reason, the strain values after the initial failure of this set of the

specimen were calculated from the cross-head extension using a correction factor. The correction factor was derived from the extensometer strain value divided by cross-head displacement at the point of initial failure.

Table 5.4: Normalised tensile test results of T700/S-G hybrid composites

Specimen Type	T700/S-G SBS UD	T700/S-G MW UD	T700/S-G MW UD woven
Pseudo-yield Stress (MPa)	1024.2±19.82	970.8±26.1	889.8±18.8
Stress drop (MPa)	283.7±58.0	85.5±47.9	33.6±23.7
Maximum stress (MPa)	1024.2±19.82	973±37.7	921.3±31.5
Initial modulus (GPa)	56.05±0.62	61.3±1.7	61.9±0.67
Final modulus (GPa)	16.6±7.69	24.5±2.80	23.34±3.81
Pseudo-yield strain (%)	1.79±0.03	1.61±0.09	1.50±0.06
Final failure Strain (%)	2.50±0.15	2.83±0.17	2.79±0.24
Difference between two failure strains (%)	0.71±0.16	1.22±0.17	1.29±0.21

Tensile stress-strain graph of T700/S-G side-by-side hybrid composite is shown in Figure 5.9 where images at different strain levels during the tensile tests (recorded using video extensometer) have also been shown. The side-by-side hybrid specimens displayed conventional hybrid failure behaviour, with a significant stress drop (27.7%) after the initial failure and prior to the redistribution of the stress to the S-G. As the T700 fibre has a lower strain to failure compared to that of S-G, T700 fibres failed initially and S-G fibre carried the load to ultimate failure. The initial failure occurred at a strain of 1.79% leading to a major crack formation on the specimen surface (Figure 5.9b) which caused the unstable load transfer from T700 to S-G, followed by a significant drop in the stress value. After the initial failure glass fibre carried the load (since glass fibre strain to failure is higher than carbon) and the stress-strain curve starts to rise but continuous delamination was observed on the specimen surface (Figure 5.9c) till final failure occurred. This result showed that random distribution of the LS and HS materials on the specimen surface (Figure 5.8 a) did not allow a smooth transition of the load from T700 to S-G. The pristine and failed images of the specimen are shown in (Figure C1-b, Appendix C).

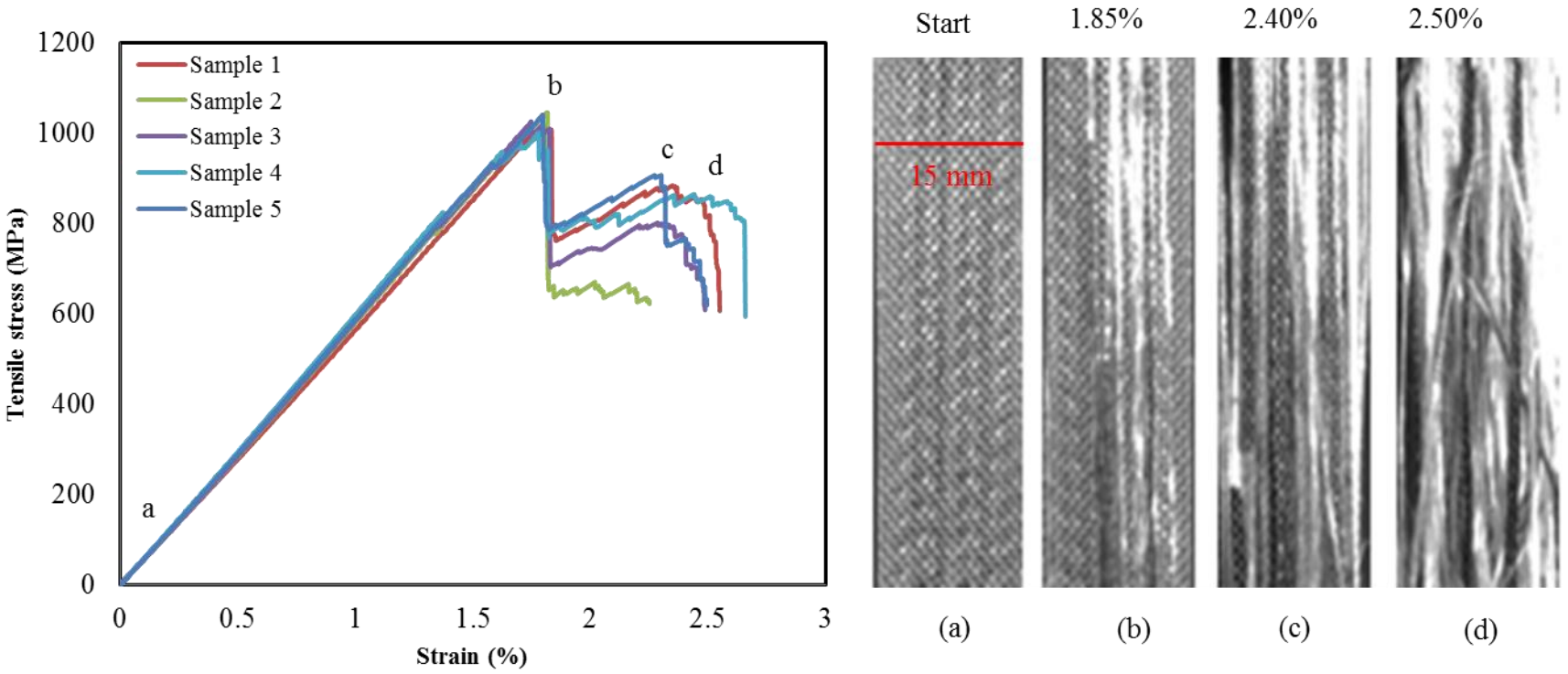

Figure 5.9: Stress-strain graph of T700/S-G side by side hybrid tow UD composite. Right side video extensometer images of the specimen at different strain levels during tensile loading; (a) start, (b) after initial failure, (c) just before ultimate failure and (d) after ultimate failure.

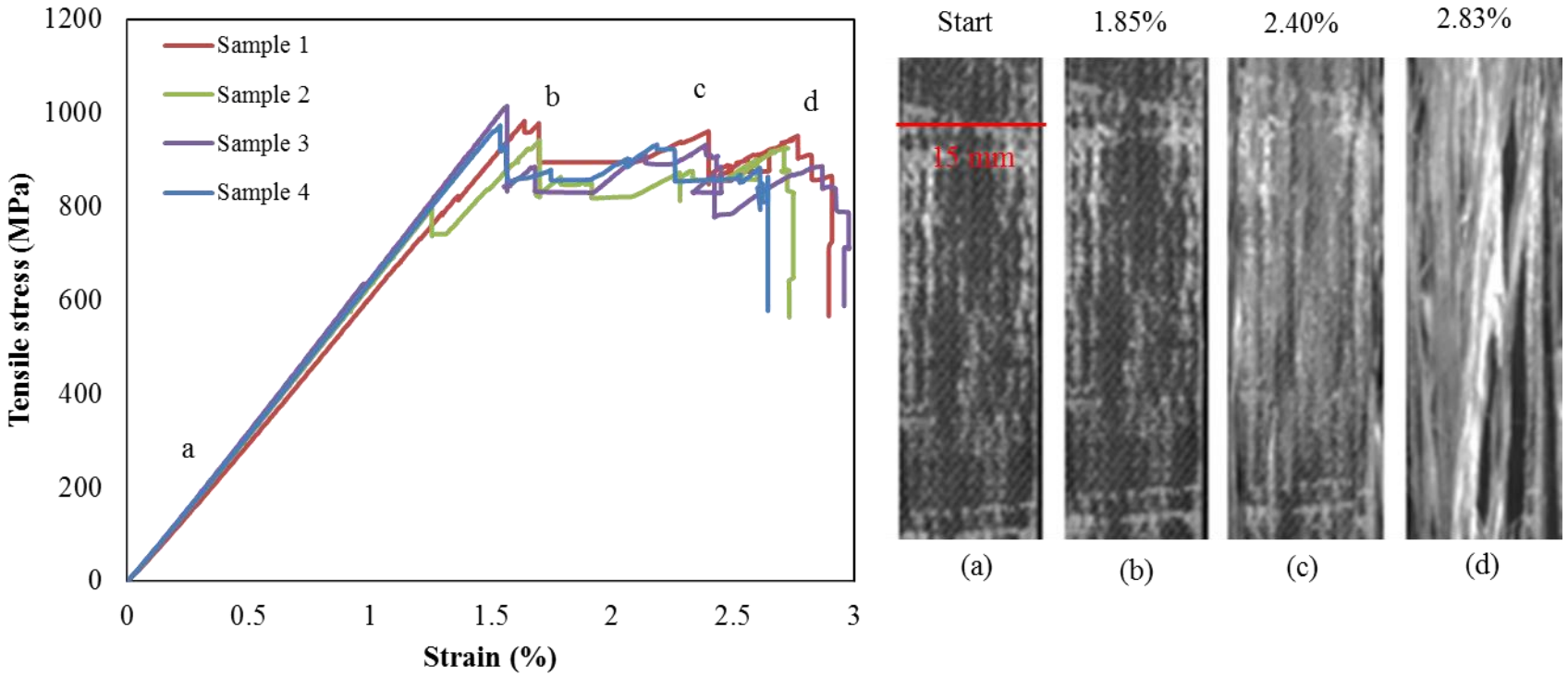

Figure 5.10: Stress-strain graph of T700/S-G micro-wrapped hybrid tow UD composite. Right side video extensometer images of the specimen at different strain levels during tensile loading: (a) start, (b) after initial failure, (c) just before ultimate failure and (d) after ultimate failure.

5.3.2.3 Tensile behaviour of T700/S-G micro-wrapped hybrid UD composite

T700/S-G micro-wrapped hybrid tow UD composite exhibited very interesting results. The stress-strain curves showed a gradual failure mode instead of normal sudden catastrophic failure (Figure 5.10). The initial failure of T700 occurred at a strain of 1.61% which is similar to T700 carbon composite but less than T700/S-GF side by side hybrid composite. After initial failure, there was a little stress drop (8.9%) but no visual change was observed on the specimen surface (Figure 5.10b). In the micro-wrapped architecture, when the applied longitudinal stress was sufficient to induce a fracture in the core (T700) the surrounding sheath (S-G) restricted crack propagation from core to sheath and caused stable pull out of the sheath elements. De-bonding of the matrix in the specimen started from edges at 2.40% strain and spread slowly across the sample. The specimen appearance also started to change (Figure 5.10c). This helps to infer that the fragmentation and dispersed delamination occurred inside the specimen. When the strain reached about 2.83% the final failure happened. The pristine and failed images of the specimen are shown in (Figure C1-c, Appendix C).

5.3.2.4 Tensile behaviour of T700/S-G micro-wrapped hybrid UD woven composite

To compare the UD and UD woven composite, UD woven composite was manufactured from T700/S-G micro-wrapped hybrid tow UD fabrics. Stress-strain response of T700/S-G micro-wrapped hybrid tow UD woven composite is shown in Figure 5.11. This composite laminate also demonstrated excellent pseudo-ductile response during tensile loading. An initial failure happened at 1.50% strain which is less compared to UD composite. It might happen because the UD fabric has some waviness, which could cause the early failure of the low strain material. However, stress drop after initial failure was reduced significantly (3.7%) (Table 5.4). A smooth stress transfer occurred between core and sheath material. Even after the final failure, the structural integrity of this specimen was better than UD composites (Figure 5.11d). The difference between initial failure and final strain to failure was higher in UD woven composite compared to UD composites. A slightly lower value of maximum stress was observed in UD woven composite compared to UD composite which might be due to fibre damage during the weaving process. The pristine and failed images of the specimen are shown in (Figure C1-d, Appendix C).

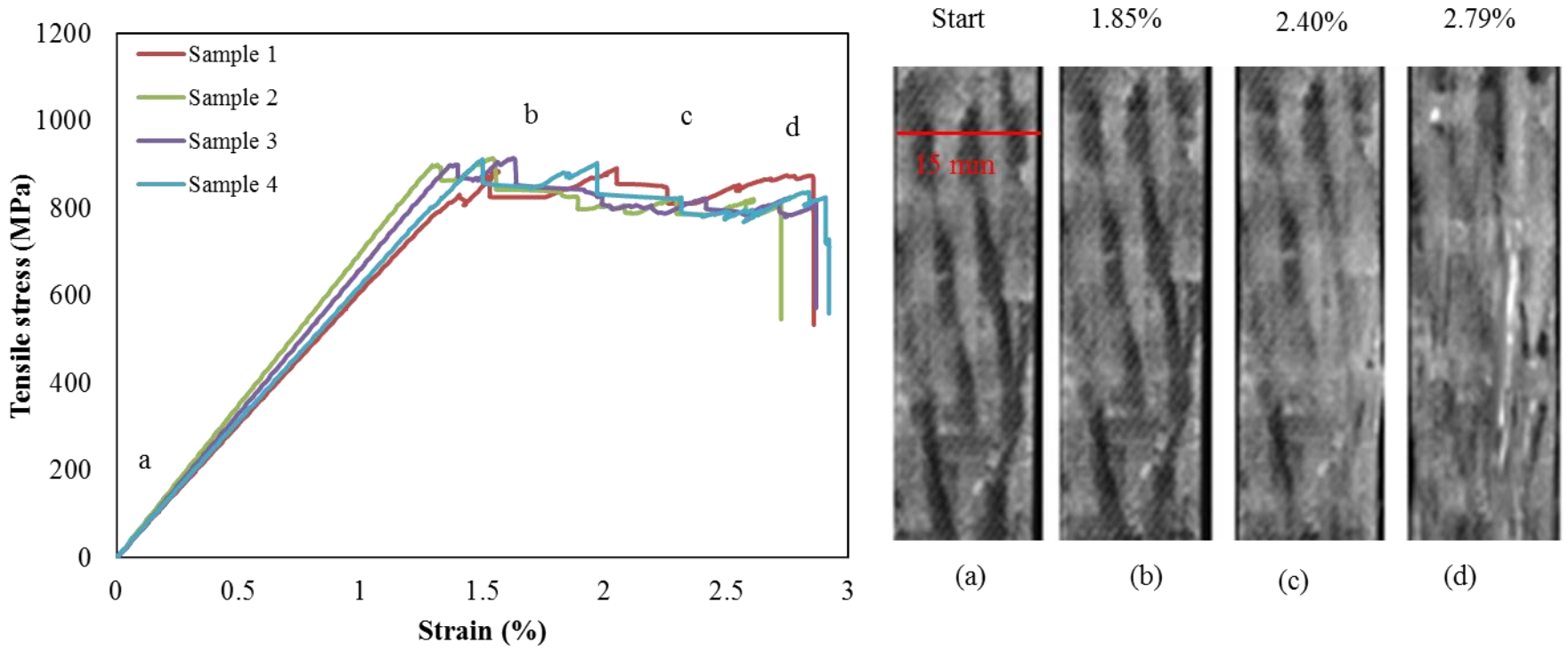

Figure 5.11: Stress-strain graph of T700/S-G micro-wrapped hybrid tow UD woven composite. Right side video extensometer images of the specimen at different strain levels during tensile loading; (a) start, (b) after initial failure, (c) just before ultimate failure and (d) after ultimate failure.

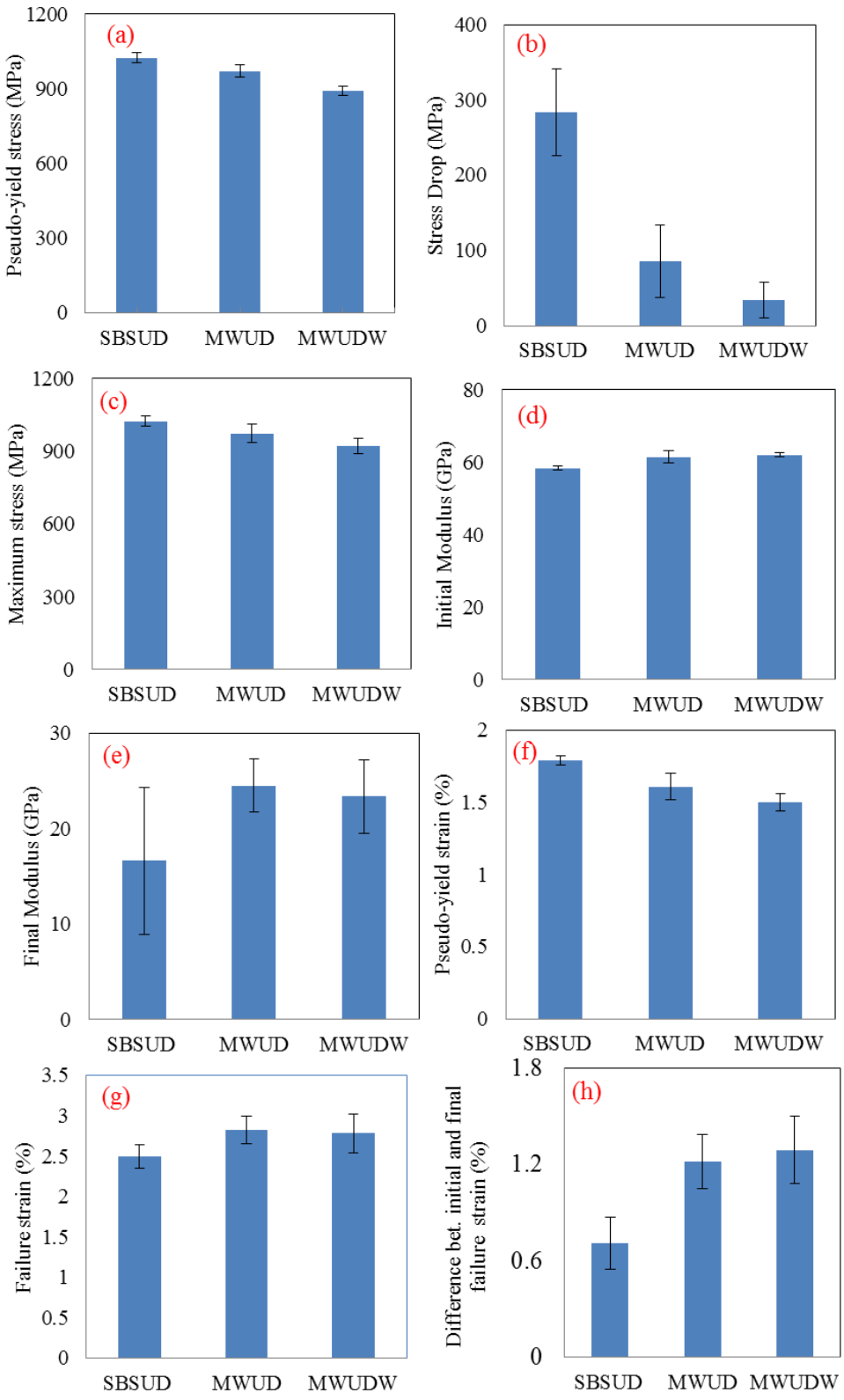

Figure 5.12: Normalised tensile properties of T700/S-G hybrid composites. Sample notation: SBSUD = side-by-side UD, MWUD = micro-wrapped UD and MWUDW = micro-wrapped UD woven.

Normalised tensile properties of different T700/S-G hybrid composites are presented in Figure 5.12. There were significant differences observed in stress drop (Figure 5.12b), final modulus (Figure 5.12e) and the difference between initial and final failure strain (Figure 5.12h) between the side by side and micro-wrapped hybrid tow composites. Minimum stress drop after initial failure was observed in the UD woven composite (Figure 5.12b). However, no major variation was detected in the other mechanical properties of the composites.

5.3.3 M55/S-G hybrid configuration

T700/S-G micro-wrapped hybrid tow composite exhibited plastic deformation but the stress value did not increase further after pseudo-yield point. To achieve the higher stiffness and extended stress-strain value, another type of hybrid configuration (M55/S-G) composite was investigated. In this hybrid configuration, the M55 was used as low strain and S-G was used as a high strain fibre in the prepared micro-wrapped hybrid tow. UD fabric was manufactured using M55/S-G micro-wrapped hybrid tow. UD woven composite was fabricated using M55/S-G micro-wrapped hybrid tow UD fabric with RTCR.

5.3.3.1 Microscopic analysis of composites

The transverse and longitudinal cross-sectional images of M55/S-G micro-wrapped hybrid tow woven UD composites are shown in Figure 5.13. Both images clearly showed that the core tow (M55) was evenly surrounded by S-G. The longitudinal image also indicates that M55 stayed at the straight position and outer S-G oriented at a certain angle.

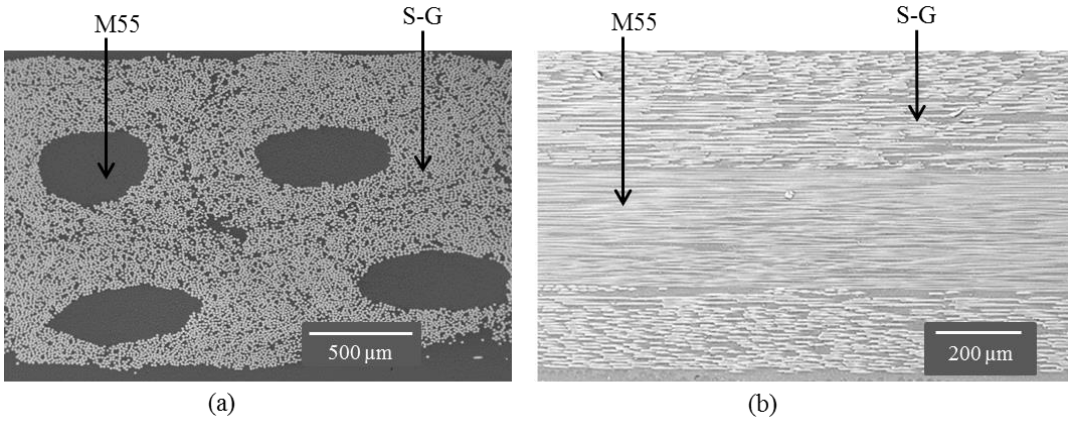

Figure 5.13: Microscope images of M55/S-GF micro-wrapped hybrid tow UD woven composite (a) transverse cross-sectional and (b) longitudinal cross-sectional image.

5.3.3.2 Tensile behaviour of M55/S-G micro-wrapped hybrid tow UD woven composite

This hybrid configuration also shows the good non-linear response with a smooth stress transition between the initial and second linear part of the stress-strain curves (Figure 5.14). Normalised tensile test results of this configuration are presented in Table 5.5. The pristine and failed images of the specimen are shown in (Figure C1-e, Appendix C). The initial failure occurred at 0.72% strain with about 10% stress drop. A flat plateau region was observed after initial failure with small stress fluctuations which indicated that low strain material (M55) fragmented gradually and transferred the load to high strain material (S-G) without any catastrophic delamination. There was no damage or crack observed on the specimen surface after initial failure (Figure 5.14b). After a certain strain level matrix delamination was started which were visible in this specimen (Figure 5.14c). As the S-G have higher failure strain than the matrix, therefore, damage development in the matrix before the final failure was observed. Some stress drops were observed in the second part of the stress-strain curves because crack propagation started at one edge of the sample (image c). This might have happened due to misalignment of the tows inside the composites. The pseudo-yield stress (stress at damage initiation) was 642 MPa which was less compared to T700/S-G hybrid configuration (970 MPa). A higher initial modulus about 90 GPa was achieved compared to T700/S-G configuration. The final failure strain of the composite was 3.47% which was higher than T700/S-G. The composite laminate was manufactured using RTCR which contributed to the higher ultimate failure strain. The detail of the resin effect has been discussed in chapter 6 in this thesis. The highest value of pseudo-ductile strain (the difference between initial and ultimate failure strain) was attained in this hybrid configuration. Jalalvand *et al*. [11] reported that any increase in the modulus ratio of LS and HS materials leads to an increase in the pseudo-ductile strain and simultaneous decrease in the pseudo-yield stress values. The obtained results were well matched with their analytical results.

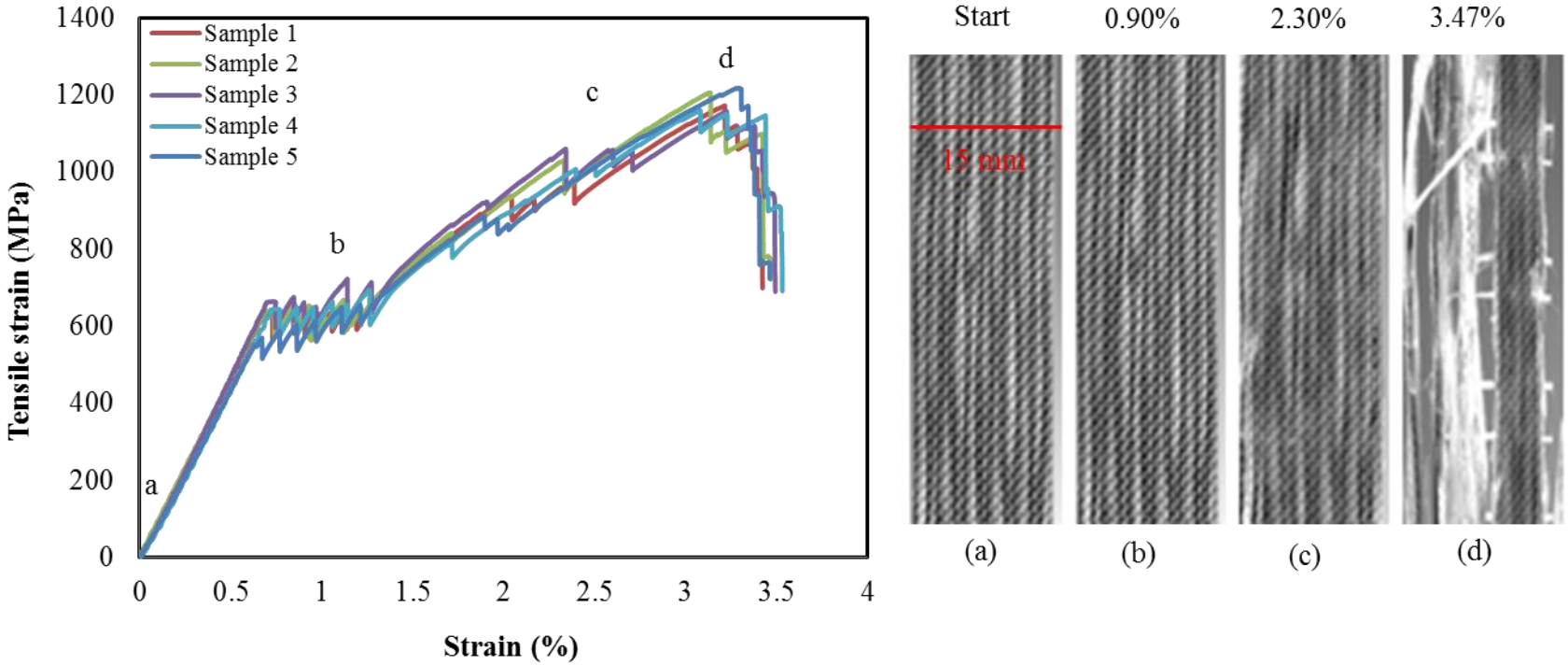

Figure 5.14: Stress-strain graph of M55/S-G micro-wrapped hybrid tow UD woven composite. Right side video extensometer images of the specimen at different strain levels during tensile loading; (a) start, (b) after initial failure, (c) specimen colour start change a and (d) after ultimate failure.

Table 5.5: Tensile test results of M55/S-G micro-wrapped hybrid tow UD woven composite

Specimen Type	M55/S-G MW UD woven
Pseudo-yield Stress (MPa)	642.19±22.7
Stress drop (MPa)	64.5±5.6
Maximum stress (MPa)	1188.3±31.7
Initial modulus (GPa)	90.33±2.24
Final modulus (GPa)	40.48±0.50
Pseudo-yield strain (%)	0.72±0.04
Final failure strain (%)	3.47±0.03
Difference between two failure strain (%)	2.75±0.03
Pseudo-ductile strain (%)	2.05±0.04

5.3.4 M55/T700 hybrid configuration

There are a limited number of published studies that describe the mechanical performance of hybrid composites manufactured from different types of carbon fibres [14], [21]. Naito *et al.* [21] studied the tensile properties of high strength (HS) and high modulus (HM) interlayer hybrid carbon fibre reinforced epoxy composites. The fibre volume fraction of HS and HM carbon fibre was 29.3 and 26.4%respectively. A significant load drop after low strain material fracture was observed. Czel *et al*. [14] recently reported the stable pseudo-ductile response (metal-like stress-strain response) in their different types of thin ply carbon-carbon interlayer hybrid composites with high initial modulus. The major problem of this kind of composite is higher manufacturing cost. The main objective to study the M55/T700 hybrid configuration to demonstrate pseudo-ductility with high strength and stiffness as an alternative of expensive thin-ply laminate. To achieve this, M55/T700 micro-wrapped hybrid tow UD and UD woven composite laminates were manufactured with room temperature curing resin (RTCR) and the pseudo-ductile properties were investigated. To compare micro-wrapped hybridisation with traditional hybridisation, M55/T700 side by side hybrid composite laminates were also manufactured and studied.

5.3.4.1 Microscopic analysis of composites

The cross-sectional images of M55/T700 side-by-side and micro-wrapped hybrid tow composites are shown in Figure 5.15. A similar distribution like T700/S-G (Figure 5.8)

was observed in this configuration. In side-by-side composites, M55 and T700F distributed randomly inside and on the surface of the composites (Figure 5.15a) but in micro-wrapped hybrid, the core tows (M55) were fully covered by a sheath (T700) (Figure 5.15b).

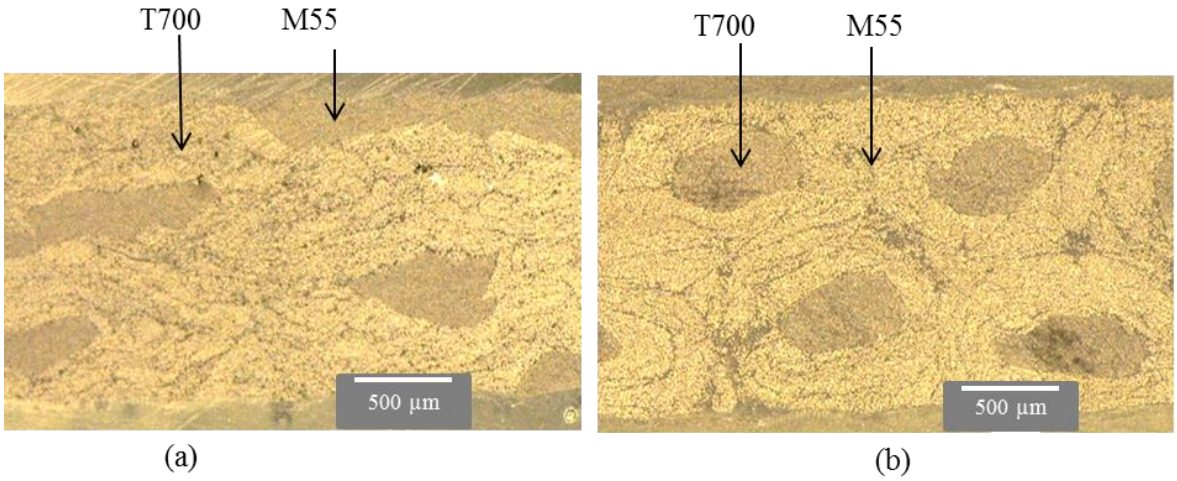

Figure 5.15: Cross-sectional images of M55/T700 UD composites: (a) side-by-side and (b) micro-wrapped hybrid.

5.3.4.2 Tensile behaviour of M55/T700 side-by-side and micro-wrapped hybrid tow UD composites

Normalised tensile test results of different M55/T700 micro-wrapped hybrid composites are presented in Table 5.6. Stress-strain graph of M55/T700 side-by-side and micro-wrapped hybrid tow composites show in Figure 5.16 and Figure 5.17 respectively. In this hybrid configuration, failure behaviour similar to that of the T700/S-G hybrid configuration was observed. A significant drop in stress (around 16.1%) was observed after initial failure with some cracks on the specimen surface (Figure 5.16 b) in the case of the side-by-side hybrid composite. The initial failure happened at 0.75% strain which is slightly smaller than M55 carbon fibre strain to failure. As shown in Figure 5.16 after initial failure a plateau region follows then the stress again increases to an ultimate value higher than pseudo-yield stress. The pristine and failed images of the specimen are shown in (Figure C1-f, Appendix C). In contrast, micro-wrapped hybrid tow composite shows the good pseudo-ductility response with a smooth stress transition between the initial and second linear part of the stress-strain curves (Figure 5.17). A horizontal plateau region in the stress-strain curve was observed between the first and second straight section with little stress drop (about 8%). The flat stress plateau region

indicated that M55 fragmented gradually and transferred the load to T700 without any catastrophic delamination. Czel *et al.* [14] reported similar results in thin-ply interlayer high modulus and high strength carbon/epoxy composites. They sandwiched the thin-ply high modulus carbon fibre with thin-ply high strength carbon fibre and manufactured the composites. The tensile test results demonstrated that the central high modulus carbon plies fragmented and delaminated steadily from the outer high strength carbon layer under tensile loading. It is interesting to note, that a higher initial modulus around 150 GPa with high pseudo-yield stress around 1110 MPa was attained in the configuration (Table 5.6). The obtained initial modulus was about 35% higher than the T700 carbon epoxy composites but the final modulus was around 104 GPa which was similar to T700 carbon-epoxy composites. The low strain material (M55) failure happened at 0.73% strain and there was no crack or damage observed on the specimen surface after an initial failure (Figure 5.17b). After the M55 failure, the load was transferred to surround T700, smoothly and there no change on the specimen surface up to 1.80% strains. The final strain to failure of the specimen was 2.05%. This specimen delivered large stress and strain boundary between the first fracture of the LS material and ultimate failure of the HS material. This metal-like failure behaviour of micro-wrapped hybrid tow composite was a significant achievement compared to the brittle failure of the conventional carbon fibre UD composite.

Table 5.6: Normalised tensile test results of M55/T700 hybrid composites

Specimen Type	M55/T700 SBS UD	M55/T700 MW UD	M55/T700 MW UD woven
Pseudo-yield Stress (MPa)	1113.3±20.2	1128.9±30.0	1111.1±21.9
Stress drop (MPa)	179.7±25.1	90.9±18.5	83.4±2.2
Maximum stress (MPa)	1863.9±18.1	1845.9±30.9	1804.1±66.3
Initial modulus (GPa)	146.01±3.50	151.1±4.92	152.2±2.19
Final modulus (GPa)	101.61±8.61	104.34±6.14	102.13±5.62
Pseudo-yield strain (%)	0.75±0.01	0.73±0.01	0.71±0.01
Final failure Strain (%)	2.03±0.04	2.05±0.03	2.05±0.04
Difference between two failure strains (%)	1.29±0.05	1.32±0.04	1.34±0.03
Pseudo-ductile strain (%)	0.80±0.04	0.84±0.04	0.80±0.05

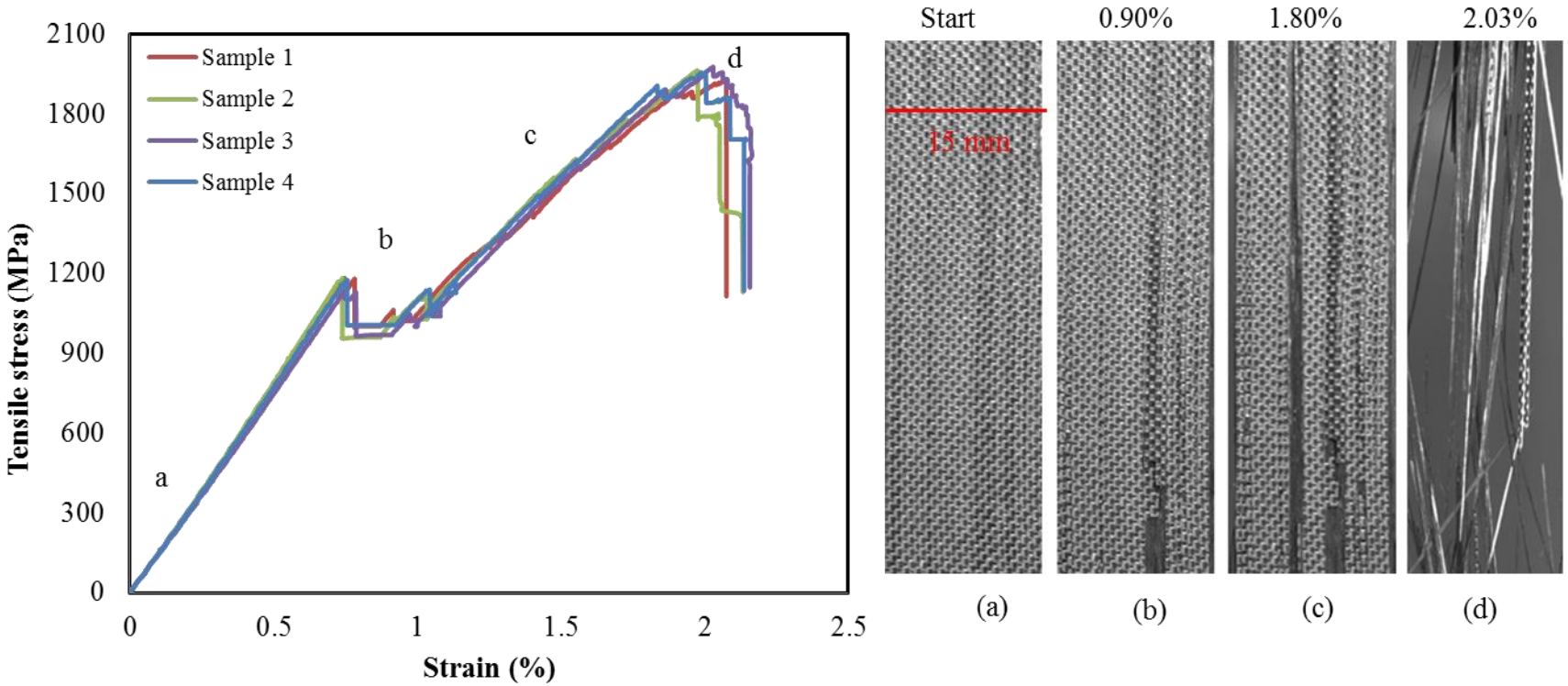

Figure 5.16: Stress-strain graph of M55/T700 side by side hybrid tow UD composite. Right side video extensometer images of the specimen at different strain levels during tensile loading; (a) start, (b) after initial failure, (c) just before ultimate failure and (d) after ultimate failure.

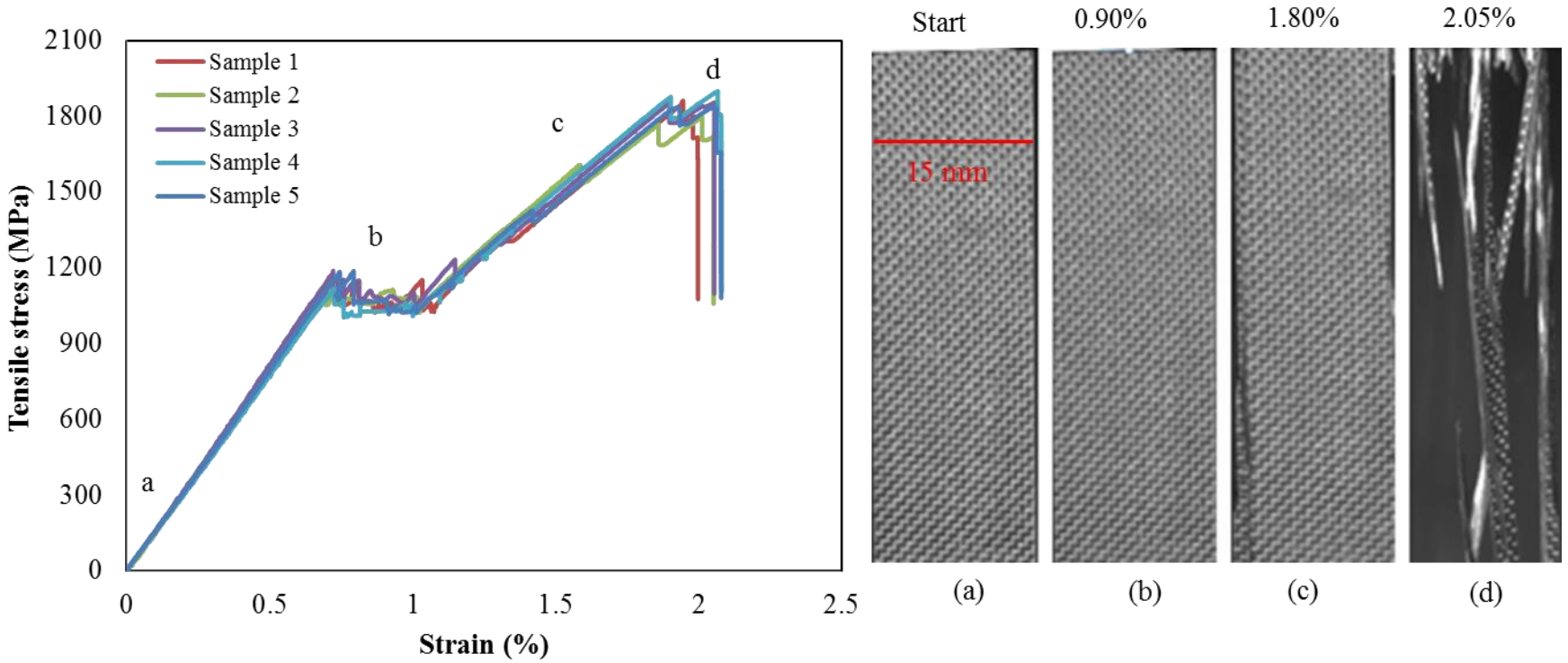

Figure 5.17: Stress-strain graph of M55/T700 micro-wrapped hybrid tow UD composite. Right side video extensometer images of the specimen at different strain levels during tensile loading; (a) start, (b) after initial failure, (c) just before ultimate failure and (d) after ultimate failure.

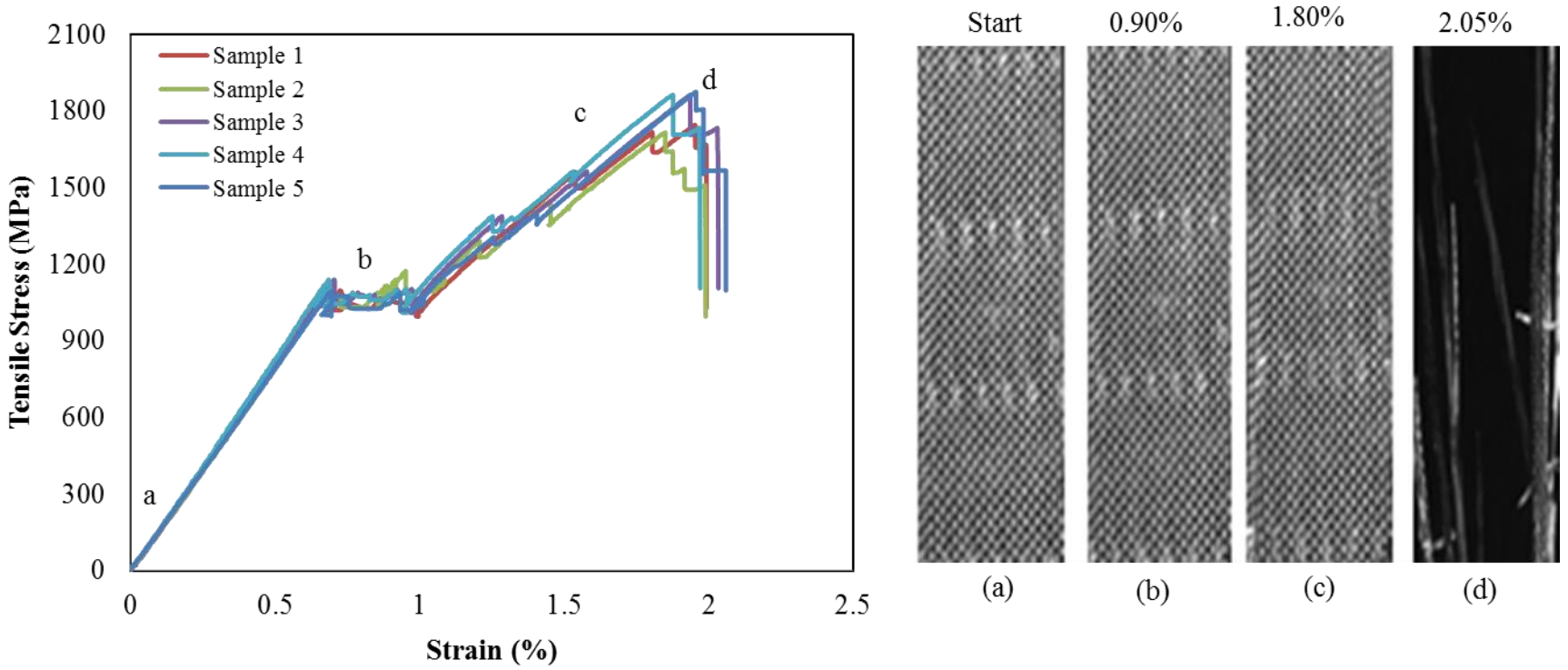

Figure 5.18: Stress-strain graph of M55/T700 micro-wrapped hybrid tow UD woven composite. Right side video extensometer images of the specimen at different strain levels during tensile loading; (a) start, (b) after initial failure, (c) just before ultimate failure and (d) after ultimate failure.

5.3.4.3 Tensile behaviour of M55/T700 micro-wrapped hybrid UD woven composite

To study the effect of UD woven fabric on the composite properties, UD woven composite was also manufactured from M55/T700 micro-wrapped hybrid tow UD fabrics. Similar results to those of the T700/S-G hybrid configuration were observed. The M55/T700 micro-wrapped UD woven composite also demonstrated good pseudo-ductile response during tensile loading (Figure 5.18). There was some difference observed in the tensile test results between micro-wrapped UD and micro-wrapped UD woven composites (Table 5.6). Less stress drop was observed in the UD woven composite and a smooth stress transfer occurred between core and sheath material. There was no major variation in other properties compared to the M55/T700 micro-wrapped UD composites. Only a slightly lower ultimate stress value was detected in UD woven composite than UD composites (Table 5.6). This may have been caused by some fibre damage that happened during weaving. The pristine and failed images of M55/T700 micro-wrapped hybrid tow UD woven composite specimen are shown in (Figure C1-g, Appendix C).

Figure 5.19 shows the normalised tensile properties of different M55/T700 hybrid composites. There was a significant difference observed in stress drop between the side by side and micro-wrapped hybrid tow composites. Minimum stress drop after initial failure was observed in micro-wrapped UD woven composite (Figure 5.19b). However, there was no major difference detected in the other properties of the composites.

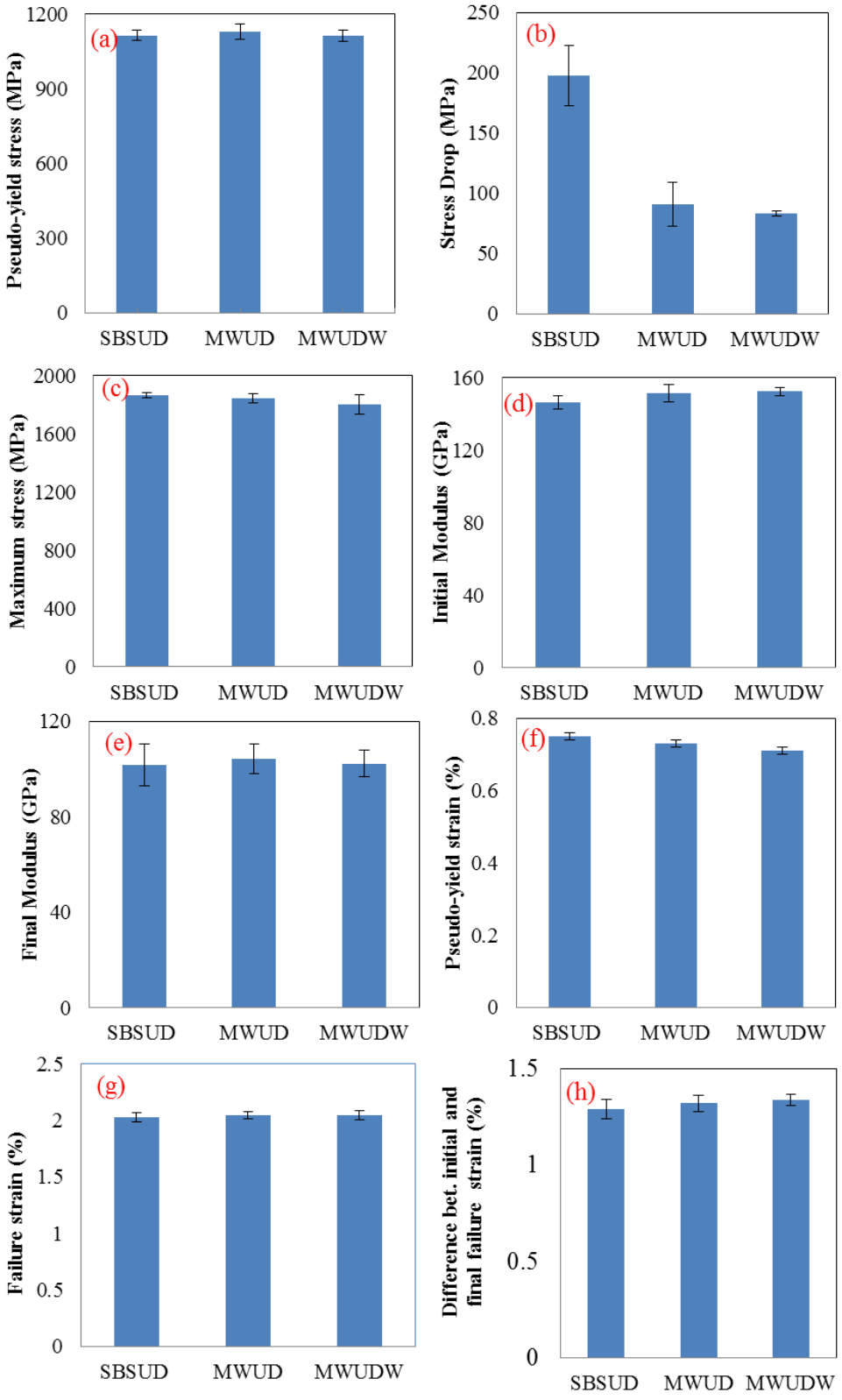

Figure 5.19: Normalised tensile properties of M55/T700 hybrid composites. Sample notation: SBSUD = side-by-side UD, MWUD = micro-wrapped UD and MWUDW = micro-wrapped UD woven.

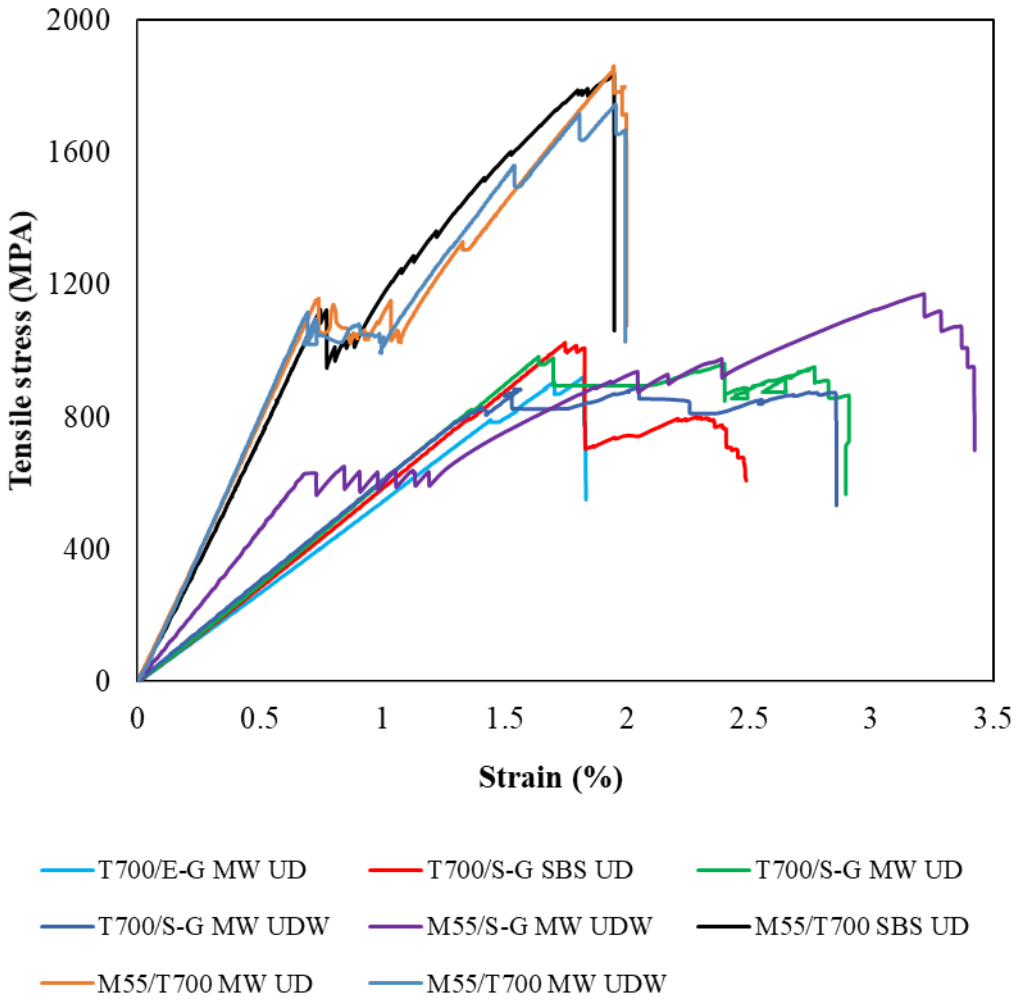

Figure 5.20: A typical normalised stress-strain graph of different hybrid composites.

A typical normalised stress-strain graph of different hybrid configurations with micro-wrapped and side by side hybrid architectures are shown in Figure 5.20. Details of the curves have been described in the above individual hybrid configuration sections.

5.4 Summary

This experimental study reported the effect of micro-wrap hybridisation on the ductile or pseudo-ductile properties of the UD and UD woven composites. The following conclusions were drawn from the study:

- Different types of UD woven preforms were made from micro-wrapped hybrid tow for the manufacturing of UD woven composites.
- A wide range of new high performance, micro-wrapped and side by side hybrid tow UD and UD woven composites with different hybrid configurations were presented. Micro-wrapped hybrid architectures demonstrated pseudo-ductility for all hybrid configurations.
- T700/E-G micro-wrapped hybrid configuration did not have enough strain after pseudo-yielding (low pseudo-ductile strain) because of a small difference between the failure strain of the T700 and E-G composites.
- T700/S-G micro-wrapped hybrid configuration offered good strain after pseudo-yielding but a very low increase in stress value was attained. A significant stress drop was observed in side by side hybrid architectures compared to micro wrapped hybrid architectures in this configuration. Micro-wrapped UD woven fabric composite showed less stress drop compared to the T700/S-G micro-wrapped UD composite.
- The M55/S-G combination provided extended stress and strain after pseudo-yield strain and before final failure (good pseudo-ductility) with high initial modulus providing about 104% increase compared to the high strain material baseline (S-G).
- After initial failure, a plateau region was observed between the first and second straight section of the stress-strain graph for M55/S-G and M55/T700 micro-wrapped hybrid configurations. It means that the low elongation core fibre fragmented, instead of causing unstable delamination or immediate fracture of the high elongation sheath fibre.
- In M55/T700 hybrid combination, micro-wrapped hybrid tow composites also demonstrated good pseudo-ductility compared to the side by side hybrid composites with high initial modulus and pseudo-yield stress. A significant difference in stress drop after pseudo-yielding was also observed between side by side and micro-wrapped hybrid architectures.
- The novel micro-wrapped hybrid architecture was a suitable approach to produce low-cost textile preform alternatives to expensive thin-ply concepts for high-performance pseudo-ductile composites.

References

[1] K. Allaer, I. De Baere, P. Lava, W. Van Paepegem, and J. Degrieck, “On the in-plane mechanical properties of stainless steel fibre reinforced ductile composites,” *Compos. Sci. Technol.*, vol. 100, pp. 34–43, Aug. 2014.

[2] M. G. Callens, L. Gorbatikh, and I. Verpoest, “Ductile steel fibre composites with brittle and ductile matrices,” *Compos. Part A Appl. Sci. Manuf.*, vol. 61, pp. 235–244, Jun. 2014.

[3] J. D. Fuller and M. R. Wisnom, “Exploration of the potential for pseudo-ductility in thin ply CFRP angle-ply laminates via an analytical method,” *Compos. Sci. Technol.*, vol. 112, pp. 8–15, May 2015.

[4] J. D. Fuller and M. R. Wisnom, “Pseudo-ductility and damage suppression in thin ply CFRP angle-ply laminates,” *Compos. Part A Appl. Sci. Manuf.*, vol. 69, pp. 64–71, Feb. 2015.

[5] J. D. Fuller, M. Jalalvand, and M. R. Wisnom, “Combining fibre rotation and fragmentation to achieve pseudo-ductile CFRP laminates,” *Compos. Struct.*, vol. 142, pp. 155–166, May 2016.

[6] S. Ogihara and H. Nakatani, “Effect of ply thickness on mechanical properties in CFRP angle-ply laminates,” in *Proceedings of ECCM-15*, 2012, no. June, pp. 1–6.

[7] H. Diao, P. Robinson, M. R. Wisnom, and A. Bismarck, “Unidirectional carbon fibre reinforced polyamide-12 composites with enhanced strain to tensile failure by introducing fibre waviness,” *Compos. Part A Appl. Sci. Manuf.*, vol. 87, pp. 186–193, Aug. 2016.

[8] S. Pimenta and P. Robinson, “Wavy-ply sandwich with composite skins and crushable core for ductility and energy absorption,” *Compos. Struct.*, vol. 116, pp. 364–376, Sep. 2014.

[9] G. Czél and M. R. Wisnom, “Demonstration of pseudo-ductility in high performance glass/epoxy composites by hybridisation with thin-ply carbon prepreg,” *Compos. Part A Appl. Sci. Manuf.*, vol. 52, pp. 23–30, Sep. 2013.

[10] M. R. Wisnom, G. Czél, J. D. Fuller, and M. Jalalvand, “High performance pseudo-ductile composites,” *20th Int. Conf. Compos. Mater. Copenhagen,* no. July, pp. 3–7, 2015.

[11] M. Jalalvand, G. Czél, and M. R. Wisnom, “Parametric study of failure mechanisms and optimal configurations of pseudo-ductile thin-ply UD hybrid composites,” *Compos. Part A Appl. Sci. Manuf.*, vol. 74, pp. 123–131, Jul. 2015.

[12] M. Jalalvand, G. Czél, and M. R. Wisnom, “Damage analysis of pseudo-ductile thin-ply UD hybrid composites – A new analytical method,” *Compos. Part A Appl. Sci. Manuf.*, vol. 69, pp. 83–93, Feb. 2015.

[13] M. Fotouhi, P. Suwarta, M. Jalalvand, G. Czel, and M. R. Wisnom, “Detection of fibre fracture and ply fragmentation in thin-ply UD carbon/glass hybrid laminates using acoustic emission,” *Compos. Part A Appl. Sci. Manuf.*, vol. 86, pp. 66–76, Apr. 2016.

[14] G. Czél, M. Jalalvand, M. R. Wisnom, and T. Czigány, “Design and characterisation of high performance, pseudo-ductile all-carbon/epoxy unidirectional hybrid composites,” *Compos. Part B Eng.*, vol. 111, pp. 348–356, Feb. 2017.

[15] M. Jalalvand, G. Czél, and M. R. Wisnom, “Numerical modelling of the damage modes in UD thin carbon/glass hybrid laminates,” *Compos. Sci. Technol.*, vol. 94, pp. 39–47, 2014.

[16] M. Jalalvand, G. Czél, M. W.-C. S. and Technology, and undefined 2014, “Numerical modelling of the damage modes in UD thin carbon/glass hybrid laminates,” *Elsevier*.

[17] L. Greve and A. K. Pickett, “Modelling damage and failure in carbon/epoxy non-crimp fabric composites including effects of fabric pre-shear,” *Compos. Part A Appl. Sci. Manuf.*, vol. 37, no. 11, pp. 1983–2001, Nov. 2006.

[18] S. COSTA, “Physically based fibre kinking model for crash of composites,” *THESIS Licent. Eng. Dep. Appl. Mech. CHALMERS Univ. Technol. Gothenburg, Sweden,* 2016.

[19] “ASTM D3039 Standard Test Method for Tensile Properties of Polymer Matrix Composite Materials -D3039 2008, Annual Book of ASTM Standards.”

[20] X.-S. Y. • S. D. • L. Z. Editors, “Composite Materials Engineering, Volume 1: Fundamentals of Composite Materials,” *B. Springer*, p. 618, 2018.

[21] K. Naito, J.-M. Yang, and Y. Kagawa, “Tensile properties of high strength polyacrylonitrile (PAN)-based and high modulus pitch-based hybrid carbon fibers-reinforced epoxy matrix composite,” *J. Mater. Sci.*, vol. 47, no. 6, pp. 2743–2751, Mar. 2012.

Chapter 6: Effect of Matrix Properties on the Ductility of Composites

In this chapter, an effect of matrix properties on the mechanical properties of the micro-wrapped hybrid tow composites has been described. Room temperature and high temperature curing epoxy resin were used to manufacture thermoset composites. An investigation has been carried out on single tow composite rods and UD fabric composite laminates.

6.1 Introduction

High-performance fibre reinforced composites like carbon or glass fibre composites have lower strain to failure and have a brittle failure. The reason for this is the inherent brittleness of the fibres. Different attempts have been undertaken to improve the failure strain and change the brittle failure behaviour of the composites such as fibre hybridisation and introducing extra length in the fibre. On the other hand, the resin systems also have a significant effect on the mechanical properties of the composites [1]–[4]. The mechanical properties of the composites can be enhanced by improving the fibre matrix bonding. The fracture behaviour of the composites depends on the strength of the fibre-matrix interface. A strong interface provides high strength and stiffness but low resistance to fracture which causes brittle failure. Alternatively, a weak interface offers low strength and stiffness but high resistance to failure fracture [5].

In the manufacturing of high-performance composites, thermoset epoxy-based resins are the best matrix material. Epoxy resin is a low viscosity reactive liquid which has good wettability. Composites manufactured with epoxy matrix provides exceptional mechanical properties and a wide range of environmental stability. The epoxy matrix is most prevalent to manufacture of thermoset composite for aircraft application. There are three main damage initiation modes in the composites which are, matrix cracking, matrix debonding and fibre rupture [1], [6]. As the initial damage in the composite is controlled by matrix cracking and matrix deboning, so the matrix properties have high influence in the composite failure. The curing process of a matrix plays an important role in the formation of the final cross-linking network, which influences the mechanical properties of the composite [5]. Higher crosslink density lowers the failure

strain but improves the chemical resistance and increases T_g. In contrast, lower crosslink density enhances the toughness by allowing the higher strain to failure. Caux *et al.* reported that in some cases plastic deformation may occur in epoxy resin by uncoiling covalent bonds rather than breaking them [7].

Lavengood and Ishai [4] summarised the mechanical characteristics of the unfilled resins and corresponding unidirectional (UD) composites from the previous studies. The results are presented in Table 6.1. The UD transverse composites fabricated with ductile matrix has higher strength and ultimate strain than the brittle matrix composites. In contrast off-axis, ductile composites have lower strength but significantly higher ultimate failure strain than the brittle matrix composites. They studied the effect of matrix ductility on the mechanical performance of glass fibre epoxy cross-plied composites. Their study also has shown that composite with a ductile matrix has higher initial modulus, slower crack propagation in the transverse layer and higher ultimate stress and strain.

Table 6.1: Mechanical characteristics of brittle and ductile glass-epoxy composites

Orientation	0º		10 º		20 º		30 º		45 º		60 º		90 º		Unfilled matrix	
Composite type	B	D	B	D	B	D	B	D	B	D	B	D	B	D	B	D
Ultimate stress $x10^3$ psi	145	150	45	32	25	18	16	12	11	10	9	9	8	9	12	8
Ultimate strain (%)	2.2	2.5	.95	2.2	1.4	1.7	.80	2.1	.85	3.0	.55	1.7	.45	.95	3.5	5.6
Young modulus $x10^6$ psi	6.0	6.1	5.6	5.2	3.7	3.3	3.2	2.2	1.4	1.7	1.2	1.6	1.2	1.3	.44	.31

B = brittle matrix and D = ductile matrix

Callens *et al.* [2] investigated the steel fibre composites with brittle (epoxy) and ductile (PA-6) matrices. They used two different matrix systems thermoset and thermoplastic. The steel fibre composite with a ductile matrix system provided higher strain to failure (12.7%) than the brittle matrix system (7.3%). The study also showed that the tensile stress and stiffness of the ductile matrix composites was higher than the brittle matrix composites. These results suggested that the strength of the interface plays a major role in the fracture mechanism of the steel fibre composites. Izuka *et al.* [8] studied the effect of resin elongation (2, 4 and 6%) in the longitudinal strength of UD carbon fibre

composites. The study showed that as the elongation of the resin was increased, the ultimate strength of the composite improved by 10-20%.

The current study investigated two epoxy resin systems on the mechanical performance of micro-wrapped hybrid tow composites. Two different types of epoxy resins, room temperature curing resin (RTCR) and high temperature curing resin (HTCR) were used to manufacture the composite rods and UD woven composites. Finally, the mechanical behaviour of different composites was studied by longitudinal tensile test. Emphasis was given to the effect of the matrix curing temperature on the ultimate strain to failure of the composites.

6.2 Experimental

6.2.1 Raw materials

Two different hybrid configurations, M55/T700 and M55/S-G micro-wrapped hybrid tows were used as reinforcement materials for this study. The studies were conducted using single hybrid tow composite rods and UD woven composite laminates. The preparation method of micro-wrapped hybrid tow and UD fabric were presented in chapter 4 (section 4.2.4) and 5 (section 5.2.2). The properties of the micro-wrapped hybrid tows were reported in chapter 4 (Table 4.2).

Two different types of epoxy resin that differ in their curing cycle and ductility were used for this study. Araldite ® LY 564 resin and Aradur ® 2954 hardener (Huntsman) was used as a matrix for high-temperature curing resin (HTCR) and EL2 epoxy laminating resin and AT30 slow hardener (easy composites) were used as a matrix for room temperature curing resin (RTCR). Details of two different matrix properties are shown in Table 6.2

Table 6.2: Properties of different resins [9], [10]

Resin & Hardener	Curing Temp. and time	Post curing Temp. and time	Tensile Strength (MPa)	Elongation at Break (%)	Tensile Modulus (GPa)	T_G (°C)
Araldite LY564 and Aradur 2954	80 °C 2 h	140 °C 6 -8 h	71-77	4.5-5.5	2.5-2.6	123-130
EL2 Epoxy and AT30 Slow	Room temp. 48 h	None	70-80	6.0-10.0	-	82-88

6.2.2 Manufacture of composites rods and laminates

Details of the manufacturing procedure of the composite rods used for the present study were discussed clearly in chapter 4 (section 4.2.6). Single hybrid tow composite rods were manufactured by using manual resin infusion method with the help of a pinboard keeping the tow under tension to ensure the tow remain straight. M55/T700 and M55/S-G micro-wrapped hybrid tow were used to fabricate the composite rods. RTCR and HTCR were used for both hybrid configurations. In case of RTCR, the curing was carried out at room temperature for 48 hrs and for HTCR, curing and post-curing were carried out in an oven at 80 ºC for 2 hours and 140 ºC for 6 hours. Four different micro-wrapped single tow composite rods were prepared.

Composite laminates were also manufactured from M55/T700 micro-wrapped hybrid tow UD woven fabrics with RTCR and HTCR using a vacuum-assisted resin infusion process. Two metal plates were used on the bottom and top of the laminate to control the same surface on both sides of the laminate. Details of the fabrication process of UD woven composites were described in chapter 5 (section 5.2.3)

6.2.3 Preparation of specimen for in-plane shear stress-strain measurement

Measurement of in-plane shear properties of composites is not straightforward. There are several test methods available to measure the in-plane shear properties. Tensile testing of a $(\pm 45)_{ns}$ laminate is the simplest test method to measure the in-plane properties (such as shear stress, shear strain and shear modulus) of the composites. For the manufacturing of in-plane shear stress-strain measurement specimen, M55/T700 micro-wrapped hybrid tow UD fabrics were used. A 2-ply 0/90° composite was manufactured from M55/T00 micro-wrapped hybrid tow UD woven fabric. Room temperature curing resin (RTCR) and high temperature curing resin (HTCR) were used to prepare two pieces laminates. Two metal plates were used on the bottom and top of the laminate to control the same surface on both sides of the laminate. Specimens for the ±45° in-plane shear-stress test were cut from 0/90° laminate. The specimen preparation process is shown in Figure 6.1

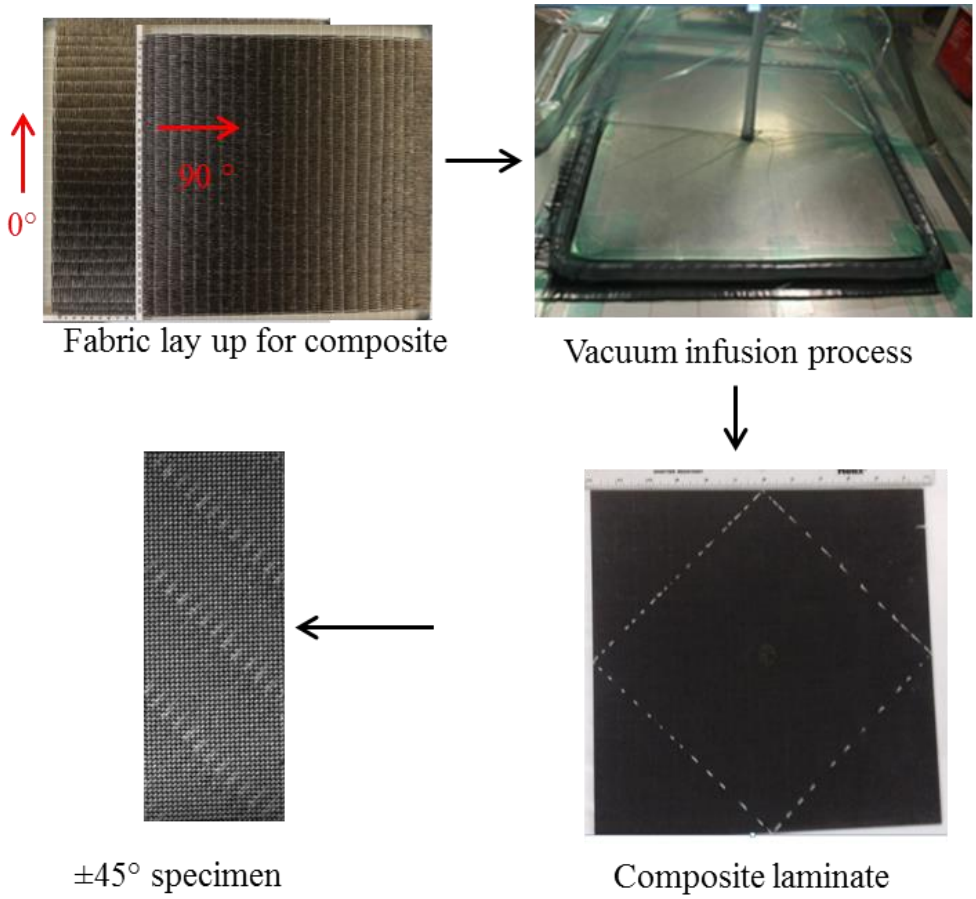

Figure 6.1: Preparation of M55/T700 micro-wrapped hybrid tow ±45°composites for in-plane shear stress-strain measurement.

6.2.4 Mechanical Testing of the composites

The longitudinal tensile test was performed to determine the pseudo-ductile properties of the composite rods and UD woven fabric composites. The test was carried out according to ASTM D3039 [11] on an Intron 5982 machine with a cross-head speed of 2 mm/min. The load was recorded using a 100 kN load cell and the strain was measured using Imetrum video extensometer with a nominal gauge length of 50 mm. In-plane shear stress-strain test was also carried out in the same machine as per ASTM D3518 [12].

6.3 Results and Discussion

6.3.1 In-plane shear stress-strain of two resin systems:

The in-plane shear stress-strain response of M55/T700 micro-wrapped hybrid tow laminates with HTCR and RTCR curing resins are shown in Figure 6.2 a and b respectively. Normalised results are presented in Table 6.3. The maximum shear stress values for both samples were low compared to prepreg. It might be due to the lower number of fabric layers on the prepared samples. Initial shear stress-strain behaviour up to a certain shear strain for both samples was linear and it was followed by a non-linear transition. The nonlinearity of the RTCR was much prominent than HTCR specimen. Ideally, the RTCR laminate exhibited ductile behaviour during the shear loading. On the other hand, HTCR showed brittle failure behaviour (Figure 6.2a) compared to the RTCR specimen (Figure 6.2b). A higher ultimate shear-stress value was obtained in HTCR compared to RTCR but higher shear modulus was observed in RTCR. However, about 28% higher shear-strain at failure was observed in RTCR than the HTCR. This failure behaviour of the ±45° composites indicated that the RTCR can contribute to the extended strain in the UD composites. This ductile behaviour could allow the stressing of the filament easily which can contribute to the higher strain to failure in the composite.

Table 6.3: Normalised in-plane shear stress-strain results of ±45° M55/T700 micro-wrapped UD woven composites

Specimen type	Maximum shear stress (MPa) ±SD	Shear strain at failure (%) ±SD	Shear modulus (GPa) ±SD
M55/T700 MW ±45° UD woven (HTCR)	55.83±1.58	2.24±0.11	3.83±0.09
M55/T700 MW ±45° UD woven (RTCR)	50.00±2.25	2.86±0.27	4.54±0.21

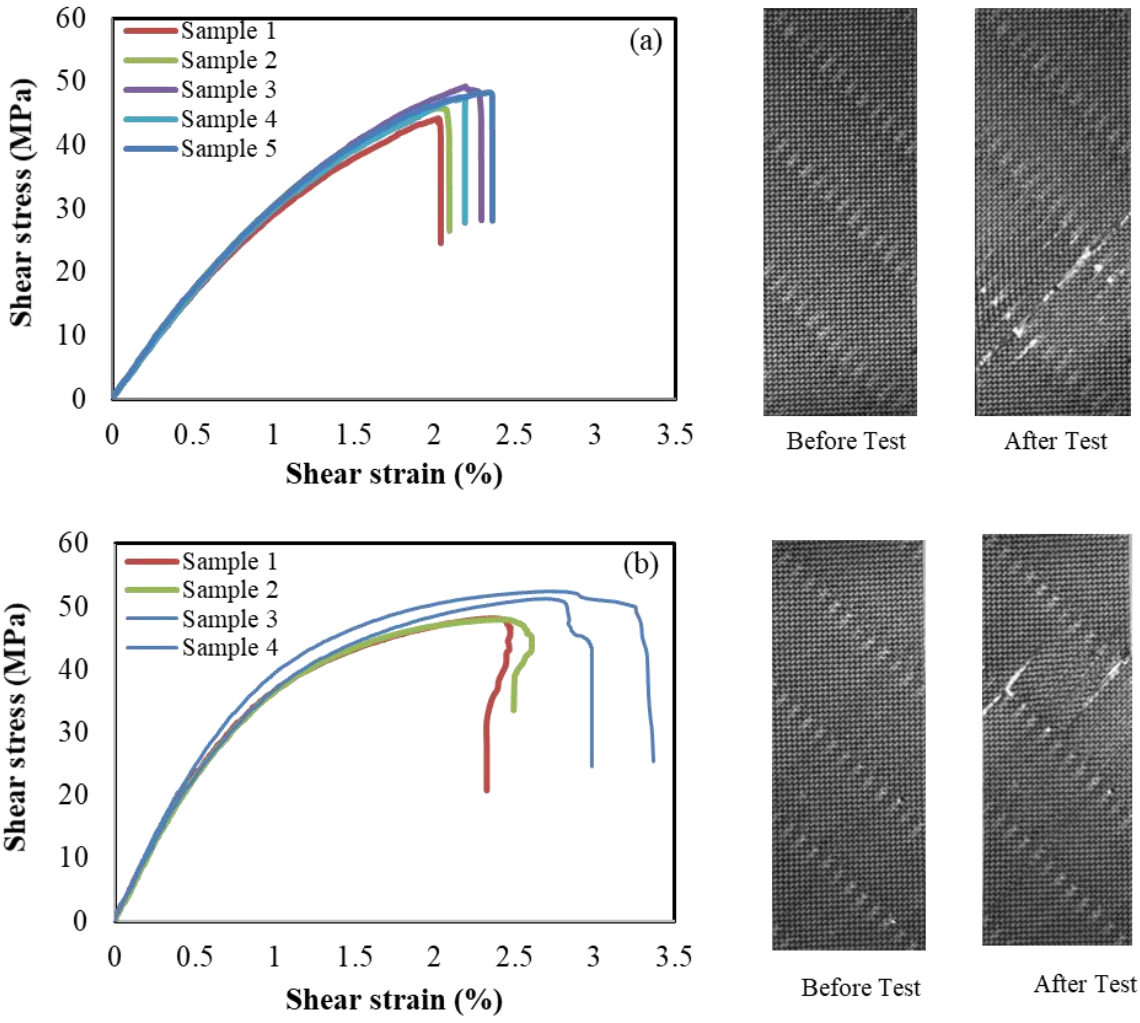

Figure 6.2: In-plane shear stress-strain curve of ±45° M55/T700 micro-wrapped hybrid tow laminate: (a) high temperature curing resin and (b) room temperature curing resin. Right side video extensometer images of the specimen before and after the test.

6.3.2 Effect of resin on T55/T700 hybrid architecture

To study the influence of matrix ductility on the composite mechanical properties, composite rods and composite laminates were manufactured from M55/T700 micro-wrapped hybrid tow with HTCR and RTCR. Figure 6.3 and Figure 6.4 shows the tensile stress-strain graph of M55/T700 micro-wrapped hybrid tow composite rods and composite laminates with two different resin systems respectively. The data were normalised to adjust the raw test values to a single specified fibre volume fraction. The data normalised method was explained in chapter 4 (section 4.2.8) and chapter 5 (section 5.2.6) for composite rods and composites laminate respectively. The fibre

volume fraction of different composite rods and laminates are presented in (Table D1 and Table D2, Appendix D). Normalised pseudo-ductile properties of composite rods and composite laminates are presented in Table 6.4 and Table 6.5 respectively. All the specimens exhibited pseudo-ductile response on their stress-strain curves. The initial failure happened around 0.72% strain for RTCR and HTCR composites. The low strain material (M55) failure start at this strain. After that, a flat plateau region was observed with small stress fluctuations which indicated that low strain material (M55) fragmented gradually and transferred the load to high strain material (T700) without any catastrophic delamination. The stress drop after initial failure was less in case of HTCR for both composite rod and laminate than the RTCR. The cause for lower stress drop in HTCR composites was not clear, further study needs to understand the reason.

The interesting finding of this study is that the RTCR composite has higher stress and ultimate strain to failure than the HTCR composite in both composite rod and laminate (Table 6.4 and Table 6.5). The use of RTCR resin increased the ultimate strain to failure of the composite about 27%. This results indicated that the ductility of the matrix has a vital impact on the ductility of the composite. As shown in Figure 6.2 the RTCR specimen showed ductile behaviour in-plane shear stress-strain response. This ductile behaviour of the matrix could allow the stressing and reoriented of the filament easily which caused the higher strain to fail in the composites.

Table 6.4: Normalised tensile test results of M55/T700 micro-wrapped hybrid tow composite rods with two resins system

Specimen Type	HTCR	RTCR
Pseudo-yield Stress (MPa)	934.74±73.1	918.68±34.96
Stress drop (MPa)	83.98±23.30	129.70±20.90
Maximum stress (MPa)	1530.67±73.30	1788.4±43.91
Initial modulus (GPa)	128.44±4.19	130.51±11.86
Final modulus (GPa)	92.27±3.18	88.2±5.86
Pseudo-yield strain (%)	0.71±0.06	0.72±0.06
Final failure Strain (%)	1.65±0.07	2.09±0.04
Difference between two failure strain (%)	0.94±0.08	1.38±0.07
Pseudo-ductile strain (%)	0.48±0.03	0.71±0.06

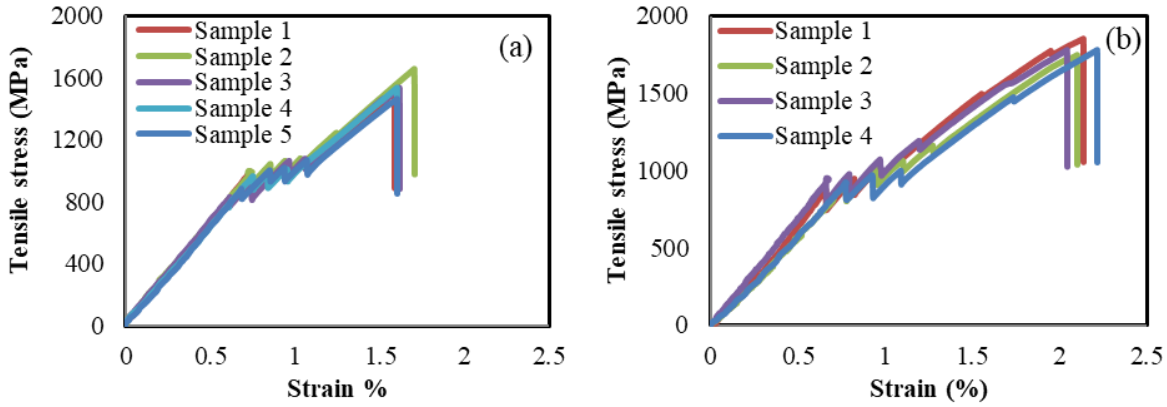

Figure 6.3: Stress-strain graph of M55/T700 micro-wrapped hybrid composite rods with two different resin system: (a) high temperature curing resin and (b) room temperature curing resin.

Table 6.5: Normalised tensile test results of M55/T700 micro-wrapped hybrid tow UD woven composite laminates with two resins system

Specimen Type	HTCR	RTCR
Pseudo-yield Stress (MPa)	1153.85±33.78	1111.1±21.9
Stress drop (MPa)	56.64±10.45	83.4±2.2
Maximum stress (MPa)	1666.8±55.60	1804.1±66.3
Initial modulus (GPa)	154.31±6.86	152.2±2.19
Final modulus (GPa)	100.75±4.88	102.13±5.62
Pseudo-yield strain (%)	0.72±0.03	0.71±0.01
Final failure Strain (%)	1.59±0.03	2.05±0.04
Difference between two failure strains (%	0.87±0.02	1.34±0.03
Pseudo-ductile strain (%)	0.57±0.03	0.80±0.05

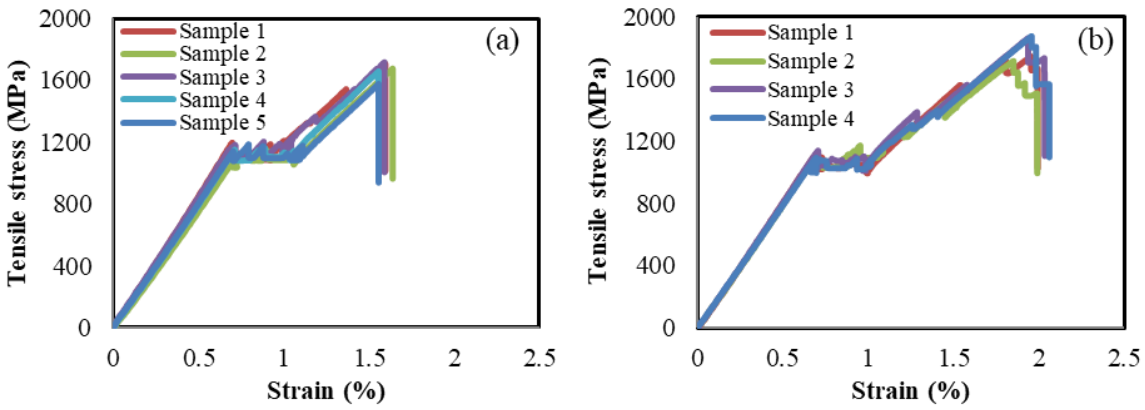

Figure 6.4: Stress-strain graph of M55/T700 micro-wrapped hybrid tow UD woven composite laminates with two different resin system: (a) high temperature curing resin and (b) room temperature curing resin.

A typical normalised stress-strain graph of M55/T700 micro-wrapped hybrid tow UD woven composite laminates with RTCR and HTCR are shown in Figure 6.5.

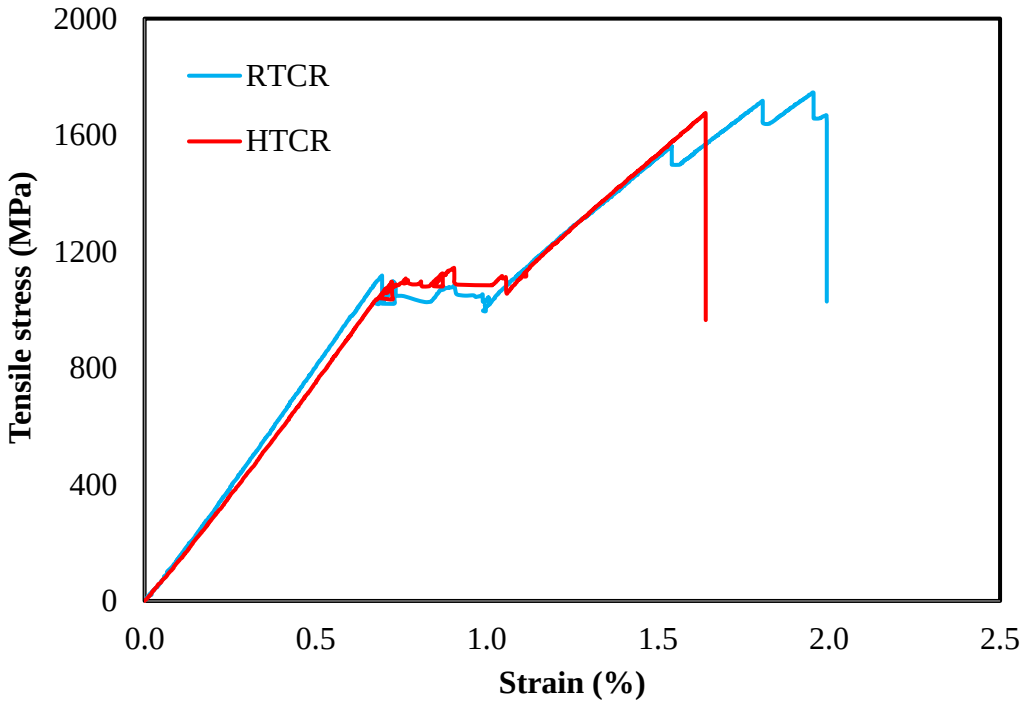

Figure 6.5: A typical normalised stress-strain graph of RTCR and HTCR composites.

6.3.3 Effect of resin on M55/S-G hybrid architecture

A similar investigation was carried out on the M55/S-G hybrid configuration. Composite rods were manufactured from M55/S-G micro-wrapped hybrid tow with RTCR and HTCR. The stress-strain curves of M55/S-G specimens along with video extensometer images are shown in Figure 6.6. A similar pseudo-ductile response was also observed in both resin system in this hybrid configuration. The initial failure of the specimens occurred about the same strain (Table 6.6) in both cases and was followed by a plateau region with small fluctuation of the stress. There were no changes observed after initial failure on the specimen surface in both RTCR and HTCR composites rods (Figure 6.6 d and h). In this hybrid configuration, lower stress drop was also observed in HTCR composite rods. However, RTCR composite rods have higher ultimate stress and strain value while the HTCR composites have slightly higher modulus. A significant improvement (about 25%) of the ultimate failure strain was attained with RTCR.

Table 6.6: Normalised tensile test results of M55/S-G micro-wrapped hybrid tow composite rods with two resins system.

Specimen Type	HTCR	RTCR
Pseudo-yield Stress (MPa)	571.43±14.35	515.4±21.63
Stress drop (MPa)	69.08±27.75	87.58±17.48
Maximum stress (MPa)	1220.1±58.67	1275.6±55.47
Initial modulus (GPa)	72.83±3.03	68.92±5.60
Final modulus (GPa)	40.25±3.45	34.65±3.07
Pseudo-yield strain (%)	0.75±0.03	0.72±0.05
Final failure Strain (%)	3.02±0.13	3.78±00.11
Difference between two failure strain (%)	2.34±0.15	3.06±0.08
Pseudo-ductile strain (%)	1.41±0.03	1.94±0.20

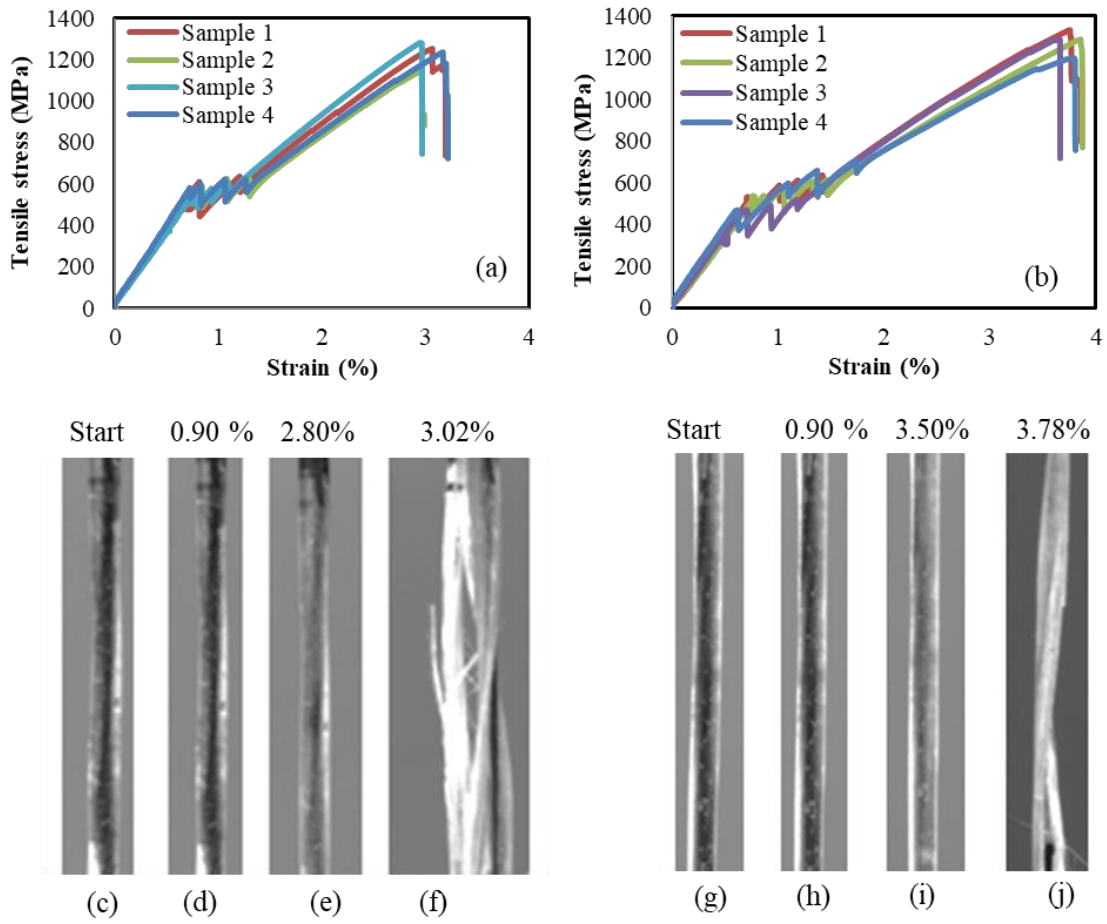

Figure 6.6: Stress-strain graph of M55/S-G micro-wrapped hybrid tow composite rods (a) HTCR and (b) RTCR with video extensometer images.

6.4 Summary

This study investigated the effect of two epoxy resin systems on the mechanical properties of the micro-wrapped hybrid tow composite rods and UD woven fabric composite laminate. In-plane shear stress-strain results revealed that room temperature curing resin (RTCR) laminate has higher ductility compared to high temperature curing resin (HTCR) laminate. Composites with both resin system showed pseudo-ductile response on their stress-strain curve during tensile loading. The ductile failure behaviour of the RTCR plays a significant role in the composites ultimate failure strain. About 27% higher failure strain was attained with RTCR composite compared to HTCR composites. The modulus and ultimate failure stress were also higher in RTCR composite than HTCR composite. However, lower stress drop after initial failure was observed with HTCR. Both hybrid configurations (M55/T700 and M55/S-G) showed similar results in the composite rods and laminates.

Reference

[1] C. Soutis, “Carbon fiber reinforced plastics in aircraft construction,” *Mater. Sci. Eng. A*, vol. 412, no. 1–2, pp. 171–176, Dec. 2005.

[2] M. G. Callens, L. Gorbatikh, and I. Verpoest, “Ductile steel fibre composites with brittle and ductile matrices,” *Compos. Part A Appl. Sci. Manuf.*, vol. 61, pp. 235–244, Jun. 2014.

[3] K. W. Garrett and J. E. Bailey, “The effect of resin failure strain on the tensile properties of glass fibre-reinforced polyester cross-ply laminates,” *J. Mater. Sci.*, vol. 12, no. 11, pp. 2189–2194, Nov. 1977.

[4] R. E. Lavengood and O. Ishai, “The mechanical performance of cross-plied composites,” *Polym. Eng. Sci.*, vol. 11, no. 3, pp. 226–232, May 1971.

[5] A. C. Garg and Y.-W. Mai, “Failure mechanisms in toughened epoxy resins—A review,” *Compos. Sci. Technol.*, vol. 31, no. 3, pp. 179–223, Jan. 1988.

[6] Y. Swolfs *et al.*, “Synchrotron radiation computed tomography for experimental validation of a tensile strength model for unidirectional fibre-reinforced composites,” *Compos. Part A Appl. Sci. Manuf.*, vol. 77, pp. 106–113, Oct. 2015.

[7] X. Caux, G. Coulon, and B. Escaig, “Influence of the degree of crosslinking on the plastic deformation behaviour of epoxy resins,” *Polymer (Guildf).*, vol. 29, no. 5, pp. 808–813, May 1988.

[8] K. Izuka, Y., Norita, T., Nishimura, T. & Fujisawa, “Manufacturing advance towards high strain fibres,” *Toray Industries Technical Data Sheet, Toray Industries Inc., Shiga, Japan*, 1986. .

[9] “Araldite ® LY564 Aradur ® 2954 Advanced Materials Araldite ® LY 564* / Aradur ® 2954*, Technical data sheet Huntsman.”

[10] “El2 Epoxy Laminating Resin, Technical Data Sheet, easycomposites.”

[11] “ASTM D3039 Standard Test Method for Tensile Properties of Polymer Matrix Composite Materials -D3039 2008, Annual Book of ASTM Standards.”

[12] A. International and F. indexed by mero, “ASTM, Standard Test Method for In-

Plane Shear Response of Polymer Matrix Composite Materials by Tensile Test of a ± 45° Laminate - D 3518/D 3518M 2001, Annual Book of ASTM Standards."

Chapter 7: Effect of Wrapping Directions of Micro-Wrapped Hybrid Tow in the Composite Properties

A novel process for the production of double helix micro-wrapped hybrid tow was presented in this chapter. The effect of wrapping direction (single and double helix) of micro-wrapped hybrid tow on the composite properties was also studied in the composite rods and laminates stage. Two-hybrid configurations M55/T700 and M55/S-G were considered for this study.

7.1 Introduction

The conventional filament-wrapped yarn is prepared by wrapping a continuous filament helically around the twistless or twisted fibrous core. The wrapping filament can be introduced in either clockwise (Z) or anti-clockwise (S) direction. The combination of the two wrapping methods is also used to prepare the X-wrap or double wrap (S and Z wrap) yarn. Louis and Salaun [1] showed that the X-wrap yarns have higher strength and elongation than the single Z-wrap yarn. Recently Shang *et al.* [2] reported that highly twisted double helix carbon nanotube yarn has a more stable structure compared to a single helical yarn. The double helix yarn is prepared from two single helical yarn segments by the conventional twisting method. The tensile test results showed that the double helix yarn breaks by two steps with one of the yarns breaking early and the other yarn breaking noticeably later with a large difference in tensile strain. A huge stress drop was observed after the fracture of first yarn and followed by fracture of second yarn. This type of failure is fully different than two-ply straight yarn.

Merter *et al.* [3] studied the effect of the hybrid yarn preparation technique on the mechanical properties of glass and polypropylene hybrid composites. Two different types of co-wrapped hybrid yarns were produced by twisting polypropylene fibre around the glass fibre by single wrap (S turn) and double wrapped (S and Z turn). The study showed that single co-wrapped hybrid yarn composite was better than double wrapped hybrid yarn composite. Movahhed *et al.* [4] studied the influence of covering percentage of glass/polyester co-wrapped hybrid yarn on physical and mechanical

properties of the composites. The study showed that wrapping percentage of co-wrapped yarn has a vital effect on the surface fracture of the composites.

To the best of the knowledge, very limited research has been done in composites using co-wrapped hybrid yarn. However, a few numbers of researches have been carried out using the conventional co-wrapped hybrid yarn in the thermoplastic composite where the wrapper yarn did not cover the core fully [3], [5]. So far no research has been carried out to study the effect of wrapping direction in the thermoplastic composites.

In this study, the effect of wrapping direction of micro-wrapped hybrid tow on the mechanical properties of the composite was investigated. Single and double-helix micro-wrapped hybrid tow composite rods and UD woven composite laminates were manufactured with epoxy resin and tested under tensile loading. Two-hybrid configurations M55/T700 and M55/S-G were considered for this study.

7.2 Experimental

7.2.1 Raw materials

In order to produce the double helix micro-wrapped hybrid tow AGY S-glass fibre (S-G), Torayca 6K high modulus carbon fibre tow (M55) and Torayca 6K high tenacity carbon fibre tow (T700) were used. Details of the fibre properties were presented in chapter 4 (Table 4.1). Two different hybrid configurations (M55/T700 and M55/S-G) were considered for this study. EL2 epoxy laminating resin and AT30 slow hardener (easy composites) were used. Details of matrix properties were shown in chapter 6 (Table 6.2).

7.2.2 Process Development for double helix micro-wrapped hybrid tow

In order to produce the double helix (S and Z turn) micro-wrapped hybrid tow, the single helix wrapping process which was explained in chapter 4 was modified. In this process, the straight core tow was helically wrapped with two sheath tows in the opposite directions. First, the straight core tow was wrapped with sheath in S directional turn (anti-clockwise) then the S turn wrapped tow was wrapped again with another sheath tow in the Z directional turn (clockwise). Flow chart and schematic of double helix micro-wrapped hybrid tow manufacturing process is shown in Figure 7.1. The

machine consists of the following units; core filament let-off, sheath filament wrapping (two units), nip roller speed control and winding system.

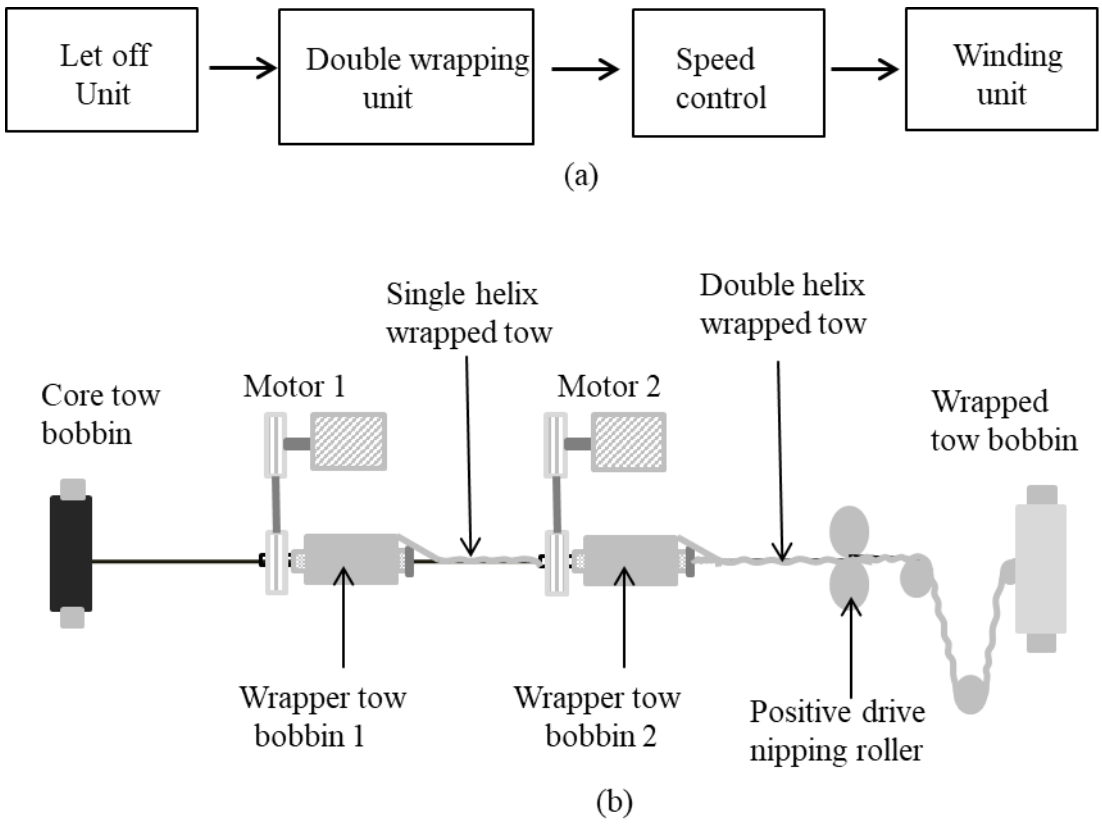

Figure 7.1: (a) Flow chart and (b) schematic of the double helix micro-wrapped hybrid tow manufacturing process.

7.2.3 Preparation of Double helix Micro-wrapped Hybrid Tow

To observe the effect of wrapping direction of sheath tow on the mechanical properties of the micro-wrapped hybrid tow and composite, double helix micro-wrapped hybrid tows were manufactured. The following different types of double helix micro-wrapped hybrid tows were prepared by using the new developed micro-wrapping process:

7.2.3.1 Preparation of M55/T700 double helix micro-wrapped hybrid tow

In this architecture, two 6K T700 tows were wrapped around the 6K M55 at two different directions. At first, 6K M55 tow was helically wrapped with 6K T700 in S turn then the S turn wrapped tow was again wrapped with another 6K T700 tow in Z

turn to finally produce the double-helix micro-wrapped hybrid tow. In this case, the second motor run in the reversed direction of the first motor. Figure 7.2 shows the photograph of the wrapping unit of the double helix micro-wrapped hybrid tow production line. As shown in Figure 7.2b, 6K T700 tow was wrapping around a 6K M55 tow and the wrapped tow again wrapping with 6K T700 in the opposite direction (Figure 7.2c). Finally, the wrapped tow was wound on a bobbin by the cross winding method. The resultant linear density of the hybrid tow was 1026 tex. The volume fraction of M55 and T700 fibre in the micro-wrapped hybrid tow was 20.20 and 79.80% respectively. The hybrid tow was labelled as M55/T700 DH micro-wrapped hybrid tow.

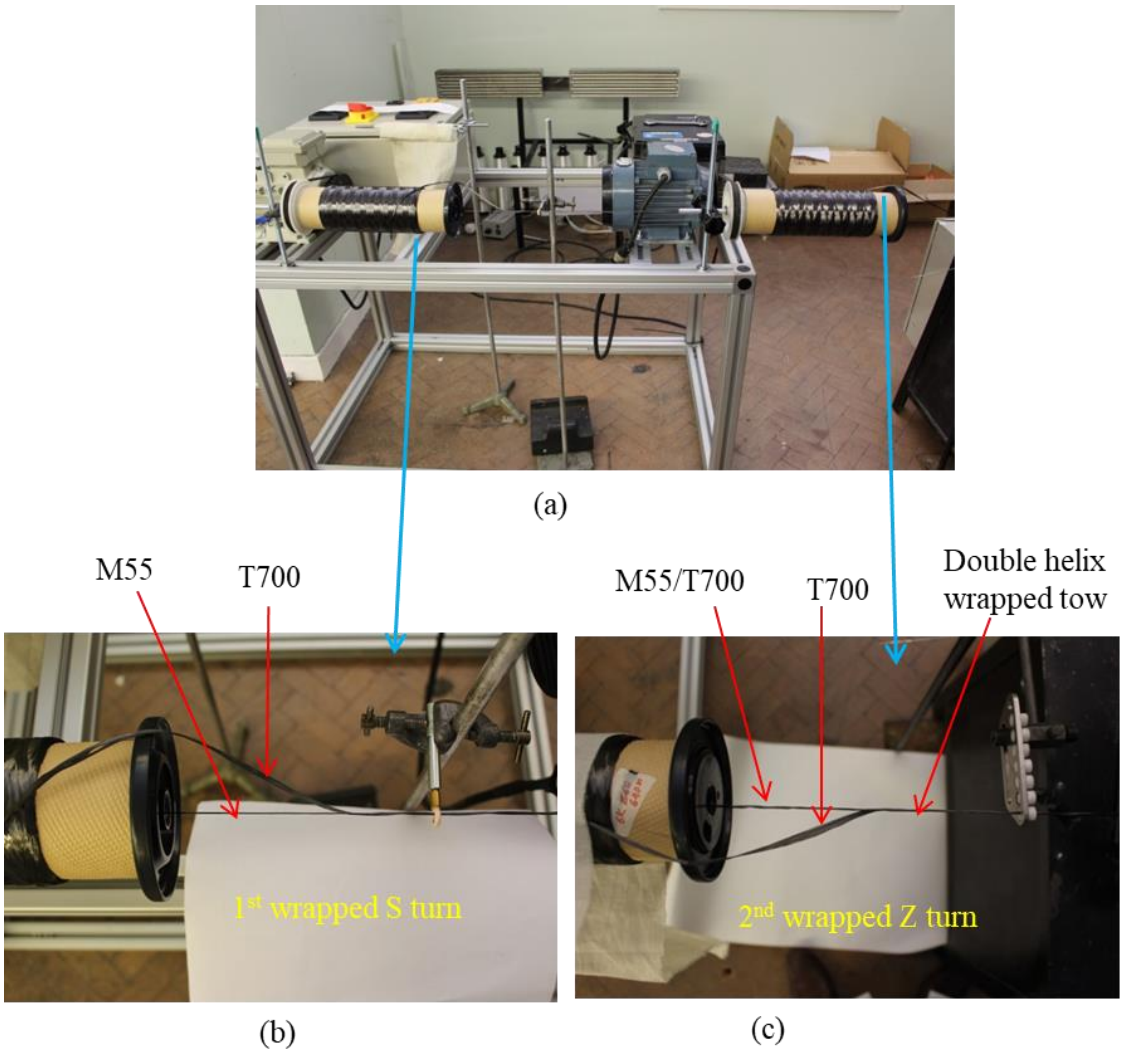

Figure 7.2: Photographs of the double-helix micro-wrapped hybrid tow production line (a) wrapping unit, (b) first wrapping unit (S wrap) and (c) second wrapping unit (Z wrap).

7.2.3.2 Preparation of M55/S-G double helix micro-wrapped hybrid tow

At first 6K M55 tow was helically wrapped with 735 tex S-G in S turn then the S turn wrapped tow was again wrapped with 735 tex S-G in Z turn to finally prepare the double-helix micro-wrapped hybrid tow. The resultant linear density of the hybrid tow was 1704 tex. The volume fraction of M55 and S-G fibre in the micro-wrapped hybrid tow was 15.90 and 84.10% respectively. The hybrid tow was labelled as M55/S-G DH micro-wrapped hybrid tow.

Schematic illustration and optical microscopic images of the M55/T700 and M55/S-G double helix micro-wrapped hybrid tows are shown in Figure 7.3. The images clearly show that the low strain to failure filament tow was helically wrapped with two high strains to failure filament tows in two different directions. Low strain filament was not visible in these images because it was fully covered with high strain material. Detail specifications of the double-helix micro-wrapped hybrid tows are presented in Table 7.1 and single helix micro-wrapped hybrid tows specification are also included here which were already presented in chapter 4 (Table 4.2).

Table 7.1: Parameters of single and double-helix micro-wrapped hybrid tows

Micro-wrapped hybrid configuration	Linear density (Tex) ±SD	No of wraps (Z) (per metre) ±SD	No of wraps (S) (per metre) ±SD	Angle of wrapped (degree) ±SD	Volume of LS fibre (%)	Volume of HS fibre (%)
M55/T700 SH	1026±1.11	26.74±1.82	nil	7.72±0.98	20.30	79.70
M55/T700 DH	1027±1.41	26.22±1.8	26.18±1.7	7.90±1.6	20.28	79.72
M55/S-G SH	1702±1.25	27.07±2.00	nil	7.90±1.24	16.00	84.00
M55/S-G DH	1704±1.52	26.40±1.9	26.20±1.8	7.90±1.44	15.90	84.10

SH = Single helix, DH = Double helix

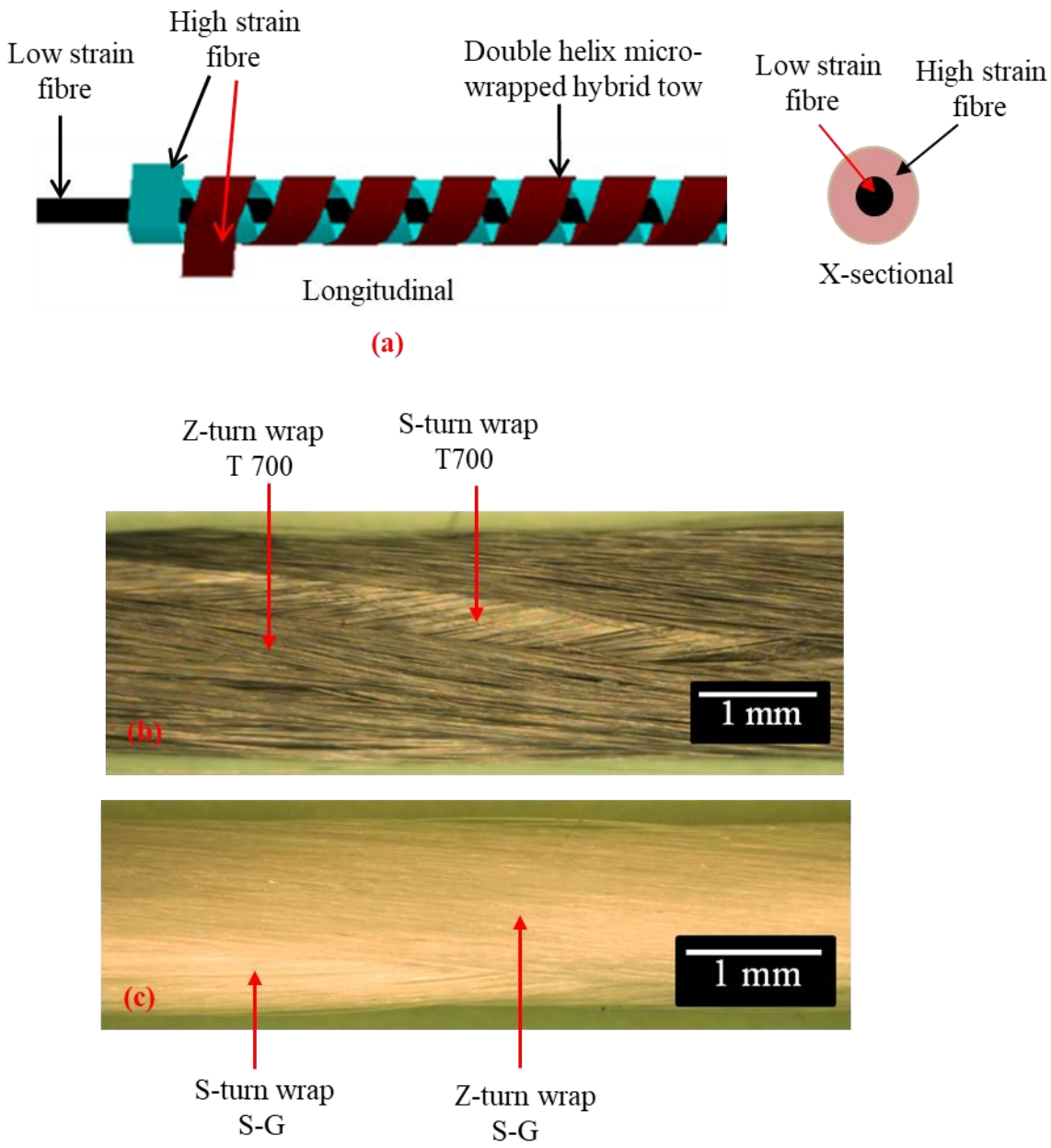

Figure 7.3: (a) Schematic illustration of double helix micro-wrapped hybrid tow, (b) and (c) optical microscopic images of M55/T700 and M55/S-G double helix micro-wrapped hybrid tows

7.2.4 Manufacture of composites rods and laminates

Composite rods were manufactured using M55/S-G double helix micro-wrapped tow with RTCR with manual resin infusion process with the help of a pinboard. The manufacturing procedure of the composite rods used for the present study was described in chapter 4 (section 4.2.6).

Composite laminates were also manufactured from M55/T700 and M55/T700 double helix micro-wrapped hybrid tow UD woven fabric with RTCR using a vacuum-assisted resin infusion process. The manufacturing process of UD woven fabric and UD composite laminates were described in chapter 5 (section 5.2.3).

7.2.5 Mechanical Testing of the composites

The test was carried out according to ASTM D3039 [6] standard on an Intron 5982 machine with a cross-head speed of 2 mm/min. The load was recorded using a 100 kN load cell and the strain was measured using Imetrum video extensometer with a nominal gauge length of 50 mm.

7.3 Results and discussion

7.3.1 M55/S-G micro-wrapped hybrid architecture

7.3.1.1 M55/S-G composite rods

To study the effect of wrapping direction on the failure mechanism during tensile loading, M55/S-G single and double helix micro-wrapped hybrid tow composite rods were manufactured and tested. Both composite rods were translucent and it was easy to observe the change of composite structure during tensile testing. Tensile stress-strain curves of M55/S-G single and double helix micro-wrapped hybrid tow composite rods with video extensometer images with different strain level are shown in Figure 7.4a and b respectively. Both architectures showed non-linearity on their stress-strain graph. Fracture of the composite rods occurred in two steps with LS (M55) material failure and fragmentation early and the HS (S-G) material failed noticeably later. As the LS strain material position was the same in both architectures, so the initial failure of both composite rods occurred at the same strain. Lower stress drop after initial failure in double helix micro-wrapped hybrid tow composite rod was detected Table 7.2. After initial failure, no change was noticed on the specimen surface in both composite rods (Figure 7.4d and m). After initial failure, a plateau region was observed which indicated that the LS material fragmentation occurred in this segment followed by rising stress and strain. The matrix cracking was started after a certain level of strain. The specimen colour change started at 2.0% strain (Figure 7.4g) in single helix composite

which became more visible with increasing strain. The matrix cracking process was not noticeable in the single helix composite rod. This matrix cracking was more visible in double helix composite rod than a single helix one. The matrix cracking started at 1.60% strain (Figure 7.4 o) in double helix composite rod and propagated slowly. The crack formation continued with an increase in stress-strain and covered the whole specimen surface (Figure 7.4s) before ultimate failure. In a single helix composite, all the high strain material reoriented (extended) in one direction but in a double helix composite the high strain material reoriented in two opposite direction (scissoring effect). When two bundles of filament extend in two opposite directions they create more matrix cracking. About 1.95% pseudo-ductile strain was achieved in both composite rods. This kind of failure behaviour is very important for structural application where a warning is needed before the ultimate failure of the composite.

The initial modulus of the single helix and double helix composites were 68.92 and 74.94 GPa respectively. According to the rule of mixture, the calculated value of the modulus was 72 GPa which is close to the experimental results.

Table 7.2: Summary of the normalised tensile test results of M55/S-G single and double helix hybrid tow composite rods

Specimen Type	Single helix	Double helix
Pseudo-yield Stress (MPa)	515.4±21.63	573.74±20.77
Stress drop (MPa)	87.58±17.48	66.96±23.81
Maximum stress (MPa)	1275.6±55.47	1332.86±62.58
Initial modulus (GPa)	68.92±5.60	74.94±0.84
Final modulus (GPa)	34.65±3.07	34.44±2.50
Pseudo-yield strain (%)	0.72±0.05	0.73±0.04
Final failure Strain (%)	3.78±00.11	3.75±0.14
Difference between two failure strain (%)	3.06±0.08	3.01±0.14
Pseudo-ductile strain (%)	1.94±0.20	1.93±0.05

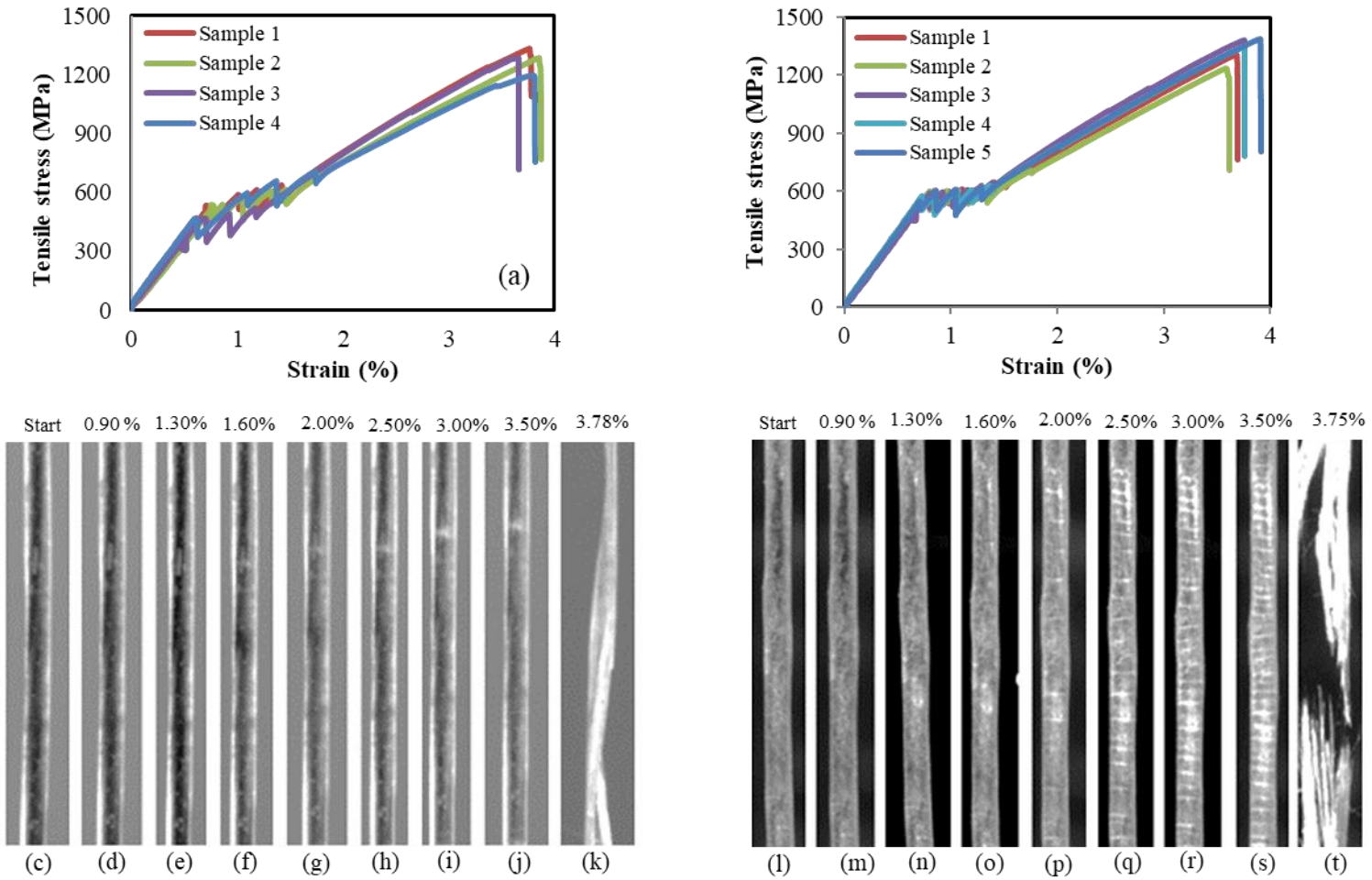

Figure 7.4: Stress-strain graph of M55/S-G micro-wrapped hybrid tow composite rods: (a) single helix micro-wrapped and (b) double helix micro-wrapped. Bottom video extensometer images of the specimens at different strain levels during tensile loading.

7.3.1.2 M55/S-G composite laminates

A similar study was also carried out in M55/S-G single and double helix micro-wrapped hybrid tow UD woven composite laminates. The stress-strain response of M55/S-G single and double-helix micro-wrapped hybrid tows UD woven composite laminates are shown in Figure 7.5a and b respectively. The composite laminates also showed the excellent pseudo-ductile response with a smooth transition between the initial and second linear part of the stress-strain curves in both laminates. Normalised tensile test results of this configuration are shown in Table 7.3. The initial failure occurred at 0.72% strain for both specimens. The stress drop after pseudo-yielding of single-helix and double helix composites was 10.01% and 11.54% respectively which was almost the same. A higher stress drop was detected in the single helix composite rod than double helix composite rods (Table 7.2) but in the composite laminate, no major variation was observed (Table 7.3). A flat plateau region was observed after initial failure indicating that low strain material fragmented gradually and transferred the load to high strain material without any catastrophic delamination. In both specimens, there was no damage or crack observed on the specimen surface after initial failure (Figure 7.5d and l). After a certain strain level matrix delamination was started which was visible in both composite laminates. The delamination was more visible in the double-helix micro-wrapped composite than single-helix composite (Figure 7.5e and m). The pristine and failed images of the specimen are presented in (Figure E1, Appendix E).

Table 7.3: Summary of the normalised tensile test results of M55/S-G single and double helix hybrid tow UD woven composite laminates.

Specimen Type	Single helix	Double helix
Pseudo-yield Stress (MPa)	642.19±22.7	616.33±22.14
Stress drop (MPa)	64.5±5.6	71.05±7.12
Maximum stress (MPa)	1188.3±31.7	1245.28±38.36
Initial modulus (GPa)	90.33±2.24	87.27±1.71
Final modulus (GPa)	40.48±0.50	38.37±1.72
Pseudo-yield strain (%)	0.72±0.04	0.71±0.01
Final failure strain (%)	3.47±0.03	3.54±0.08
Difference between two failure strain (%)	2.75±0.03	2.83±0.09
Pseudo-ductile strain (%)	2.05±0.04	2.05±0.14

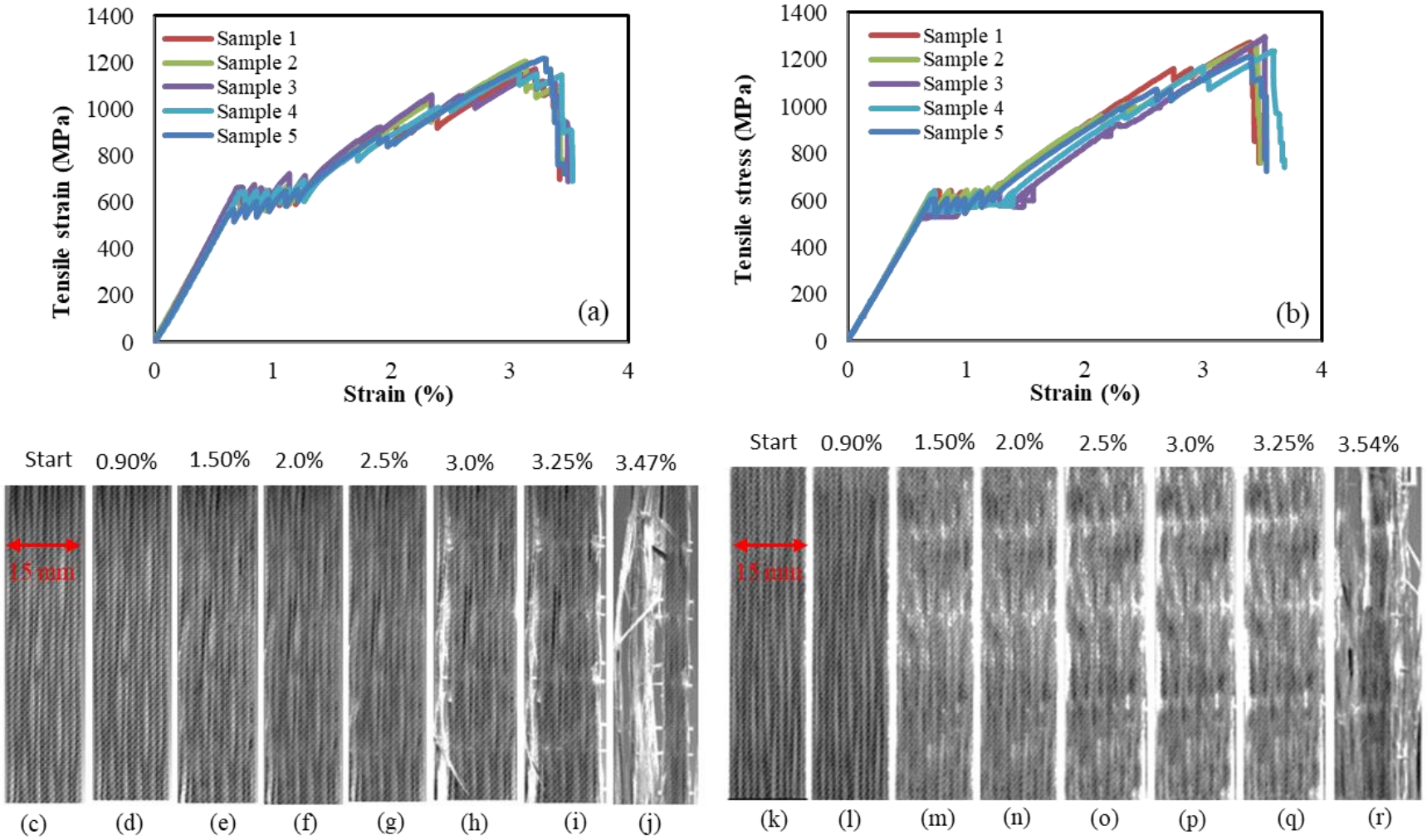

Figure 7.5: Stress-strain graph of M55/S-G micro-wrapped hybrid tow UD woven composites: (a) single helix micro-wrapped and (b) double helix micro-wrapped. Bottom video extensometer images of the specimens at different strain levels during tensile loading.

Some stress drops were observed in the second part of the stress-strain curves because crack propagation started at one edge of the sample (Figure 7.5 h and p). It might have happened due to miss alignment of the tows inside the composite laminates. A good pseudo-ductile strain (about 2.05%) was achieved in this configuration. The initial modulus of the single helix and double helix composites were 90 and 87 GPa respectively. According to the rule of mixture, the calculated value of the modulus was 90 GPa which is close to the experimental results.

7.3.2 M55/T700 micro-wrapped hybrid architecture

To clarify the effect of wrapping direction in the micro-wrapped hybrid tow composite another hybrid configuration (M55/T700) composite were investigated.

7.3.2.1 M55/T700 composite laminates

To study the effect of wrapping direction in the composites laminate, UD woven composite laminates were manufactured from M55/T700 single and double helix micro-wrapped hybrid tow UD woven fabric. Figure 7.6 a and b shows the stress-strain curve of M55/T700 single and double helix micro-wrapped hybrid composite laminate respectively. The single and double-helix architecture composite laminates showed similar failure behaviour and demonstrated excellent pseudo-ductile response. No significant difference was observed between the two architectures. The pseudo-yield strain of both composites was the same. There was no influence of wrapping direction on the low strain material failure as it stayed in the core at a straight position in both hybrid architectures. The stress drop after pseudo-yielding of the double-helix composite was 7.4% which is almost similar to single-helix micro-wrapped composite (7.5%). The ultimate strain to failure of the single-helix micro-wrapped tow was a bit higher (2.05%) than double-helix composite (1.94%). In a single helix composite, all the high strain material extended in one direction but in a double helix composite the high strain material extended in two opposite direction. The two bundles of filament extended in two opposite directions and reoriented which created more matrix cracking. The matrix cracking generated the stress concentration which caused early failure of the composite.

Table 7.4: Summary of the normalised tensile test results of M55/T700 single and double helix hybrid tow composite laminates

Specimen Type	Single helix	Double helix
Pseudo-yield Stress (MPa)	1111.1±21.9	1087.3±21.4
Stress drop (MPa)	83.4±2.2	79.4±20.2
Maximum stress (MPa)	1804.1±66.3	1726.4±88.1
Initial modulus (GPa)	152.2±2.19	152.5±5.62
Final modulus (GPa)	102.13±5.62	100.47±5.01
Pseudo-yield strain (%)	0.71±0.01	0.72±0.02
Final failure Strain (%)	2.05±0.04	1.94±0.06
Difference between two failure strains (%	1.34±0.03	1.22±0.06
Pseudo-ductile strain (%)	0.80±0.05	0.79±0.04

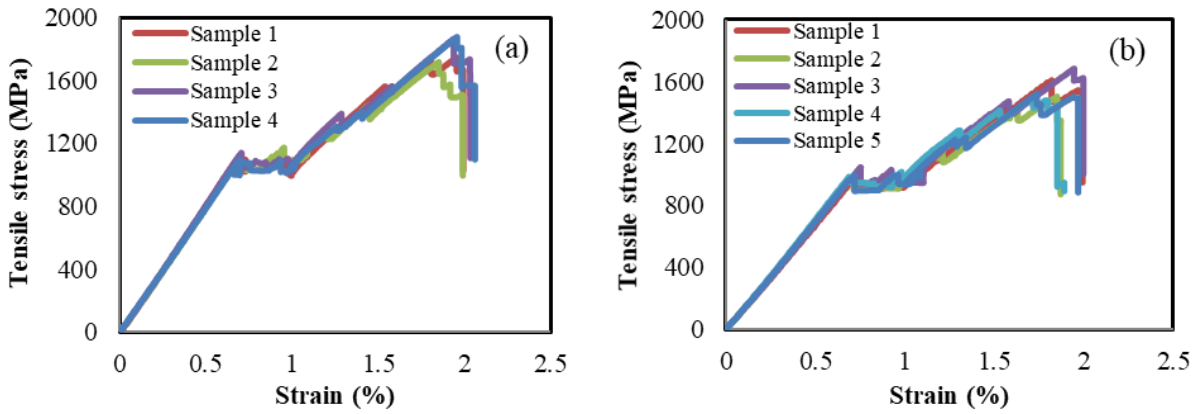

Figure 7.6: Stress-strain graph of M55/T700 micro-wrapped hybrid tow UD woven composites: (a) single helix micro-wrapped and (b) double helix micro-wrapped.

A typical normalised stress-strain graph of different single and double helix micro-wrapped hybrid tow UD woven composites are shown in Figure 7.7.

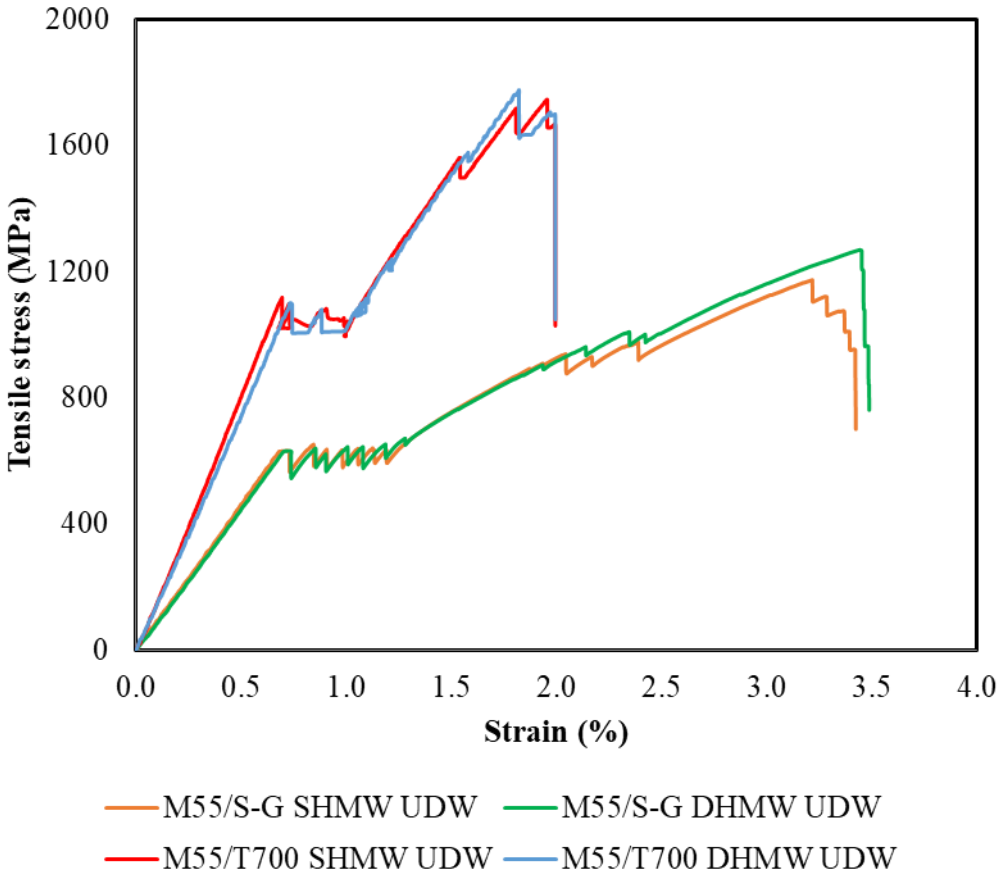

Figure 7.7: A typical normalised stress-strain graph of different single and double helix micro-wrapped hybrid tow UD woven composites.

7.4 Summary

The process which was developed for the manufacture of double helix micro-wrapped hybrid tow for pseudo-ductile composite has been discussed in this chapter. Two different hybrid configurations (M55/S-G and M55/T700) double helix micro-wrapped hybrid tows were prepared and it was observed that this process was also suitable for the production of core-shell type hybrid tow. Tensile test results of composite rods and laminates showed that double helix micro-wrapped hybrid architecture also demonstrated pseudo-ductile behaviour with little stress drop after LS material failure. No significant difference in the tensile properties of single and double helix composite was observed. The video extensometer images during the tensile test of M55/S-G micro-wrapped composite rod and laminate showed that the matrix cracks started earlier in the double helix micro-wrapped hybrid composite testing than in single helix testing. The matrix cracking process was more noticeable in double helix composites. This kind

of fracture mechanism could be useful as a warning sign before the final failure of the composite if it is monitored by using acoustic emission system.

References

[1] G. L. Louis and H. L. Salaun, "'X' Direction Filament-Wrapped Yarn," *Text. Res. J.*, vol. 56, no. 3, pp. 161–163, Mar. 1986.

[2] Y. Shang *et al.*, "Highly Twisted Double-Helix Carbon Nanotube Yarns," *ACS Nano*, vol. 7, no. 2, pp. 1446–1453, Feb. 2013.

[3] N. E. Merter, G. Başer, and M. Tanoğlu, "Effects of hybrid yarn preparation technique and fiber sizing on the mechanical properties of continuous glass fiber-reinforced polypropylene composites," *J. Compos. Mater.*, vol. 50, no. 12, pp. 1697–1706, May 2016.

[4] B. M. H. Arefazar A., Movahed H.R., Eskandarnejad S., "Study of the effect of core-twist hybrid yarn glass/pet on mechanical properties of unsaturated polyester resin," vol. 16, no. 163. Iranian Journal Of Polymer Science And Technology (Persian), pp. 31–40, 01-Jan-2003.

[5] B. Baghaei, M. Skrifvars, and L. Berglin, "Manufacture and characterisation of thermoplastic composites made from PLA/hemp co-wrapped hybrid yarn prepregs," *Compos. Part A Appl. Sci. Manuf.*, vol. 50, pp. 93–101, Jul. 2013.

[6] "ASTM D3039 Standard Test Method for Tensile Properties of Polymer Matrix Composite Materials -D3039 2008, Annual Book of ASTM Standards.

Chapter 8: Conclusions and Future Research

8.1 Summary of findings

The aim of this research was to design and develop the processes for tow scale dry fibre architectures to prepare inherent ductile reinforced material for achieving ductility or pseudo-ductility in high-performance composites. Two different processes were developed to prepare hybrid preform for ductile or pseudo-ductile composites. Detailed manufacturing processes of hybrid preforms and their composites were extensively studied and their mechanical behaviour was investigated. The findings described in this research provided a better understanding of the mechanism that can be used to create ductility in the high-performance composites. A summary of the key findings of this study has been presented in the following sections.

8.1.1 Spread and commingled carbon/glass hybrid composites

A novel process for spreading and commingling of carbon and glass fibre tow was developed to make fibre hybridisation at the spread-tow level. The tows were commingled once they were spread. The process was capable of spreading carbon and glass fibre tow separately using compressed air which allowed increasing the width 4-5 times without noticeable filament damage. The experimental studies showed that airflow rate, angle of airflow, tow tension and entanglement of filament in the tow affect the spreadability of the tow. Followed by spreading, a commingled tow was prepared from one carbon and two glass fibre spread tows by using air-assisted spreading process. The volume fraction of the carbon and glass fibre in the commingled tow was 20% and 80% respectively. Finally, four different types of composites were manufactured i) spread tow carbon ii) spread tow glass (iii) carbon and glass spread tow-in different layers (layer by layer) and (iv) commingled carbon/glass composites. SEM observation confirmed that carbon and glass fibres were partially hybridised at the tow level during commingling process. The tensile properties studies revealed that both hybrid composites exhibited more gradual and improved tensile failure strain compared to 100% carbon fibre spread tow composite. Non-linearity in the stress-strain graphs was observed during tensile testing. No significant differences in mechanical properties were observed between the two-hybrid architectures. The ultimate strain to failure of the hybrid composites increased about 26% compared to carbon fibre composite but it was

25% lower than that of glass fibre composite. In this process, some ductility or pseudo-ductility were achieved. However, another process for dry fibre architecture was developed and studied for improvement in ultimate failure strain.

8.1.2 Process development and evaluation of micro-wrapped hybrid tows

A novel micro-wrapping process was developed for dry fibre hybrid architectures to manufacture reinforced material for ductile or pseudo-ductile composites. In order to produce the micro-wrapped hybrid tow, a laboratory-scale machine was designed and assembled. In this process, hybridisation of two different dry fibres with different strain to failure was carried out through a micro-wrapping where low strain (LS) fibre was kept straight in the core and high strain (HS) fibre helically wrapped around the low strain fibre. The process was suitable for the production of core-shell type hybrid tow. Micro-wrapped hybrid tows were produced using two different types of wrapping arrangement: single helix and the double helix. In the single helix micro-wrapping process, the straight LS fibre (core tow) wrapped with a single bundle of HS fibre (sheath tow) either clockwise (Z) or anti-clockwise (S) direction. Whereas for the double helix micro-wrapping process, the straight LS fibre (core tow) was helically wrapped with two bundles of HS fibre (sheath tows) in both S and Z direction. Four different types of hybrid configurations (T700/E-G, T700/S-G, M55/S-G and M55/T700) single helix micro-wrapped and two types of (M55/S-G and M55/T700) double helix micro-wrapped hybrid tows were prepared and their structural and tensile properties were studied. Various types of UD woven textile preform were manufactured from micro-wrapped hybrid tows. In order to compare the mechanical properties of micro-wrapped hybridised composites, other types of composites were produced without micro-wrapping. In this process instead of micro-wrapping hybridisation, a side-by-side parallel placement of two different strain to failure fibres were kept together in the same axial direction.

Microscopic observation revealed the core-sheath architectures of micro-wrapped hybrid tow where sheath filament wrapped the core at the angle of 7-degree. Dry tow tensile test results displayed the non-linearity on their stress-strain graph. In comparison with side by side hybrid tows, the micro-wrapped hybrid tows had higher stress and strain to failure for all hybrid configurations. The reason for the higher strength of micro-wrapped hybrid tow was that the wrapping increased the filament-filament

interaction. Dry fibre tow test also demonstrated lower stress drop after initial failure compared to the side by side hybrid tow.

8.1.3 Mechanical characterisation of micro-wrapped hybrid tow composites

A detailed study on the effect of micro-wrap hybrid architectures on the ductile or pseudo-ductile properties of the composite was carried out and compared with side by side hybrid architectures. The investigations were carried out in three stages- mesoscale composite (single hybrid tow composite rod), UD composite laminates and UD woven composite laminates. A wide range of composite rods and laminates with different hybrid configurations were fabricated and studied. The main findings of this research are summarised below.

- The cross-sectional study of the composites confirmed that the LS fibre (core tow) were distributed inside the HS fibre (sheath tow) at different shapes but it was fully covered by HS fibre in the micro-wrapped hybrid composites. However, in side-by-side hybrid composites, LS and HS fibre distributed randomly inside and on the surface of the composite.
- Tensile test results demonstrated that micro-wrapped hybrid composites (rods and laminates) demonstrated pseudo-ductile behaviour with little stress drop after LS fibre failure for all four hybrid configurations. In the micro-wrapped architectures after the initial failure of the LS fibre (core), the surrounded HS fibre (sheath) restricted the crack propagation and transferred the stress to HS fibre without major stress drop. In addition, the video extensometer images confirmed that there was no visual change on the surface of the specimen after LS fibre failure. In contrast, a significant stress drop was observed in side by side hybrid composites after LS fibre failure and some damage on the specimen surface were observed.
- T700/E-G configuration did not demonstrate any pseudo-ductile behaviour in the composite rod though the dry micro-wrapped hybrid tow of this configuration demonstrated nonlinearity on their stress-strain curve (similar results were observed in the literature). However, some hybrid effect was observed because the final strain to failure of the composite rod was 2.09% which is higher than T700 UD composite (1.63%). Although, T700/E-G micro-wrapped hybrid composite shown non-linearity on their stress-strain graph, but it did not have enough strain

after pseudo-yielding (low pseudo-ductile strain) because of a small difference between the failure strain of the T700 and E-G composites.

- T700/S-G micro-wrapped hybrid configuration offered good strain after pseudo-yielding (initial failure) but the very low increase in stress value was attained in both composite rod and laminate. A significant improvement of stress drop after initial failure in the micro-wrapped hybrid composite (8.9%) was achieved compared to side by side hybrid composite (27.7%). In addition, T700/S-G micro-wrapped UD woven composite showed lower stress drop (3.7%) compared to the T700/S-G micro-wrapped UD composite. Elastic modulus was increased by 41% compared to the HS material baseline.
- By using M55/S-G micro-wrapped hybrid configuration, after pseudo yielding, the stress to failure was also increased along with strain in contrast with T700/S-G hybrid composite that showed only higher strain but little increase in stress. Higher pseudo ductile strain (2.05%) and higher modulus were achieved with M55/S-G configuration. An increase of 104% modulus was recorded with respect to the high strain material baseline (S-G).
- The M55/T700 micro-wrapped hybrid configuration also demonstrated good pseudo-ductility with the high initial modulus (150 GPa), pseudo-yield stress (1128 MPa) and pseudo-ductile strain (0.84%). A significant difference in stress drop after pseudo-yielding was also observed in this configuration between side by side (16.1%) and micro-wrapped hybrid architecture (8%).
- After initial failure, a plateau region was observed between the first and second straight part of the stress-strain curves for M55/S-G and M55/T700 micro-wrapped hybrid composites. It means that the LS fibre fragmentation occurred, instead of causing unstable delamination or immediate fracture of the HS fibre. If this fracture is monitored (e.g. by acoustic emission) it could be exploited as a warning sign before final failure.

8.1.4 Effect of resin ductility

A significant effect of two epoxy resin systems, room temperature curing resin (RTCR) and high temperature curing resin (HTCR) on ultimate failure strain of the micro-wrapped hybrid composite was observed. In-plane shear stress-strain results revealed that room temperature curing resin composites have higher ductility compared to high temperature curing resin composites. Composites with both resin systems showed

pseudo-ductile response on their stress-strain curve during tensile loading. Higher ductile behaviour of the RTCR promoted the stressing and reorientation of the filament easily, resulting in an increase in ultimate strain to failure of composite about 27% compared to HTCR. The modulus and ultimate failure stress were also higher in RTCR composite than HTCR composite. However, higher stress drop after initial failure was observed with RTCR compared to HTCR composite.

8.1.5 Effect of wrapping directions

The double helix wrapping process was also suitable for the production of core-shell type hybrid tow. The effect of wrapping directions of micro-wrapped hybrid tow on the pseudo-ductile properties was investigated in two-hybrid configurations (M55/S-G and M55/T700). Tensile test results of composite rods and laminates showed that the double helix micro-wrapped hybrid architecture demonstrated similar pseudo-ductile behaviour of the single helix micro-wrapped hybrid composites. No significant differences in the tensile properties of single and double helix composite were observed. The video extensometer images during the tensile test of M55/S-G micro-wrapped composite rod and laminate showed that the matrix crack started earlier in the double helix micro-wrapped hybrid composite than in the single helix one. The matrix cracking process was more noticeable in the images of the double helix composite. This kind of fracture mechanism can be useful as a warning sign before the final failure of the composite if it is monitored by acoustic emission system.

Textile preforms are considered the structural backbone of the composites as these are used as reinforcement. The micro-wrapped hybrid tow could be used to manufacture different types of textile preforms. Therefore, this study indicates that the novel micro-wrapped hybrid architecture can be a suitable approach to produce low-cost textile preform alternative to existing expensive thin ply concepts for achieving ductility or pseudo-ductility.

.

8.2 Future research

- In this research, two promising processes of dry fibre architectures to demonstrate ductility or pseudo-ductility in high-performance composites were designed, developed and investigated. This research work has been limited to the

tensile behaviour studies of dry preforms and various types of composites. However, there are several aspects (such as compressive and flexural behaviour) of the hybrid composites that could be investigated in the future.

- To clarify the failure mechanism of the micro-wrapped hybrid tow composite, the mesoscale composite specimen (single micro-wrapped hybrid tow composite rod) could be tested using in-situ X-ray computed tomography for improved understanding of the hybrid tow composite failure mechanism under the tensile loading.
- It was found that carbon/E-glass commingled spread tow can increase the failure strain of the composites compared to controlled carbon fibre composite with the 20% and 80 % volume ratio. However, different hybrid configurations (carbon/S-glass, carbon/carbon) should be investigated to further understand the failure mechanism of the commingled spread tow composite under tensile loading.
- In this study, only one wrapping angle micro-wrapped hybrid tow was investigated. Influence of wrapping density (wrapping angle) and tow fineness of micro-wrapped hybrid tow on the mechanical properties of high-performance composites can be investigated.
- Loading-unloading behaviour of the micro-wrapped hybrid composites should be studied to understand the energy dissipation.
- 3D fabric can be manufactured from micro-wrapped hybrid tows and mechanical properties of the 3D woven composite laminates can be studied.

Appendices

Appendix A: Chapter 3

Figure A1: Pristine and failed specimen images of CF/E-G layer by layer and commingled hybrid composites.

Layer by layer hybrid

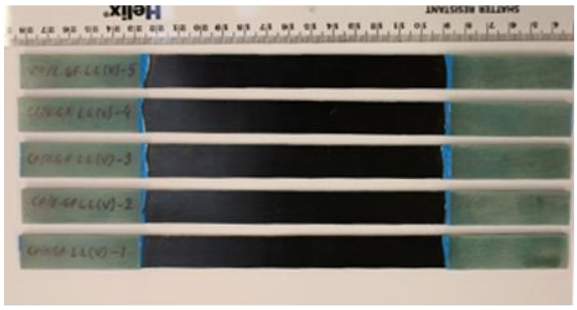

Pristine specimens

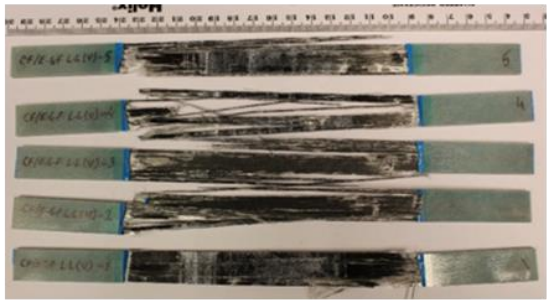

Failed specimens

Commingled hybrid

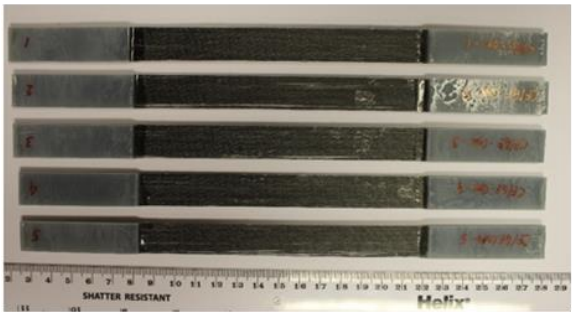

Pristine specimens

Failed specimens

Appendix B: Chapter 4

Table B1: Fibre volume fraction of different hybrid tow composite rods.

Hybrid tow configuration	Hybrid architecture	Types of Resin	Fibre volume fraction (%) ± SD		
			LS fibre	HS fibre	Total
T700/E-G	SBS	HTCR	6.51±0.26	27.37±1.06	33.88±1.32
T700/E-G	SHMW	HTCR	7.42±0.24	31.23±0.98	38.65±1.22
T700/S-G	SBS	HTCR	7.28±0.18	29.16±1.08	36.44±1.26
T700/S-G	SHMW	HTCR	8.04±0.21	32.18±0.83	40.22±1.04
M55/T700	SBS	HTCR	6.67±0.25	26.67±0.99	33.42±1.24
M55/T700	SHMW	HTCR	8.22±0.12	32.28±0.96	40.50±1.08
M55/S-G	SBS	HTCR	5.17±0.19	27.17±0.99	32.34±1.18
M55/S-G	SHMW	HTCR	6.42±0.18	33.70±0.94	40.12±1.12

SSB = side by side, SHMW = single helix micro-wrapped, RTCR = room temperature curing resin.

Figure B1: Failure images of different side by side and micro-wrapped hybrid tows.

(a) Failure images of M55/T700 hybrid tows

Side by side hybrid

Micro-wrapped hybrid

(b) Failure images of M55/S-G hybrid tows

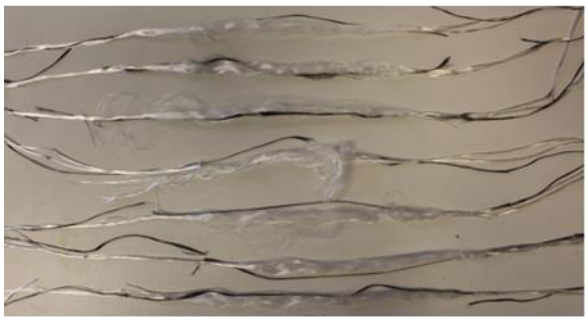

Side by side hybrid

Micro-wrapped hybrid

Figure B2: Pristine and failed specimen images of different side by side and micro-wrapped hybrid tow composite rods.

(a) T700/S-G side by side hybrid composite rods

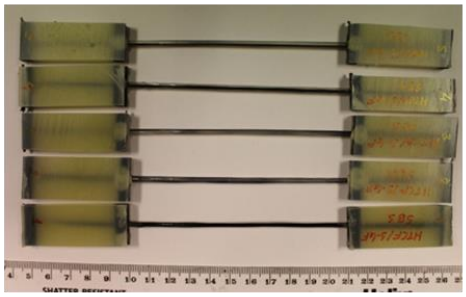

Pristine specimens

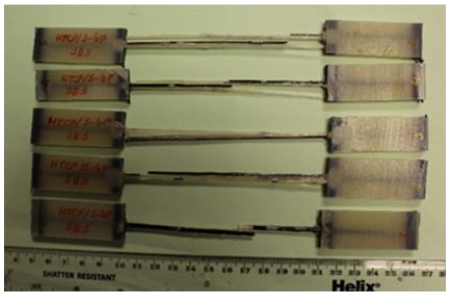

Failed specimens

(b) T700/S-G micro-wrapped hybrid composite rods

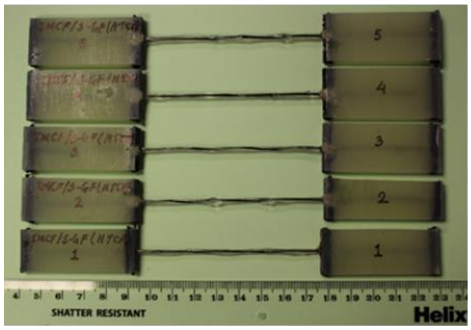

Pristine specimens

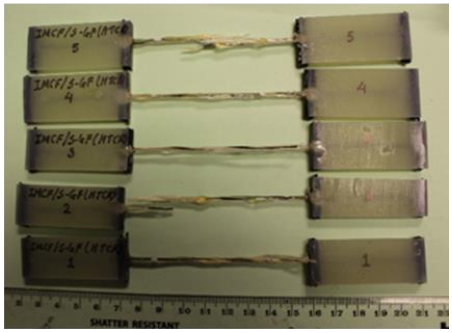

Failed specimens

(c) M55/T700 side by side hybrid composite rods

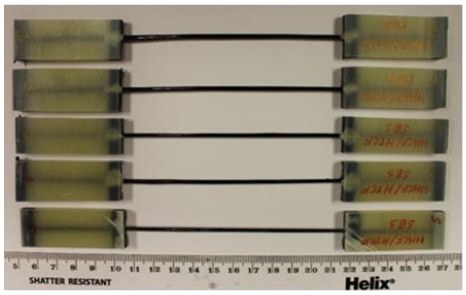

Pristine specimens

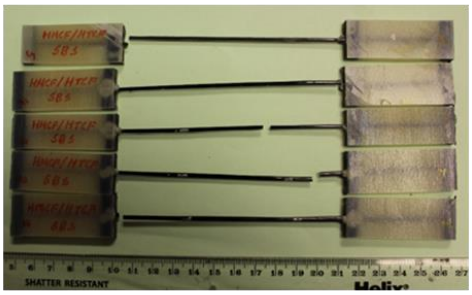

Failed specimens

(d) M55/T700 micro-wrapped hybrid composite rods

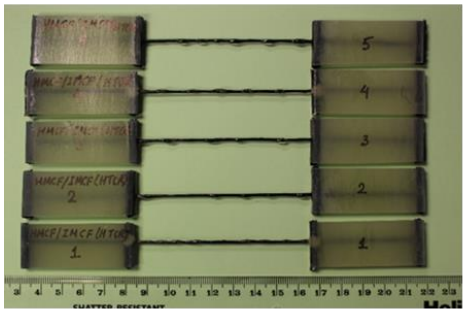

Pristine specimens

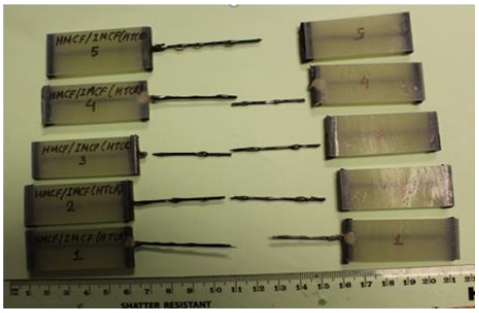

Failed specimens

(e) M55/S-G side by side hybrid composite rods

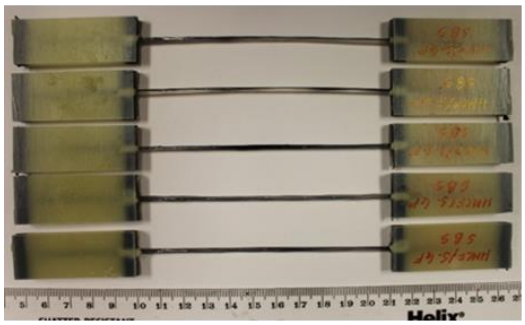

Pristine specimens

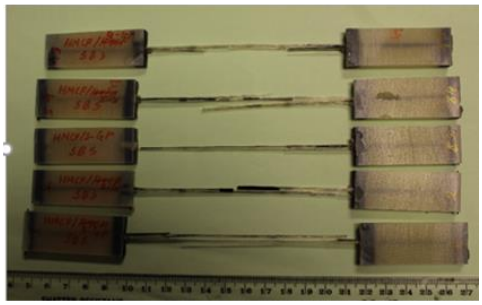

Failed specimens

(f) M55/S-G micro-wrapped hybrid composite rods

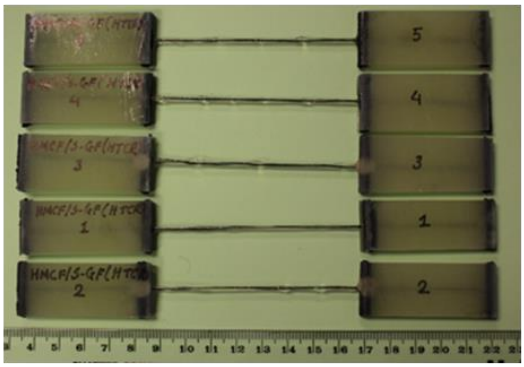

Pristine specimens

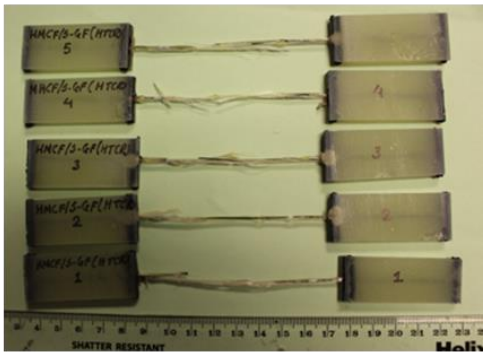

Failed specimens

Appendix C: Chapter 5

Table C1: Fibre volume fraction of different composite laminates

Hybrid configuration	Hybrid process	Type of specimen	Resin type	Fibre volume fraction (%) ± SD			
				LS fibre	HS fibre	Weft	Total
T700/E-G	SHMW	UD	HTCR	11.37±0.04	47.83±0.19	-	59.20±0.23
T700/S-G	SBS	UD	HTCR	12.56±0.06	48.16±0.26	-	60.20±0.32
T700/S-G	SHMW	UD	HTCR	11.2±0.05	44.8±0.19	-	56.00±0.24
T700/S-G	SHMW	UDW	HTCR	9.87±0.7	39.46±0.29	0.17	49.50±0.36
M55/T700	SBS	UD	RTCR	12.19±0.05	47.87±0.21	-	60.06±0.26
M55/T700	SHMW	UD	RTCR	11.08±0.07	43.48±0.27		54.56±0.34
M55/T700	SHMW	UDW	RTCR	10.15±0.07	39.85±0.28	0.16	50.16±0.35
M55/S-G	SHMW	UDW	RTCR	8.05±0.03	42.24±0.15	0.16	50.45±0.18

SSB = side by side, SHMW = single helix micro-wrapped, UD = Unidirectional, UDW = Unidirectional woven, RTCR = room temperature curing resin, HTCR = High temperature curing resin

Figure C1: Pristine and failed specimen images of different side by side and micro-wrapped hybrid composites.

(a) T700/E-G micro-wrapped hybrid UD

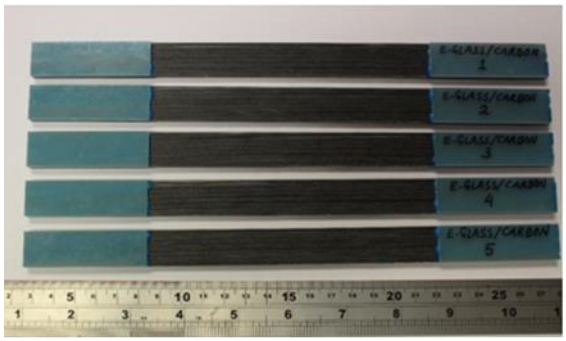

Pristine specimens

Failed specimens

(b) T700/s-G side by side hybrid UD

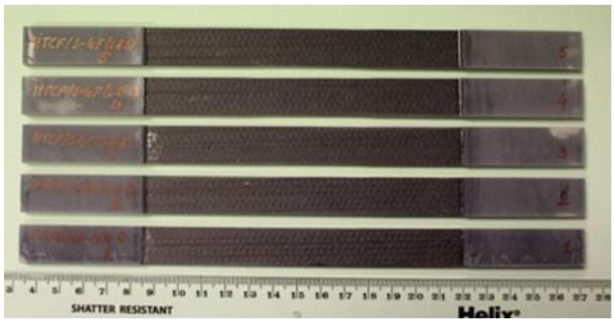

Pristine specimens

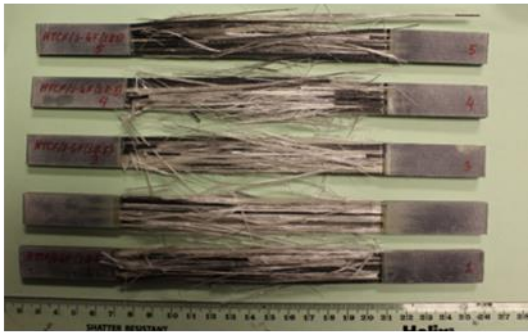

Failed specimens

(c) T700/S-G micro-wrapped hybrid UD

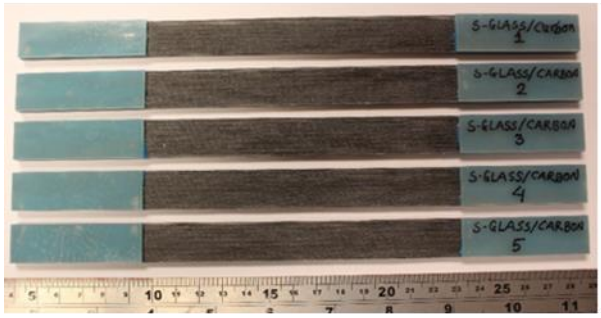

Pristine specimens

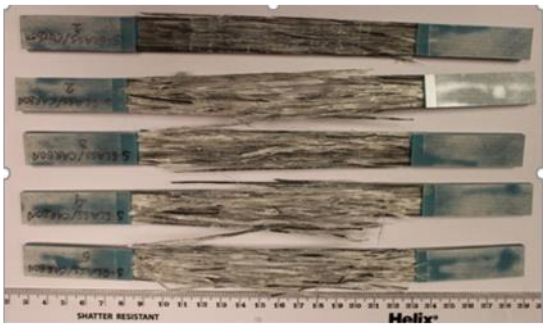

Failed specimens

(d) T700/S-G micro-wrapped hybrid UD woven

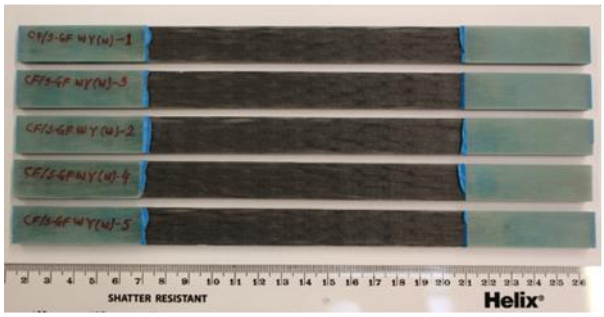

Pristine specimens

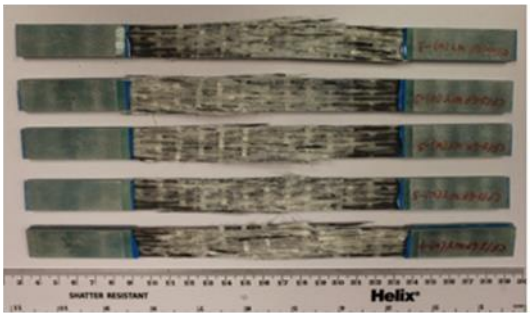

Failed specimens

(e) M55/S-G micro-wrapped hybrid UD woven

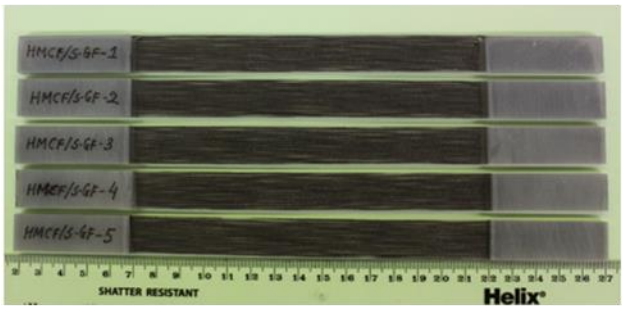

Pristine specimens

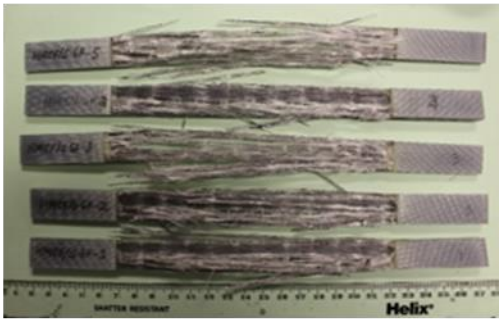

Failed specimens

(f) M55/S-G side by side hybrid UD

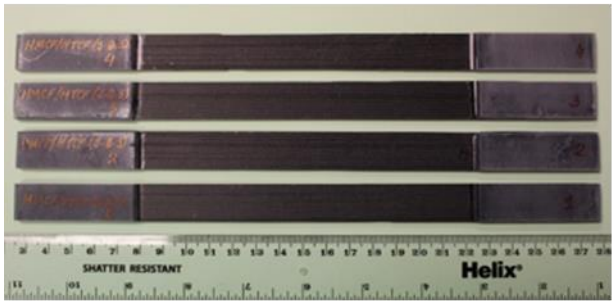

Pristine specimens

Failed specimens

(g) M55/T700 micro-wrapped hybrid UD woven

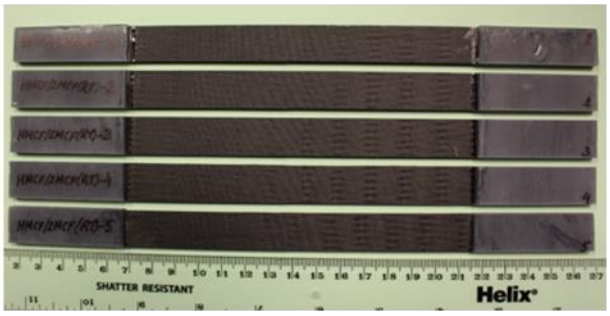

Pristine specimens

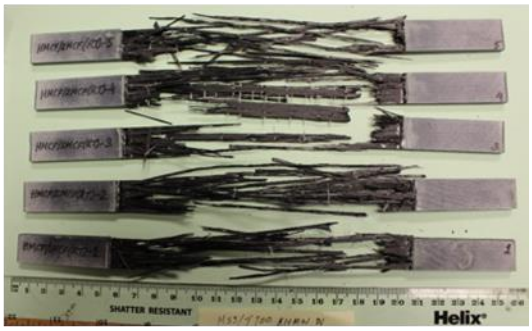

Failed specimens

Appendix D: Chapter 6

Table D1: Fibre volume fraction of different hybrid tow composite rods.

Hybrid tow configuration	Hybrid architecture	Types of Resin	Fibre volume fraction (%) ± SD		
			LS fibre	HS fibre	Total
M55/T700	SHMW	HTCR	8.22±0.12	32.28±0.96	40.50±1.08
M55/T700	SHMW	RTCR	7.77±0.22	30.49±0.92	38.26±1.14
M55/S-G	SHMW	HTCR	6.42±0.18	33.70±0.94	40.12±1.12
M55/S-G	SHMW	RTCR	6.21±0.17	32.63±0.89	38.84±1.06

Table D2: Fibre volume fraction of different composite laminates

Hybrid configuration	Hybrid process	Type of specimen	Resin type	Fibre volume fraction (%) ± SD			
				LS fibre	HS fibre	Weft	Total
M55/T700	SHMW	UDW	HTCR	9.96±0.07	39.10±0.29	0.16	49.22±0.36
M55/T700	SHMW	UDW	RTCR	10.15±0.07	39.85±0.28	0.16	50.16±0.35
M55/T700	SHMW	±45° W	HTCR	9.95±0.06	39.06±0.22	0.16	49.17±0.28
M55/T700	SHMW	±45° W	RTCR	10.32±0.06	41.28±0.04	0.16	51.76±0.30

Appendix E: Chapter 7

Table E1: Fibre volume fraction of different hybrid tow composite rods.

Hybrid tow configuration	Hybrid architecture	Types of Resin	Fibre volume fraction (%) ± SD		
			LS fibre	HS fibre	Total
M55/S-G	SHMW	RTCR	6.21±0.17	32.63±0.89	38.84±1.06
M55/S-G	DHMW	RTCR	6.01±0.18	31.53±0.93	37.54±1.11

SHMW = single helix micro-wrapped, DHMW = Double helix micro-wrapped

Table E2: Fibre volume fraction of different composite laminates

Hybrid configuration	Hybrid process	Type of specimen	Resin type	Fibre volume fraction (%) ± SD			
				LS fibre	HS fibre	Weft	Total
M55/T700	SHMW	UDW	RTCR	10.15±0.07	39.85±0.28	0.16	50.16±0.35
M55/T700	DHMW	UDW	RTCR	9.97±0.08	39.72±0.30	0.15	49.84±0.38
M55/S-G	SHMW	UDW	RTCR	8.05±0.03	42.24±0.15	0.16	50.45±0.18
M55/S-G	DHMW	UDW	RTCR	8.08±0.04	42.45±0.22	0.15	50.68±0.26

SHMW = single helix micro-wrapped, DHMW = Double helix micro-wrapped

Figure E1: Pristine and failed specimen images of the single helix and double helix micro-wrapped hybrid composites.

(a) M55/S-G single helix micro-wrapped hybrid UD woven

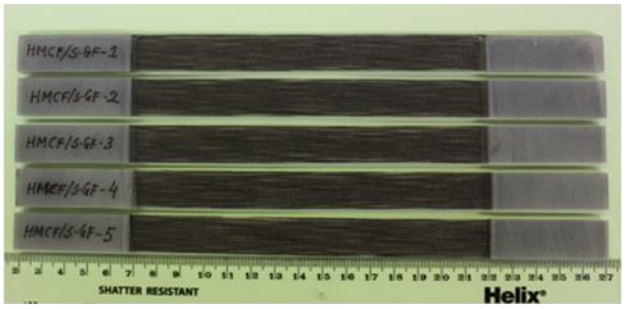

Pristine specimens

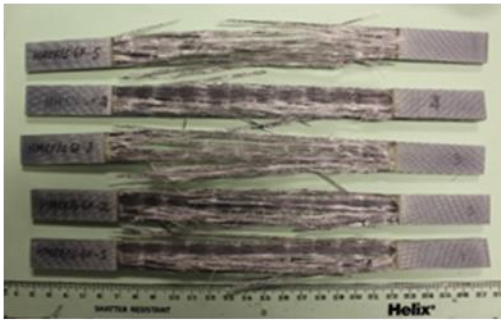

Failed specimens

(b) M55/S-G Double helix micro-wrapped hybrid UD woven

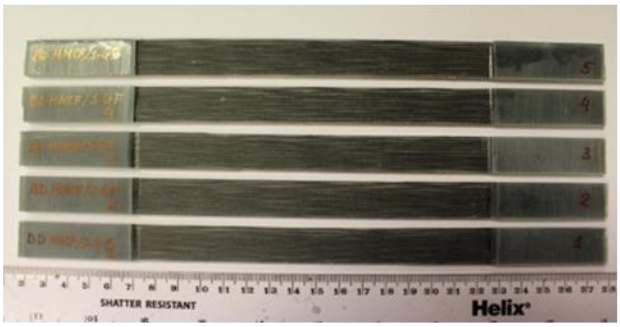

Pristine specimens

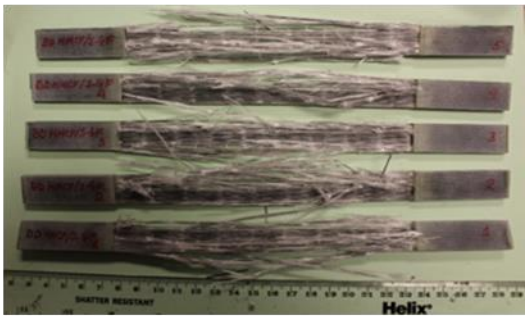

Failed specimens